Department of Naval Architecture and Marine Engineering

DEVELOPMENT OF NUMERICAL WAVE POWER PREDICTION TOOL FOR OFFSHORE OSCILLATING WATER COLUMN WAVE ENERGY CONVERTER

Ahmed Seif-Eldine Mohamed Bayoumi, M.Sc.

A thesis presented in fulfilment of the requirements for the degree of Doctor of Philosophy

2013

Signed: *Date:*

Summary

Marine renewable energy sources are crucial alternatives for a sustainable development. The idea of generating electrical power from water waves has been realized for many years. In fact, waves are now considered as an ideal renewable energy source since a Wave Energy Converter (WEC) has no fuel cost and provides cleanly a high power density that is available most of the time. The third generation of WECs is intended to be installed offshore. This allows the device to harvest the great energy content of waves found in deep water and minimise the environmental impacts of the device. On the other hand, moving WECs to offshore locations will increase the initial and maintenance costs.

So many types of device may be suggested for wave power extraction that the task of selecting a particular one is made complicated. Therefore modelling of different WECs allows the comparison between them and the selection of the optimum choice. Recent studies showed that the SparBuoy Oscillating Water Column (OWC) has the advantage of being simple, axi-symmetrical, and equally efficient at capturing energy from all directions, but its efficiency (capture factor) is affected significantly by the incident wave periods variation due to the dynamic coupling of the water column and the floating structure. The proper modelling of the device allows the optimization of the geometries and the Power Take-Off (PTO) mechanism in order to maximise the power absorbed.

The main objective of this research is to develop experimentally validated numerical wave power prediction tool for offshore SparBuoy OWC WEC. The numerical tool should be able to predict the spar motions and the water column oscillations inside the structure, in addition to the estimation of the pneumatic power absorber and the evaluation of the device performance.

Three uncoupled linear second order differential equations have been used to predict the spar surge, heave and pitch motions, where wave forces have been calculated analytically in frequency domain in inertia and diffraction regimes. Mooring system has been involved in surge motion only using static and quasi-static modelling

approaches. Finite element multi-static model have been developed using OrcaFlex to validate the analytical results.

Single Degree of Freedom (DOF) mechanical oscillation model has been presented to simulate the water column oscillations inside captive cylindrical OWC where PTO damping and stiffness due to air compressibility inside the pneumatic chamber have been taken into account linearly. Later on, nonlinearity due to large waves has been investigated. Linearized frequency domain model based on classical perturbation theory and nonlinear model where wave forces are calculated in time domain have been proposed. Furthermore, nonlinearity due to damping forces has been considered. First, iterative procedure has been used to optimise the linear and quadratic damping coefficients in frequency domain. Then, another model has been provided where equivalent viscous damping coefficients are calculated in time domain by taking into consideration the instant oscillation amplitude. Finally the nonlinear effects due to air compressibility inside the OWC chamber has been considered in a time domain model which include the water column oscillations amplitudes.

Two different dynamic models have been implemented to describe floating OWC and will be referred to in the text as *simplified 2DOF model* and *Szumko model*. Both models considered two translational modes of motions in heave direction. Simplified 2DOF model has been solved analytically in frequency domain due to its simplicity, while numerical solutions in time domain have been provided for both models using Matlab. Different approaches have been adopted to modify both models in order to obtain a satisfactory agreement between the predicted and measured results.

A floating platform consists of four similar SparBuoy OWC WECs rigidly attached together by trusses where spars are located at the corners have been tested experimentally. Numerical model has been developed to predict the platform motions. Finally the experimental results have been compared to those obtained from the modelling of single SparBuoy OWC.

Acknowledgements

First of all, I gratefully acknowledge my sincere veneration and indebtedness and express my profound gratitude and deep respect to my supervisor **Professor Atilla Incecik**, Head of Department of Naval Architecture and Marine Engineering, University of Strathclyde, for his valuable guidance, suggestions, and encouragement throughout all phases of this research work. It is also a great honor and privilege for me to be supervised by him and to share his valuable knowledge and expertise.

I would like to pay my gratefulness to **Professor Hassan El-Gamal**, Department of Mechanical Engineering, Alexandria University, for his continuous supports and valuable suggestions during my research work. I am greatly indebted to him for his sincere support and technical assistance during the development of the numerical programs.

I also wish to express my profound gratitude to **Professor Nigel Baltrop, Professor Sandy Day** and **Mr. David Clelland** for their treasured and continuous help.

I am also deeply indebted to the friendly and helpful laboratory team; **Mr. Charles Keay, Mr. Bill McGuffie, Mr. Grant Dunning** and **Mr. Bill Wright** for the appreciated efforts during tank experiments.

I would like to thank the department administrative Staff, **Mrs. Carol Georges** and **Mrs. Fiona Cameron** for their professional services during my visits.

The financial support provided by the **Arab Academy for Science, Technology and Maritime Transport** to carry out this research work is gratefully acknowledged.

Finally and forever I am indebted to **my parents** for their support in all respects, **my wife** for her love, encouragement and patience, **Mr. & Mrs Mabrouk** and **Mrs. Thelma Will**, my family in Scotland.

Table of Contents

Abbreviations

CFD	Computational Fluid Dynamics
DOF	Degree of Freedom
EVD	Equivalent Viscous Damping
ODE	Ordinary Differential Equation
OWC	Oscillating Water Column
PTO	Power Take-Off
RANS	Reynolds Averaged Navier-Strokes
RM	Relative Motion (m)
VD	Viscous Damping
WEC	Wave Energy Converter

Nomenclature

A	Area (m^2)
$\mathbf{A_P}$	Projected area (m^2)
[B]	Damping matrix
BM	Metacentric radius (m)
$\mathbf{b_1}$	Damping coefficient of the structure
$\mathbf{b_2}$	Damping coefficient of the water column and the PTO mechanism
$\mathbf{b_{PTO}}$	Damping coefficient of the PTO mechanism
$\mathbf{b_s}$	Damping coefficient of the structure
$\mathbf{b_{wc}}$	Damping coefficient of the water column
$\mathbf{C_D}$	Hydrodynamic drag coefficient
$\mathbf{C_{Da}}$	drag coefficient
$\mathbf{C_F}$	Capture Factor
$\mathbf{C_H}$	Aerodynamic height coefficient
$\mathbf{C_M}$	Hydrodynamic inertia coefficient
$\mathbf{C_S}$	Aerodynamic shape coefficient
$\mathbf{C_W}$	Capture Width
d	Draught (m)

D	Diameter (m)
E	Elevation (m)
f	Frequency (Hz)
f_I	Incident wave force (N)
f_A	Diffraction wave force (N)
F_T	Total wave forces (N)
F_W	Wave/fluid induced force/moment vector
F_{1TY} cos (ωt)	Vertical wave force acting on the structure (N)
F_{2TY} cos (ωt)	Vertical wave force acting on the water column (N)
g	Gravitational acceleration (m/s^2)
GM_T & GM_L	Transverse and the longitudinal metacentric heights (m)
H	Section height (m)
H_{av}	Average wave height (m)
H_s	Significant wave height (m)
H_W	Wave height (m)
I'	Pitch actual inertia ($kg.m^2$)
I_a	Pitch added inertia ($kg.m^2$)
I_p	Pitch total inertia ($kg.m^2$)
j	Second moment of area (m^4)
K	Wave number
[K]	Restoring matrix
k_{air}	Stiffness due to air compression (N/m)
k_s	Hydrostatic stiffness of the water column (N/m)
k_{wc}	Hydrostatic stiffness of the water column (N/m)
k_1	Structure hydrostatic stiffness (N/m)
k_2	Stiffness due to air compression and hydrostatic effects of the water column (N/m)
KB	Distance from center of the under-water volume to keel (m)
KG	Distance from center of gravity to keel (m)
l	Total mooring line length (m)
l_S	Suspended (lifted) mooring line length (m)
L	Wave length (m)

[M]	Mass (inertia) matrix
M_a	Added mass (kg)
M_{ahm}	Added horizontal mass (kg)
M_{avm}	Added vertical mass (kg)
M_1	Total mass (mass and added mass) of the structure (kg)
M_2	Total mass (mass and added mass) of the water column (kg)
$\vec{n}$	Unit normal vector
p	Pressure (N/m^2)
P_{cap}	Power captured (W)
P_{max}	Maximum power captured (W)
Pre-T	Mooring line pre-tension (N)
P*	Dimensionless mean power capture
P'	Power per unit width of wave-front (W/m)
Q	Value of the amplitude ratio at resonance (Quality factor)
r	Radius of gyration
R_1 & R_2	Half-power points
S	Froude scaling factor
T	Wave or oscillation period (s)
T_a	Axial mooring line tension (N)
T_e	Energy period (s)
T_{ext}	External loading or the resultant tension (N)
T_H	Horizontal mooring line tension (N)
T_{HA}	Horizontal tension in mooring line A (N)
T_{HB}	Horizontal tension in mooring line B (N)
T_p	Average period between successive crests (s)
T_V	Vertical mooring line tension (N)
T_Z	Average period between successive zero up-crossing (s)
U	Wind velocity (m/s)
u, u̇, ü	Water particles displacement, velocity & acceleration (m, m/s, m/s^2)
V_0	Air volume inside the pneumatic chamber (m^3)
w	Mooring line submerged weight per unit length (N/m)
w_d	Water depth (m)

$\{\ddot{\mathbf{X}}\}, \{\dot{\mathbf{X}}\}, \{\mathbf{X}\}$	Acceleration, velocity and displacement vectors
$\mathbf{y_1}, \dot{\mathbf{y}}_1, \ddot{\mathbf{y}}_1$	Displacement, velocity, and acceleration of the structure (m, m/s, m/s^2)
$\mathbf{y_2}, \dot{\mathbf{y}}_2, \ddot{\mathbf{y}}_2$	Displacement, velocity, and acceleration of the water column (m, m/s, m/s^2)
$\mathbf{Z}$	Distance between the centre of gravity of the section and the centre of gravity of the whole structure (m)
$\boldsymbol{\gamma}$	Specific heat ratio for air
$\boldsymbol{\delta}$	Logarithmic decrement
$\boldsymbol{\theta}$	Solidity ratio
$\boldsymbol{\xi}$	Damping ratio
$\boldsymbol{\xi_t}$	Damping ratio (by Logarithmic decrement method)
$\boldsymbol{\xi_f}$	Damping ratio (by Half-power bandwidth method)
$\boldsymbol{\rho}$	Water density (kg/m^3)
$\boldsymbol{\rho_{air}}$	Air density (kg/m^3)
$\boldsymbol{\tau}$	Shielding factor
$\boldsymbol{\phi}$	Phase angle between waves and water column oscillations in captive OWC
$\boldsymbol{\phi_1}$	Phase angle between waves and structure heave in floating OWC
$\boldsymbol{\phi_2}$	Phase angle between waves and water column oscillations in floating OWC
$\boldsymbol{\varphi}$	Angle to the horizontal made by the line at the fairlead (deg.)
$\emptyset$	Wave (velocity) potential
$\emptyset_{\mathbf{I}}$	Incident wave potential
$\emptyset_{\mathbf{D}}$	Diffraction wave potential
$\emptyset_{\mathbf{S}}$	Scattered wave potential
$\emptyset_{\mathbf{R}}$	Radiated wave potential
$\boldsymbol{\omega}$	Angular frequency (rad/s)
$\boldsymbol{\omega_n}$	Angular natural frequency (rad/s)
$\boldsymbol{\omega_{R1}}$ & $\boldsymbol{\omega_{R2}}$	Half-power points frequencies (rad/s)
$\boldsymbol{\Delta_{st}}$	Static deflection
$\boldsymbol{\nabla}$	Under-water volume (m^3)

List of Figures

List of Tables

Chapter 1

Introduction

1.1. Background

The world population and their energy demands are increasing significantly throughout the past decades. The world depends on depleting fossil fuels to fulfil this increasing demand which leads to serious social, economic and environmental problems.

Eventually all fossil fuels resources will run out, if their use is not relieved by change of technology or lapse of demand due to other reasons. Moreover, during the past 20 years, about three-quarters of anthropogenic (human-caused) emissions came from the burning of fossil fuels for industrial processes, transportation and electricity production.

The Kyoto Protocol adopted on 11 December 1997 commit industrial countries to limit or reduce their emissions of four greenhouse gases (carbon dioxide, methane, nitrous oxide, sulphur hexafluoride) and two groups of gases (hydrofluorocarbons and perfluorocarbons). December 2012, the UN's 18th conference on climate change in Doha, Qatar, produced an agreement that would see the Kyoto Protocol continuing for a further seven years.

Renewable energies are required to provide the world with alternative energy sources in an economical and environmentally friendly fashion. The currents of energies passing continuously as renewable energies through the earth are shown in Fig.1.1 provided by (Twidell and Weir, 1986)

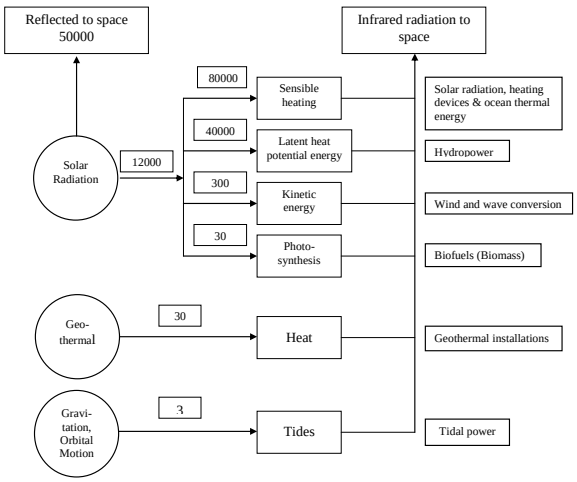

Fig.1.1. Currents of energies passing continuously as renewable energies through the earth, units terawatts

The above renewable energy sources have different advantages and disadvantages which may limit their use at a specific location besides other reasons. These advantages and disadvantages are presented in Table 1.1.

Table1.1: Advantages and disadvantages of renewable energies

Energy Type	Advantages	Disadvantages
Solar	Clean power source	Not available round the clock
	Inexhaustible power source	Solar panels are visually obstructive
	Free power source	Expensive to build
Wind	Clean power source	Not available round the clock
	Inexhaustible power source	Wind mills are visually obstructive
	Free power source	Expensive transmission of electricity
Geo Thermal	Clean power source	Not available in many locations
	Theoretically inexhaustible power source	Not much power per vent
	Free power source	Occasional escape of harmful gases & minerals
	Do not require structures like solar panels and wind mills	
Hydel	Clean power source	Requires high initial investment
	Water is free power source	Nearby areas are flooded
	Cost of hydro-electricity is very low	Availability of water depends upon rains
Bio Mass	Cheap source of energy	Not clean power source
	Theoretically inexhaustible power source	Requires ample space to grow bio mass crops
	Available throughout the world	Conversion into alcohol is expensive
	Easy to convert into high energy portable fuel such as alcohol or gas	
Tidal	Clean power source	Not available round the clock
	Inexhaustible power source	Only produce electricity during tidal surges
	Free power source	
	Tides are predictable	Construction of dams to capture tidal energy is expensive
	Generation of electricity is reliable	
Ocean Wave	Clean power source	Output from wave power plant is fluctuating but can be accommodated by using dump loads
	More consistent	
	Available round the clock	
	No visual obstruction	
	Higher power production owing to high density of water	
	Costs per net kilowatt are in the range of wind and below solar [6]	

1.2. Ocean wave energy

1.2.1. Wave energy resources

Wind generated waves are produced by the differential heating of the earth caused by the Sun. As solar energy is converted to wind energy, the time-averaged power flow is spatially concentrated, from an intensity of typically 0.1–0.3 kW/m2 horizontal surface of the earth to 0.5 kW/m2 envisaged area perpendicular to wind direction. As wind energy is converted to wave energy, even more spatial concentration takes place. Just below the ocean surface, average power flow intensity is typically 2–3kW/m2 of envisaged area perpendicular to direction of wave propagation. Therefore the wave energy intensity is the highest energy intensity among all other renewable energy sources and the estimated world-wide wave energy potential exceeds 1TW (Falnes, 2007). The faster the wind, the longer the wind blows, and the bigger the area over which the wind blows (fetch), the bigger the waves (Stewart, 2008). The process of wave generation from wind is illustrated in Fig.1.2.

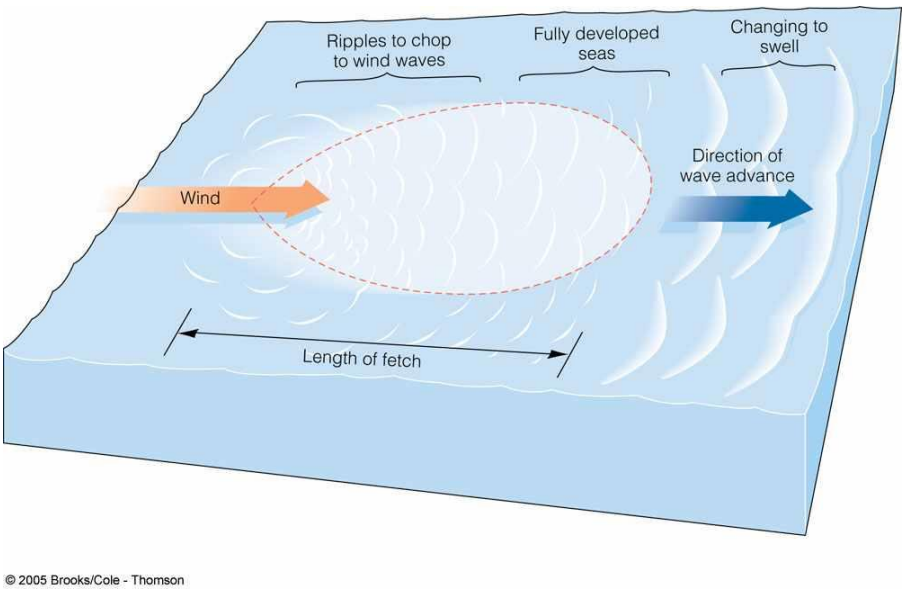

Fig.1.2. Wind generated wave process

Waves generated in deep water travel great distances with little loss in energy. In deep water it may be considered to travel along the surface with an approximate sinusoidal profile (Southgate, 1981). The power in Watts per unit meter of wave width is expressed as:

$$P' = \frac{\rho g^2 T H^2}{32\pi} \qquad \textbf{Eq.1.1}$$

One may note that the above formula is for regular waves. Real ocean wave are irregular and may be presented by linear theory as the superposition of wave of varying height, period and direction (Dunnett and Wallace, 2009). In order to present the irregularity, the sea condition for certain length of time can be considered constant and may be presented by a directional wave spectrum where the energy in the wave is distributed over the frequency range of ocean waves as it is presented in Fig.1.3 provided by Hals (2010)

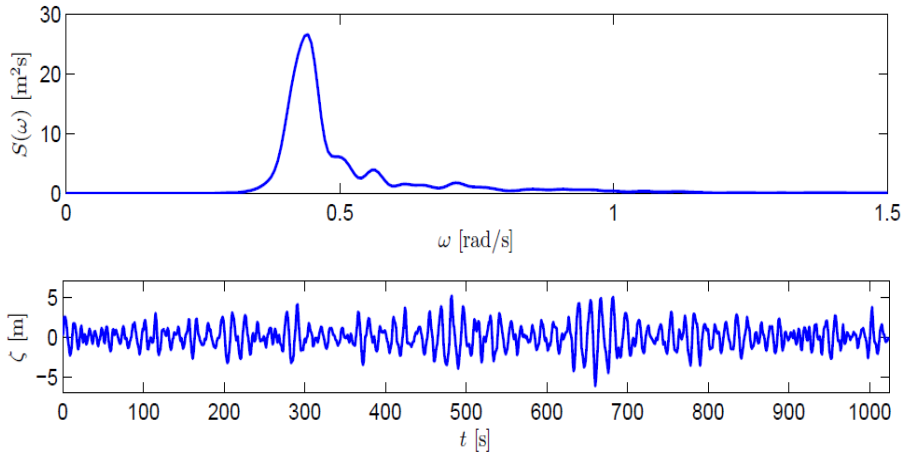

Fig.1.3. Pierson-Moskowitz wave spectrum for 20m/s wind speed

Various mathematical models have been proposed to represent the real sea spectra. (Sarpakaya and Isaacson, 1981) reported that the most commonly used spectra are JONSWAP, Bretschneider and Pierson-Moskowitz. In this case the power in Watts per unit meter of wave width is expressed in term of significant wave height in meters and energy period in seconds.

The power density spectrum is formulated as:

$$S(\omega) = \frac{\alpha g^2}{\omega^5} \exp[-\beta(\frac{g}{U\omega})^4] \qquad \textbf{Eq.1.2}$$

α = 8.1*10^{-3}, β = 0.74, g is the gravitational acceleration and U is the wind speed in m/s.

In order to find the significant wave height and energy period, the n^{th} spectral moment is used:

$$\boldsymbol{m_n = \int_0^\infty \omega^n s(\omega) d\omega} \qquad \textbf{Eq.1.3}$$

The significant wave height is obtained from the area under the spectrum m_0 as:

$$\boldsymbol{H_s = 4\sqrt{m_0}} \qquad \textbf{Eq.1.4}$$

And the average wave height as:

$$\boldsymbol{H_{av} = \sqrt{2m_0}} \qquad \textbf{Eq.1.5}$$

The observed average period in an irregular sea state:

$$\boldsymbol{T = 2\pi \frac{m_o}{m_1}} \qquad \textbf{Eq.1.6}$$

The average period between successive crests:

$$\boldsymbol{T_p = 2\pi \sqrt{\frac{m_2}{m_4}}} \qquad \textbf{Eq.1.7}$$

The average period between successive zero up-crossing:

$$\boldsymbol{T_z = 2\pi \sqrt{\frac{m_0}{m_2}}} \qquad \textbf{Eq.1.8}$$

Energy period:

$$\boldsymbol{T_e = 1.12\ T_z} \qquad \textbf{Eq.1.9}$$

Finally the power per unit width of wavefront in this case is:

$$\boldsymbol{P' = 0.5\ H_s^2 T_e} \qquad \textbf{Eq.1.10}$$

The constant (0.5) in the above equation depends on the spectrum used originally.

1.2.2. Wave energy conversion

Waves are considered as an ideal renewable energy source that can provide cleanly a high power density that is available most of the hours during a year (Mueller, 2002). The idea of generating electrical power from water waves has been realized for many years. Several reviews such as (Thorpe, 1999; Falnes and Budal, 1987, and Drew et al., 2009) marked that there are many configurations of WEC; over 1000 wave energy conversion techniques have been invented all over the world, only few devices have been tested at large scale, and deployed in the oceans.

(Vantorre et al, 2004) reported that a successful wave absorber for a specific sea condition should fulfil the following conditions: a) the frequency for which the converter is most receptive should coincide with the dominant component in the wave spectrum; b) it should be possible to adapt this frequency to variations of the sea state; c) the converter should be able to absorb the energy of other wave components with acceptable efficiency as well; d) if the performance of the absorber depends on the wave direction, these considerations are also valid for the directional distribution.

1.2.3. Classification of WEC

Previous studies categorised the WECs in many ways. In general, WECs may be categorized in term of:

- **Geometry and orientation: point absorbers, attenuators and terminators**

A point absorber is a device that possesses small dimensions relative to the incident wavelength. A heaving buoy and Oscillating Water Column are examples of point absorbers. Attenuators lie parallel to the predominant wave direction and ‘ride’ the waves. An example of an attenuator WEC is the Pelamis. Terminator devices have their principal axis parallel to the wave front (perpendicular to the predominant wave direction) and physically intercept waves like TAPCHAN device (Rhinefrank, 2006

and Leijon et al., 2006). Scale and orientation of different concepts are illustrated in Fig.1.4.

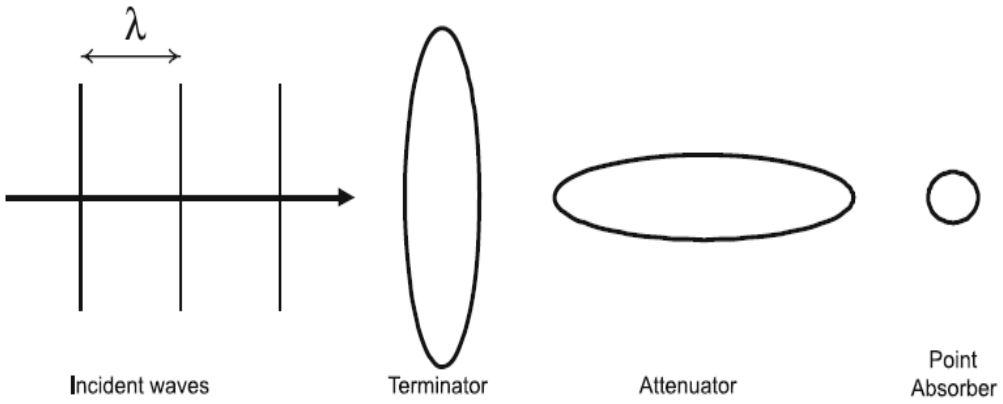

Fig.1.4. Schematic showing scale and orientation of a Terminator, Attenuator and Point-Absorber

- **Location: shoreline, near shore and offshore.**

Shoreline devices are fixed structures mounted on the coastline or wave-breakers. The initial, operational and maintenance costs are relatively low compared to near and offshore devices. They do not require deep-water moorings and long underwater electrical cables. Near shore devices are defined as devices that are in relatively shallow water. Shallow water depth varies between 10 and 20m at a distance of between 0.5 and 2.0km from the coastline or a depth of less than one-quarter wavelength. The annual average incident wave power is higher than shoreline and environmental impacts are decreased. Offshore devices are generally in deep water. Deep water may be defined as tens of meters water depth, water depth greater than 40 meters, and depth exceeding one-third of the wave length. Deep water device are subjected to higher annual average incident wave power, severe weather conditions and minimal topographic constrains (Drew et al., 2009; Folley et al., 2007, Ringwood, 2006).

- **Mode of motion for energy absorption: Pitch, heave and surge**

WEC may be classified according to the motion in which the wave energy is absorbed (Fig.1.5). Wave pitching, heaving and/or surging forces cause relative motion between the absorber and the reactor to drive a PTO mechanism.

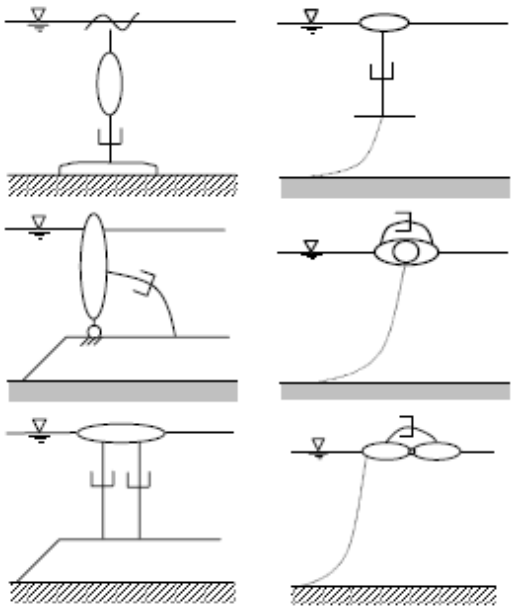

Fig.1.5. Classification of WEC according to mode of motion (Boyle, 2004)

- **Power take off mechanism: pneumatic, hydraulic, mechanical and directly electrical**

Several PTO mechanisms have been proposed for wave energy converters (Falnes, 2007). According to the configuration of the WEC the suitable PTO is selected. It may be pneumatic as in case of OWC. Hydraulic PTO is used in other cases as in Pelamis. Sometimes the PTO is directly electrical, example of such system is a point absorber (floating buoy) connected to a linear generator (sided piston equipped with permanent magnets) at the seabed by a tether. The generator piston is driven by the motion of the buoy and counteracted by a spring.

- **Wave-structure interaction: active and passive devices**

Active devices are devices where the interface element responds to the wave action and produces the mechanical work, while passive devices remain stationary and the

water movement relative to the structure is made to work. The first category includes different types of floating bodies; the second one includes constructions fixed rigidly to the sea bottom or shore (Vantorre, 2004).

- **Mooring: motion-independent and motion-dependent devices**

Johanning et al., (2006) defined a motion-independent device as the device in which the mooring acted in a conventional manner to keep the device on station (an example would be a floating oscillating water column). In this case, the needs of the mooring would be similar to that for a conventional oil and gas floating installation. In particular, the resonant period of the mooring would be designed to fall outside the range of wave forcing periods. Motion-dependent device are devices in which the dynamics of the device and its primary modes of energy extraction requires the application of an interactive mooring system. The mooring must be designed such that the resonant period of the device and mooring system should match the wave periodicity as far as is practicable.

1.2.4. Most common WEC

- **Pelamis**

The Pelamis presented in Fig.1.6 is a semi-submerged, articulated structure composed of cylindrical sections linked by hinged joints and is held on station by a compliant mooring system that allows the machine to weathervane to align itself head-on to incoming waves (it takes its 'reference' from spanning successive wave crests). As waves travel down the length of the machine they cause the structure to articulate around the joints. The induced motion of these joints is resisted by hydraulic rams that pump high-pressure oil through hydraulic motors via smoothing accumulators. The hydraulic motors drive electrical generators to produce electricity. Power from all the joints is fed down a single umbilical cable to a junction on the seabed. A number of devices can be connected together and linked to shore through a single seabed cable (Primer, 2007).

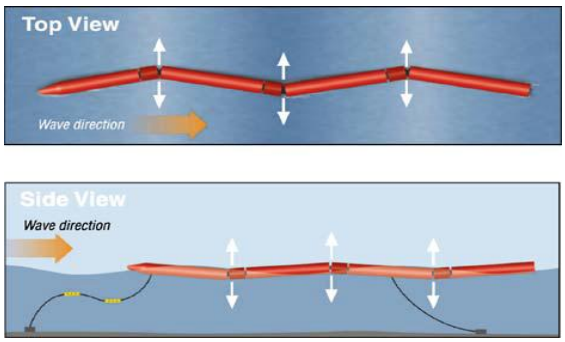

Fig.1.6. Pelamis WEC

- **Wave Dragon and TAPCHAN**

Wave Dragon is one of the foremost technologies within the field of wave power (Fig.1.7). Unlike most other devices it does not oscillate with the waves; it gathers the wave energy passively by utilising the overtopping principle. The front face of the device is a curved ramp, oncoming waves surge up it, as if it were a beach. Behind the crest of this ramp lies a reservoir which gathers the water "overtopping" the ramp which now has higher potential energy than the surrounding water. The effect of Wave Dragon is amplified by long reflector wings. Mounted to the reservoir, they channel the waves towards the ramp. The energy is extracted as the water drains back to the sea through low head hydro turbines within the reservoir. Wave Dragon operation is quite similar to the TAPCHAN. Instead of the dragon reflector, TAPCHAN comprises a gradually narrowing channel with wall heights typically 3 to 5 meters above mean water level that guides the water to the floating reservoir.

Tello Ruiz, 2010 reported that the advantage of such overtopping device is that turbine technology has already been in use in the hydropower industry for long time and is well understood (Powertech, 2009). However, the disadvantage is the strongly non-linear hydrodynamics of overtopping devices and therefore the hydrodynamic problem of the overtopping principle cannot be addressed by linear water wave theory (Falcão, 2010).

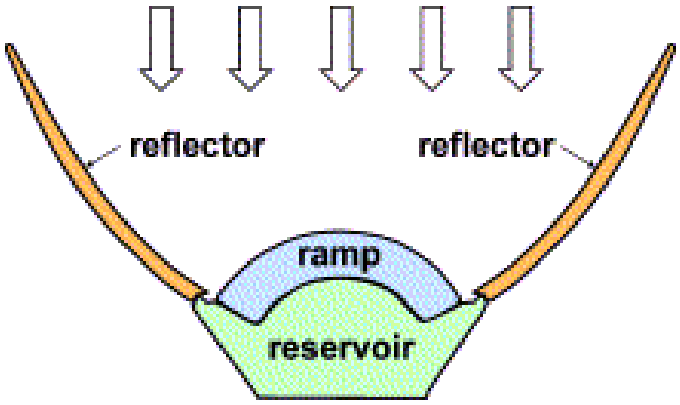

Fig.1.7. Wave Dragon WEC

- **Archimedes Wave Swing**

The AWS consists of an air filled chamber fixed to the seabed and open at the top (the silo), closed by another cylinder (the floater). An air lock is created between the two cylinders and so water cannot flood the silo. The floater can move up (or down), due to the pressure increase (decrease) linked with the incoming wave crest (trough) directly above the device as shown in Fig.1.8. By adding a PTO system this oscillation can be converted into electrical power. In the case of the AWS, the PTO is a permanent-magnet linear generator.

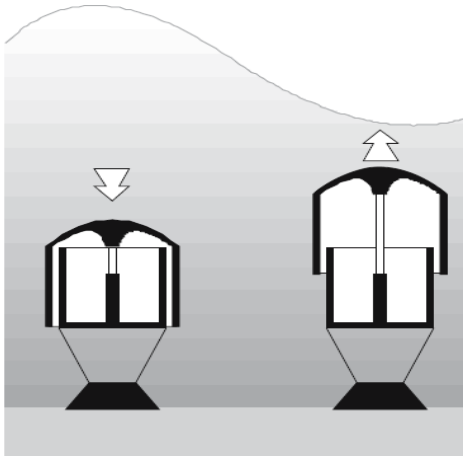

Fig.1.8. Archimedes Wave Swing WEC

- **Oscillating Water Column**

A shoreline OWC is formed by a chamber which is filled with air above the water line. Driven by wave action, the water level inside the chamber rises and falls,

alternately pressurising and rarefying the air within the chamber. As the water level inside the chamber rises, and pressurised air escapes from the chamber through a turbine-generator unit producing electrical power. As the water level in the chamber falls air is drawn back into the chamber through the turbine-generator assembly to continue power production. Wells turbines are self-rectifying so that the direction of turbine rotation remains constant throughout the power cycle.

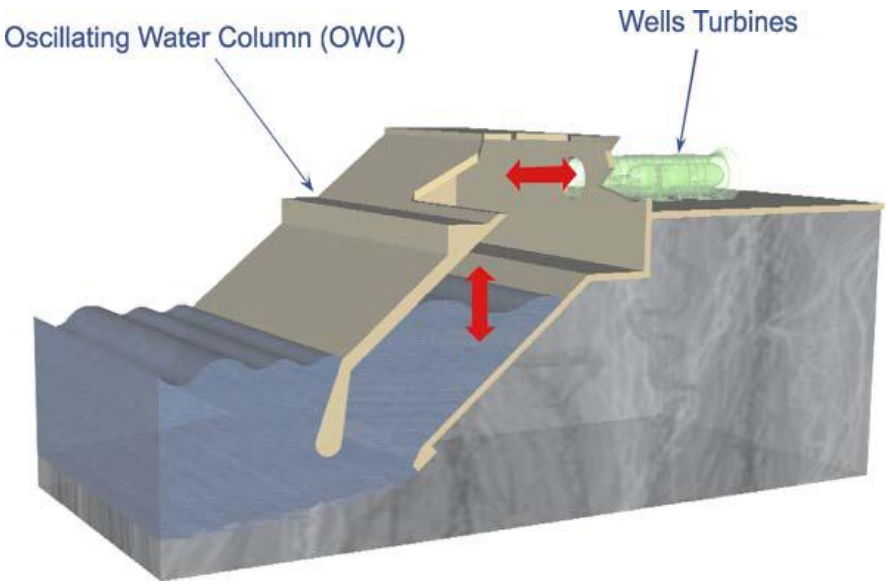

Fig.1.9. Shoreline OWC WEC

- **Sloped-Buoy OWC**

The sloped buoy (Fig.1.10) is a floating buoy with three parallel, immersed tail tubes that float at an angle of some 45 degrees to the vertical. The length of the tail tubes constrains the buoy to move in the direction of the sloped tubes. The tail tubes, which are open to the sea at the bottom end contain a mass of sea water against which a moving buoy can react, utilising the energy in both surge and heave motions (DTI, 2006).

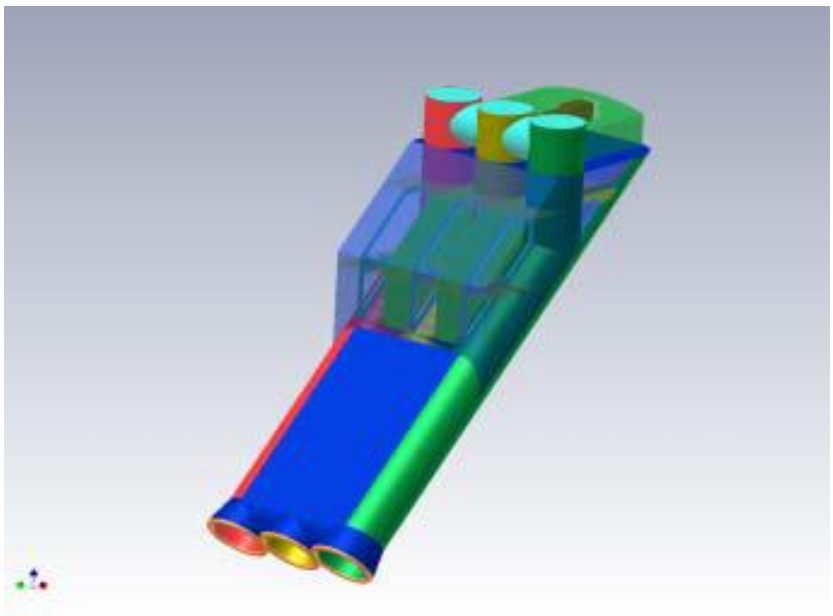

Fig.1.10. Sloped-Buoy OWC WEC

- **Backward Bent Duct Buoy (BBDB) OWC**

The BBDB (Fig.1.11) has a horizontal tail tube that uses the surge and pitch motion of the buoy to create relative movement between the device and its constrained water columns (DTI, 2006).

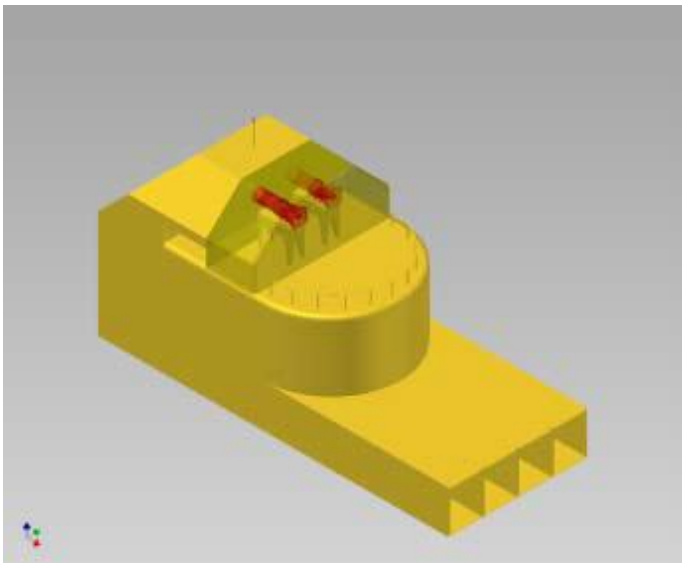

Fig.1.11. Backward Bent Duct Buoy OWC WEC

- **Spar-Buoy OWC**

Spar technology has been utilized for offshore structures such as research vessels, communication relay stations, and storage and offloading platforms. Recently its application has extended to the deep draft cylindrical spar for deep-water production. The shape of spar platforms is usually a long hollow cylinder with a large diameter. It is normally moored by means of conventional spread chains. In general spar is an attractive design solution for regions where the environment is harsh (Rho & Choi, 2002).

The Spar Buoy (Fig.1.12) is possibly the simplest concept for a floating OWC. It is an axisymmetric device (and so insensitive to wave direction) consisting basically of a submerged vertical tube open at both ends, fixed to a floater.

The buoy has a predominant heave motion and generates pneumatic power through the relative motion between the water column in the vertical draught tube and the buoy's whole body motion, which is designed to be out of phase with the water column motion.

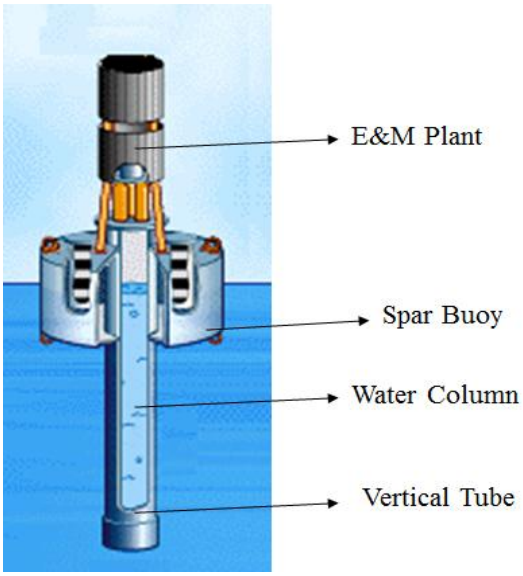

Fig.1.12. Spar-Buoy OWC WEC

Each type of buoy was tested in Wavegen's wave tank. The Spar-Buoy has the advantage of being symmetrical and equally efficient at capturing energy from all directions. Both the Sloped Buoy and BBDB are particularly efficient in one

direction but their efficiency falls off when waves approach them from an angle to the normal operating direction.

A report prepared for the British Department of Trade and Industry compared the three types of floating OWCs for electricity generation in an Atlantic environment: and considered the Spar Buoy to be the lowest risk and most economic option for further development.

1.2.5. Evaluation of WEC

There has been considerable debate about evaluating the performance of WEC. (Caska and Finnigan, 2008; Retzler et al., 2008) quoted that a generally applicable measure of performance, known as the capture width C_W, it represents the equivalent width of incident wave power that is completely absorbed by the device and converted to mechanical power. In other words C_W at a given frequency is defined to be the ratio of the total mean power absorbed by the body to the mean power per unit crest wave width of the incident wave train, where mean refers to the average value per wave period for regular waves or per energy period for irregular waves

Capture width has the unit of meter and may be divided by the device diameter D to develop further comparative measure known as Capture Width Ratio (CWR) or Capture Factor (C_F). Capture factor is a good measure for comparing the performance of devices of same configuration (type) as it is defined in relation to the width of the structure.

The overall efficiency of wave power plant from wave to wire includes the capture factor (efficiency) of the WEC, the efficiency of the PTO mechanism and the efficiency of the power chain (generator, transmission lines, etc.) (Thorpe, 1999).

1.2.6. Environmental impacts of WEC

One of the main driving forces behind the development of wave energy (and other renewables) is their environmental benefits compared to conventional generation. However, no energy producing technology is without environmental impacts. (Iglesias et al, 2009) mentioned that wave energy has a significant advantage over other renewable energy sources with respect to its environmental impact.

WEC produce no gaseous, liquid or solid emissions and hence, in normal operation, wave energy is virtually a non-polluting source. However, the deployment of wave power schemes could have a varied impact on the environment. Some of these effects may be beneficial and some potentially adverse. Therefore environmental impacts should be assessed considering the construction, operation and decommissioning phases of the plant. Many of the potential impacts would be site specific as it is shown in Table 1.2 provided by (Thorpe, 1999) and impacts will be greatly reduced for floating devices and increased for shore-based devices.

Table 1.2: Environmental impact of wave energy converters (Thorpe, 1999)

Environmental Effect	Shoreline	Near-shore	Offshore
Land use / sterilization	Low	------	------
Construction / maintenance sites	Low	------	------
Coastal erosion	Low	Low-Medium	Low-Medium
Recreation	Low	Low	------
Sedimentary flow patterns	------	Low	Low
Navigation hazards	------	Low	Low
Fish and marine biota	Low	Low	Low
Acoustic noise	Low	------	------
Working fluid losses	------	Low	Low
Endangered species	Low	Low	------
Device/mooring damage	------	Low-Medium	Low-Medium

1.2.7. Economics of WEC

The conventional way of describing the size of an electricity generation power plant is in term of the rated or maximum power. For a wave power plant, the rated power can only be generated at times of maximum wave height. The average power is considerably less that the rated power and it turns out that for wave power plants the average power is typically between 30 and 40% of the rated power. It could be useful in this case using the capacity factor which is defined as the actual yearly electrical energy output of a generation plant divided by the electrical energy produced if the plant was operated at rated power continuously during the entire year (Hagerman, 1992 and Primer, 2007).

The relative costs distribution of a wave power plant is varying according to the type and location of the WEC. In general, initial (capital) cost consists of four major cost centres for any wave power scheme:

- Device structure
- Mechanical and electrical plant
- Electrical transmission
- Transportation and installation.

The factors which make up the annual running cost of wave power plant governing the cost of electricity are:

- Annual sum involved in repayment of the capital cost
- Annual Operational & Maintenance (O&M) costs
- Annual insurance

The annual sum involved in repayment of the capital cost of a wave power scheme can be assessed in a number of ways. The common approach adopted by (Thorpe, 1999), namely amortisation of the capital costs over the complete lifetime of the scheme using various discount rates.

Good maintenance procedures are essential to ensure successfully performance with high availability. However, in addition to the planned maintenance there will be other, unscheduled outages due to component failure. Therefore, any estimation of annual O&M costs has to include:

- Cost of Spares
- Cost of repair
- Operational cost

Costs of Spares are the costs associated with providing spares to replace faulty equipment. Adequate supply of replacement parts should be ensured for minimal downtime. Repair Costs are the cost of repairing the faulty replaced equipment to be used as spares in the future. This would entail an additional repair cost. Operational Costs are the costs associated with providing maintenance crews and vessels to enable repairs (manpower costs, vessel hire rates etc.). The availability assessment provides an estimation of the number and types of repair crews required to provide the level of availability for each device.

However, the cost of electricity from the existing designs of wave energy devices is unlikely to be economically competitive in the short to medium term. From an economical point of view, the large waves dictate the costs while the small and medium waves give the incomes. If a wave energy converter is to survive the peak powers in the ocean, it must have large safety margins. This usually raises the total costs of the system without giving a corresponding increase of the income. One way of reducing this problem is to place the WEC in areas of moderated or lower environment sensibility. Another idea promoted by Budal and Falnes is constructing wave power plants consisting of many relatively small WECs, in contrast to large-scale converters reaching several megawatts (Vantorre, 2004). Methodology for Economic Appraisal to determine the cost of electricity proposed by Thorpe, 1999, is illustrated in Fig.1.13.

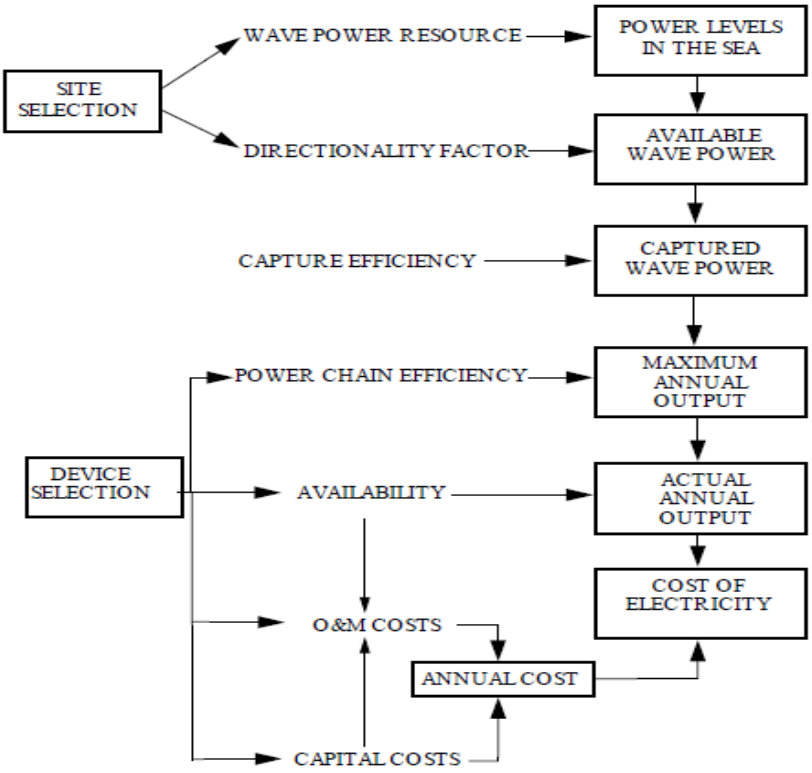

Fig.1.13. Methodology for Economic Appraisal

1.2.8. Wave energy challenges

Many challenges are facing the wave energy development (Twidell and Weir, 1986; Boyle, 2004) highlighted some of these challenges. Wave patterns are irregular in amplitude, phase, and direction. It is difficult do design devices to extract power efficiently over the wide range of variables even if they can be predicted. Wave periods are commonly 5 to 10 seconds (frequency 0.1 Hz). It is extremely difficult to couple this irregular slow motion to electrical generators requiring 500 times greater frequency (50 Hz). There is always a probability of extreme gales or hurricanes (storm) producing waves of freak intensity. The structure of the power device must be able to withstand this, which will increase the device cost and reduce normal efficiency of power extraction. Peak power is generally available in deep water waves from open sea swells where difficulties of constructing, maintaining and fixing or mooring the WEC in position, and of transmitting power to land, are major.

So many types of device may be suggested for wave power extraction that the task of selecting a particular method is made complicated and somewhat random.

1.3. Research objectives

The main objective of this research is to develop experimentally validated numerical wave power prediction tool for offshore SparBuoy OWC WEC.

From the literature review presented in Chapter 2, several researchers used mechanical oscillatory systems to model OWCs. Obviously, mechanical modelling of OWC provides simple and efficient modelling tool and provides easy test for the phase and amplitude conditions. Most of the researchers considered one or two translational modes of motion in heave direction and disregarded the mooring system. Others assumed linear PTO damping and linear air compressibility stiffness or did not consider them in the modelling.

The numerical tool to be developed in this research should be able to:

- Model the environment,
- Predict the WEC structure motions,
- Consider the mooring system employed,
- Predict the water column oscillations inside the structure,
- Estimate the pneumatic power absorber,
- Evaluate the device performance,

In order to perform this task minor objectives were targeted:

- Acquire an understanding of the water column oscillations in captive and floating OWCs.
- Model the OWC (structure/water column system) mathematically.
- Analytically and/or numerically solve the mathematical (dynamic) models
- Develop reduced scale models

- Experimentally test the reduced scale models to measure the damping and to validate the mathematical model

Such tasks require an understanding of:

- Linear wave theory
- Hydrodynamics of OWC
- Vibrational (structure) analysis
- Dynamic modelling procedures
- Numerical tool (Matlab)
- Finite element package (OrcaFlex)
- Tank experiments
- Experimental data analysis software (Spike)

1.4. Thesis plan

Chapter 2 presents an overview on the models used to describe the OWC. This is in addition to the hydrodynamics and the optimal operation conditions of OWCs. Finally a critical review on recent researches in this area is included.

In **Chapter 3** the loading on offshore structures due to waves and wind will be discussed. Wave forces are examined in diffraction and inertia regimes using velocity potential and Morison approaches. Wind forces calculations are provided by American Petroleum Institute (A.P.I.) and American Bureau of Shipping (A.B.S.).

SparBuoy motion response prediction, considering oscillating rigid-body theory, will be presented in **Chapter 4,** followed by methodologies used to determine mass, damping and stiffness matrix.

Single and multi-catenary mooring lines analysis suitable for wave energy converters will be highlighted in **Chapter 5**. Determination of load excursion and reaction curves will be explained and presented in addition to static and quasi-static

modelling of surge motion. A 2D multi-static mooring modelling using computational fluid dynamic (CFD) package will be presented in this chapter as well.

Furthermore, **Chapter 6** provides one dynamic model used to model captive OWCs and two dynamic models for the floating ones. Linear power take-off damping and stiffness due to air compressibility inside the pneumatic chamber will be taken into account. In addition, the analytical and numerical solution of the proposed mathematical models will be provided, as well as an overview of the numerical tool and procedures. Later on, approaches adopted to obtain better agreement with the measured results will be presented.

Nonlinearity due to large waves will be investigated in **Chapter 7**. Linearized model based on classical perturbation theory in frequency domain and nonlinear model where wave force is calculated in time domain will be proposed. Later on, nonlinearity due to damping forces will be considered. First, iterative procedure will be used to optimise the linear and quadratic damping coefficients in frequency domain. Finally, another model will be proposed where viscous forces will be calculated in time domain by taking into consideration the instant water column oscillation amplitude.

Finally the nonlinear effects due to air compressibility inside the OWC chamber has been studied by a time domain model which include the water column oscillations amplitudes.

Chapter 8 presents innovative idea for hybrid renewable energy converting platform.

The experimental work performed to validate the mathematical models is shown in **Chapter 9**. The wave tank, reduced model and measuring devices are illustrated and defined in addition to the experimental aims and procedures.

The conclusions of the research and the contributions to the research field achieved are presented in **Chapter 10** along with recommendations for further work.

1.5. Results and discussions

Graphical representation of Pierson-Moskowitz spectrum which represents the distribution of wave energy as a function of frequency is illustrated in Fig.1.14 using Eq.1.2.

The seasonal weather data (seasonal mean wind speed) used are referred to Meteorology, Synoptic Charts & Weather Routing course provided by The Arab Academy for Science, Technology, and Maritime Transport (AASTMT), for a region on the Mediterranean Sea called Sidi-Barrani, Egypt within 32-31˚N latitudes and 25-27˚W longitudes.

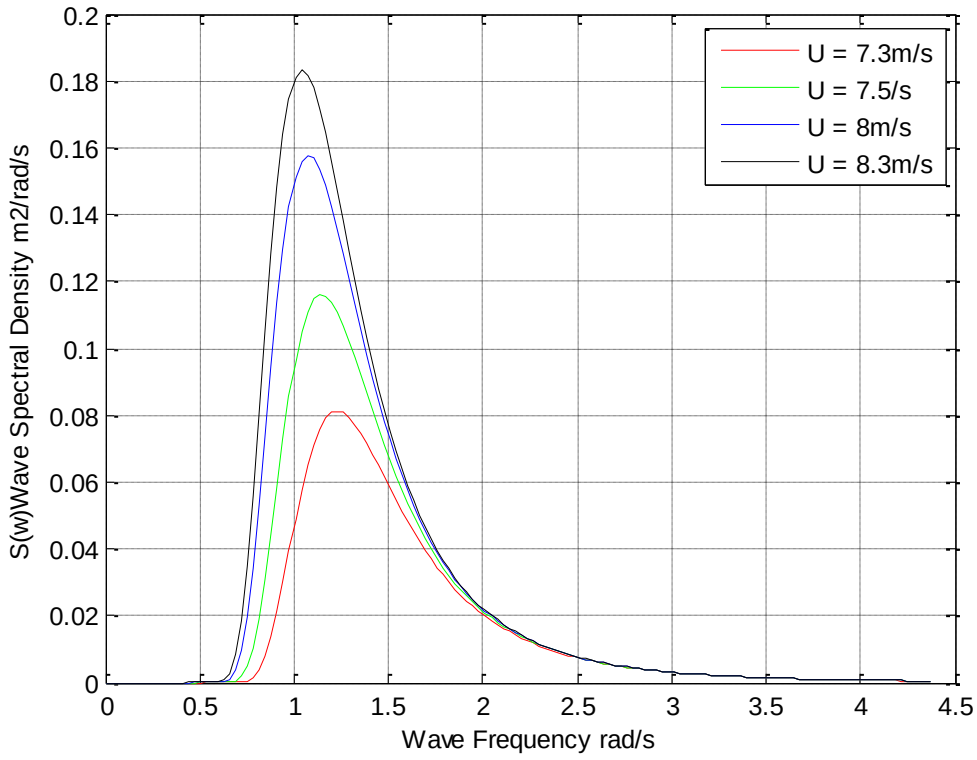

Fig.1.14. Pierson-Moskowitz spectrum for seasonal wind speeds at Sidi-Barrani, Egypt (32-31˚N latitudes and 25-27˚W longitudes).

Table 1.3 presents results obtained from Eq.1.3 to Eq.1.10 used to calculate significant wave height Hs, peak period Tp, zero up-crossing period Tz, energy period and the power per unit width of wavefront P' according to different wind speeds U during each season.

Table 1.3: U, Hs, Tp, Tz, Te and P' for the 4 seasons at Sidi-Barrani, Egypt

	U (m/s)	**Hs (m)**	**Tp (s)**	**Tz (s)**	**Te (s)**	**P'(kW/m)**
Spring	8.27	1.4587	1.48315	4.2924	4.8075	5.1147
Summer	7.55	1.2158	1.3555	3.9193	4.3896	3.2443
Autumn	7.03	1.0541	1.2687	3.6488	4.0867	2.2704
Winter	8.0275	1.3744	1.4354	4.1667	4.6667	4.4076

References of Chapter 1

Boyle G, **Renewable energy**, 2nd edition, 2004, Oxford University Press, Oxford, UK.

Caska A.J., Finnigan T.D., 2008, 'Hydrodynamic characteristics of a cylindrical bottom-pivoted wave energy absorber', Ocean Engineering Vol. 35 pp 6–16

DTI, 2006, 'Near shore floating oscillating wave column: Prototype development and evaluation', A report for The UK Department of Trade and Industry, Contract number: V/06/00201/00/00, URN number: 05/581

Drew B, Plummer A R, and Sahinkaya MN, 2009, 'A review of wave energy converter technology', In Proceeding of IMechE Part A: J. Power and Energy, Vol. 223 pp 887 - 902

David Dunnett, and James S. Wallace, 2010, 'Electricity generation from wave power in Canada' Renewable Energy Vol. 34 pp 179–195

Falcão, A.F.O., 2010, "Wave Energy Utilization: A Review of the Technologies", Renewable and Sustainable Energy Reviews, Vol. 14 pp 899–918.

Falnes J, Budal K., 1978, "Wave-power conversion by point absorbers," Norwegian Maritime Res Vol. 6(4) pp2–11

Folley M., Whittaker T.J.T., Henry A., 2007, 'The effect of water depth on the performance of a small surging wave energy converter', Ocean Engineering, Vol. 34, pp 1265–1274

Hagerman G. Wave energy resource and economic assessment for the state of hawaii. Technical report, SEASUN Power Systems, 1992

Iglesias G., Lo´ pez M., Carballo R., A. Castro, J.A. Fraguela, P. Frigaard, 2009, 'Wave energy potential in Galicia (NW Spain)', Renewable Energy, pp 1–11

Johanning L., Smith G H, and Wolfram J., 2006, 'Mooring design approach for wave energy converters', Proc. IMechE Vol. 220 Part M: J. Engineering for the Maritime Environment

Leijon M., Danielsson O., Eriksson M., Thorburn K., Bernhoff H., Isberg J., Sundberg J., Ivanova I., Sjo¨stedt E., Agren O., Karlsson K.E., & Wolfbrandt A., 2006, 'An electrical approach to wave energy conversion', Renewable Energy Vol. 31 pp 1309–1319.

Mueller MA., 2002, "Electrical generators for direct drive wave energy converters," Gen Transm Distrib IEE Proc 149(4) pp 446–56.

Primer: Power from Ocean Waves and Tides, Electric Power Research Institute, Report 1015267, June 2007, California, USA.

Powertech Labs Inc., 2009, "Ocean Energy: Global Technology Development Status", IEA-OES Document No.: T0104.

Retzler, C., Pizer, D., Henderson, R., Ahlqvist, J., Cowieson, F., Shaw, M., 2003, 'Pelamis WEC –Advances in the numerical and experimental modelling program', In: Fifth European Wave Energy Conference, Cork, Ireland.

Rhinefrank K, Agamloh EB, von Jouanne A, Wallace AK, Prudell J, Kimble K, 2006, 'A novel ocean energy permanent magnet linear generator buoy'. Renewable Energy Vol. 31(9) pp 1279–98.

Rho Jun B., and Choi Hang S., 2002, 'Heave and Pitch Motions of a Spar Platform with Damping Plate', In Proceedings of the 12th International Offshore and Polar Engineering Conference Kitakyushu, Japan

Ringwood John, 2006, "The dynamics of wave energy," Irish Signal and Systems Conference, June 28-30, Dublin, Ireland

Sarpkaya T., Isaacson. M., 1981, **Mechanics of Wave Forces on Offshore Structures**, Van Nostran Reinhold Company, New York

Southgate H.N., 1981, Ray Methods for Combined Refraction and Diffraction Problems, Report Number IT 214, Hydraulics Research, Wallingford, Oxon. UK.

Stewart Robert H. 2008, **Introduction to Physical Oceanography**, Department of Oceanography Texas A & M University.

Thorpe T.W., 1999, 'A Brief Review of Wave Energy', ETSU Report Number R-120 for the DTI

Tello Ruiz Manases, 2010, 'Dynamics and hydrodynamics for floating wave energy converters', M.Sc. thesis, Universidade Tecnica de Lisbone.

Twidell John W. and Weir Anthony D., 1986, **Renewable energy resources**, E&FN Spon, London, UK

Vantorre M., Banasiak R., Verhoeven R., 2004, "Modeling of hydraulic performance and wave energy extraction by a point absorber in heave," Applied Ocean Research Vol. 26 pp 61–72

Chapter 2

Critical Review

2.1. Introduction

The oscillating water column wave energy converter equipped with air turbine has been studied, possibly more than any other type of wave energy device.

A conventional OWC-WEC has a three-stage energy conversion process, wave-to-pneumatic power conversion inside the OWC chamber, then pneumatic-to-mechanical power conversion through the PTO mechanism (turbine), and finally mechanical-to-electrical power conversion using electrical generators coupled with the turbine.

Gomes et al., 2012 reported that shoreline full-scale prototypes were built in the 1980s and 1990s. These were the cases of the Kværner multi-resonant OWC, in Norway, the Pico plant in Azores, Portugal and the LIMPET in Islay, Scotland. The Pico and LIMPET plants are still operational. Those particular devices have proved the principle of operation and the extraction of energy under real sea conditions.

More recently, floating OWC devices have been studied and developed, namely the OE Buoy, the Orecon and the Oceanlinx Mk3. A 1/4th scale model of the OE Buoy device has been tested in the Galway Bay, Ireland since 2006. The Oceanlinx Mk3 prototype was tested at an offshore location in 2010.

The principle of operation of a floating OWC is similar to that of a fixed one. The main difference is that the structure oscillates, which consequently leads to radiation

of waves. In this case, the relative motion between the device and the internal free surface provides the air flow. From oscillating body theory it is known that a system with two bodies is supposed to have two resonance peaks, due to the dynamics of each body. If the system is tuned to have those peaks placed close to the dominant wave frequency, it is possible to widen the range of frequencies within which the system performs well. This is one of the main advantages of floating OWC devices Gomes et al. (2012).

2.2. Modelling of OWC

The pioneering work on the mathematical modelling of WECs assumed that the waves were of small amplitude, relative to both the wavelength and the water depth, and of permanent regular form, which are the basic hypotheses of linear wave theory Cruz (2008).

From performance perspective adoption of linear wave theory is valid, since linear waves may be assumed for most of the WEC operating times. However, from the survivability perspective linear wave theory may not be suitable for such modelling application.

Considering the linear wave theory has been generally successful in predicting the hydrodynamics and performance of a wide range of marine structures. In modelling, it provides many benefits. Folley & Whittaker (2009) reported that, linear wave theory allows exact solutions to be produced with relative ease for both monochromatic and mixed seas. It allows the system dynamics to be represented in the frequency domain, using linear superposition and Fourier analysis. The efficacy and simplicity of linear wave theory has meant that few other procedures have been used in the design of wave energy converters.

OWC-WEC can be described by mathematical models equivalent to each energy conversion process in the power chain, and therefore the overall efficiency of the OWC WEC depends on the individual efficiencies of these processes.

The performance of OWC may be evaluated stochastically or through frequency or time domain approach. Stochastic and frequency domain analysis allow a prompt evaluation of the device dynamics. For a more detailed analysis, in which, the forces imposed by the PTO and the anchoring system are strongly non-linear, a time domain approach is required, as stated by Alves, Costa et al. (2010). From readings, one may conclude that frequency domain modelling is usually adopted in studies concerned about design and especially for geometry optimization, while time domain approach is implemented for operation control models.

A theoretical model of the hydrodynamics of a fixed OWC device was developed by Evans (1978) by considering the internal free surface as a rigid weightless piston which allowed the application of rigid (oscillating) body theory.

In this approach fixed OWC modelling process is best described by considering a single translational mode in heave direction. For offshore OWC the dynamic coupling of the water column and the floating structure is very important to achieve the desired efficiency and therefore the system is described by considering two translational modes in heave direction (two DOF model). Advanced modelling requires the prediction of the amplitudes of the six DOF motion of the structure, to select the optimum mooring configuration and to know if modes such as surge or sway may store energy enough to significantly alter the system.

Another approach helps in accounting of the deformation of the internal free surface through the application of an oscillating surface-pressure distribution condition. In this way, the behaviour of these devices is modelled with better accuracy, essentially when the chamber dimensions are not small compared to the wavelength. The application of this approach to particular OWC geometries was performed using boundary element methods.

2.3. Power absorbed and optimal operation conditions

The power absorbed by OWC WEC may be defined according to the pressure distribution theory as the product of the net volume flux of the interior water surface and the air pressure in the chamber above the OWC. For mechanical modelling the power absorbed is defined as the product of the net wave force acting on the interior water surface and the vertical velocity of this surface. Detailed mathematical representation of the power absorbed by an oscillating body WEC is provided by many authors including Brendmo, Falnes et al. (1996) and Falnes (2002). Conditions for maximum (optimum) power absorption have to be considered in plant design and operation for efficient energy conversion process. Many publications including Hals (2010) highlighted the optimum phase and amplitude conditions for optimum power absorption from point absorber WEC and their control strategies.

The optimum phase condition is satisfied when the velocity of the water surface in the chamber is in phase with the excitation force, and it corresponds to the situation when the system is in resonance.

The optimum amplitude condition when the velocity amplitude of the internal water surface is 90° out of phase with the excursion amplitude. Thus, at the optimum, the elevation in the OWC chamber is lagging the incident wave by a quarter of a period. Furthermore, to satisfy the amplitude condition, the oscillation amplitude must be adjusted such that the radiated power equals half the excitation power which occurs when the chamber is open Brendmo, Falnes et al. (1996).

For floating OWC where heave motions are modelled as two DOF, if the water column and the structure are moving in phase the absorbed power is very low, separation of the natural frequencies results in significant increases in maximum power capture Stappenbelt & Cooper (2009).

2.4. Review of recent research investigations

Recent published researches related to the current research area will be highlighted in this section. Most of the modelling studies focused either on evaluating or improving the performance of floating OWC by implementing control strategies or optimization models. Time and frequency domain models using analytical, numerical and Computational Fluid Dynamics (CFD) approaches will be discussed.

Sykes et al. (2009) provided a preliminary assessment of the validity of employing a boundary element method code to predict the displacement and associated hydrodynamic properties of a simple floating un-damped OWC in the form of a hollow vertical circular cylinder. Predictions obtained from the WAMIT code are compared with experimental measurements at selected frequencies and with increasing wave amplitude. In their paper reasonable agreement between the predicted and measured motions of the device appeared while poorer agreement between the measured and predicted pressures for the moving cylinder appeared.

Stappenbelt & Cooper (2009) studied the OWC WEC performance including analysis of the dynamic coupling of the water column and the floating structure. They presented a two DOF mechanical oscillator model in order to examine this relationship for the heave motion. The basis of the heave motion model adopted in their research was the fixed OWC model proposed by Szumko (1989) and more recently adopted by Folley & Whittaker (2005) where the PTO damping is modelled by linear damper and the air compressibility by linear stiffness. They also assumed that wave forces on the water column, and the floating structure, are to be related via a complex parameter allowing for both a magnitude and phase difference between the forces. Following Froude-Krylov approximation it may be shown that this parameter is real. In the limit of large wavelength, or small wave number, this parameter can also be shown to be equivalent to the area ratio of the OWC opening to the total base area of the floating wave energy converter.

Their results showed the importance of separating the OWC and structure natural frequencies. The optimal damping at resonance approaches the radiation value, but is

also strongly influenced by other system parameters. Air compressibility appears to have little influence on the dynamic response and power capture of a typical floating OWC. In order to validate their results, the authors compared their results with the floating OWC experimental results from the study by Sykes et al., (2009).

In this paper, neither the numerical tool (procedure) used in the modelling, nor the wave force estimation procedure were provided. Moreover the damping of the water column itself was ignored and the PTO damping value was assumed constant.

Nunes et al. (2011) modelled the behaviour of a floating OWC including the hydrodynamic and the aerodynamic parts using MATLAB. The ode3 (Bogacki-Shampine) solver was chosen due to its precision and computation speed to solve the structure and water column equations of motion. They applied a dimensional optimisation technique to the turbine and the pneumatic chamber to improve the device performance for a wide number of sea states and developed a control strategy to improve the quality of the energy absorbed by the device.

In their study the diffraction component was not taken into account with the wave forces. Conversion of wave-pneumatic and coupling of the two bodies was modelled based on the pressure inside the chamber. The air inside the device was assumed as an ideal gas; the processes of filling and emptying the chamber were assumed as being isentropic where compressibility was considered. They assumed linear PTO response then performed experiments considering a variable pitch Wells turbine with the objective of applying phase and amplitude control to maximize the power absorbed by controlling the turbine characteristics.

Results concluded that the optimisation of the turbine's characteristic would bring an improvement on the device efficiency. In addition, the use of the proposed control strategies smoothed the power absorption in case of regular waves. It is conceivable that a more suitable predictive controller may improve the performance, in particular for irregular waves.

It is noticed that the optimization procedure was not applied to the whole device geometry. It included parameter related to the aerodynamic part only. Some doubts

concerning the reliability and performance of the proposed controller in real sea may appear. Another disadvantage is that this control technique consumes energy to allow the device to absorb more energy which will have a negative effect of the overall efficiency of the device. Non-linear losses associated with the increase of air volume flow rate across the turbine were not considered in the mathematical model.

Gervelas et al. (2011) presented a one DOF time-domain model for an OWC based on previous works on trapped air cavities for marine vehicles (also known as motion control tanks). Their paper describes the coupling between the hydrodynamic and thermodynamic problems of the proposed OWC. They presented two coupled differential equations, the first one governs the heave motion of the water column itself and the second one governs the pressure inside the chamber. The differential equations were solved using MATLAB ode45 solver. Regular and irregular tests were performed on a 1:20 scale model of a three chambers floating OWC having equal draught. The water elevation and the pressure variation inside the chamber were measured in order to validate their numerical model.

Far from being perfect, the model exhibits a relatively good agreement with measured data except when diffraction effects are predominant.

The model considered the OWC as a single degree of freedom system and completely ignored the effect of the buoy motion. In the proposed model diffraction forces were not taken into account. The PTO damping was assumed linear and taken as 10% of the critical damping. Decay tests would have been useful to determine the damping in this case since experimental facilities were available. In addition, the reduced scale OWC had three non-circular chambers. In the numerical model, the water column was assumed to be a single cylinder.

Alves et al. (2010) performed numerically a frequency domain modelling, in order to optimize the shape of a floating OWC. Computation of the excitation force and the hydrodynamic coefficients (damping and added mass) was performed using (WAMIT), which is a three-dimensional radiation-diffraction panel model based on

linear water wave theory and potential flow. Different buoy shapes were considered in their investigated.

Results obtained indicated that in a heave motion device, the shape of the surface buoy is a minor important parameter if its volume and water plane area are kept the same. In addition, the volume of the buoy should be as small as possible to improve the radiation capabilities and consequently the power absorption.

The study highlighted the importance of the submerged mass not only to enhance the device vertical stability but to tune the device in accordance with the predominant waves.

Another research to optimize the geometry of a floating OWC is presented by Gomes et al. (2012). Several cases, considering different values of the floater diameter and total submerged length were numerically tested in order to have a perspective on how the dimensions of the device influence the annual average power.

The distance between the floater and the submerged mass is a very important parameter because it influences the radiation capabilities of the device. The study of the absorption capabilities of the device for each sea state of the wave climate showed a relationship between the total submerged length and energy period. Sea states with small energy periods tend to be more favourable for the energy absorption by devices with small total submerged length. However, these sea states with small energy period represent a very small percentage of the total energy and are always not favourable in terms of annual average power when compared with large total submerged length devices.

They verified that for some cases with small submerged length, the air chamber height influences only slightly the annual average power if the turbine damping coefficient is optimal. However, as the submerged length increases, the air chamber height becomes more preponderant.

For all cases studied during their research, it was shown that relatively large variations in the turbine damping coefficient about its optimum value have only small influence on the annual average power.

It is noted that all of the previous researches considered one or two translational modes of motion in heave direction and disregarded the remaining motions and the mooring effects. In addition, PTO damping was assumed linear or not considered in the modelling as in the case of Alves et al. (2010)

A.F.O. Falcão et al (2012) adopted the pressure distribution theory to analyse the performance of an OWC spar buoy wave energy converter with a non-uniform inner cross section of the tube. Analysis was performed in frequency domain, for regular as well as in irregular waves where phase control wasn't considered.

Authors highlighted that some simplifying assumptions made to perform the analysis may, in some situations of practical interest, fail to be met. However, even in this case, the analysis and results are expected be significant and to provide useful insights. Researchers linearized the equation involving the air compressibility effect, neglected the excitation force and the radiation damping at the tube lower end and neglected the interference between the buoy and the lower segment of the tube.

Their results showed that adoption of a draught tube with a lower segment of larger inner diameter may result in a significant reduction in the optimal tube length and in the turbine coefficient. Identical results can be achieved to a lesser extent by widening the tube upward inside the buoy in both regular and irregular waves. Later on optimization procedure cover a wide range of values, including on what concerns the turbine showed that the volume of the air chamber significantly affects the optimal freeboard tube length (length decreasing with increasing volume), but not the optimal turbine coefficient.

Aubault et al., 2011, worked on the incorporation of an OWC-WEC into the WindFloat hull. The WindFloat is a floating structure has 3 cylindrical columns connected through a tubular truss to transfer lateral loads. At the base of each

column, a hexagonal heave plate controls the wave induced motions of the structure. On top of the structure a very large wind turbine.

In order to investigate the effect of the PTO on the internal free surface of the OWC They presented an eight degree of freedom system of motion equations, in the frequency domain to consider the six DOF motion of the structure in addition to the water column pumping and sloshing modes of motion.

This analysis has shown that the effect of the OWC structure on platform motions is limited. However, when a PTO is introduced on one column, pitch and roll motions increase. The discrepancies between numerical and experimental results in the floating cases may be linked to corresponding differences in predicted and measured roll and pitch angles of the platform. Moreover, changing the OWC dimensions would solve the sloshing issue and make the water surface acts as a rigid piston.

Muliawan et al, 2013 proposed a combined concept involving the combination of a Spar-type Floating Wind Turbine (FWT) and a Wavebob-type WEC referred as 'SpareTorus Combination (STC) aiming to reduce the total capital cost compared with segregated deployment of a Spar-type FWT and a Wavebob-type WEC. As wave passes, the floating torus will heave and slide along the spar-type FWT to extract energy from waves while the wind turbine generates power from the wind.

The specified STC concept has been modelled and analysed coupled in the time domain to study the motions, power production and mooring load of the combined concept under operational conditions. Hydrodynamic properties of two rigid bodies involved in the STC, including its interactions, are calculated in the frequency domain using HydroD and then applied in SIMO (computer program that was developed by MARINTEK for simulating the motions and station-keeping behaviour) to carry out the coupled motion (wave- and wind-induced responses)-mooring analysis of two bodies in given environmental conditions in the time domain through retardation functions. Aerodynamic force at the wind turbine; are obtained (borrowed) from Statoil's informal implementation of a simplified method called TDHMILL (Thrust-Dynamic-Horizontal-Mill) to calculate the aerodynamic

forces as a function of the relative wind velocity. It simplifies the aerodynamics of the turbine system to be represented as a thrust force at the top of the tower that is calculated using the relative wind speed at each time step.

The dimensions and parameters of the present STC are directly adopted from the properties of existing Spar-type FWT and WEC publicly available, which is an advantage from modelling prospective, but a dimensional optimization between the two devices would result in better performance or reduction in initial cost.

Their study ignored the drag and inertia forces due to mooring line motion, which is reasonable since its motion has minor effect on the power absorption process and important for the mooring system design which is not the scope of their research.

El Marjani et al. (2008) adopted the CFD approach in order to investigate the air flow inside the OWC chamber and the turbine. They presented a three-dimensional numerical simulation of unsteady viscous flows using FLUENT code. Their results proved that the level of useful energy is higher in the inhalation than in the exhalation process, due to losses appeared in the outer and the inner guide vanes for the exhalation. Aiming to validate their models, authors compared the numerical results with the experimental results obtained from the Pico plant built in Azores. Comparisons showed good agreement.

The study did not include energetic aspects connected with the conversion of the initial incident wave energy by the air chamber (wave-pneumatic conversion). In other words they assumed that the hydrodynamic problem is already solved because the inclusion of the hydrodynamic part in the modelling using Fluent is complex, time consuming, expensive and requires multi-phase models.

Cashman et al., 2009, studied a quarter scale offshore OWC-WEC and used results from a prototype device to validate their work.

Their paper investigated the modelling of Well's turbine and studied the electrical output from a generator to be coupled to the turbine under multiple sea state conditions.

Despite simplifying assumptions and experimental error the model was found to predict the mechanical and electrical performance of the system to a satisfactory level of accuracy.

Dizadji & Sajadian (2011) performed extensive experimental research in order to optimize the OWC chamber geometry. Various geometrical designs of shoreline OWC system were constructed to measure the air pressure, flow and velocity in the duct toward the intake of the turbine, consequently the optimal design was obtained. Their results revealed that mounting the turbine vertically at the top of the chamber increases the power output.

In this study the turbine damping was not considered in the experimental model. Moreover the tank dimensions may affect the accuracy of the experimental measurements. Most of the experiments considered the measured parameters during the compression process only and ignored the expansion process measurements.

The experimental study would have been better if the number of tests were increased. The proposed designs had sharp edges and corners, application of very simple air flow visualisation method would have been very useful to investigate the behaviour of the air flow inside the chamber for further minor design modification later on from the aerodynamic point of view since the experimental facilities were available and the model was made of plexi-glass.

Based on the above survey and considering the report objectives, methodology adopted throughout the research should be able to model the water column oscillations inside the device considering the air compressibility and PTO damping. In addition, the structure heave motion should be coupled with the water column oscillations and the structure surge motion should be coupled with the mooring system deployed. Due to the symmetry of the structure the coupling between the heave and pitch motions may be ignored. It is also important to investigate nonlinear effects of the device performance

References of Chapter 2

Alves MA, Costa IR, Sarmento AJNA, Chozas JF., 2010, 'Performance evaluation of an axysimmetric floating OWC', In Proceeding of 20th International Offshore and Polar Engineering Conference; Beijing, China

Brendmo A., Falnes J., Lillebekken P.M., 1996 'Linear modelling of OWCs including viscous loss', Applied Ocean Research, Vol. 18, pp 65–75.

Cashman D., Sullivan D., Egan M.G., Hayes J.G., 2009 'Analysis and Modelling of an Off-shore Oscillating Water Column Wave Energy Converter', In proc. of European Wave and Tidal Energy Conference

Cruz J., 2008, **Ocean wave energy**. ISBN 978-3-540-7489-6. Springer

Dizadji Nader, Seyed Ehsan Sajadian, 2011, 'Modeling and optimization of the chamber of OWC system', Energy Vol. 36 pp 2360-2366

El Marjani A., Castro Ruiz F.,Rodriguez M.A., & Parra Santos M.T., 2008, 'Numerical modelling in wave energy conversion systems'. Energy, Vol 33, pp 1246 – 1253.

Evans DV., 1978, 'Oscillating water column wave-energy device', Journal of the Institute of Mathematics and Its Applications Vol. 22(4) pp 423-433.

Falcão A.F.O., Henriques João C.C., Cândido José J., 2012, 'Dynamics and optimization of the OWC spar buoy wave energy converter ', Renewable Energy Vol. 48 pp 369-381

Falnes, J., 2002. **Ocean Waves and Oscillating Systems: Linear Interactions Including Wave-energy Extraction**. Cambridge University Press, Cambridge.

Folley M., Whittaker T.J.T., 2009, 'Analysis of the nearshore wave energy resource' Renewable Energy pp 1–7

Folley, M. & Whittaker, *T.*, 2005, 'The effect of plenum chamber volume and air turbine hysteresis on the optimal performance of oscillating water columns', In *Proceedings of 24th International Conference on Offshore Mechanics and Arctic Engineering* (OMAE2005), Halkidiki, Greece.

Gervelas R., Trarieux F. amd Patel M., 2011,' A time domain simulator for an oscillating water column in irregular waves at model scale' Ocean Engineering, Vol 38, pp 1007–1013.

Gomes R.P.F., Henriques J.C.C., Gato, A.F.O. Falcão L.M.C, 2012, 'Hydrodynamic optimization of an axisymmetric floating oscillating water column for wave energy conversion' Renewable Energy Vol. 44 pp 328-339

Hals Jørgen, 2010, 'Modelling and phase control of wave-energy converters', PhD. Thesis Norwegian University of Science and Technology, Norway

Muliawan Made Jaya, Karimirad Madjid, and Moan Torgeir, 2013, 'Dynamic response and power performance of a combined Spar-type floating wind turbine and coaxial floating wave energy converter' Renewable Energy 50 (2013) 47-57

Nunes Guilherme, Duarte Valério, Pedro Beirão, and José Sá da Costa, 2011, Modelling and control of a wave energy converter, Renewable *Energy,* Vol 36, pp 1913-1921.

Stappenbelt Brad and Cooper Paul, 2009, 'Mechanical Model of a Floating Oscillating Water Column Wave Energy Conversion Device', Annual Bulletin of the Australian Institute of High Energetic Materials pp. 34-45, USBN: 978-0-9806811-3-0

Sykes, R., Lewis, A. & Thomas, G., 2009, 'A hydrodynamic study of a floating OWC', In Proceedings of the 8th European Wave and Tidal Energy Conference, Uppsala, Sweden

Szumko, S., 1989, 'Mechanical Model for Oscillating Water Column with Compressibility', Journal of Engineering Mechanics, Vol. 115, No.9, pp 1851-1865

Chapter 3

Wave and Wind Forces on Offshore Structures

3.1. Introduction

Environmental loads on offshore structures are differentiated between static and dynamic loads. In this Chapter, dynamic loads on offshore structures due to waves and wind will be discussed.

At first a review on the methods used in the evaluation of wave loading on structures is presented. This is followed by analysis of the inertia and diffraction regimes including Morison's equation and the linear diffraction problem. Wave forces calculations will be used later on in this research during the modelling of the spar and OWC motions.

Later on, methodologies for wind force calculations on offshore structures based on guidelines provided by American Petroleum Institute (A.P.I.) and American Bureau of Shipping (A.B.S.) are provided. Wind forces calculations are essential during the determination of the environmental loads for modelling of the mooring system.

Several readings have been made to understand wave and wind forces on offshore structure and especially wave energy converters. It is worth to mention that wave mechanics, theories, and regimes are clearly explained by (Dean & Dalrymple, 1991), (Sarpkaya & Isaacson, 1981), (Chakrabarti, 2005.a) and (Hudspeth, 2006). The hydrodynamics of OWC are well presented by Cruz (2008). This chapter is mainly based on the knowledge collected from the above references, and basic hydrodynamic courses.

3.2. Wave Forces

The calculation of hydrodynamic forces on offshore structures is of great importance to designers involved in offshore engineering. The hydrodynamic force calculations for design represent a very difficult task because the environmental conditions are very complex because interaction occurs between waves and structure (Soylemez, 1995).

Moreover most of the WEC are located in harsh environment and exposed to dense wave loads. Therefore proper modelling of the environmental loads is very important to investigate the performance and the survivability of the WECs

During the early development of North Sea drilling activities, several analytical tools were developed to predict wave forces on offshore structures. There are common features between most of the analysis tools developed within the early 1960s and the early 1970s. First, the Airy wave theory is adopted. Amplitudes of wave and platform motions are assumed to be small. This assumption permits the linear superposition of the wave forces acting on the restrained structure due to the wave particle motions and hydrodynamic forces acting on the structure due to rigid-body oscillations of the platform in calm water. Second, the wave and motion induced forces are calculated on each volume element, assuming that the rest of the structure is not present. In other words, the interference between the elements of the structure is not taken into account. The total force acting on the structure is obtained by summing the forces on each volume element. Third, the structure can be divided into several volume elements. If the sectional dimensions of these elements are less than about $1/5^{th}$ of the wave length, the wave and motion induced forces can be assumed to be concentrated in the centre of these volume elements. If one of the dimensions of these volume elements is large compared to the wave length, the two or three dimensional source distribution methods should be adopted Fourth, the free-surface effects are neglected, since most of the volume elements of a floating structure are deeply submerged (Incecik, 1982).

As experience from the floating platforms operated for oil and gas industry all over the world gave evidence of the shortcomings in the design calculations, the need was felt for more rational design methodologies.

Several attempts were made to derive generalised calculation methods by which the hydrodynamic and the structural loading on a floating platform under wave excitation can be predicted. These attempts led to the panel method, sometimes known as the boundary integral equation method or Boundary element method. This occupies a central position in the prediction of wave effects on large offshore structures, since it can be applied to a wide variety of practical applications, with sufficient confidence that it can be used by practitioners, not just by researchers. The 3D panel method was first developed by Hess and Smith at the Douglas Aircraft Company. The name came from their representing the body surface by a large number of small flat quadrilateral `panels'. This approach was extended by several groups to include free surface effects. The common features to the computational methods of structural analysis based on boundary element method may be found in (Incecik, 1982) and (Lee & Newman, 2004).

As offshore activities extended to deeper waters and more hostile environments a number of challenges appeared, regarding more efficient computation of linear solutions and the need to consider second-order nonlinearities. Recent developments include higher-order panel methods, and more exact and convenient representations of the geometry, also the development of accelerated solvers which are essential for extremely large complex structures, and coupled solutions of the potential and viscous problems (Lee & Newman, 2004).

In the present days Computational Fluid Dynamic (CFD) approach based on the Reynolds Averaged Navier-Strokes (RANS) are being tested. Some of the CFD codes developed for industry are validated against theoretical / published results. It has been shown that the codes replicate severe nonlinearities which are not accounted in second order diffraction theory or the third order long wave length theory. CFD programs are still complicated, expensive and time consuming since it

requires mesh generation. In addition simulations on powerful processing unit are required for accurate results (Repalle et al, 2007).

3.3. Wave forces regimes

Theoretically, wave forces are computed by two different approaches that depend on the size of structure. In this regard structures are classified as small or large.

If the structure characteristic dimension is relatively small compared to the wave length, flow separation dominates the loading behaviour. In this case forces are assumed to be within the inertia regime where inertia and viscous forces calculations are significantly important. As the structure dimension increase relatively to the wave length, this assumption is no longer valid since the incident waves undergo significant scattering or diffraction. Such diffraction force should be taken into account. This situation is considered in the diffraction regime (Sarpkaya & Isaacson (1981).

The small vs. large structures may be determined by a chart similar to the one shown in Fig.3.1 which summarise various regimes provided by (Chakrabarti, 2005.a).

It is important to mention that in the present study the Morison equation was used to calculate the forces on the structure (spar) since it proved efficiency in predicting loads on small structures. On the other hand, considering preliminary models of WECs, it is usually assumed that forces remain within the diffraction regime (Sphaier Torres, Masetti, Costa & Levi, 2007) and that the importance of other known forces can be considered at a later stage. Consequently understanding of the linear diffraction theory is needed to evaluate vertical (heave) forces applied on the water column and the structure in case of OWC modelling (Chapter 6).

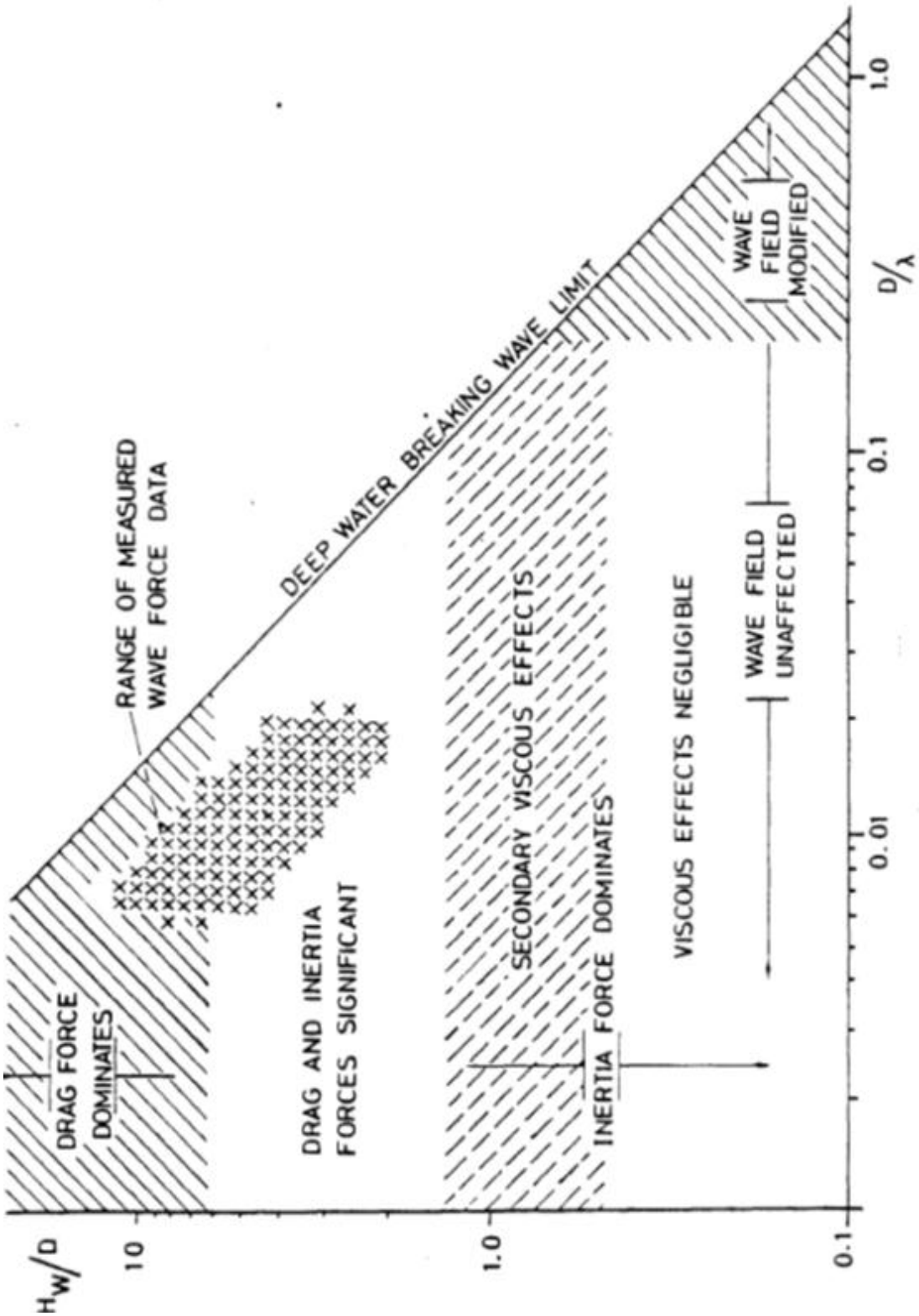

Fig.3.1. Various regimes according to which wave forces may be calculated.

Note that in the above figure λ denotes the wave length.

3.3.1. Inertia regime

For small structures, when the ratio between diameter and wave length is less than 0.2, force calculations are carried out in the inertia regime. Within the inertia regime as the ratio between diameter D and the wave height H_W gets smaller viscous forces become significant (Incecik, 1982). The inertia regime may be summarised from Fig.3.2 as follows:

$D/H_W > 0.2$, inertia increasingly dominant

$0.125 < D/H_W < 0.2$, inertia + drag significant

$D/H_W < 0.125$, drag predominant

In this case Morison's equation is often considered as a valid alternative for the calculation of hydrodynamic force, and it has been used in previous studies to calculate wave forces on deep-draught slender structures such as spars (Anam & Roësset, 2004). The empirical Morison formula includes both inertia and drag forces.

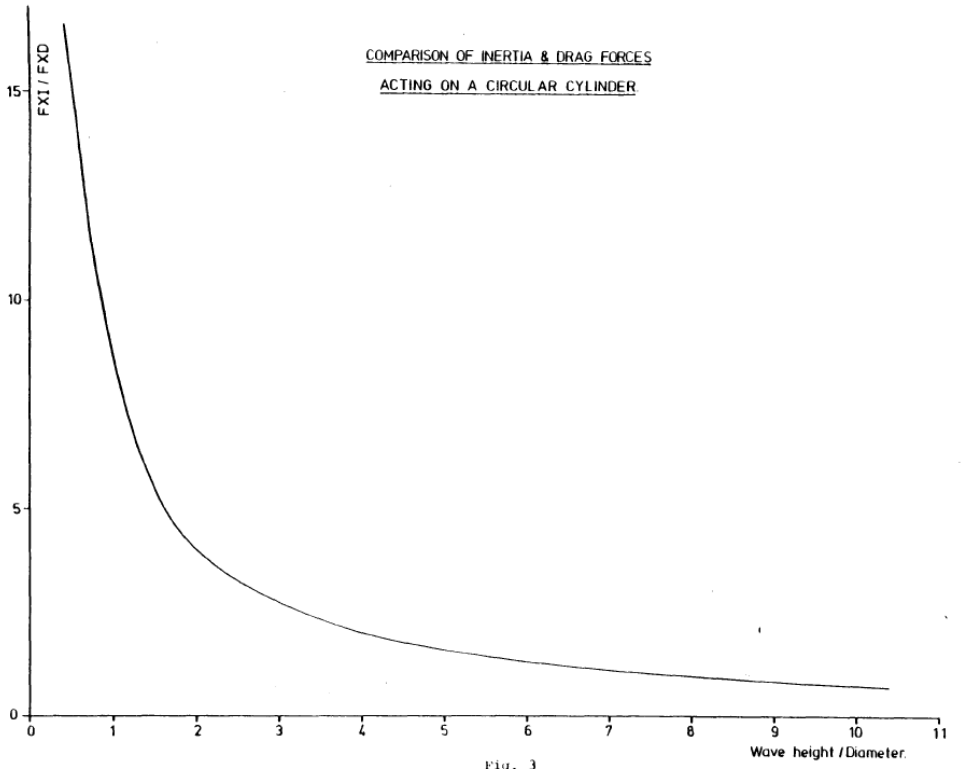

Fig.3.2. Comparison of inertia and drag forces acting on a circular cylinder

3.3.1.1. Morison Equation

In a simplified description one may say that the oscillatory flow over one cycle will change the low-pressure (wake) region immediately behind the structure every half cycle.

As the flow changes direction, the low-pressure region will move from the downstream to the upstream side. Thus the force on the structure will change direction every half a wave cycle.

Combining the effects of water particle velocity and acceleration on the structure, the loading on the structure due to regular waves is computed from the empirical formula known as Morison equation

The following formula known as the Morison equation for the total wave force F_T, which is just the sum of the two forces, drag and inertia (Sarpkaya & Isaacson, 1981):

$$\boldsymbol{F_T = \frac{1}{2} C_D \rho A \dot{u}|\dot{u}| + C_M \rho \ddot{u} \nabla} \qquad \textbf{Eq. 3.1}$$

where;

C_D and C_M are the drag and inertia coefficients.

A is the area

∇ is the underwater volume

ρ is the water density

$\dot{u}$ and $\ddot{u}$ are the velocity and acceleration of the water particles which may be obtained for linear wave theory from Table 3.1 provided by (Moe, 2009).

It is noted that an absolute value sign on one of the velocity terms in Eq.3.1 ensures that the drag force is in the direction of the velocity, which changes direction as the

wave passes. To determine the total force on a vertical pile, the force per unit elevation must be integrated over the immersed length of the pile.

Table 3.1: The profile, dynamic pressure, particle velocities and accelerations in a regular, harmonic wave (Linear wave theory) (Moe, 2009)

Wave property	LOW WATER ($d/\lambda < 1/20$)	INTERMEDIATE WATER ($1/20 < d/\lambda < 1/2$)	DEEP WATER ($d/\lambda > 1/2$)
Velocity potential ($u = \nabla\phi$)	$\phi = \frac{ag}{\omega}\frac{\cosh k(z+d)}{\cosh kd}\cos(\omega t - kx)$	$\phi = \frac{ag}{\omega}\frac{\cosh k(z+d)}{\cosh kd}\cos(\omega t - kx)$	$\phi = \frac{ag}{\omega}e^{kz}\cos(\omega t - kx)$
Dispersion relation	$\omega^2 = gk^2 d$	$\omega^2 = gk\tanh kd$	$\omega^2 = gk$
Wave length - wave period relation	$\lambda = T\sqrt{gd}$	$\lambda = \frac{g}{2\pi}T^2\tanh\frac{2\pi d}{\lambda}$	$\lambda = \frac{g}{2\pi}T^2 \ (\approx 1.56\,T^2)$
Wave profile	$\eta = a\sin(\omega t - kx)$	$\eta = a\sin(\omega t - kx)$	$\eta = a\sin(\omega t - kx)$
Dynamic pressure	$p_d = \rho g a\sin(\omega t - kx)$	$p_d = \rho g a\frac{\cosh k(z+d)}{\cosh kd}\sin(\omega t - kx)$	$p_d = \rho g a e^{kz}\sin(\omega t - kx)$
Horizontal particle velocity	$u = \frac{\omega a}{kd}\sin(\omega t - kx)$	$u = \omega a\frac{\cosh k(z+d)}{\sinh kd}\sin(\omega t - kx)$	$u = \omega a e^{kz}\sin(\omega t - kx)$
Vertical particle velocity	$w = \omega a\frac{z+d}{d}\cos(\omega t - kx)$	$w = \omega a\frac{\sinh k(z+d)}{\sinh kd}\cos(\omega t - kx)$	$w = \omega a e^{kz}\cos(\omega t - kx)$
Horizontal particle acceleration	$\dot{u} = \frac{\omega^2 a}{kd}\cos(\omega t - kx)$	$\dot{u} = \omega^2 a\frac{\cosh k(z+d)}{\sinh kd}\cos(\omega t - kx)$	$\dot{u} = \omega^2 a e^{kz}\cos(\omega t - kx)$
Vertical particle acceleration	$\dot{w} = -\omega^2 a\frac{z+d}{d}\sin(\omega t - kx)$	$\dot{w} = -\omega^2 a\frac{\sinh k(z+d)}{\sinh kd}\sin(\omega t - kx)$	$\dot{w} = -\omega^2 a e^{kz}\sin(\omega t - kx)$
Group velocity	$c_g = c$	$c_g = \frac{1}{2}c\left(1 + \frac{2kd}{\sinh 2kd}\right)$	$c_g = \frac{1}{2}c$

$\omega = 2\pi/T$, $k = 2\pi/\lambda$ T = wave period λ = wave length a = wave amplitude g = acceleration of gravity $c = \lambda/T$ = phase speed	t = time x = direction of propagation z = vertical co-ordinate positive upward, origin at still water level d = water depth	p_d = dynamic pressure $p_d - \rho gz + p_o$ = total pressure in the water ($-\rho gz$ = hydrostatic pressure, p_o = atmospheric pressure). $E = \frac{1}{2}\rho g a^2$ = wave energy (per unit surface area) $P = Ec_g$ = wave energy flux (per unit width along the wave crest)

Note that for the above table, the waves are propagating in the direction of the positive *x*-axis. It should also be noted that the phase is arbitrary, thus a phase angle of θ_0 could be added in all expressions for $\theta=\omega t-kx$ above. For instance, if $\theta_0 = \pi/2$, then and $\sin(\theta+\pi/2)=\cos\theta$. Hence, in the expressions above, the potential, vertical

velocity etc. may instead be expressed through -sin(ω*t*-*kx*)) and the wave profile, horizontal velocity, etc. through cos(ω*t*-*kx*). Complex notation in which the harmonic functions are expressed through real or imaginary parts of *exp(ωt-kx)* may also be used (Moe, 2009).

In general C_D and possibly C_M vary over the length of the pile; as the Reynolds number surely does. Therefore, we cannot integrate this equation directly. If, however, we take constant values of C_D and C_M (Table 3.2) and use linear wave theory and consider only the local acceleration term, the integration can be carried out up to the mean free surface to give an approximation to the total force (Dean & Dalrymple, 1991).

Table 3.2: Hydrodynamic drag and inertia coefficients (Chakrabarti, 2005.a)

Wave Theory	**C_D**	**C_M**	**Comments**	**Reference**
Linear Theory	1.0	0.95	Mean values for ocean wave data on 13-24in cylinder	Wiegel et al (1957)
	1.0 – 1.4	2.0	Recommended design values based on statistical analysis of published data	Agerschou and Edens (1965)
Stokes 3rd order	1.34	1.46	Mean values for oscillatory flow for 2-3in cylinders	Keulegan and Carpenter (1958)
Stokes 5th order	0.8 – 1.0	2.0	Recommended design values based on statistical analysis of published data	Agerschou and Edens (1965)

We can see from the above table that for linear waves the recommended values for drag and inertia coefficients are 1.2 and 2.0, respectively.

3.3.2. Diffraction regime

For large structures as the ratio between diameter and wave length gets larger the wave force calculations should be done in diffraction regime since the structure alerts the form of the incident waves over a large area in its vicinity.

The diffraction parameter *(D/L)* is to be considered the measure of the importance of diffraction. The diffraction should be included whenever $D/L > 0.2$. (or $\pi\ D/L > 0.5$) This condition is important from a modelling perspective Sarpkaya & Isaacson (1981).

If we assume linear-free surface conditions, in other words the wave height is small compared to the wave length ($H_W/L<0.14$ for deep water waves) in diffraction regime the viscous forces become negligible and the linear diffraction theory may be adopted.

The first part of the theory determines the first order exciting forces due to scattered waves (incident and diffracted) while the radiation part considers the moving structure in water and computes the added mass and damping coefficients.

3.3.2.1. Linear diffraction problem

For large bodies, the flow remains attached to the body and the flow may be well described by the velocity potential (potential flow) (Chakrabarti, 2003.a and Hudspeth, 2006). Assuming incompressible fluid and ir-rotational motion the velocity potential satisfies Laplace equation within the region so that:

$$\boldsymbol{\nabla^2 \emptyset = 0} \qquad \textbf{Eq. 3.2}$$

In Eq.3.2, ∇^2 is a second order differential operator, $\emptyset$ is the velocity potential and presents the harmonic function in the equation. For a 2D analysis Eq.3.2 may be written as:

$$\boldsymbol{\frac{\partial^2 \emptyset}{\partial x^2} + \frac{\partial^2 \emptyset}{\partial z^2} = 0} \qquad \textbf{Eq. 3.3}$$

In the XZ plane where z is measured from the free surface, it is subject to the following boundary conditions:

$$\frac{\partial^2 \emptyset}{\partial t^2} + g\frac{\partial \emptyset}{\partial z} = 0 \qquad at\ the\ free\ surface,\ z = 0 \qquad \textbf{Eq. 3.4}$$

$$\eta = -\frac{1}{g}\left(\frac{\partial \emptyset}{\partial t}\right) \qquad at\ the\ free\ surface,\ z = 0 \qquad \textbf{Eq. 3.5}$$

$$\frac{\partial \emptyset}{\partial z} = 0 \qquad at\ the\ seabed,\ z = -w_d \qquad \textbf{Eq. 3.6}$$

$$\frac{\partial \emptyset}{\partial n} = 0 \qquad at\ the\ body\ surface \qquad \textbf{Eq. 3.7}$$

where

g is the gravitational acceleration.

w_d is the water depth and;

η is the surface elevation

Eq.3.4 and Eq.3.5 derive from the linearized kinematic and dynamic free surface boundary conditions assuming small amplitude wave theory. Eq.3.6 and Eq.3.7 correspond to the kinematic boundary conditions at the seabed and at the body surface respectively.

If a body is present, either fixed or undergoing small body motions, then the potential is decomposed into:

$$\emptyset = \emptyset_S + \emptyset_R \qquad \textbf{Eq. 3.8}$$

with the component potentials $\emptyset_S$ and $\emptyset_R$ associated with the Scattered and Radiated wave fields respectively. For the scattering problem, it is usual to employ a further decomposition and write:

$$\emptyset_S = \emptyset_I + \emptyset_D \qquad \textbf{Eq. 3.9}$$

where ϕ_I and ϕ_D are the Incident and Diffraction potentials respectively. Therefore by ignoring the Radiation contribution, the velocity potential is assumed to be the sum of Incident and Diffraction potentials only.

The incident wave potential itself satisfies Laplace equation Eq.3.2 and the boundary conditions Eq.3.4 – Eq.3.7. It is specified in a complex form as:

$$\emptyset_I = \varepsilon \frac{\cosh(k(z+w_d))}{\cosh(k\, w_d)} e^{-i(kx-\omega t)} \qquad \textbf{Eq. 3.10}$$

where

$$\varepsilon = -\frac{igH_w}{2\omega} \qquad \textbf{Eq. 3.11}$$

k is the wave number

ω is the wave frequency

Due to the linearity of the problem the diffraction potential as well satisfies the same equations. Given Eq.3.7 and Eq.3.9 the corresponding boundary condition of zero flux across the body boundary becomes:

$$\frac{\partial \emptyset_D}{\partial n} = -\frac{\partial \emptyset_I}{\partial n} \qquad \textbf{Eq. 3.12}$$

And the pressure, *p* throughout the fluid may be evaluated by the linearized Bernoulli equation as:

$$p = -\rho\left(\frac{\partial \emptyset}{\partial t} + gz + \frac{1}{2}|\nabla \emptyset|^2\right) \qquad \textbf{Eq. 3.13}$$

and reduced in case of small amplitude waves to:

$$p = -\rho\left(\frac{\partial \emptyset}{\partial t} + gz\right) \qquad \textbf{Eq. 3.14}$$

Using the above analysis, sectional forces, total forces and overturning moments may be obtained.

Once again the second part of the theory is concerned about the radiated waves. The corresponding radiation problem utilises the decomposition:

$$\emptyset_R = \sum_{j=1}^{6}(-i\omega X_j \emptyset_j) \qquad \textbf{Eq. 3.15}$$

associated with the motion being composed of six independent body modes, where X_j is the complex amplitude of motion in the j^{th} mode (Sykes et al, 2009).

3.3.2.2. Scattering force

In order to describe the flow in diffraction regime around an arbitrary body geometry one may use the Green function method. However, the flow field in diffraction regime around a circular cylinder can be represented with a velocity potential whose analytical solution can be obtained. This form of solution first given by Havelock, 1940 and presented in MacCamy 1954 and Incecik 1982 and will be presented in this section.

As mentioned in Eq.3.9, the scattering potential is assumed to consist of Incident and Diffraction potentials. The incident potential on the rigid cylinder Eq.3.10 can be expressed as an infinite series using the polar co-ordinates r and θ:

$$\phi_I = -\frac{0.5H_w g}{\omega}\frac{Cosh[k(z+w_d)]}{Cosh(kw_d)}\sum_{m=0}^{\infty}\varepsilon_m i^m Cos(m\theta)J_m(kr)e^{-i\omega t} \qquad \textbf{Eq. 3.17}$$

where Jm(kr) are Bessel functions of the first kind of orders of 0, 1, 2, …..m. ε0=1 and ε0=2 for m>1.

A cylindrical wave is reflected from the cylinder and may be described by the velocity potential $\emptyset_D$

$$\phi_D = -\frac{0.5H_w g}{\omega}\frac{Cosh[k(z+w_d)]}{Cosh[kw_d]}\sum_{m=0}^{\infty}A_m Cos(m\theta)[J_m(kr)+iY_m(kr)]e^{-i\omega t} \textbf{ Eq. 3.18}$$

where A_m is numerical constant and $Y_m(kr)$ are Bessel functions of the second kind.

From Eq.3.9, the scattered potential may be obtained from Eq.3.17 and Eq.3.18

$$\phi_S = -\frac{0.5H_w g}{2\omega}\frac{Cosh[k(z+w_d)]}{Cosh(kw_d)}\sum_{m=0}^{\infty}[\varepsilon_m i^m Cos(m\theta)J_m(kr) + A_m Cos(m\theta)H\ \ (kr)]e^{-i\omega t}$$

Eq. 3.19

where $H_m^{(1)}(kr) = J_m(kr) + iY_m(kr)$ is the Henkel function of the first kind.

The constants A_m are evaluated by using the boundary condition that the fluid velocity normal to the cylinder is zero, that is:

$\frac{\partial \phi}{\partial r} = 0$ at r=D/2=R **Eq. 3.20**

where D and R are the diameter and radius of the cylinder respectively.

Thus:

$$A_m = -\varepsilon_m i^m \frac{J_m^{'}(kR)}{H_m^{'(1)}(kR)}$$ **Eq. 3.21**

for m = 0, 1, 2, 3,….. where $J_m^{'}(kR)$ and $H_m^{'}(kR)$ are the derivatives of $J_m(kr)\ \ and\ \ H_m^{(1)}(kr)$ at r=R. Therefore the total potential is:

$$\phi_S = -\frac{0.5H_w g}{\omega}\frac{Cosh[k(y+d)]}{Cosh(kd)}\sum_{m=0}^{\infty}\varepsilon_m i^m\left[J_m(kr) - \frac{J'_m(kR)}{H_m^{'(1)}(kR)}H_m^{(1)}(kr)\right]Cos(m\theta)e^{-i\omega t}$$

Eq. 3.22

The water surface elevation η and the dynamic pressure at the surface of the cylinder are calculated using the total velocity and potential and the linear Bernoulli equation Eq.3.14.

At the water surface p=0 and y=η so from Eq.3.14

$$\eta = 0.5H_w\sum_{m=0}^{\infty}\varepsilon_m i^{m+1}\left[J_m(kr) - \frac{J_m^{'}}{H_m^{'(1)}(kR)}H_m^{(1)}(kR)\right]Cos(m\theta)e^{-i\omega t}$$ **Eq. 3.23**

Similarly, the dynamic pressure is:

$$p = -\rho g 0.5H_W \frac{Cosh[k(z+w_d)]}{Cosh(kw_d)}$$
$$\sum_m^{\infty}\frac{\varepsilon_m i^{m+1}}{H_m^{'(1)}}\left[J_m(kR)H_m^{'(1)}(kR) - J_m^{'}(kR)H_m^{(1)}(kR)\right]Cos(m\theta)e^{-i\omega t}$$ **Eq. 3.24**

which reduces to:

$$p = -\frac{\rho g H_W}{\pi k R} \frac{Cosh[k(z+w_d)]}{Cosh(kw_d)} \sum_m^{\infty} \frac{\varepsilon_m i^{m+1}}{H_m^{'(1)}} Cos(m\theta) e^{-i\omega t} \qquad \textbf{Eq. 3.25}$$

since

$$\left[J_m(kR) H_m^{'(1)}(kR) - J_m^{'}(kR) H_m^{(1)}(kR)\right] = \frac{2i}{(\pi kR) H^{'(1)}(kR)} \qquad \textbf{Eq. 3.26}$$

and

$$J_{m+1}(x) Y_m(x) - J_m(x) Y_{m+1}(x) = \frac{2}{\pi x} \qquad \textbf{Eq. 3.27}$$

The horizontal force per unit length of the cylinder is calculated by integrating the pressure around the cylinder:

$$p = -\frac{\rho g H_W}{\pi k} \frac{Cosh[k(z+w_d)]}{Cosh(kw_d)} \int_0^{\infty} \sum_m^{\infty} \frac{\varepsilon_m i^{m+1}}{H_m^{'(1)}} Cos(m\theta) Cos\theta d\theta e^{-i\omega t} \qquad \textbf{Eq. 3.28}$$

After integration, Eq.3.28 becomes:

$$f_x = \frac{2\rho g H_W}{k} \frac{Cosh[k(z+w_d)]}{Cosh(kw_d)} \left[J_1^{'}(kR) + iY_1^{'}(kR)\right]^{-1} ie^{-i\omega t} \qquad \textbf{Eq. 3.29}$$

and taking the real part only:

$$f_x = \frac{2\rho g H_W}{k} \frac{Cosh[k(z+w_d)]}{Cosh(kw_d)} A(kR) Cos(\omega t - \alpha) \qquad \textbf{Eq. 3.30}$$

where α is the phase angle between the force and the wave crest

$$\alpha = \tan^{-1}\left(\frac{J_1^{'}(kR)}{Y_1^{'}(kR)}\right) \qquad \textbf{Eq. 3.31}$$

$$A(kR) = \frac{1}{\sqrt{J_1^{'2}(kR) + Y_1^{'2}(kR)}} \qquad \textbf{Eq. 3.32}$$

$J_1^{'}$ *and* $Y_1^{'}$ can be approximated from the asymptotic expansions of the derivatives of Bessel functions as follows:

$$J_1^{'}(kR) = \frac{1}{2} \qquad \textbf{Eq. 3.33}$$

$$Y_1^{'}(kR) = \frac{2}{\pi(kR)^2} \qquad \textbf{Eq. 3.34}$$

Eq.3.30 can also be generalised for the application of circular members both in inertia and diffraction regimes. If we set Eq.3.30 equal to the inertia component of Morison's equation the following relation can be obtained:

$$f_x = \rho\pi R^2 C_M \omega^2 0.5 H_W e^{kz} Sin(kx-\omega t) = \frac{2\rho g k e^{kz}}{k} A(kR) Cos(kx-\omega t+\alpha) \qquad \textbf{Eq. 3.35}$$

The right hand side of Eq.3.35 can also be written as:

$$\frac{2\rho g k e^{kz}}{k} A(kR) \frac{0.5\pi R^2 \omega^2}{0.5\pi R^2 \omega^2} \frac{Sin(kx-\omega t)}{Sin(kx-\omega t)} Cos(kx-\omega t+\alpha) \qquad \textbf{Eq. 3.36}$$

Comparing Eq.3.36 and the left hand side of Eq.3.35 it can be seen that C_M can be written as:

$$C_M = \frac{4}{\pi} \frac{1}{(\pi D/\lambda)^2} A(kR) \qquad \textbf{Eq. 3.37}$$

Now the horizontal wave force on large diameter cylinders can also be written in the following form:

$$f_x = C_M \rho\pi(D^2/4)\ddot{u} \qquad \textbf{Eq. 3.38}$$

Where C_M will be calculated from Eq. 3.37 and ü is the horizontal wave particle acceleration. Fig.3.3 presents values of C_M versus D/L.

In this context, if D/L is very small (D/L<0.2) C_M approach 2 and the diffraction force is calculated by multiplying the added mass of the cylinder by the acceleration of the water particles this is also called acceleration force. Acceleration force component in heave direction on a vertical cylinder can be written as:

$$\boldsymbol{f_A = -0.5 H_w g\, KM_a \ \frac{sinh(-dk+w_d k)}{cosh(w_d k)} cos(-\omega t)} \qquad \textbf{Eq. 3.39}$$

where;

M_a is the added mass and will be discussed later. This method has been used by Gervelas et al., 2011.

If diffraction component is too small compared to the incident wave component, then the diffraction component can be neglected and the excitation force is represented by the contribution from the incident waves alone as:

$$\boldsymbol{f_I = 0.5 H_w \rho g A \frac{cosh(-dk+w_d k)}{cosh(w_d k)} cos(-\omega t)} \qquad \textbf{Eq. 3.40}$$

and this case is known as the Froude-Krylov Approximation and it is useful when circumstances permit.

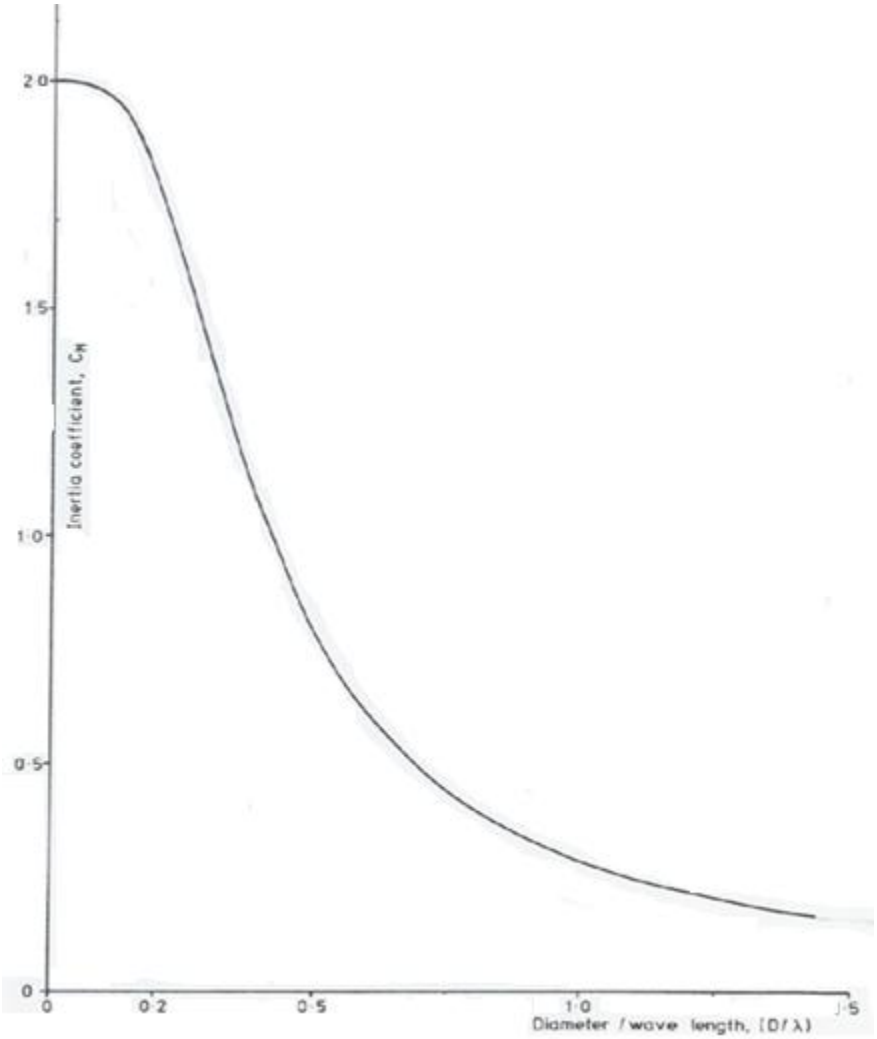

Fig.3.3. Values of C_M versus D/L

Note that in the above figure λ denotes the wave length.

3.3.2.3. Radiation force

The radiation force corresponds to the force experienced by the body due to its own oscillatory movement in the absence of an incident wave field. It is proportional to the immersed shape of the body and the complex amplitude of the motion in the linear theory. The complex radiation force generated by unit amplitude body motion can be calculated by conventional numerical techniques at any number of frequency points.

The standard practice is to regard the force as being composed of two components: one in phase with the body acceleration and the other in phase with the body velocity. These force components may be written as function of the added mass M_a and damping coefficients d_j respectively, therefore:

$$\vec{f}_R = \iint_S -\rho\left(\frac{\partial \emptyset_R}{\partial t}\right)\vec{n}dS = -M_{a_j}\ddot{x}_j - d_j\dot{x}_j \qquad \textbf{Eq. 3.41}$$

Electrical analogy presents the radiation force in term of impendence. The radiation resistance and the radiation reactance are the equivalent of added mass and damping coefficient respectively which will be discussed in Chapter 4.

3.4. Wind forces

The wind force acting on an ocean structure is the sum of the wind force acting on its individual parts. For any part such a structural member, storage tank, deck house, derrick, helicopter deck, etc., the wind force arises from the viscous drag of the air on the body and from the difference in pressure on the windward and leeward sides. In the present study wind forces are calculated in order to include the wind loads in mooring modelling only.

3.4.1. Wind forces by American Petroleum Institute

Wind force calculations as recommended by A.P.I. can be summarised as follows:

$$\boldsymbol{F_{wind} = \frac{1}{2}\rho_{air} C_{Da} A_P U^2} \qquad \textbf{Eq. 3.45}$$

where;

ρ_{air} is the density of air (1.225 kg/m^3 for dry air).

C_{Da} is the aerodynamic drag coefficient (dimensionless force coefficient)

A_P is the projected (characteristic) area of the body.

U is the wind velocity.

The drag coefficient depends on the shape of the body and on the Reynolds number.

Table 3.3 gives typical C_D values used in calculations. Data given in Table 3 are recommended by American Petroleum Institute.

Published wind speeds given in the design guidelines refer to values 10 metres above the sea surface. To determine the wind speeds at other elevations, E, a one-seventh power law has generally been found to be adequate for elevations to about 200 metres. Thus, if U denotes the wind speed at an elevation, and U_O denotes the wind speed at the 10 metres elevation, then:

$$\boldsymbol{U = U_o \left(\frac{E}{10}\right)^{1/7}} \qquad \textbf{Eq. 3.46}$$

3.4.2. Wind forces by American Bureau of Shipping

Wind force calculations as recommended by American Bureau of Shipping (A.B.S.) can be summarised as follows:

$$\boldsymbol{F_{wind} = \frac{1}{2}\rho C_H C_S A_P U^2} \qquad \textbf{Eq. 3.47}$$

where;

C_S is the shape coefficient (see Table 3.4).

C_H is the height coefficient (see Table 3.5)

If two or more parallel frames or members are located behind each other in the wind direction, the shielding effect must be taken into account. The wind force on a shielded member can be calculated as:

$$\boldsymbol{F_{shielded} = \frac{1}{2}\rho C_D \theta A_P U^2 \tau} \qquad \textbf{Eq. 3.48}$$

θ is the solidity ratio defined as the projected exposed area of the frame normal to the direction of the force divided by the area enclosed by the boundary of the frame normal to the direction of the force. τ is the shielding factor (see Table 3.6).

If more than two members are located in line with the wind direction, the wind force on the third and subsequent members should be taken equal to the wind load on the second member.

Table 3.3: Aerodynamic drag coefficient (A.P.I.)

Object	**Force Coefficient**
Beams	1.5
Cylinders	0.5
Sides of Buildings	1.5
Projected Area of Platform	1.0

Table 3.4: Shape coefficient (A.B.S)

Object	**C_S**
Cylinders	0.5
Hull (surface type)	1.0
Deck House	1.0
Isolated Structural Shapes (cranes, angles, channels, beams, etc.)	1.5
Under deck areas (smooth surfaces)	1.0
Under deck areas (exposed beams and girders)	1.3
Rig derrick (each face)	1.25

Table 3.5: Height coefficient (A.B.S)

Height (Metres)	**C_H**
0 – 15.3	1.0
15.3 – 30.5	1.10
30.5 – 46.0	1.20
46.0 – 61.0	1.30
61.0 – 76.0	1.37
76.0 – 91.5	1.43
91.5 – 106.5	1.48
106.5 – 122.0	1.52
122.0 – 137.0	1.56
137.0 – 152.5	1.60
152.5 – 167.5	1.63
167.5 – 183.0	1.67
183.0 – 198.0	1.70
198.0 – 213.5	1.72
213.5 – 228.5	1.75
228.5 – 244.0	1.77
244.0 – 256.0	1.79
256.0	1.80

Table 3.6: Shielding factor (A.B.S.)

Spacing ratio α	**Values of τ for an aerodynamic solidity ratio β of**							
	0.1	0.2	0.3	0.4	0.5	0.6	0.7	0.8&over
Up to 1	1.0	0.96	0.90	0.80	0.68	0.54	0.44	0.37
2.0	1.0	0.97	0.91	9.82	0.71	0.58	0.49	0.43
3.0	1.0	0.97	0.92	0.84	0.74	0.53	0.54	0.48
4.0	1.0	0.98	0.93	0.86	0.77	0.67	0.59	0.54
5.0	1.0	0.98	0.94	0.88	0.80	0.71	0.64	0.60
6.0&over	1.0	0.99	0.95	0.90	0.83	0.75	0.69	0.66

Spacing ratio is the distance centre to centre of the frames, beams or girders divided by the least overall dimension of the frame, beam or girder measured at right angles to the direction of the wind. For triangular or rectangular framed structures diagonal to the wind, the spacing ration should be calculated from the mean distance between the frames in the direction of the wind.

3.5. Results and discussions

Wave forces calculations methodologies presented in this chapter will be used during modelling of OWC WEC to predict the water column oscillations and the structure motion response in case of floating OWC. Surge forces and pitch moments will be assumed to consist of inertia and drag components. Heave forces will be assumed to consist of pressure and acceleration components.

Fig.3.4 Fig.3.5 and Fig.3.6 present surge, heave and pitch forces/moments expected to be applied on the water column of experimental model1. Fig.3.7 Fig.3.8 and Fig.3.9 present the same forces/moment on the water column of experimental model2.

Calculations of Surge, heave and pitch force/moment acting on the spar are presented in details in Appendices A, B and C respectively

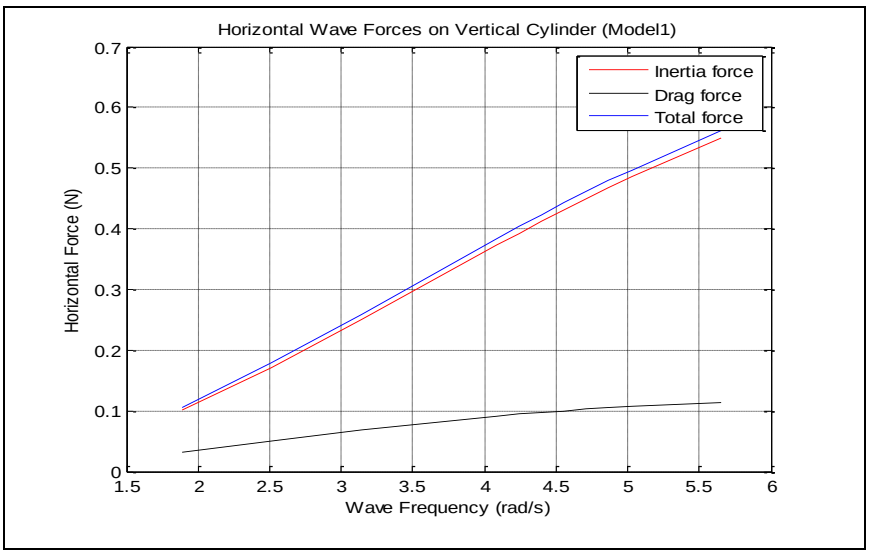

Fig.3.4. Inertia, drag and total horizontal force on experimental model1

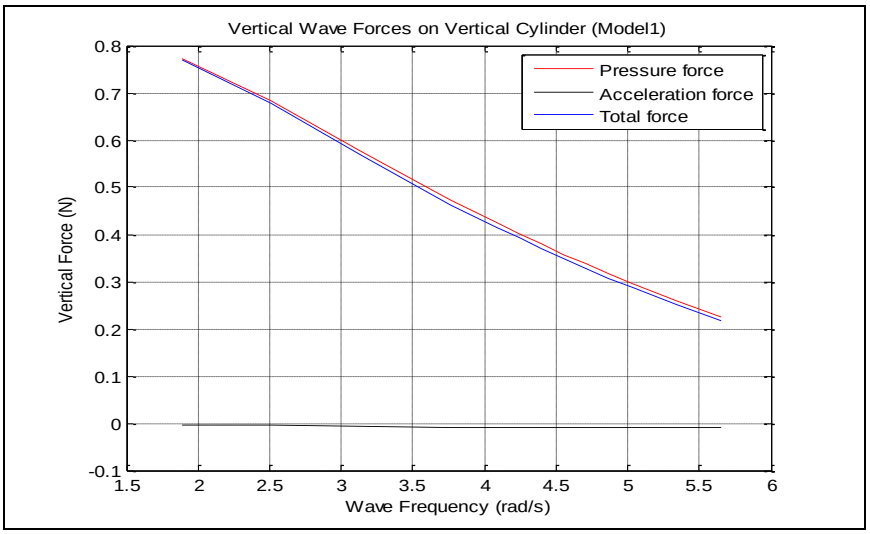

Fig.3.5. Pressure, acceleration and total vertical force on experimental model1

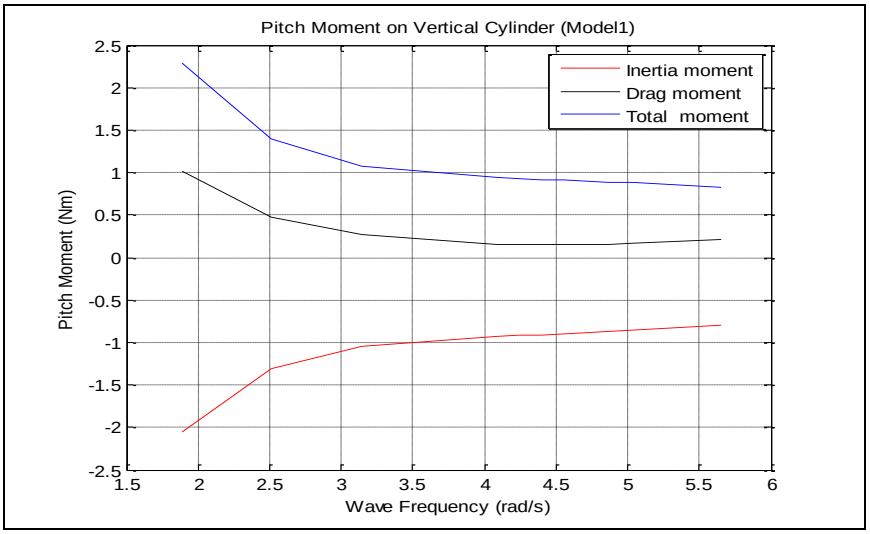

Fig.3.6. Inertia, drag and total pitch moment on experimental model1

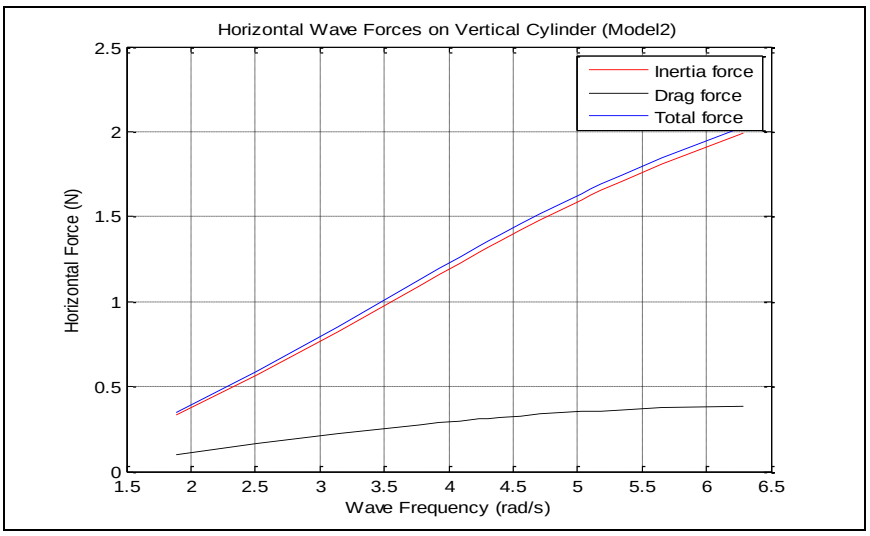

Fig.3.7. Inertia, drag and total horizontal force on experimental model2

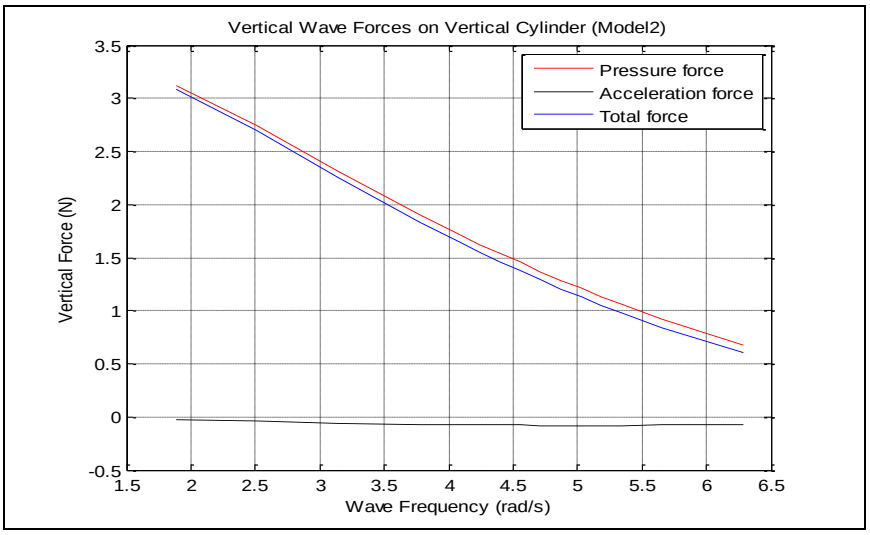

Fig.3.8. Pressure, acceleration and total vertical force on experimental model2

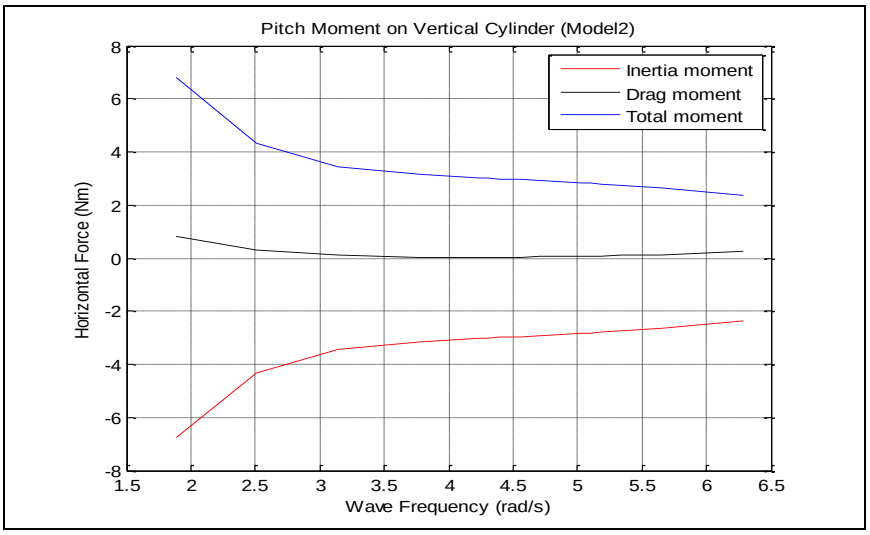

Fig.3.9. Inertia, drag and total pitch moment on experimental model2

Results showed that the drag contribution in the total horizontal force (Fig.3.4 and Fig3.7) and pitch moment (Fig.3.6 and Fig.3.8) is very small compared to the inertia contribution, which agrees with the chart present in Fig.3.2, since the wave height to diameter ratios are 1 and 0.5 for experimental model 1 and 2 respectively.

Fig.3.5 and Fig.3.8 showed that the total vertical force consists mainly of the pressure components and that acceleration component may be neglected. This case corresponds to Froude-Krylov approximation.

In order to validate the wave forces calculations presented above, Keulegan-Carpenter and the diffraction parameters were calculated for the two experimental models (see chapter 9 for more details on reduced scale models). Table 3.7 present comparisons between those parameters for buoys and water columns of experimental models 1 and 2 assuming wave height of 0.02m and wave length of 3.2m.

Table 3.7: Keulegan-Carpenter and the diffraction parameters for experimental model1 and 2

	Experimental model1		Experimental model2	
	Buoy	Water column	Buoy	Water column
KC	0.4	1.0	0.2	0.4
D/L	0.04	0.01	0.09	0.03

The above table showed that Keulegan-Carpenter parameter KC<1 and diffraction parameter D/L<0.2, therefore viscous forces may be ignored, forces are to be calculated in diffraction regime, and Froude-Krylov approximation is valid which verify the results obtained. In addition results are compared to (Incecik, 2003) results and showed very good agreement.

Wind forces were calculated only to estimate the environmental loads on the structure for proper mooring modelling. Wind forces calculation methodology presented in this chapter is applied to a full scale structure (scale 1:50 of experimental model1), results obtained are presented in Fig.3.10.

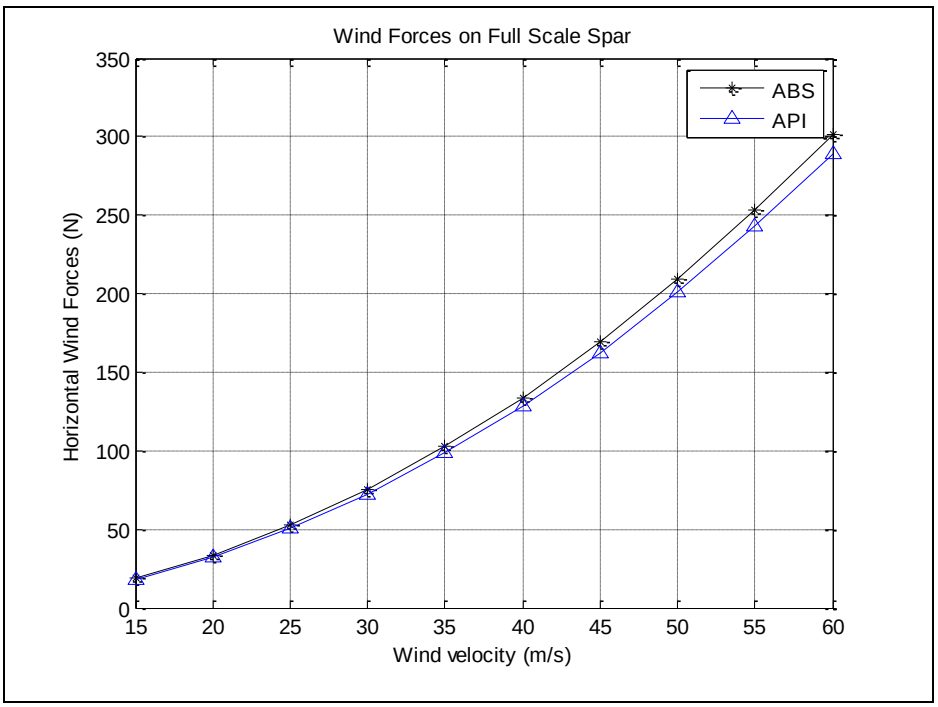

Fig.3.10. Wind forces on full scale SparBuoy OWC WEC

Results obtained following the API and ABS recommendations are quite similar. It is important to mention that wind forces were only used to estimate a range of environmental loads on the mooring system.

References of Chapter 3

Anam Iftekhar & Roësset José M., 2004, 'Slender-body approximations of hydrodynamic forces for spar platforms', International journal of offshore and polar engineering Vol. 14, No.2

Chakrabarti, S., 2005a, **Handbook of Ocean Engineering vol. 1**. Planfield: Elsevier.

Dean, R. G. and Dalrymple, R. A., 1991, **Water wave mechanics for engineers and scientists**. Advanced Series on Ocean Engineering. Vol. 2. Singapore: World Scientific. ISBN 978-981-02-0420-4

Havelock, T.H. 1940, 'The Pressure of Water Waves upon a Fixed Obstacle", Proc. Of the Royal Society A175

Hudspeth, R.T., 2006. **Wave forces on coastal and ocean structures**. Advanced Series on Ocean Engineering, Vol. 21. World Scientific Publishing, Singapore.

Incecik A., 1982, 'Design aspects of hydrodynamic and structural loading on floating offshore platforms under wave excitation', Ph.D. thesis, University of Glasgow, U.K.

Incecik A., 2003, 'Dynamic motion response analysis of a spar buoy', Report prepared for WAVEGEN Limited, Inverness

Lee C.H. and Newman J.N., 2004, 'Computation of wave effects using the panel method', in Numerical models in fluid-structure interaction, Preprint, Editor S. Chakrabarti, WIT Press, Southhampton.

MacCamy, R.C. and Fuchs, R.A., 1954, **Wave Forces on Piles: A Diffraction Theory**, Technocal Memorandum No. 69, U.S. Army Beach Erosion Board, Office of the Chief of Engineers

Moe G., 2009, **Linear wave theory** NTNU, Trondheim, Norway.

Repalle Nitin, Thiagarajan Krish, and Michael Morris-Thomas, 2007, 'CFD simulation of wave run-up on a spar cylinder', 16th Australasian Fluid Mechanics Conference, Australia

Sarpkaya T., Isaacson. M., 1981, **Mechanics of Wave Forces on Offshore Structures**, Van Nostran Reinhold Company, New York

Soylemez M., 1996,'General method for calculating hydrodynamic forces' Ocean Engineering, Vol. 23, No. 5, pp. 423-445

Sphaier S. H., Torres F.G.S, Masetti I.Q., Costa A.P. & Levi C., 2007, 'Monocolumn behavior in waves: Experimental analysis', Ocean Engineering Vol. 34, pp. 1724-1733.

Sykes, R., Lewis, A. & Thomas, G., 2009, 'A hydrodynamic study of a floating OWC', In Proceedings of the 8th European Wave and Tidal Energy Conference, Uppsala, Sweden

Chapter 4

Motion Response of Floating Cylinder under Wave Forces

4.1. Introduction

In Chapter 3, the question 'how to compute loads on offshore structures?' was answered. How the structure will respond to these loads will be discussed in this chapter.

The wave excitation on floating stable structures will result in small six DOF rigid body motions shown in Fig.4.1 which can be resolved into three translational modes of motion (surge, sway, heave) and three rotational modes of motion (roll, pitch and yaw) in the directions of about the (x,y,z) coordinate axes (Incecik, 1982).

If one interested in a particular direction the structure is treated as a single DOF oscillating body. If two floating bodies are moving independently in the vicinity of one another in waves, the two body motion problem may be solved and modelled as a two DOF (this approach will be adopted for modelling floating OWC and will be discussed in Chapter 6).

4.2. Ship rigid body motions

When a cylinder is considered as an oscillating rigid-body, the motions equation can be derived from Newton's second law as follows:

$$\boldsymbol{F_W} = [\boldsymbol{M}]\{\ddot{\boldsymbol{X}}\} \qquad \textbf{Eq. 4.1}$$

where;

F_W is the total wave/fluid induced force/moment vector

[M] is the mass matrix;

$\{\ddot{X}\}$ is the acceleration vector of the cylinder.

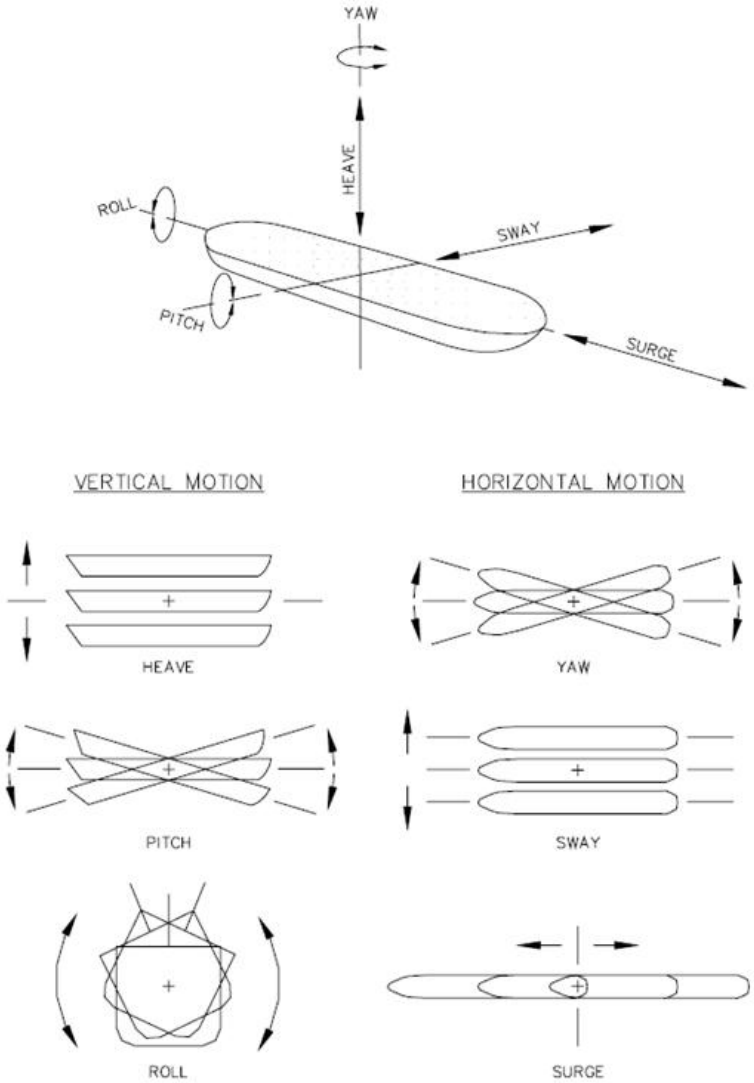

Fig.4.1. Ship rigid body motions

In Eq.4.1 the total force vector, F_W can be replaced by the sum of the force and moment components (discussed in Chapter 3) and the external forces applied.

If the forces/moments are rearranged as motion dependant terms on the left hand side and time dependant forcing terms on the right hand side, the following six linear, second-order differential equations can be obtained in its matrix form:

$$[\boldsymbol{M}]\{\ddot{\boldsymbol{X}}\} + [\boldsymbol{B}]\{\dot{\boldsymbol{X}}\} + [\boldsymbol{K}]\{\boldsymbol{X}\} = \{\boldsymbol{F_W}\} \qquad \textbf{Eq. 4.2}$$

where;

[*M*], [*B*] and [*K*] are the total mass, hydrodynamic damping, and restoring coefficient matrix.

$\{\ddot{X}\}, \{\dot{X}\}$ and $\{X\}$ are the acceleration, velocity and displacement vectors of the cylinder.

If we assume no coupling between the different modes of motions, the previous equation may then be reduced to six uncoupled linear second order differential equations, for which the standard form is written as:

$$\boldsymbol{m_j\ddot{x}_j + b_j\dot{x}_j + k_jx_j = F_{Wj}\, e^{-i\omega t}} \qquad \textbf{Eq. 4.3}$$

Sub-scripts *j* takes value from 1 to 6 denoting surge, sway, heave, roll, pitch and yaw motions respectively. In the present study motions in concern are surge, heave, and pitch.

The solution of the above equation is presented in details in Appendix A and finally gives the motion amplitude as:

$$\boldsymbol{X} = \frac{F_W/_{\boldsymbol{k}}}{\left\{\left[1-\left(\frac{\omega}{\omega_n}\right)^2\right]^2 + \left[2\xi\frac{\omega}{\omega_n}\right]^2\right\}^{1/2}} \qquad \textbf{Eq. 4.4}$$

ω_n is the natural frequency, and the phase angle between the wave and the response is:

$$\boldsymbol{\phi} = \tan^{-1}\left\{\frac{2\xi\frac{\omega}{\omega_n}}{1-\left(\frac{\omega}{\omega_n}\right)^2}\right\} \qquad \textbf{Eq. 4.5}$$

4.3. Total mass calculations

In a fluid medium such water of a given density, the determination of the effective mass of the body is not easy and requires the consideration of the motion of the fluid as well as that of the body. Therefore the total mass of a moving body consists of the actual mass and the added mass in a specific direction. The basic definition of added mass provided by Sarpkaya & Isaacson, 1981 is 'the quotient of the additional force required to produce the acceleration throughout the fluid divided by the acceleration of the body'. In other words, the motion of a body through an inviscid fluid media is always accompanied by a fluid mass transport and that is the added mass which may be expressed in many ways. The use of each analytical expression depends on the simplicity of its evaluation.

Sarpkaya & Isaacson, 1981 presented in their book a table for added masses of various body shapes including circular disk. The horizontal added mass of a circle M_{ahm} per unit length may be calculated as:

$$\boldsymbol{M_{ahm} = \rho \, \frac{\pi}{4} \, D^2} \qquad \textbf{Eq. 4.6}$$

And the vertical added mass M_{avm} for heave motion is:

$$\boldsymbol{M_{avm} = \rho \, \frac{4}{3} \left(\frac{D}{2}\right)^3} \qquad \textbf{Eq. 4.7}$$

For pitch motion the total inertia, I_p, consists of the actual inertia, I', and the added inertia, I_{ap} of the structure.

$$\boldsymbol{I' = \rho \, \nabla_T \, r^2} \qquad \textbf{Eq. 4.8}$$

The radius of gyration, r is the square root of the water plane moment of area divided by the water plane area. The added inertia of the circular cylinder may be calculated as:

$$\boldsymbol{I_{ap,T} = \rho \frac{\pi}{4} (A \, d \, Z)} \qquad \textbf{Eq. 4.9}$$

A is the cross-section area of the section, *d* is the section draught and *Z* represents the distance between the centre of gravity of the section and the centre of gravity of the whole structure in case the cylinder makes a part of a floating structure.

4.4. Damping measurement

Perhaps the simplest approach to the definition of damping will be through the measurements of the dissipated energy of the system. In the absence of damping, once a system is excited and set into motion theoretically the motions will continue indefinitely. As a consequence of damping, some energy is dissipated, and a continuous source of energy is required to maintain these motions. In the steady state, the energy generated by the excitation is equal to the energy dissipated.

Ankudinov, 1991 reported that for marine platforms and vessels, vibration damping is customarily separated into the following main types:

- **Hysteretic damping**

Hysteretic damping includes material damping due to the energy losses caused by irreversible internal processes. These losses typically accompany the cyclic deformation of a solid material and convert strain energy to heat. This phenomenon is due to the local micro-plastic strains in the nonhomogeneous material of marine structures. This component is thought to be small but might increase significantly from stress concentration.

Hysteretic damping also includes structural damping due primarily to the energy losses in the structural joints during bending and shear of the hull girder. Structural damping also increases in the areas of stress concentration.

- **Energy losses due to resonance**

These losses are typically associated with the resonant vibrations of various local structures and equipment, including superstructure, machinery fittings etc. The losses

become larger at higher modes, possibly due to the fact that more local structure becomes involved.

- **External (hydrodynamic) damping**

This form of damping includes two major types of damping that may be experienced on the floating structures which oscillate near or on the free surface. First, wave damping due to the dissipation of energy in the form of surface waves which are generated as a result of rigid body motion of floating structures (radiation waves). Second, viscous damping which are due to the turbulent flow in the lee of a body. In addition to damping effects associated with mooring lines

Hydrodynamic damping can be studied somewhat differently than other components of vibration damping. Unlike structural damping it can be estimated using a variety of available analytical and numerical hydrodynamic methods.

In the present study the hydrodynamic damping coefficients were evaluated experimentally. There are many methods to identify modal damping ratios both in the frequency domain and in the time domain from experimental measurements. Methods of the time domain include logarithmic-decrement method, ITD method, STD method, random decrement technique, weighted response-integral method, etc. Methods of the frequency domain include half-power bandwidth method, peak picking method, admittance circle method, etc. Further possibilities include wavelet transform and EMD-HT method (Huang et al., 2007).

Viscous damping model is used for simplicity as it leads to linear equation of motion. The first damping identification method used in the study is based on logarithmic decrement, δ obtained experimentally from decay tests in time domain (Fig.4.2). The logarithmic decrement is obtained from:

$$\boldsymbol{\delta = \frac{1}{n} ln \left| \frac{X_i}{X_{i+n}} \right|} \qquad \textbf{Eq. 4.10}$$

where X_i and X_{i+n} stand for the amplitudes of the i^{th} and $(i+n)^{th}$ cycles, respectively. The damping ratio ξ_t is related to the logarithmic decrement by the equation:

$$\xi_t = \sqrt{\frac{\delta^2}{4\pi^2+\delta^2}} \qquad \textbf{Eq. 4.11}$$

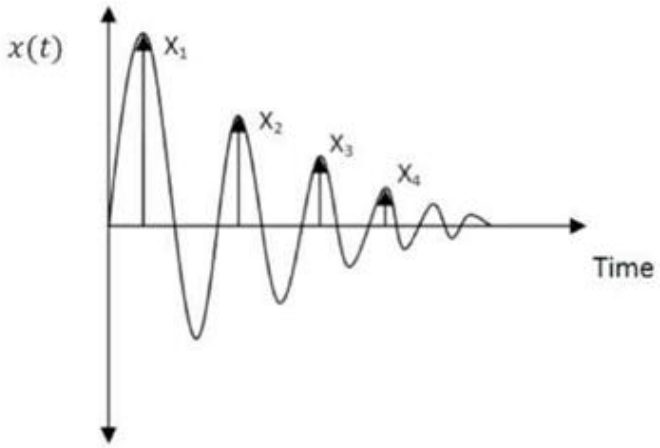

Fig.4.2. Logarithmic decrement method

There are two problems with the logarithmic-decrement method. The first one is that peak values are sampling values, and might not be equal to the actual maximum values. The second one is that the accuracy of this method is easily contaminated by noise (Huang et al., 2007). Another problem appeared throughout the experiments is the insufficient number of cycles within the decay test which affect the accuracy as well.

The second damping identification method used is the half-power bandwidth method, also known as Quality Factor (Fig.4.3).

From the forced oscillation tests expressed in frequency domain The value of the amplitude ratio at resonance is called *Q* factor of the system, the points R_1 and R_2 where the amplification factor falls to $Q/\sqrt{2}$ are called half-power points because the power absorbed by the damper in proportional to the square of the amplitude (Rao, 1991). In this case the damping ratio ξ_f is obtained by implementing the frequencies corresponding to the half-power points (ω_1 *and* ω_2) and the peak frequency (ω_n) of the forced oscillation tests expressed in frequency domain in:

$$\xi_f = \frac{\omega_2-\omega_1}{2\omega_n} \qquad \textbf{Eq. 4.12}$$

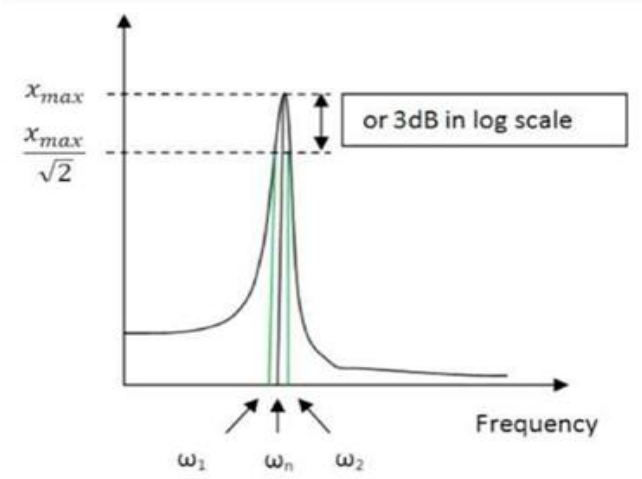

Fig.4.3. Half-power bandwidth method

4.5. Stiffness calculations

Stiffness *k*, in the equation of motion is the effect of the restoring forces and moments is due to the hydrostatic loads and the displacement of a floating structure from its equilibrium state.

A floating structure when at rest in still water will experience hydrostatic pressures on its submerged part, which act normal to the surface of the structure. The forces generated from these pressures have a vertical component, which is equal to the gravitational force acting on the mass of the structure. In other words this force is equal to the displacement weight of the structure. In other directions the hydrostatic force is zero.

The restoring forces and moments can be hydrostatic or elastic. The total force and moments due to the mass of the body plus the external forces such as mooring forces must be in equilibrium at rest. When the floating structure's under water displacement changes by movements in translational or in rotational modes, restoring forces and moments occur to satisfy the static equilibrium.

For floating structures the restoring forces and moments can be related to the translational or rotational displacements with the following matrix equation by

making use of standard naval architectural formulae provided by (Gerritsma & Beukelman, 1967).

$$\begin{bmatrix} f_{h1} \\ f_{h2} \\ f_{h3} \\ f_{h4} \\ f_{h5} \\ f_{h6} \end{bmatrix} = - \begin{bmatrix} 0 & 0 & 0 & 0 & 0 & 0 \\ 0 & 0 & 0 & 0 & 0 & 0 \\ 0 & 0 & \rho g A_W & 0 & 0 & 0 \\ 0 & 0 & 0 & \rho g \nabla GM_T & 0 & 0 \\ 0 & 0 & 0 & 0 & \rho g \nabla GM_L & 0 \\ 0 & 0 & 0 & 0 & 0 & 0 \end{bmatrix} \begin{bmatrix} x_1 \\ x_2 \\ x_3 \\ x_4 \\ x_5 \\ x_6 \end{bmatrix} \quad \textbf{Eq. 4.13}$$

GM_T and GM_L are the transverse and the longitudinal metacentric heights respectively. For cylindrical sections both values are equal and calculated as:

$$GM = KB + BM - KG \quad \textbf{Eq. 4.14}$$

KB is the centre of the immersed volume.

KG is the centre of gravity of the floating structure and;

$$BM = \frac{2}{3} \int_{-\frac{D}{2}}^{\frac{D}{2}} \left(\frac{D}{2}\right)^3 dx / \nabla \quad \textbf{Eq. 4.15}$$

D is the diameter and represents the breadth of the waterline. The integral part of the above equation equals the second moment of the water-plane area, *j*. Therefore:

$$BM = \frac{j}{\nabla} \quad \textbf{Eq. 4.16}$$

From Eq.4.13 it is clear that for unmoored ships the surge stiffness caused by the restoring force is equal to zero. Therefore the surge stiffness is assumed to be the horizontal tension applied on the structure by the mooring lines (Fatlinsen, 1990) which will be discussed in Chapter 5.

4.6. Results and discussion

In order to predict the rigid body motions of a spar according to the methodology presented in this chapter, Mass, damping and stiffness values should be defined, in

addition to the stability index and reference heights. The actual mass of the experimental models and the damping values are measured experimentally. The added mass/inertia of the experimental models in heave and pitch directions are calculated as presented in section 4.3. Results obtained from Eq.4.6 - to Eq.4.9 are presented in Table 4.1.

The half-power bandwidth method was not applicable in case of structure damping identification from the forced oscillation tests, therefore the structure damping in heave and pitch are obtained by the logarithmic decrement method from decay tests as presented in section 4.4. Results obtained from Eq.4.11 are presented in Table 4.2.

Heave and pitch hydrostatic stiffness results obtained from Eq.4.13 are presented in Table 4.3.

Table 4.1: Structure total mass and inertia values in heave and pitch

	Structure Mass & Inertia			
	Heave		**Pitch**	
	Actual mass (kg)	**Added mass (kg)**	**Actual Inertia ($kg.m^2$)**	**Added inertia ($kg.m^2$)**
Model1	2.065	0.502	0.276	0.08
Model2	9.045	4.592	0.5951	0.295

Table 4.2: Structures heave and pitch damping ratios

	Structure Damping Ratios (Log. decrement method)	
	Heave	**Pitch**
Model1	0.056	0.071
Model2	0.070	0.045

Table 4.3: Structure heave and pitch stiffness

	Structure Stiffness	
	Heave (N/m)	**Pitch (N.m/rad)**
Model1	123.27	3.651
Model2	580.62	27.13

Unfortunately, inclining test was performed for the second model only. However, comparison of the calculated and measured parameters of the second model is enough to validate the mathematical model. This comparison is presented in Table 4.4.

Table 4.4: Stability index and reference heights

	Stability Index and Reference Heights (m)			
	Model 1		**Model 2**	
Parameters	**Measured**	**Calculated**	**Measured**	**Calculated**
KG	NA	0.182	0.144	0.146
KB	NA	0.287	NA	0.294
BM	NA	0.010	NA	0.044
GM	NA	0.115	0.191	0.193

From the above data, and assuming uncoupled motions, the natural frequencies of the two experimental models in heave and pitch motions may be determined. Table 4.5 presents the predicted natural frequencies of both models.

Table 4.5: Structure heave and pitch natural frequencies

	Structure natural frequencies (rad/s)	
	Heave	**Pitch**
Model1	6.9	3.1
Model2	6.7	5.6

To validate the mathematical and the numerical methodologies adopted and the primary results obtained above, predicted motions are compared with experimental motion responses of the two reduced scale models (which will be discussed in details in Chapter 9). Comparisons are presented in Fig.4.4 and Fig.4.5.

Note that the numerical model adopted does not include the interaction between the different modes of structure motions and the motion response of the water column since the existence of the water column is ignored at this time. That's why the predicted RAOs are smoother than the measured ones.

Predicted heave response peak is expected to be at 6.9rad/s., unfortunately, due to the time limitations, experimental validation have been performed for a small range of frequencies.

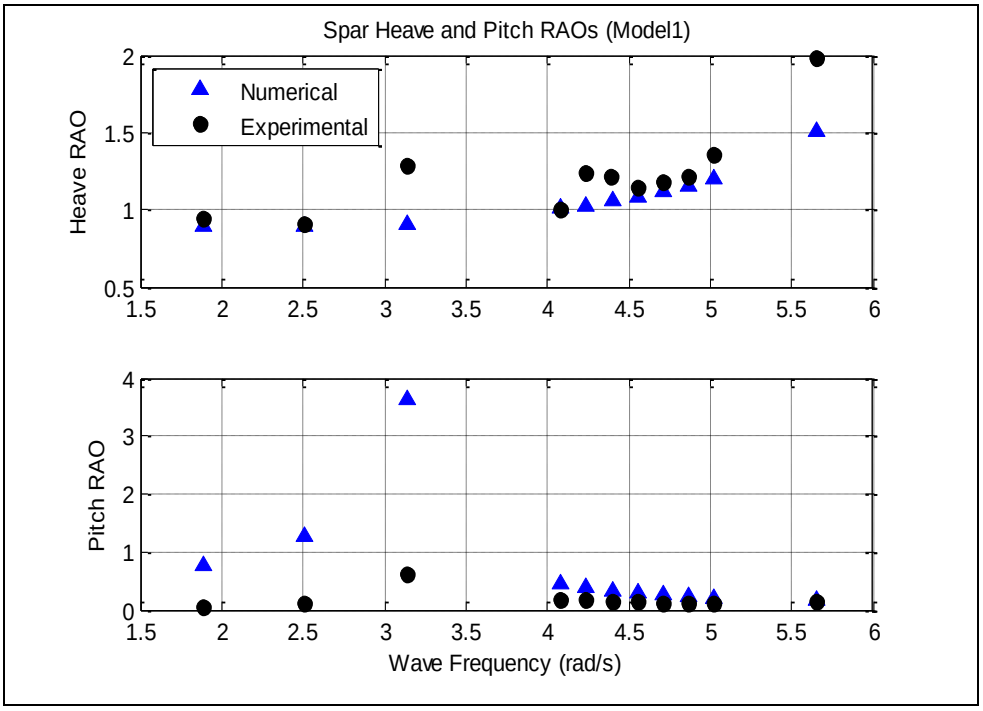

Fig.4.4. Comparison between numerical and experimental heave and pitch RAOs for experimental model1

As we can see in the experimental heave RAO of model1 (Fig.4.4) a slight increase occurs at 4.1rad/s which is the structure natural frequency in real case if the coupling with the inner water column is considered.

Another peak in the heave response appeared and was clearly observable in experimental testing around 3.1rad/s, which is the structure pitch natural frequency. This agrees with Sykes et al., 2009 research results. This increase might be because of the interaction between the pitch motion and the water column oscillations as a free surface.

For experimental model2, the predicted heave response peak is expected to be at 6.5rad/s while for pitch it was found to be 5.6rad/s,

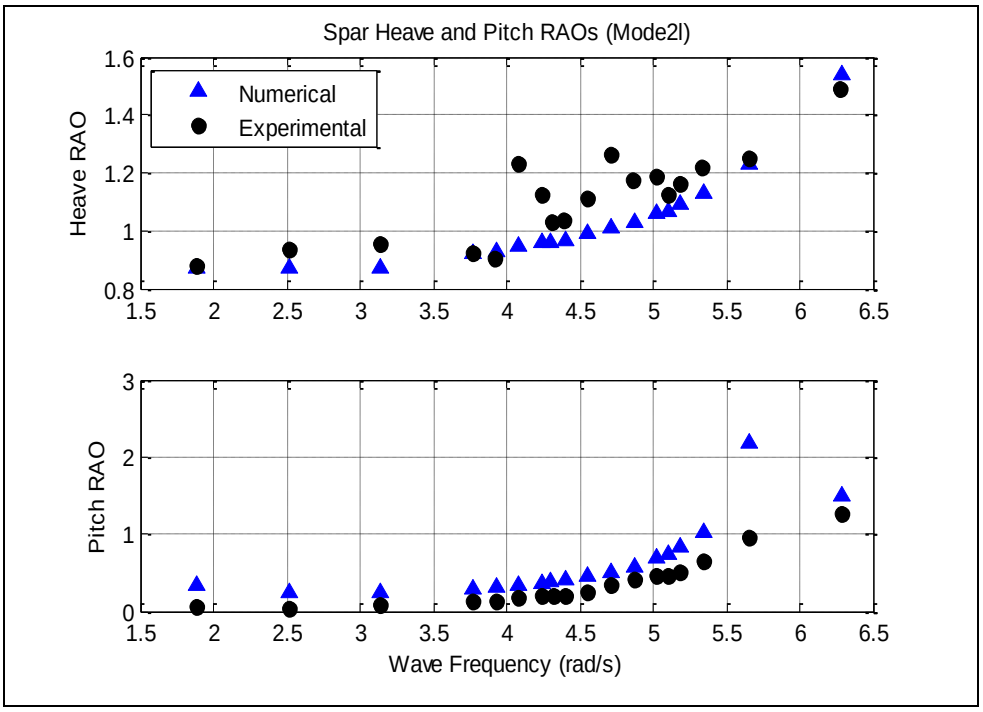

Fig.4.5. Comparison between numerical and experimental heave and pitch RAOs for experimental model2

In Fig.4.5, Experimentally two peaks appear in the measured heave motion response. The first peak corresponds to the structure heave natural frequency in case coupling is considered (at 4.1rad/s) and the second one corresponds to the natural frequency of the water column in captive mode (at 4.8rad/s).

The coupling between the structure heave and water column oscillations will be considered in chapter 6.

A very small increase appeared in the measured pitch RAO of the two models at the water column natural frequency. This could be due the free surface effect of the water column pitching.

Fig.4.4 and Fig.4.5 show that the trends of the numerical results agree with the experimental results. However, it would be expected from the limitations of linear wave theory that best agreement between prediction and experiment would be achieved for the smallest chosen wave amplitude at a given frequency. This is confirmed from the figures.

The clear disagreement between the numerical and experimental pitch results around the resonant frequencies for both experimental models presented in Fig.4.4 and Fig.4.5 is due to the inaccuracy of determining the pitch damping coefficient from the decay tests, in addition to the wave length at low frequency.

Aalbers, 1984 presented a mathematical model to incorporate empiric quadratic damping in order to obtain a satisfactory agreement with model test results.

Linear and quadratic damping coefficient determination will be discussed in chapter 7 in details.

Results obtained by introducing a quadratic damping to the pitch equation of motion are presented in comparison with the results obtained from the viscous damping approach and the experimental results for experimental model 1 & 2 in Fig.4.6 and Fig.4.7 respectively. In the following figures VD and EVD stand for Viscous Damping and Equivalent Viscous Damping approaches respectively.

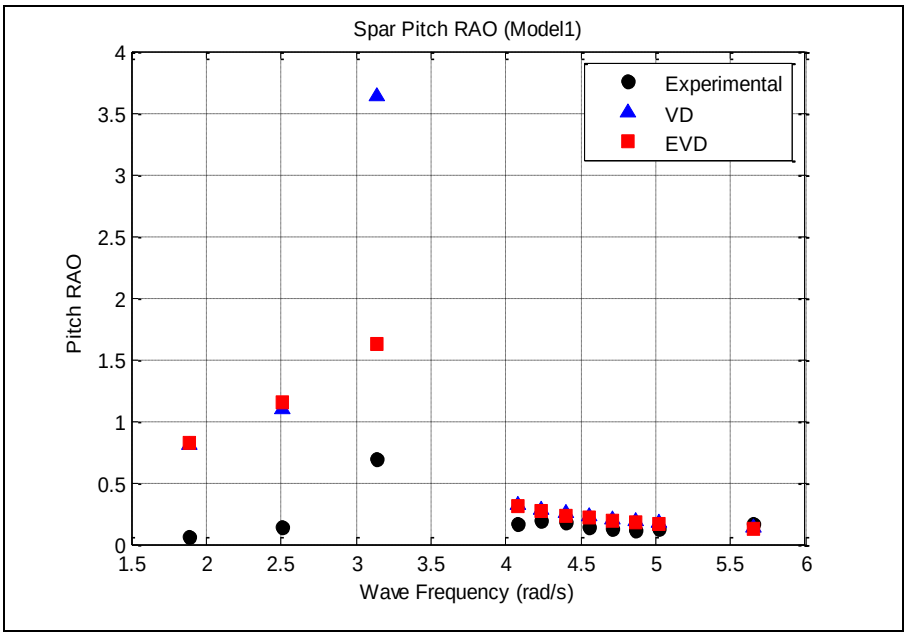

Fig.4.6. Comparison between experimental, viscous Damping and equivalent viscous damping spar pitch RAO for experimental model1

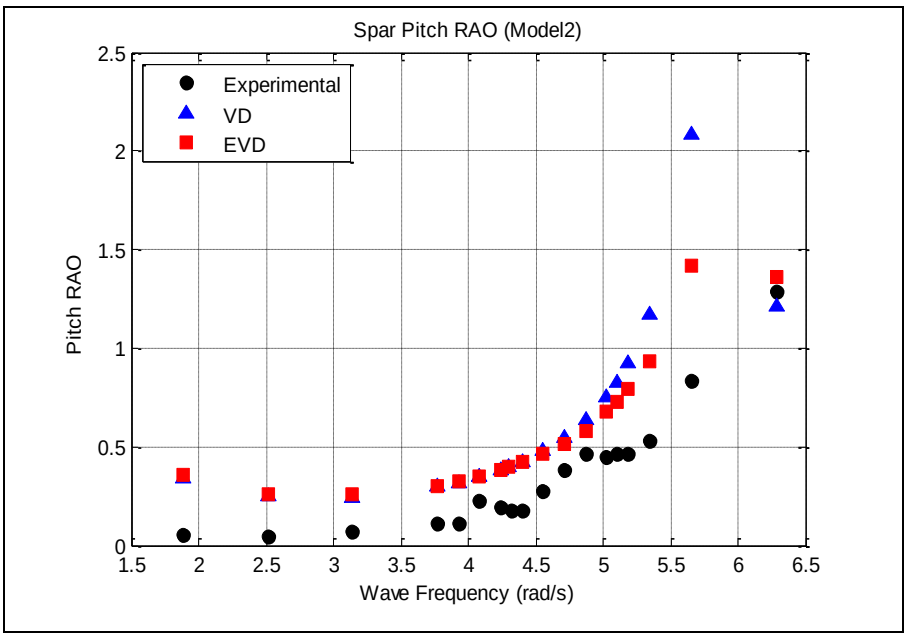

Fig.4.7. Comparison between experimental, viscous Damping and equivalent viscous damping spar pitch RAO for experimental model2

The above figures showed that results of the equivalent viscous damping approach make better agreement with the experimental results of both model especially around the natural frequency.

References of Chapter 4

Aalbers A.B., 1984, 'The water motions in a moonpool', Ocean Engineering Vol. 11 No.6, pp 557-579.

Ankudinov, 1991, 'Hydrodynamic hull damping, Ship structure', Washington DC Report No. SR-1307

Faltinsen, O. M., 1990, **Sea Loads On ships and Offshore Structures**. Cambridge: Cambridge university Press.

Gerritsma, J., Beukelman, W., 1967, 'Analysis of the Modified Strip Theory for the Calculation of Ship Motions and Wave Bending Moment', Netherlands Ship Research Centre: TNO Report No. 96S

Huang Fang-Lin, Xue-Min Wang, Zheng-Qing Chen, Xu-Hui He, Yi-Qing Ni, 2007, 'A new approach to identification of structural damping ratios', Journal of Sound and Vibration, Vol 303, pp 144–153

Incecik, A., 1982, 'Design aspects of hydrodynamic and structural loading on floating offshore platforms under wave excitation', Ph.D. thesis, University of Glasgow, U.K

Sarpkaya T., Isaacson. M., 1981, **Mechanics of Wave Forces on Offshore Structures**, Van Nostran Reinhold Company, New York

Singiresu S. Rao., 1991, **Mechanical Vibration**, Third edition, Addison-Wesley Publishing Company, ISBN 0-201-52686-7

Sphaier S. H., Torres F.G.S, Masetti I.Q., Costa A.P. &Levi C. 2007 Monocolumn behaviour in waves: Experimental analysis. Ocean Engineering Vol. 34, pp 1724-1733

Sykes, R., Lewis, A. & Thomas, G., 2009, 'A hydrodynamic study of a floating OWC', Proceedings of the 8th European Wave and Tidal Energy Conference, Uppsala, Sweden

Chapter 5

Mooring Consideration

5.1. Introduction

In the present chapter mooring systems design approaches and analysis will be discussed. Motion response of structures under wave excitation forces has been discussed in Chapter 4. Mooring system is considered in the present Chapter in order to predict its contribution in the horizontal (surge) motion response of the structure in case of single and multi-catenary mooring lines.

A method to simplify the cross system case is presented as well. This achieved by resolving the lines along two orthogonal directions and introducing an ‘imaginary’ system, where two imaginary mooring lines are opposite each other. Later on static and quasi-static surge motion modelling of a full scale spar will be performed.

5.2. Mooring of wave energy converters

It is essential that offshore vessels/structures have fit-for-purpose mooring systems. The mooring system consists of freely hanging lines connecting the surface platform to anchors or piles on seabed, positioned at some distance from the platform. The mooring lines are laid out, often symmetrically in plan-view around the vessel (Chakrabarti, b.2003).

There are a range of rules, guidelines and regulations for mooring systems published by various authorities (e.g. DNV 2001, API 1997) around the world. The most stringent of these apply to the design, analysis and maintenance regulations for the floating structures of the offshore oil and gas industry. The reasons for this stringency are the risk of substantial loss of life and the danger of environmental pollution Harris et al., (2004).

In contrast, WECs operate unmanned, and there is no danger of major environmental pollution. In addition, installation locations being considered at present for floating WEC devices have depths of over 50 m in unsheltered location with relatively high wave energy density where WECs may be distributed as an array. Therefore the major requirements for a WEC mooring are to hold the device in place without affecting its overall economics and dynamic behaviour Johanning et al., (2006).

The behaviour of the mooring 'springs' can be controlled to fine tune the structure/mooring system behaviour to achieve a specified performance. This can be controlled by the weight of chain or other tension member, scope of chain, placement of sinkers, amount the anchor penetrates the soil, and other parameters (UFC, 2005).

Some WECs perform best when constrained to a minimum surge and sway giving a maximum motion relative to the wave surface. However, it should be recognized that the heave response and tidal change will alter the tension characteristic of the mooring configuration. This is important for WECs operating in shallow water and harsh wave climates

(Hals, 2010) reported that researchers are concerned about how to design efficient devices including structures, machinery and moorings for viable conversion concepts, how to accurately model and assess the loads and stresses on the converters and moorings, how the power absorption is influenced by array and mooring configurations.

In general it is not desirable or practical to moor a floating structures especially WECs rigidly. For example, if a WEC can have a large amount of buoyancy, so it usually must be allowed to move with changing water levels. Otherwise this would

result in higher internal system loadings, particularly at the mooring being attachment points for the WEC, and the frequency response in surge will be higher which may cause dynamic problems.

The use of soft system would result in lower internal system loadings with lower frequency response in surge, but this would allow a wider excursion. It should be recognized that a soft mooring system can allow a floating body to remain relatively stationary with respect to the water surface.

Harris et al., (2004) summarized the requirements that need to be considered for WEC moorings systems:

- The primary purpose of the mooring system is to maintain the floating structure on station within specified tolerances under normal operating load and extreme storm load conditions.
- The excursion of the device must not permit tension loads in the electrical transmission cable(s) and should allow for suitable specified clearance distances between devices in multiple installations.
- The mooring system must be sufficiently compliant to the environmental loading to reduce the forces acting on anchors, mooring lines and the device itself to a minimum; unless the stiffness of the mooring itself is an active element in the wave energy conversion principle used.
- All components must have adequate strength, fatigue life and durability for the operational lifetime, and marine growth and corrosion need to be considered.
- A degree of redundancy is highly desirable for individual devices, and essential for schemes which link several devices together.
- The system as a whole should be capable of lasting for 30 years or more, with replacement of particular components at no less than 5 years.
- The mooring must be sufficient to accommodate the tidal range at the installation location.
- The mooring system should allow the removal of single devices without affecting the mooring of adjacent devices.

- Removal of mooring lines for inspection and maintenance must be possible.
- The mooring must be sufficiently stiff to allow berthing for inspection and maintenance purposes.
- Contact between mooring lines must be avoided.
- The mooring should not adversely affect the efficiency of the device, and if it is part of an active control system it must also be designed dynamically as part of the overall WEC system.

Furthermore, Harris et al., (2004) studied different mooring configuration and their suitability for wave energy converters (presented in Table 5.1), and concluded that free hanging catenary or multi-catenary moorings and CALM or SALM single point moorings appear the most favourable options at present as they have well established design criteria and relatively moderate installation costs. However, the suitability of a free hanging catenary mooring, a multi-catenary mooring or a combination of both has to be carefully evaluated in the context of the stiffness requirements of a WEC.

Their research also concluded that mooring line material and anchors should be selected in the context of the seabed condition, mooring configuration, design specification of the WEC and the costs (Table 5.2). Considerable cost differences can be identified between chain, wire ropes and synthetic ropes, but there are factors other than breaking load that must be considered in the overall system design. The choice for a mooring line material would be more likely to be based on physical attributes and technical issues rather than cost. The main technical considerations of a mooring line will be its performance in respect to its reliability and stiffness characteristics.

Concerning the anchors, the seabed condition itself could dictated a specific anchor type or allow a choice of anchor type installations. This becomes obvious for a rocky seabed where embedment would not be an option. The cost of installing a particular anchor could be significant and could negatively influence the choice of a location and/or mooring configuration.

Table 5.1: Mooring configurations and their suitability for wave energy converters (Harris et al., 2004)

Mooring Configuration	Characteristics	Suitability for WEC
Spread Moorings		
Catenary Mooring	The mooring lines of a free hanging Catenary Mooring arrive horizontal to the seabed so that the anchor point is only subject to horizontal forces. The restoring forces are mainly generated by the weight of the mooring lines returning the system to equilibrium.	High
Multi-Catenary Mooring	The catenary mooring lines incorporate weights and buoys to form S- or Wave type configurations. Steep and lazy touch down points are possible.	High
Taut Spread Mooring (Tethered Mooring)	The mooring lines of a Taut Spread Mooring arrive, typically at an angle to the seabed with the anchor point capable of resisting horizontal and vertical forces. The restoring forces are mainly generated by the elasticity of the mooring line. The mooring lines of a TLP are orthogonal to the seabed, with the restoring force mainly generated by the change in buoyancy of the topside structure.	Low
Single Point Mooring		
Turret Mooring	An internal or external catenary moored turret attached to a floating structure allows weathervaning around the turret.	Low
Catenary Anchor Leg Mooring (CALM)	The floating structure is moored to a catenary moored buoy and is able to weathervane around the moored buoy.	High
Single Anchor Leg Mooring (SALM)	The floating structure is moored to a single anchored taut buoy and is able to weathervane around the moored buoy.	High
Articulated Loading Column (ALC)	A moored floating structure can weathervane around a bottom hinged column, which has a swivel above the water line.	Medium
Single Point mooring And Reservoir (SPAR)	A catenary anchored SPAR buoy allows the storage of a medium (oil, hydrogen) and a floating structure to weathervane around a mooring point.	Medium
Fixed Tower Mooring	A fixed tower anchored into the seabed allows the moored floating structure to weathervane around the mooring point.	Medium
Dynamic Positioning		
Active Mooring	The technique for the Active Mooring consist of mooring lines which are spread around the floating structure, where the inboard end of each mooring line is held by a servo controlled winch. A central computer tensions or loosens the mooring lines in order to keep a fixed seabed position.	Low
Propulsion	The technique consists of positioning a floating structure above a fixed seabed point by the use of propellers or thrusters which are controlled from a central computer.	Low

Table 5.2: Mooring components and relative costs (Harris et al., 2004)

Mooring Components	Characteristics	Costs
Mooring line		
Chain	Depending on required proof strength Grade 3, 3S or 4 should be used for offshore moorings. Chains provide a good catenary stiffness effect and have good abrasion and bending properties. Suitable for long term moorings but require regular inspections.	Medium
Wire Rope	Spiral Strand, Six Strand and Multi-Strand wire ropes available but only the Spiral Strand is suitable for long term mooring. Due to the elasticity of wire ropes it can be used in tensioned mooring applications. Extreme bending must be avoided.	Low
Synthetic Rope	Typical fibre ropes are Polyester, Aramid, HMPE or Nylon ropes. The weight of the ropes in water is around zero allowing them to be close to neutrally buoyant or buoyant. The weight and elasticity properties make them more common for very deep water tether applications. Short term experience in real conditions results in a high safety factor being applied. Considerable change in axial stiffness after installation requires re-tensioning. Axial compression and hysteretic heating at extreme storm condition needs to be avoided and fishbites can be a problem.	High
Anchor		
Gravity Anchor	Horizontal holding capacity is generated by dead weight providing friction between seabed and anchor.	Medium
Drag-Embedment Anchor	Horizontal holding capacity is generated in the main instalment direction by the embedment of the anchor in the ground.	Medium
Driven Pile / Suction Anchor	Horizontal and vertical holding capacity is generated by forcing a pile mechanically or from a pressure difference into the ground, providing friction along the pile and the ground.	High
Vertical Load Anchor	Horizontal and vertical holding capacity is generated due to a specific embedment anchor allowing loads not only in the main instalment direction.	High
Drilled and Grouted Anchor	Horizontal and vertical holding capacity is generated by grouting a pile in a rock with a pre-drilled hole.	High

5.3. Catenary mooring lines

Fig.5.1 shows a catenary mooring line deployed from point A (fairlead) on the submerged hull of a floating vessel to point B at the anchor on the seabed. A part of the mooring line between A and B is resting on the seabed, the horizontal distance between points A and B is 5-20 times the vertical distance between the same two points.

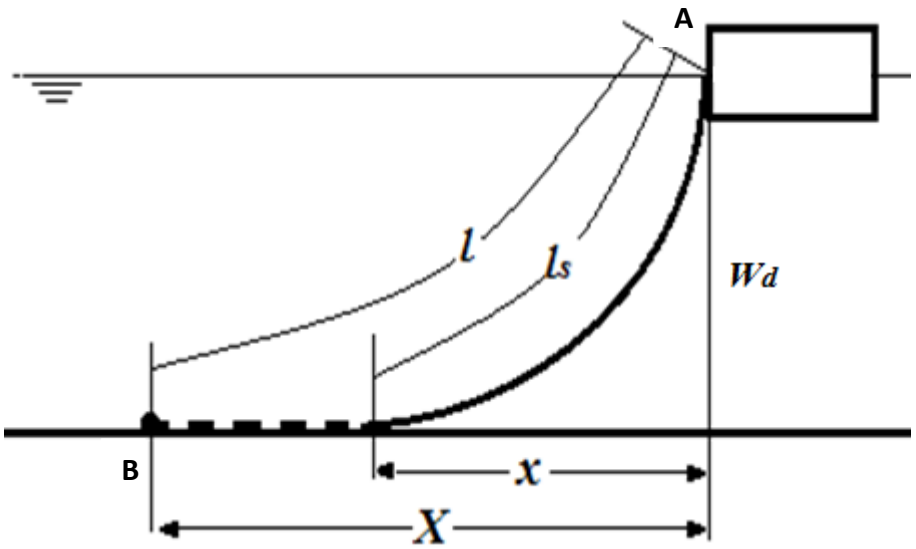

Fig. 5.1. Single catenary mooring line

From a static point of view, the cable tension in point A is due to the total weight in sea water of the suspended line length. The progressive effect of line lift-off from the seabed due to the horizontal movement of the vessel increase/decrease line tension at point A. this feature coupled with the simultaneous decrease/increase in line angle with the horizontal causes the horizontal restoring force on the vessel to increase/decrease with vessel offset in a nonlinear manner (Chakrabarti, b.2003). This behaviour can be described by the following procedure.

The axial tension T_a in the line can be found from the horizontal T_H and vertical T_V tension force component at the fairlead as:

$$\boldsymbol{T_a = \left(T_H^2 + T_V^2\right)^{1/2}} \qquad \textbf{Eq. 5.1}$$

The angle to the horizontal made by the line at the fairlead can be found from the horizontal tension T_H and the line tension T at fairlead in the form:

$$\boldsymbol{\cos \varphi = \frac{T_H}{T}} \qquad \textbf{Eq. 5.2}$$

If a mean horizontal force is applied to a moored floating object, the horizontal distance X between the anchor and the fairlead may be written as a function of the total mooring line length l, the suspended (lifted) mooring line length l_S and the corresponding scope x as:

$$\boldsymbol{X = l - l_S + x} \qquad \textbf{Eq. 5.3}$$

l_S may be found from the inelastic catenary equations as:

$$\boldsymbol{l_S = a \sinh\left(\frac{x}{a}\right)} \qquad \textbf{Eq. 5.4}$$

$$\boldsymbol{a = \frac{T_H}{w}} \qquad \textbf{Eq. 5.5}$$

where,

w is the submerged weight per unit length

5.4. Mooring system design approaches

5.4.1. Static approach

It is usually carried out at early stages of mooring system design. Load excursion curve in case of single catenary line and reaction curves in case of multi-lines are established ignoring fluid forces on the lines. In this approach it is assumed that mooring stiffness is equal to the tension force in mooring lines.

The maximum dynamic offset caused by the waves and drift frequency effects is then estimated. Certifying authority standards give guidance on this. The static method has the disadvantage that conservative assumptions are made in terms of the unidirectional environment and large safety factors need to be applied to account for uncertainties. Furthermore important features of the dynamics are absent from the methodology (Chakrabarti, b.2003).

5.4.2. Quasi-static approach

This procedure is the next level of complexity; generally one of the two types of calculations is carried out:

- A time domain simulation that allows for the wave induced vessel force and responses at wave and drift frequency, while treating wind and current forces as being steady and using the stiffness curves without considering line dynamics (this approach was adopted after determining the reaction curves).
- A frequency response method where the stiffness curve is treated as a linear and low frequency dynamic response to both wave drift and wind gust effects are calculated as if for a linear single DOF system

The basic differences between the static and quasi-static approaches are that:

- The quasi-static analysis is usually nonlinear in that the catenary stiffness at each horizontal offset is used within the equation of motion.
- The equations of motion are integrated in time domain. The influence of added mass and damping are included.
- Frequency domain solutions are possible but major assumptions associated with linearization of stiffness and damping are to be made.

A computer package especially developed for sea-keeping mooring systems will be highlighted in section 5.8.

5.4.3. Dynamic approach

Full dynamic analysis are regularly utilised in design, though there is no universal agreement in the values of mooring line damping. This can influence vessels responses and loads strongly.

Dynamic simulations use lumped mass finite element or finite difference schemes to model small segments of each line whose shape is altered from the static

catenary profile. Analysis is performed in time domain and it is computationally intensive. Difficulties associated with the adoption of the dynamic approach are:

- Time steps must be small so that the wave-induced line oscillations are included.
- Runs must be long to allow for the vessel drift oscillation period, which in deep water may be more than 15 minutes.
- For a typical vessel mooring design, the weather is multi-directional and a number of test cases must be considered.

5.5. Single catenary mooring analysis

For a preliminary static approach only, the horizontal displacement in surge (sway) needs to be considered as discussed in API RP 2SK by the American Petroleum Institution Johanning et al., (2006).

The relationship between the excursion of the structure and the horizontal loads applied on it may be found by plotting the load excursion curves. The load excursion curve for a particular line can also be used to identify the horizontal displacement or surge caused by a change in the horizontal loading.

Assuming that the fairlead connection is at the water surface, the horizontal scope for the inelastic case can be expressed as:

$$\boldsymbol{X = l - w_d\left(1 + 2\frac{a}{w_d}\right)^{1/2} + a\ \cosh^{-1}\left(1 + \frac{w_d}{a}\right)} \qquad \textbf{Eq. 5.6}$$

This basic formulation (Eq.5.6) can be used to plot the load excursion curve by applying a range of horizontal forces that are to be expected on the WEC at the installation location, for specific mooring line length , submerged weight per unit length and water depth (Fatlinsen, 1990).

5.6. Multi-catenary mooring (Spread Mooring)

Spread mooring system will have more than one mooring line. This arrangement of moorings is especially useful for securing permanently or semi-permanently moored structures (UFC, 2005) and likely to be adopted for most WECs (Johanning et al., 2006). The relationship between horizontal tension and surge displacement can be represented in the form of 'reaction curves' for pairs of opposed lines. This approach can also be used for a set of four lines when they form mutually orthogonal pairs, provided the surge displacements are small compared with the line lengths.

In contrast to a single line, no direct link between surge and the external horizontal loading can be made for two lines opposite each other. In this case, the load excursion curve is not represented through the horizontal tension of an individual line and the resultant surge, but through the horizontal external loading and the resultant surge (Johanning et al., 2006).

Considering a mooring system consists of two opposite lines with line *A* facing the incoming force and line *B* on the lee side. Therefore the external force will increase the horizontal tension in line A and reduce the horizontal tension in line B. The external loading or the resultant horizontal tension can be expressed in the form:

$$\boldsymbol{T_{ext} = T_{HA} - T_{HB}} \qquad \textbf{Eq. 5.7}$$

For this reason, the reaction curve in this case is represented by the horizontal external loading and the resultant surge as a dotted line on the over the load excursion curves. The equilibrium position, with no external loading is indicated with the crossing point of the surge–tension curves (load excursion curve of each line).

5.7. Cross system

In case of cross system (the general case), where there are not mutually orthogonal pairs of opposed lines, the approach described above must be modified. This is

achieved by resolving the lines along two orthogonal directions and introducing an 'imaginary' system, where two imaginary mooring lines are opposite each other in each of the *x* and *y* directions. Using simple geometry, the properties for the real mooring lines can be resolved into components to form the imaginary mooring lines. In the simple preliminary design approach here, it is assumed that the surge is sufficiently small that the line direction remains essentially unchanged.

Assuming an external loading F_{ext} is applied to a structure at an angle β with the x-axis, the corresponding force in the x-direction is $F_x=F_{ext}\ cos\ \beta$, and the corresponding force in the y-direction is $F_y=F_{ext}\ sin\ \beta$. The resultant forces for the *x*- and *y*- direction can then be used to produce a reaction curve for the imaginary lines *A* and *B* in each direction, by proceeding in the same manner as described above in section 5.6

The resultant real value for surge, and the real values for the line tension, horizontal tension, vertical tension, horizontal scope, lifted line length, and horizontal distance, for the individual lines, can be found by simple geometrical resolution into the *x*- and *y*-directions (Johanning et al., 2006).

5.8. Finite element approach for mooring analysis

Recently several marine dynamics computer programs have been published for research and industrial uses.

OrcaFlex is a marine dynamics program developed by Orcina for static and dynamic analysis of a wide range of offshore systems, including all types of marine risers (rigid and flexible), global analysis, moorings, installation and towed systems. OrcaFlex provides fast and accurate analysis of catenary systems such as flexible risers and umbilical cables under wave and current loads and externally imposed motions. OrcaFlex makes extensive use of graphics to assist understanding. The program can be operated in batch mode for routine analysis work and there are also special facilities for post-processing your results including fully integrated fatigue analysis capabilities.

OrcaFlex is a fully 3D non-linear time domain finite element program capable of dealing with arbitrarily large deflections of the flexible from the initial configuration. A lumped mass element is used which greatly simplifies the mathematical formulation and allows quick and efficient development of the program to include additional force terms and constraints on the system in response to new engineering requirements. In addition to the time domain features, modal analysis can be performed for individual lines and RAOs can be calculated for any results variable using the Spectral Response Analysis feature. OrcaFlex is also used for applications in the Defence, Oceanography and Renewable energy sectors. OrcaFlex is fully 3D and can handle multi-line systems, floating lines, line dynamics after release, etc. Inputs include ship motions, regular and random waves. Results output includes animated replay plus full graphical and numerical presentation (OrcaFlex manual).

In this research OrcaFlex is used to perform Multi-static (Quasi-static) analysis for a spar moored by two orthogonal lines. The installation properties are similar to those presented in (Johanning et al., 2006).

5.9. Results and discussions

In order to predict the surge behaviour of the Sparbuoy OWC, the methodologies presented in this chapter are applied to a full scale structure (scale 1:100 of experimental model1).

Load excursion curve is obtained analytically by applying a range of horizontal forces that are to be expected on the WEC at the installation location, for specific mooring line length, submerged weight per unit length and water depth. For single catenary mooring line, the solution of Eq.5.6 is presented in Fig.5.2.

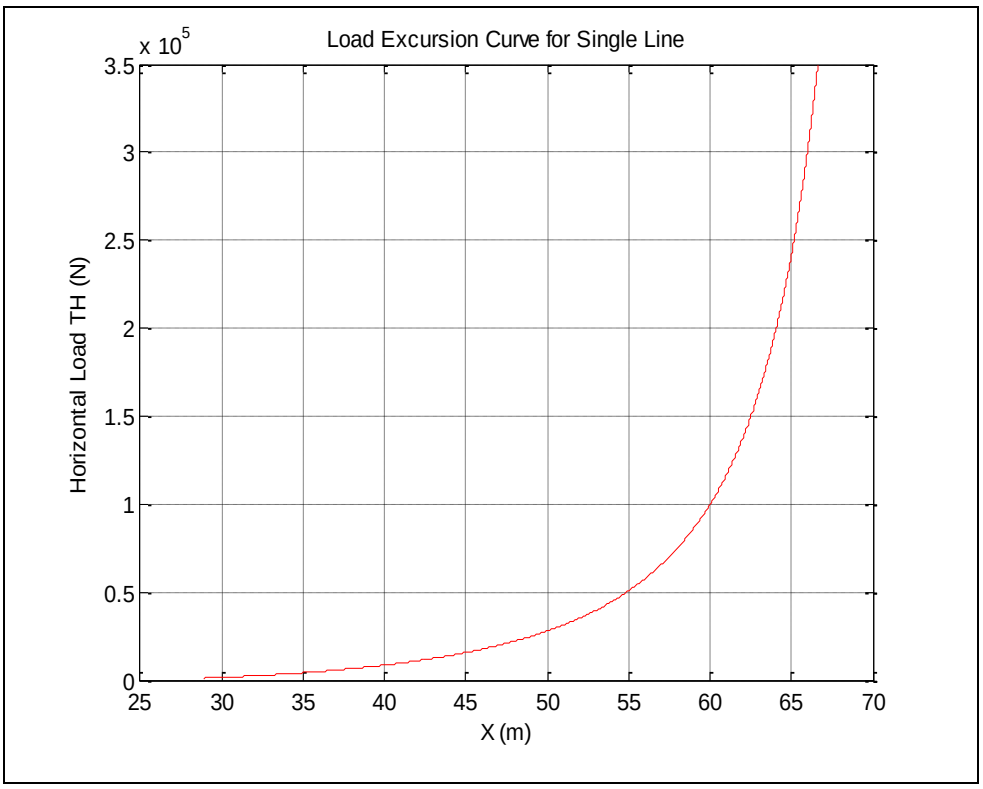

Fig.5.2. Load excursion curve for single catenary mooring line, installation properties: w_d=50m, l=75m and w=918.75N/m

Considering a mooring system consists of two opposite lines with line A facing the incoming force and line B on the lee side. The external force will increase the horizontal tension in line A and reduce the horizontal tension in line B. the crossing point of the surge–tension curves for the two lines depends on the horizontal pre-tension. In this case the reaction curve is plotted using Eq.5.7 over the load excursion curves. Load excursion curve and reaction curves for different horizontal pre-tension are presented in Fig.5.3.

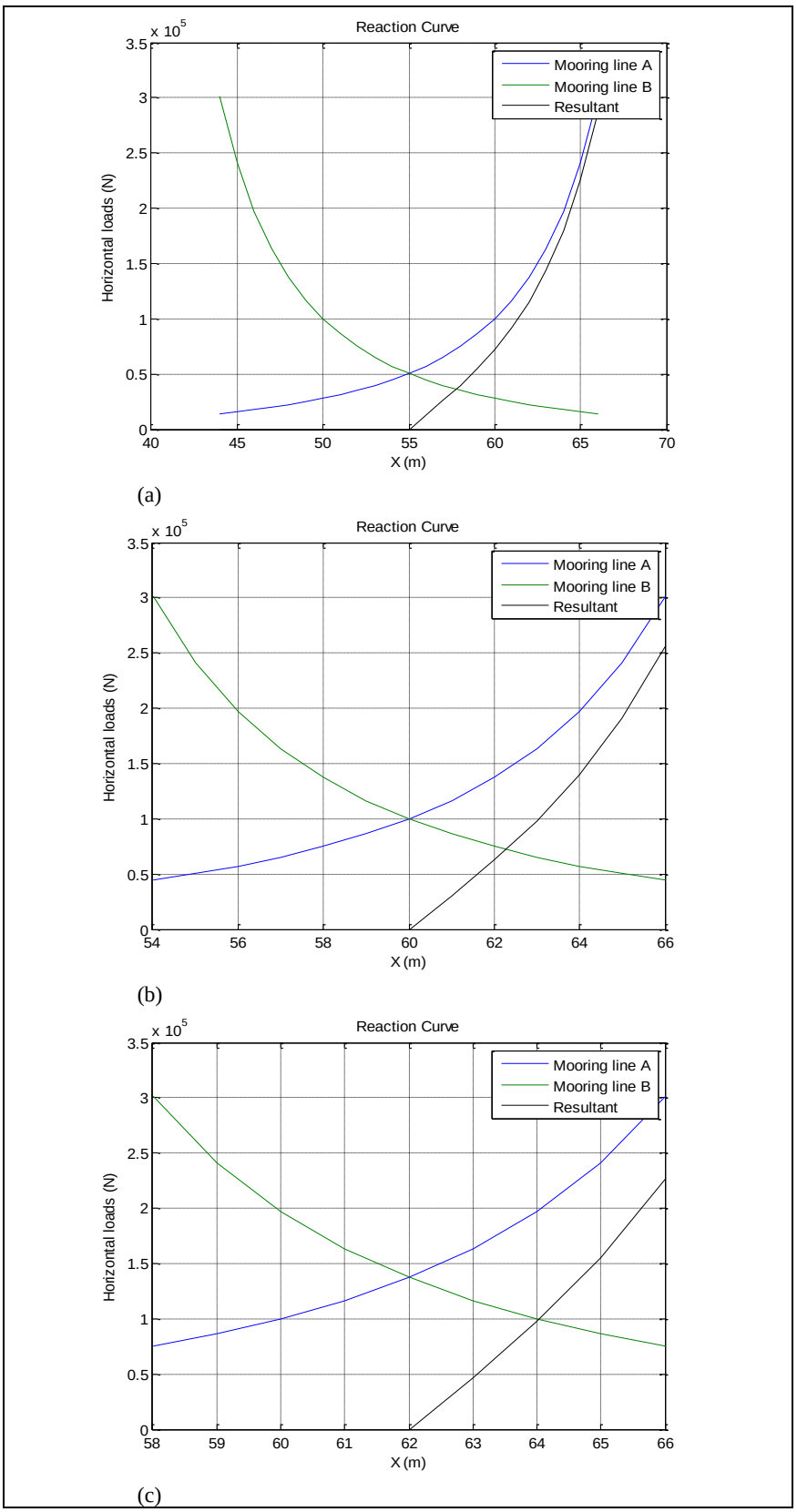

Fig.5.3. Load excursion and reaction curves for two opposite catenary mooring lines, installation properties w_d=50m, l=75m and w=918.75N/m, (a) Pre-T = 50kN (b) Pre-T = 100kN (c) Pre-T = 140kN

In order to validate the analytical rsults obtained a 2D Multi-static modelling have been performed using OrcaFlex. A snapshot of the model is presented in Fig.5.4.

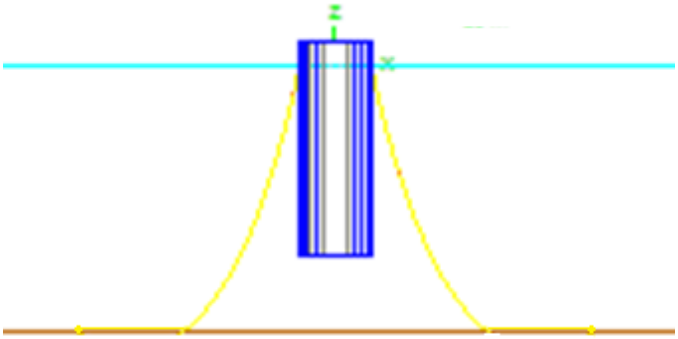

Fig.5.4. Snapshot of spar used in OrcaFlex modelling

Total restoring force obtained from the finite element model is compared to those obtained analytically in Fig.5.5.

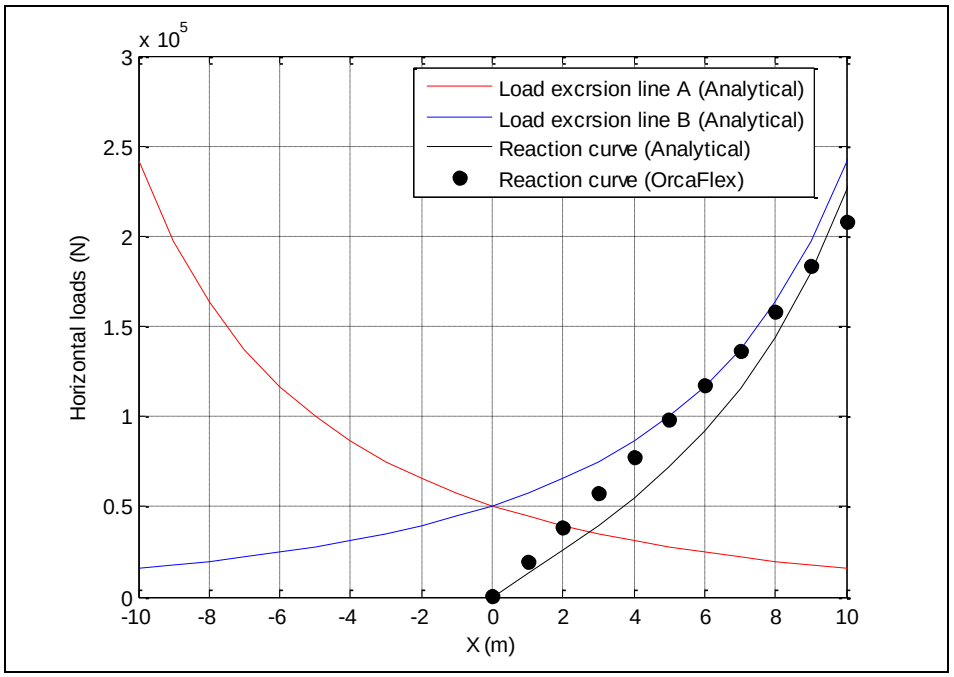

Fig.5.5. Comparison between analytical and finite element reactions curves for two opposite catenary mooring lines, installation properties w_d=50m, l=75m and w=918.75N/m, Pre-T = 50kN

Fig.5.5. showed very good agreement between the predicted results using different approaches. It was important to plot both curves to perform static and quasi-static surge modelling for moored structure. In both approaches approach it is assumed that

mooring stiffness is equal to the tension force (resultant) in mooring lines. Constant line stiffness has been used for static modelling while reaction curve obtained has been used to estimate the instant resultant mooring line tension at different offsets. Fig.5.6 and Fig.5.7 presents static and quasi-static modelling of full-scale SparBuoy structure surge motion equipped with two opposite catenary mooring lines one facing the incoming force and the other is on the lee side.

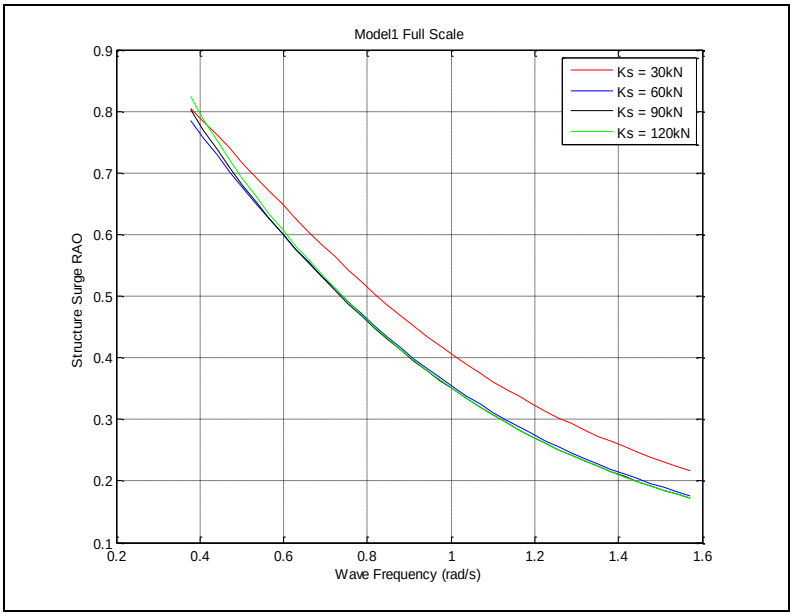

Fig.5.6. Comparison between structure surge RAO vs. wave frequency for different mooring line stiffness, using time domain static approach

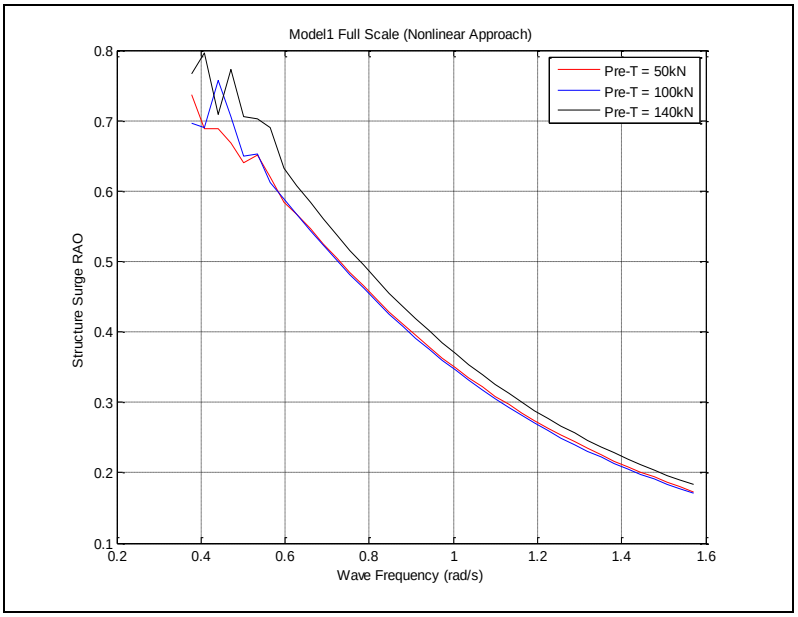

Fig.5.7. Comparison between structure surge RAO vs. wave frequency for different horizontal mooring line pre-tension, using time domain quasi-static approach

Results presented in this chapter agree with (Johanning et al, 2006) results. It is noticed that surge RAO obtained from quasi-static modelling (Fig.5.7) does not show big discrepancies than RAO obtained from static approach (Fig.5.6) except for frequencies below 0.6rad/s in case of quasi-static modelling.

References of Chapter 5

American Petroleum Institute Recommended Practice for Design and Analysis of StationkeepingSystems for Floating Structures. API RP 2SK Standard, API Stock No. G02SK2, 1997, USA

Chakrabarti, S., 2005b, **Handbook of Ocean Engineering vol. 2**. Plainfield: Elsevier

Det Norske Veritas, 2010, Gloabal Performance Analysis of Deepwater Floating Structures. Retrieved 09 15, 2012, from DNV Exchange: http://exchange.dnv.com/publishing/Codes/ToC_edition.asp#Offshore%20Standards

Det Norske Veritas, 2010, Position Mooring. Retrieved 04 15, 2012, from DNV Exchange:http://exchange.dnv.com/publishing/Codes/ToC_edition.asp#Offshore%20Standards

Faltinsen, O. M., 1990, **Sea Loads On ships and Offshore Structures**. Cambridge: Cambridge university Press.

Hals Jørgen, 2010, 'Modelling and phase control of wave-energy converters', PhD. Thesis Norwegian University of Science and Technology, Norway

Harris, R. E., Johanning, L., and Wolfram, J, 2004, 'Mooring systems for wave energy converters: a review of design issues and choices'. 3rd International Conference on Marine Renewable Energy, Blyth, UK 07–09.

Johanning L., Smith G H, and Wolfram J., 2006, 'Mooring design approach for wave energy converters', Proc. IMechE Vol. 220 Part M: J. Engineering for the Maritime Environment

Unified Facilities Criteria (UFC), 2005, **DESIGN: MOORINGS**, UFC 4-159-03, USA

Chapter 6

Linear Modelling of Oscillating Water Column

6.1. Introduction

Unlike conventional offshore structures and ships mathematical model where the wave loading on the structure and the ship response to certain sea conditions that are of interest; researchers are more concerned about the performance of the power conversion process in case of WECs

Jefferys (1980) and Brendmo et al. (1996) presented in their papers the power flows between the OWC components and the corresponding information flows, in addition to the basic models used to describe the OWC, the limitation for applying each model and the transformation from one model to another.

The general model used to describe the OWC is the so-called applied-pressure (or pressure distribution) description, where the power input to the air chamber may be obtained in terms of the air pressure fluctuation and the air volume flux in the chamber above the interior water surface. Models based on applied-pressure description are valid for a wide range of frequencies and valid also if the shape of the interior water surface is changing.

The alternative rigid-piston model (spring-mass-damper model) adopted in this research is also applicable if the wavelength is large compared to the horizontal extension of the interior water surface (low frequency), in this case it is assumed that the surface of the water column remains plane and then may be considered to be a rigid piston (heaving body). The errors introduced by this approximation are

negligible. The power input to the air chamber may then be obtained in terms of the net wave force acting on the interior water surface and the vertical velocity of this surface.

Obviously, mechanical and electrical analogy of OWC system provided simple and efficient modelling tool allowing the study of the system from different prospective. Moreover, mechanical modelling provides easy test for the phase and amplitude conditions.

6.2. Dynamic model of OWC

Following the rigid piston model, captive OWC is best described by considering a single translational mode in heave direction. For offshore OWC the dynamic coupling of the water column and the floating structure is very important to achieve the desired efficiency and therefore the system is described by considering two translational modes in heave direction.

6.2.1. Captive OWC

The water column oscillations in captive OWC is modelled as a single DOF system illustrated in Fig. 6.1(a)

M_2 represents the total mass (mass and added mass) of the water column

b_2 is the damping coefficient of the water column and the PTO mechanism

k_2 is the stiffness due to air compression and hydrostatic effects of the water column

$F_{2TY} \cos(\omega t)$ is the vertical wave force acting on the water column

$y_2, \dot{y}_2, \ddot{y}_2$ are the displacement, velocity, and acceleration of the water column.

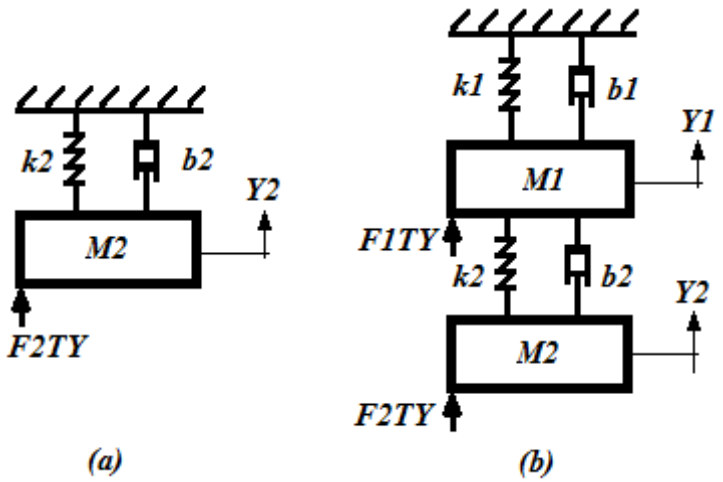

Fig.6.1. Dynamic model of (a) Captive and (b) floating OWC (simplified 2DOF model)

The equation of motion used to describe the water column oscillations in captive OWC assuming viscous damping is:

$$\boldsymbol{M_2\ddot{y}_2 + b_2\dot{y}_2 + k_2y_2 = F_{2TY}\,cos(\,\omega t)} \qquad \textbf{Eq. 6.1}$$

6.2.2. Floating OWC

In this research two different dynamic models will be used to describe floating OWC and will be referred to in the text as *simplified 2DOF model* and *Szumko model* respectively.

The simplified 2DOF model is presented in Fig. 6.1(b), where,

M_1 is the mass and the added mass of the structure (buoy, tube and collar)

b_1 is the damping coefficient of the structure

k_1 is the structure hydrostatic stiffness in heave mode

$F_{1TY}\,cos\,(\omega t)$ is the vertical wave force acting on the structure

$y_1, \dot{y}_1, \ddot{y}_1$ are the displacement, velocity, and acceleration of the structure.

The coupled equations of motion used to describe the system are:

$$\boldsymbol{M_1\ddot{y}_1 + (b_1 + b_2)\dot{y}_1 + (k_1 + k_2)y_1 - b_2\dot{y}_2 - k_2y_2 = F_{1TY}\,cos(\omega t)} \qquad \textbf{Eq. 6.2}$$

$$\boldsymbol{M_2\ddot{y}_2 + b_2\dot{y}_2 + k_2y_2 - b_2\dot{y}_1 - k_2y_1 = F_{2TY}\,cos(\omega t)} \qquad \textbf{Eq. 6.3}$$

The second model used to describe floating OWCs is originally proposed by Szumko (1989) and recently adopted by Folley & Whittaker (2005) and Stappenbelt & Cooper (2010) is presented in Fig. 6.2. In this model, it must be noted that the turbine damping is modelled by the linear damping parameter separately, not in conjunction with the water column damping as in the former model. In addition, the air compressibility is also modelled by the linear stiffness separately not in conjunction with the hydrostatic stiffness of the water column. In other words the PTO damping and air compressibility are related to the relative velocity and displacement between the two masses.

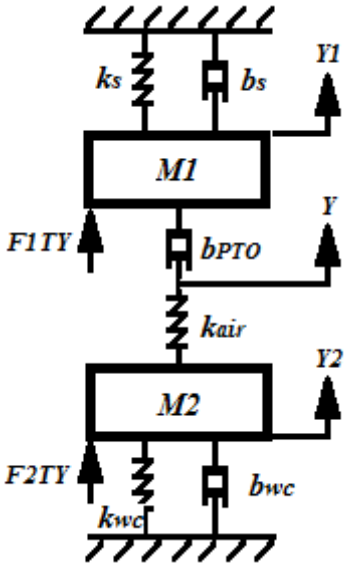

Fig.6.2. Szumko (1989) dynamic model of floating OWC

The coupled equations of motion of the system are:

$$\boldsymbol{M_1\ddot{y}_1 + b_s\dot{y}_1 + b_{PTO}(\dot{y}_1 - \dot{y}) + k_sy_1 = F_{1TY}\,cos(\omega t)} \qquad \textbf{Eq. 6.4}$$

$$\boldsymbol{b_{PTO}(\dot{y} - \dot{y}_1) + k_{air}(y - y_2) = 0} \qquad \textbf{Eq. 6.5}$$

$$\boldsymbol{M_2\ddot{y}_2 + b_{wc}\dot{y}_2 + k_{wc}y_2 + k_{air}(y_2 - y) = F_{2TY}\,cos(\omega t)} \qquad \textbf{Eq. 6.6}$$

where

b_s, b_{wc}, and b_{PTO} represent the structure, water column and PTO damping respectively

k_s, k_{wc}, and k_{air} represent the structure hydrostatic, water column hydrostatic and air compressibility stiffness respectively.

6.3. Assumptions

The assumptions made in these models are quite similar to those assumed by (Gervelas et al., 2011; and Nunes et al, 2011) in their researches:

a) Only waves with small amplitude are considered and linear theory is adopted. Linear wave theory allows the system dynamics to be represented in the frequency domain, with the associated powerful tools of linear superposition and Fourier analysis (Folley & Whittaker, 2005).
b) The added mass and added inertia of the water column and the structure are assumed to be frequency independent.
c) The air inside the device is treated as an ideal gas; the processes of filling and emptying the chamber are assumed to be isentropic and compressibility is considered.
d) The total force acting on the structure is obtained by summing the forces on each volume element and forces are assumed to be concentrated in the centre of these volume elements.

6.4. Calculations

6.4.1. Total masses

The actual mass of the structure was measured experimentally while the mass of the water column was assumed to be a solid vertical cylinder, with a mass equal to the cylinder of water from the bottom of the tube to the internal still water level. Since

the added mass was assumed to be frequency independent, the added vertical mass M_{avm} per unit length of cylindrical bodies is calculated as:

$$\boldsymbol{m_{avm} = \frac{4}{3}\,\rho\left(\frac{D}{2}\right)^3} \qquad \textbf{Eq. 6.7}$$

The total mass of the water column, M_2 consists of the mass and added mass of the water column:

$$\boldsymbol{M_2 = M_{wc} + M_{avm,wc}} \qquad \textbf{Eq. 6.8}$$

The total mass of the structure, M_1 is the sum of mass of the buoy, tube and collar with their added masses:

$$\boldsymbol{M_1 = M_s + M_{avm,s}} \qquad \textbf{Eq. 6.9}$$

6.4.2. Damping

Damping in conventional OWC consists of two parts: the turbine damping which extracts the energy from the system and the damping of the water column itself due to the wave damping.

The device geometry and the PTO damping are very important to govern the OWC damping which is crucial parameter in synchronizing the wave frequency and the natural frequency of the water column to achieve the desired performance, in addition to the structure and mooring lines damping in case of offshore OWC to tune the device motions. The optimum damping should be targeted during the plant design to ensure maximum power absorption (Thiruvenkatasamy, 1998).

In the study herein damping values were determined experimentally from forced oscillation and decay tests of the structure and water column. PTO damping was modelled experimentally by orifices plate on the top of the OWC tube. Damping identification techniques were explained in details in Chapter 4. Models including nonlinear damping will be discussed in Chapter 7.

6.4.3. Stiffness

The air compressibility inside the pneumatic chamber is modelled mechanically by a linear spring separately or in conjunction with the water column hydrostatic stiffness corresponding to its water plane area.

The hydrostatic stiffness of the structure and the water column are calculated as:

$$\boldsymbol{k_s = \rho\, g\, A_s} \qquad \textbf{Eq. 6.10}$$

$$\boldsymbol{k_{wc} = \rho\, g\, A_{wc}} \qquad \textbf{Eq. 6.11}$$

Where A_s and A_{wc} are the water plane area of the structure and the water column respectively.

The pneumatic stiffness may be expressed in term of air properties (specific heat ratio and atmospheric pressure) and chamber geometry (area and height) (Brendmo et al., 1996 and Ikoma et al., 2012). This approach was adopted in several studies by pioneer researchers. The pneumatic stiffness is calculated as:

$$\boldsymbol{k_{air} = \frac{\gamma\, p\, A_{wc}^{\,2}}{V_0}} \qquad \textbf{Eq. 6.12}$$

where, V_0 is the average air volume in the pneumatic chamber

p is the pressure

γ is the specific heat ratio for air.

Many researchers ignored the air compressibility problem following the assumption that for subsonic air flow especially at Mach number less than 0.3, air may be treated as incompressible fluid (Oosthuizen and Carscallen, 1997), or assuming that for full scale OWC the influence of the air compressibility will be minor compared to the hydrostatic (restoration) force previously discussed (Suleman & Bin Khaleeq 2010).

6.4.4. Wave forces

Once again; in the present study the total vertical wave excitation forces acting on the structure, F_{1TY} and/or the water column, F_{2TY} consist of dynamic pressure forces (incident) and acceleration forces (Incecik, 1982, Aalbers, 1984 and Sphaier et al., 2007). The total vertical force acting on the structure includes the forces acting on the buoy, tube and collar.

As mentioned in Chapter 3 the incident wave component is expressed as:

$$\boldsymbol{f_p = 0.5\, H_w\, A\, \rho g \frac{cosh(-dK+w_dK)}{cosh(w_dK)}} \qquad \textbf{Eq. 6.13}$$

And the acceleration component is calculated as:

$$\boldsymbol{f_a = -0.5\, H_w\, M_{avm}\ g\, K \frac{sinh(-dK+w_dK)}{sinh(w_dK)}} \qquad \textbf{Eq. 6.14}$$

For floating OWC, phase difference between forces applied on the structure and water column should be introduced in the modelling for proper dynamic analysis. Stappenbelt & Cooper, 2009 reported that wave forces on the water column, and the floating structure, are to be related via a complex parameter allowing for both a magnitude and phase difference between the forces. It may be noticed that this parameter is real. In the limit of large wavelength, or small wave number, this parameter can also be shown to be equivalent to the area ratio, R_O, of the OWC opening to the total base area of the floating wave energy converter. In this case wave forces applied on the water column are multiplied by R_O and wave forces applied on the structure are multiplied by $(1\text{-}R_O)$.

6.5. Computer simulation

A range of computer scripts and functions have been developed to calculate the damping coefficients from experiments. Later on; Analytical and numerical algorithms have been developed to perform the modelling of captive and floating OWC by solving the Ordinary Differential Equations (ODEs) describing the motions.

6.5.1. Analytical solutions in frequency domain

Analytical integration algorithms have been developed to solve the linear equations of motions reported in the study *(except Szumko model. It was solved numerically due to its complexity)* based on the solutions of second order linear equations provided in differential equation books such as (Ayres,1952) and mechanical vibrations book (Rao, 1991) for both single and two DOF models.

From the equation of motion used to describe the water column oscillations in captive structure assuming viscous damping (Eq.6.1), the water column oscillation amplitude is calculated as:

$$y_2 = \frac{F_{2TY}/k_2}{\sqrt{\left[1-\left(\omega/\omega_{n2}\right)^2\right]^2+\left[2\xi\left(\omega/\omega_{n2}\right)\right]^2}} \qquad \textbf{Eq. 6.15}$$

where ξ is the damping ratio and the phase angle between the water column and waves is:

$$\phi_2 = tan^{-1}\left[\frac{2\,\xi\,(\omega/\omega_n)}{1-(\omega/\omega_n)^2}\right] \qquad \textbf{Eq. 6.16}$$

The water column heave natural frequency is:

$$\omega_{n2} = \sqrt{\frac{k_2}{M_2}} \qquad \textbf{Eq. 6.17}$$

Once again the solution of a standard single DOF equation of motion is presented in Appendix D.

For the two DOF model, the general equations of motion of the system are expressed in Eq.6.2 & Eq.6.3. The complete analytical solution of a two DOF model is presented in Appendix E.

The amplitudes and the phase angles of the two bodies may be written as:

$$Y_1 = \frac{1}{\omega_{n1}^2\omega_{n2}^2 m_1 m_2}\sqrt{\frac{\left((f_1k_2+k_2f_2)-\omega^2(f_1m_2)\right)^2+\left(\omega(f_1c_2+c_2f_2)\right)^2}{\left[(1-r_1^2)^2+(2\xi_1r_1)^2\right]\left[(1-r_2^2)^2+(2\xi_2r_2)^2\right]}} \quad \textbf{Eq. 6.18}$$

$$\Phi_1 = tan^{-1}\left(\frac{2\xi_1r_1}{1-r_1^2}\right)+tan^{-1}\left(\frac{2\xi_2r_2}{1-r_2^2}\right)-tan^{-1}\left(\frac{\omega(f_1c_2+c_2f_2)}{(f_1k_2+k_2f_2)-\omega^2(f_1m_2)}\right) \quad \textbf{Eq. 6.19}$$

$$Y_2 = \frac{1}{\omega_{n1}^2\omega_{n2}^2 m_1 m_2}\sqrt{\frac{\left((f_2(k_1+k_2)+k_2f_1)-\omega^2(f_2m_1)\right)^2+\left(\omega(f_2(c_1+c_2)+c_2f_1)\right)^2}{\left[(1-r_1^2)^2+(2\xi_1r_1)^2\right]\left[(1-r_2^2)^2+(2\xi_2r_2)^2\right]}} \quad \textbf{Eq. 6.20}$$

$$\Phi_2 = tan^{-1}\left(\frac{2\xi_1r_1}{1-r_1^2}\right)+tan^{-1}\left(\frac{2\xi_2r_2}{1-r_2^2}\right)-tan^{-1}\left(\frac{\omega(f_2(c_1+c_2)+c_2f_1)}{(f_2(k_1+k_2)+k_2f_1)-\omega^2(f_2m_1)}\right) \quad \textbf{Eq. 6.21}$$

Since the system is damped, the masses vibrate with the same frequency with a time lag; assuming that:

$$y_1 = Y_1e^{i(\omega t-\Phi_1)} \quad \textbf{Eq. 6.22}$$

$$y_2 = Y_2e^{i(\omega t-\Phi_2)} \quad \textbf{Eq. 6.23}$$

$$\dot{y}_1 = Y_1i\omega e^{i(\omega t-\Phi_1)} \quad \textbf{Eq. 6.24}$$

$$\dot{y}_2 = Y_2i\omega e^{i(\omega t-\Phi_2)} \quad \textbf{Eq. 6.25}$$

$$\ddot{y}_1 = -Y_1\omega^2 e^{i(\omega t-\Phi_1)} \quad \textbf{Eq. 6.26}$$

$$\ddot{y}_2 = -Y_2\omega^2 e^{i(\omega t-\Phi_2)} \quad \textbf{Eq. 6.27}$$

Therefore the relative motion between the water column and the structure may be expressed as:

$$RM = y_1\cos(\omega t+\phi_1)-y_2\cos(\omega t+\phi_2) \quad \textbf{Eq. 6.28}$$

6.5.2. Numerical solutions in time domain

A large number of software packages offer pre-programmed numerical integration algorithms. Numerical integration of ODE is provided by the ODE solver package of Matlab. It contains both fixed-step and variable-step solvers, suitable for different degrees of stiffness and needs for accuracy (Hals, 2010).

For the models reported herein, the solver named ode23 was selected. ode23 is an implementation of an explicit Runge-Kutta, pair of Bogacki and Shampine. It may be more efficient than ode45 (In general, ode45 is the best function to apply) at crude tolerances and in the presence of moderate stiffness. Like ode45, ode23 is a one-step solver.

Matlab ode23 accepts only first-order differential equations. In order to use the ODE solver with higher-order ODEs, one must rewrite each equation as an equivalent system of first-order differential equations (Matlab 2008).

Mathematical manipulations performed to rewrite the equation of motion of water column in captive OWC as an equivalent system of first-order differential equations is presented in Appendix F.

Appendix G presents the system of first-order differential equations equivalent to the equations of motions of the simplified 2DOF model and Szumko model.

6.6. Special case (one-way coupling)

The special condition for harmonic excitation treated herein occurs when the mass ratio m_r (m_2/m_1) is large (>0.4 in this case) and the natural frequency ratio $(\omega_{n2}/\omega_{n1})$ is close to 1 with small damping ratio.

In this case the predicted frequency responses of the masses become very close to each other. Both analytical and numerical procedures fail in predicting the spar heave and the water column motion.

By examining the values of the terms making the equations of motion (Eq.6.1 and Eq.6.2) it was found that some terms are relatively very high. These terms were set to zero which leaded to the one-way coupling approach.

One-way coupling between the two masses may be a reasonable assumption in this case. This is achieved by treating the structure heave motion as single DOF system while keeping the equation of motion of the water column as it is. In other words, only single DOF motion of the structure will be taken into account in water column oscillations calculation. Therefore the equations of motion for the structure heave and the water column oscillations may be re-written as:

$$\boldsymbol{M_1\ddot{y}_1 + (c_1 + 0)\dot{y}_1 + (k_1 + 0)y_1 - 0\dot{y}_2 - 0y_2 = F_{1TY}\, cos(\omega t)} \qquad \textbf{Eq. 6.29}$$

$$\boldsymbol{M_2\ddot{y}_2 + c_2\dot{y}_2 + k_2y_2 - c_2\dot{y}_1 - k_2y_1 = F_{2TY}\, cos(\omega t)} \qquad \textbf{Eq. 6.30}$$

6.7. Power absorbed and performance measures

It is important that the numerical tool developed in this research not only simulate the OWC motions but be able to measure the performance of the device as well. The proper operation of the device is not the scope of the research while the proper modelling is. Since the same orifices were used during testing the models without being scaled, the effect of the plates is different on the two models. However the motions and damping results obtained from the numerical and the experimental modelling were used to measure the performance in the scaled environment. It is expected that full scale results will be significantly different due to the PTO damping used in real conditions.

The general applicable measures of performance were discussed in section 1.5.2. Similarly to those presented and adopted by Falnes, 2002; Stappenbelt & Cooper 2009; Gomes et al., 2012 and Falcão 2012. The mean captured power from a heaving wave energy converter is given by as:

$$\boldsymbol{P_{cap} = 0.5\, \omega^2\, b_{PTO}\, Y^2} \qquad \textbf{Eq. 6.31}$$

The theoretical maximum limit for the time-averaged wave power that can be absorbed from regular waves in deep water by a heaving wave energy converter with a vertical axis of symmetry is to be:

$$\mathbf{P_{max}} = \frac{\mathbf{1}}{\mathbf{8\ b_{PTO}}} |\mathbf{F_{2TY}}|^{\mathbf{2}} \qquad \textbf{Eq. 6.32}$$

Therefore, from Eq.6.31 and Eq.6.32, it is possible to compute the dimensionless mean power capture, given by:

$$\boldsymbol{P^*} = \frac{\boldsymbol{P_{cap}}}{\boldsymbol{P_{max}}} \qquad \textbf{Eq. 6.33}$$

For regular incident waves, the wave power per unit crest width is obtained From Eq.1.1 Then the capture width which represents the equivalent width of incident wave power that is completely captured by the device and converted to mechanical power is defined by:

$$\boldsymbol{C_W} = \frac{\boldsymbol{P_{cap}}}{\boldsymbol{P_W}} \qquad \textbf{Eq. 6.34}$$

The Capture Factor C_F also known as Capture Width Ratio C_{WR} is expressed as:

$$\boldsymbol{C_F} = \frac{\boldsymbol{P_{abs}}}{\boldsymbol{P_W\ D}} = \frac{\boldsymbol{C_W}}{\boldsymbol{D}} \qquad \textbf{Eq. 6.35}$$

6.7. Results and discussions

In this section captive and floating OWC modelling results obtained by considering one and two translational modes in heave direction respectively will be presented.

The mass of the water column is assumed to be a solid vertical cylinder from the bottom of the tube to the internal still water level. Added mass is assumed to be frequency independent. The water column total mass results are presented in Table 6.1.

Table 6.1: Water column total mass and added mass in heave

	OWC Mass (kg)	
	Mass	**Added mass**
Model1	1.1310	0.0360
Model2	4.5996	0.2953

Water column damping and PTO damping modelled experimentally by orifice plates were calculated using logarithmic decrement and half-power bandwidth methods. Water column damping results are presented in Table 6.2.

Table6.2: Water column damping results

	OWC Damping Ratios					
	WC (Open tube)		**WC + 4 Orifices**		**WC + 2 Orifices**	
	Log. dec.	**Half-power**	**Log. dec.**	**Half-power**	**Log. dec.**	**Half-power**
Model1	0.041	0.084	0.043	0.09	0.046	0.096
Model2	0.043	0.068	0.059	0.095	0.082	NA

The orifices area made about 5.6% and 11.2% of the water column area for experimental model1 in case of 2 and 4 orifices respectively. While for the second model, orifices area just made 1.2% and 2.4% of the water column area.

In case of open tube, damping obtained represents the water column damping, while damping obtained in case orifice plates are used represents the sum of the water column and the PTO damping.

The determination of damping in case of 2 orifices for experimental model 2 was not applicable due to the high damping applied.

Moreover, it is noticed that damping ratios of experimental model 2 are higher than those of experimental model 1.

We may also notice that damping values obtained from the half-power bandwidth method are higher than those obtained from logarithmic decrement method.

Results obtained from Eq.6.11 and Eq.6.12 used to calculate the hydrostatic and pneumatic stiffness are presented in Table 6.3.

Table 6.3: Stiffness results

	OWC Stiffness (N/m)	
	WC Hydrostatic	**Air Compressibility**
Model1	27.7371	1.0875
Model2	112.8053	4.4227

As mentioned earlier in section 6.4.3 the pneumatic stiffness due to air compressibility is small compared to the hydrostatic stiffness of the water column. From the above table the pneumatic stiffness makes about 3.7% of the total stiffness. It is expected that for a full scale OWC, the pneumatic stiffness be relatively smaller compared to the hydrostatic stiffness of the water column.

In the present study a single degree of freedom oscillatory system was used to model the water column oscillations inside captive OWC.

Fig.6.3 and Fig.6.4 present comparison between experimental and numerical water column RAO for experimental models 1&2 respectively.

The water column RAO is defined as the water column oscillation amplitude divided by the wave amplitude.

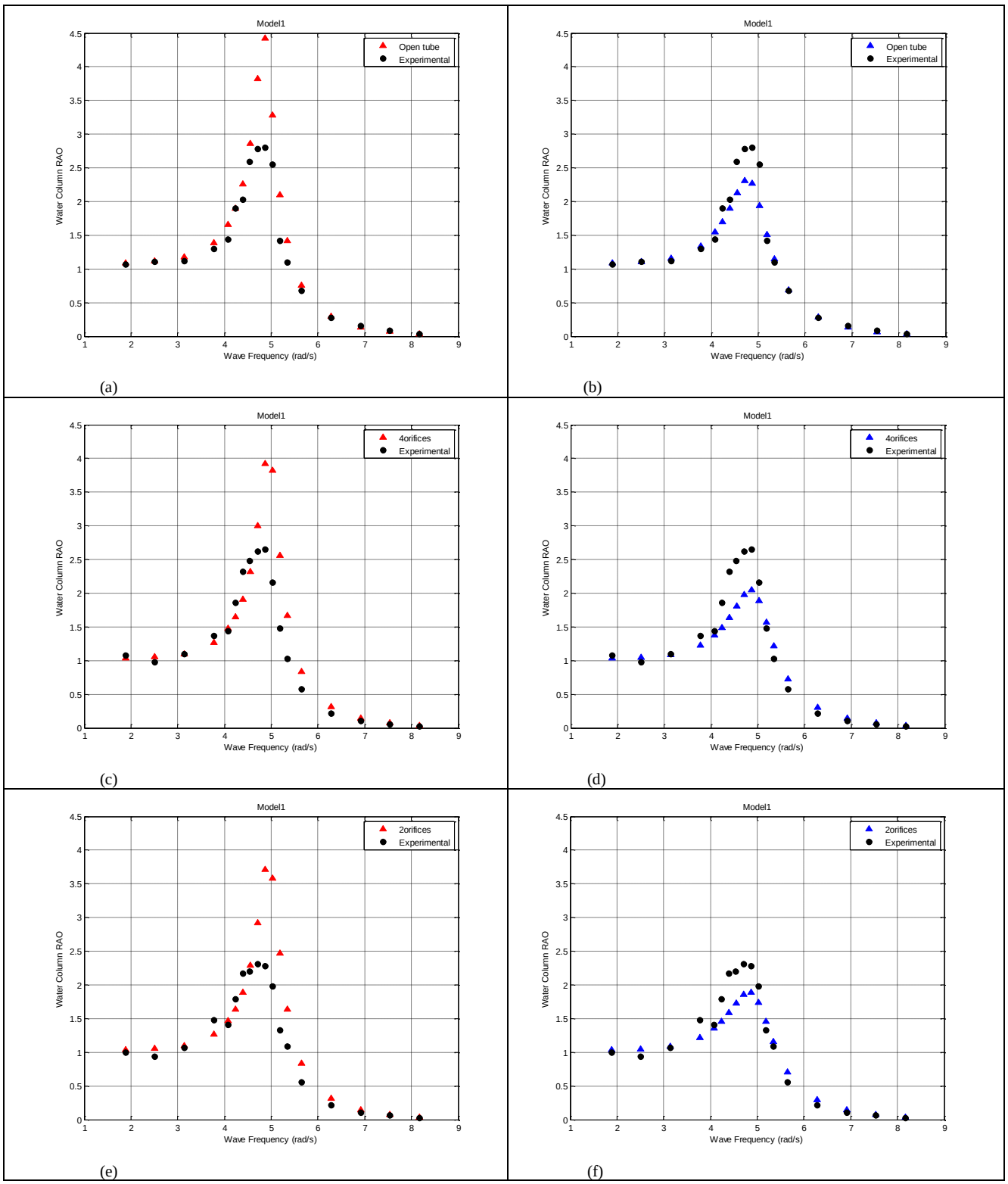

Fig.6.3. Comparison between numerical and experimental water column oscillations RAOs vs. wave frequency for experimental model1; 1DOF model, viscous damping, (left) using logarithmic decrement method, (right) using half power bandwidth method; (a,b) Open tube, (c,d) 4 orifices, (e,f) 2 orifices,

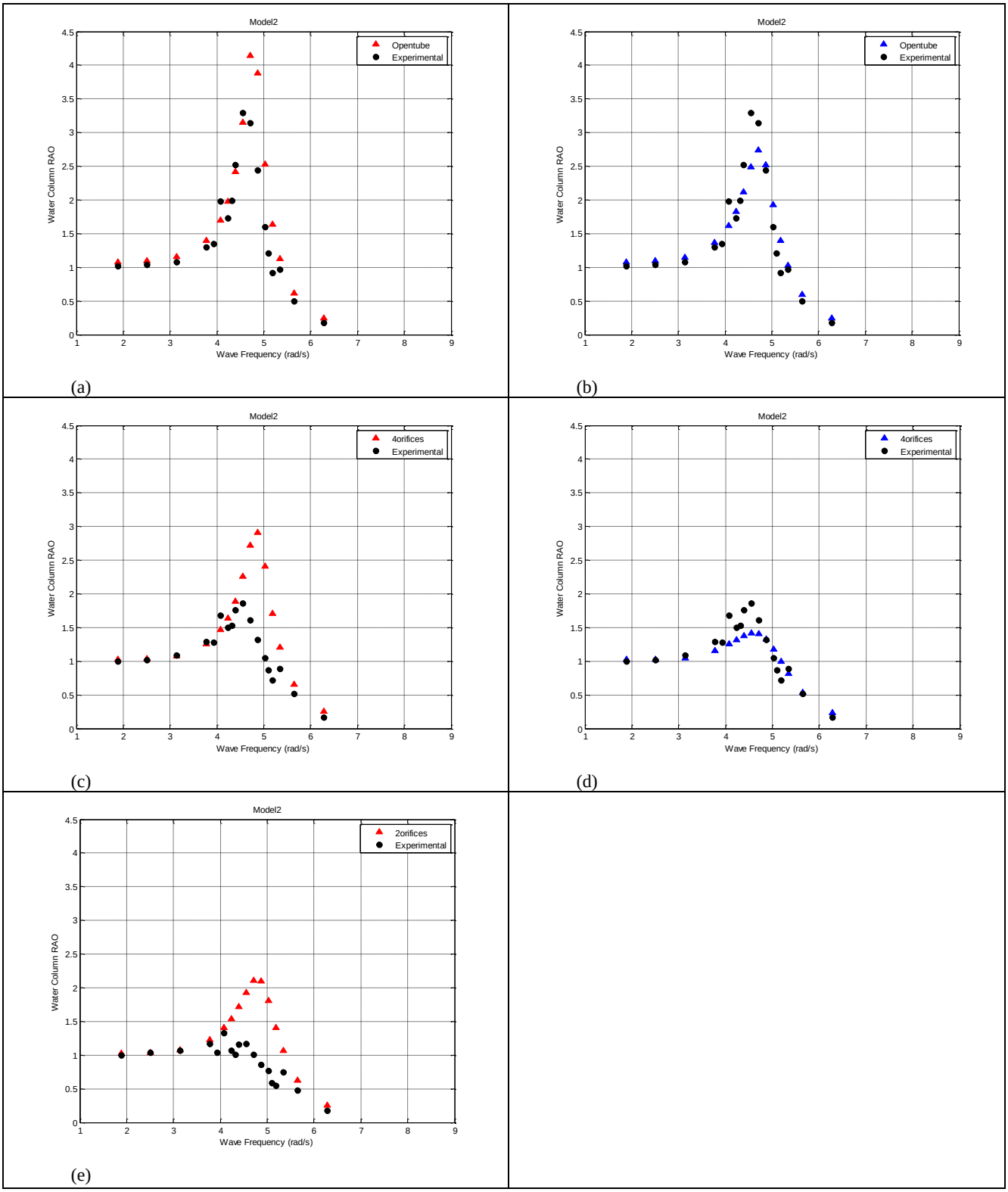

Fig.6.4. Comparison between numerical and experimental water column oscillations RAOs vs. wave frequency for experimental model2; 1DOF model, viscous damping, (left) using logarithmic decrement method, (right) using half power bandwidth method; (a,b) Open tube, (c,d) 4 orifices, (e) 2 orifices.

Fig.6.3 and Fig.6.4 showed that the pneumatic stiffness which varies according to the number of orifices in the orifice plate has a minor influence on the water column response and may be ignored. Moreover, the increase in PTO damping causes a reduction in the oscillations RAO only around the resonance frequency. It is noticed that viscous damping model results using both approaches failed to predict the response accurately around resonance.

The phase angles between waves and water column oscillations as calculated from Eq.6.16 are presented in Fig.6.5 and Fig.6.6 for experimental models 1 and 2 respectively.

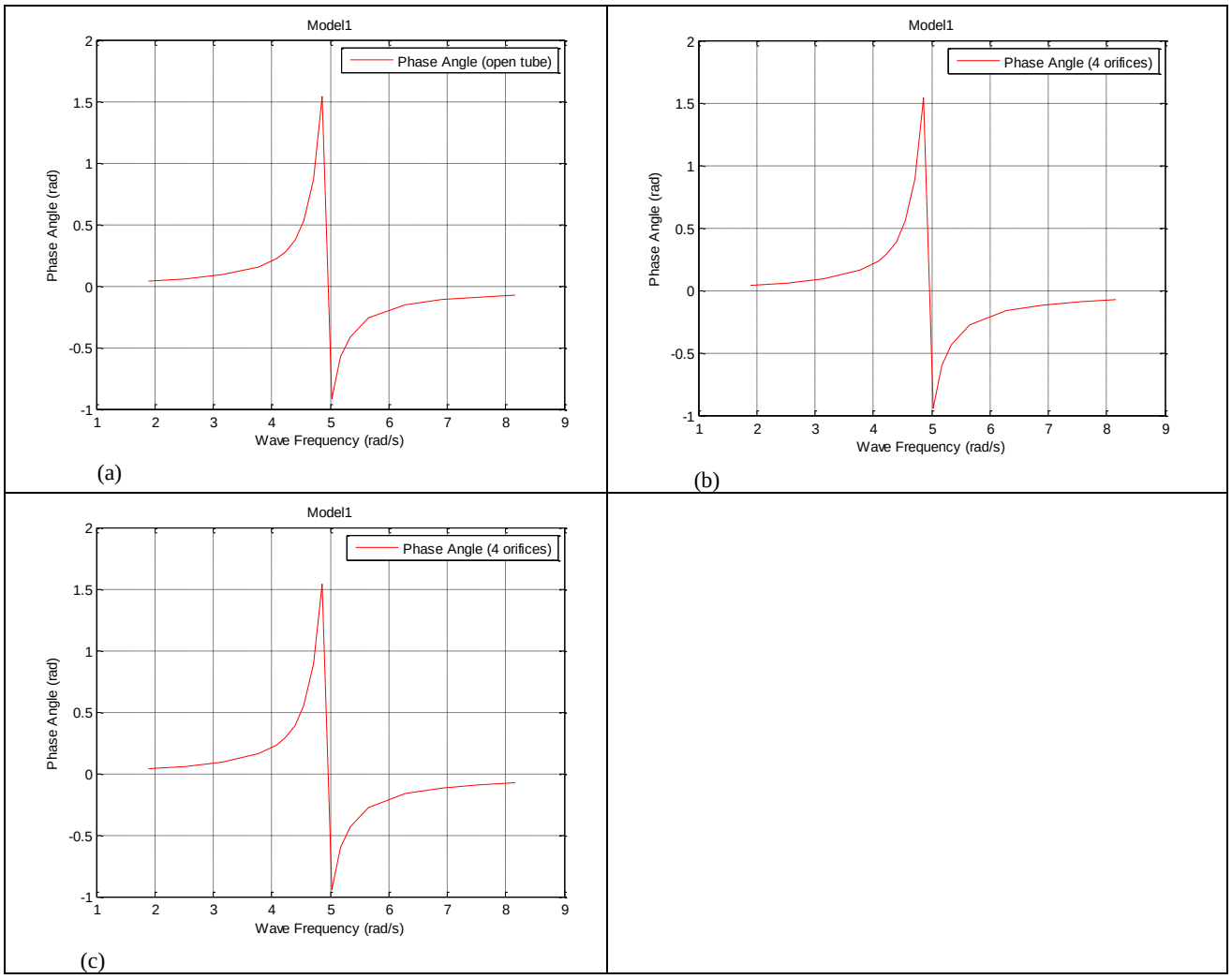

Fig.6.5. Predicted phase angle between waves and the water column oscillations for experimental model1; 1DOF model; (a) Open tube (b) 4 Orifices (c) 2 Orifices

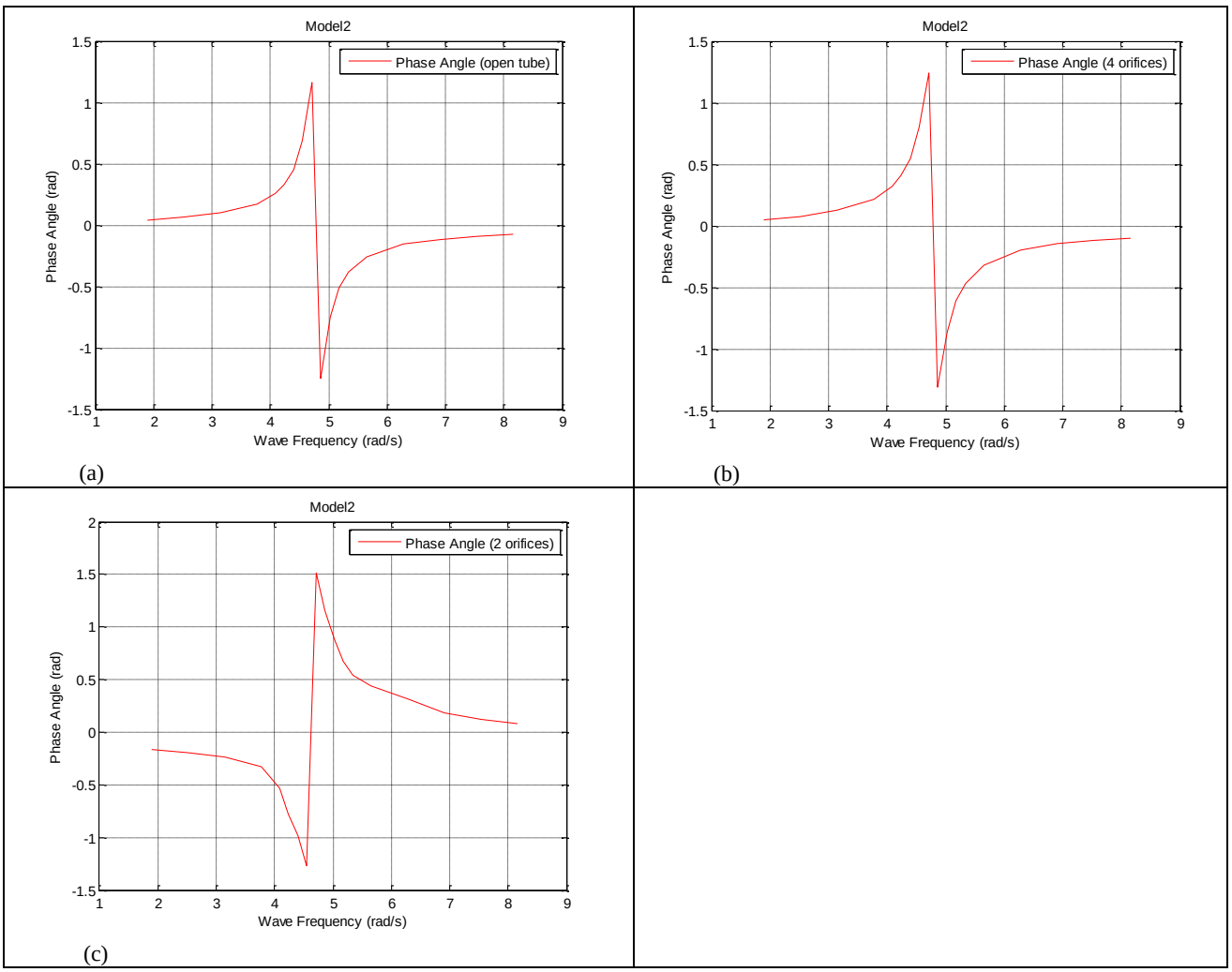

Fig.6.6. Predicted phase angle between waves and the water column oscillations for experimental model2; (a) Open tube (b) 4 Orifices (c) 2 Orifices

From the above figures, it is seen that the phase angles are quite similar except in case of 2 orifices for experimental model 2, due to the high damping applied by the orifices.

The two different dynamic models presented in this chapter used to describe floating OWC referred to in the text as *simplified 2DOF model* and *Szumko model* respectively. Simplified 2DOF model was solved analytically due to its simplicity. Predicted natural frequencies of the two experimental models are presented in Table 6.4.

Table 6.4: Coupled natural frequency results

	Structure Natural frequency	**WC Natural frequency**	**Frequency ratio**
Model1	8.0642	4.1888	1.9252
Model2	7.5828	4.1717	1.8177

Comparison between analytical and experimental results of structure heave, water column oscillations and relative RAOs for experimental model1 using simplified 2DOF model is presented in Fig.6.7.

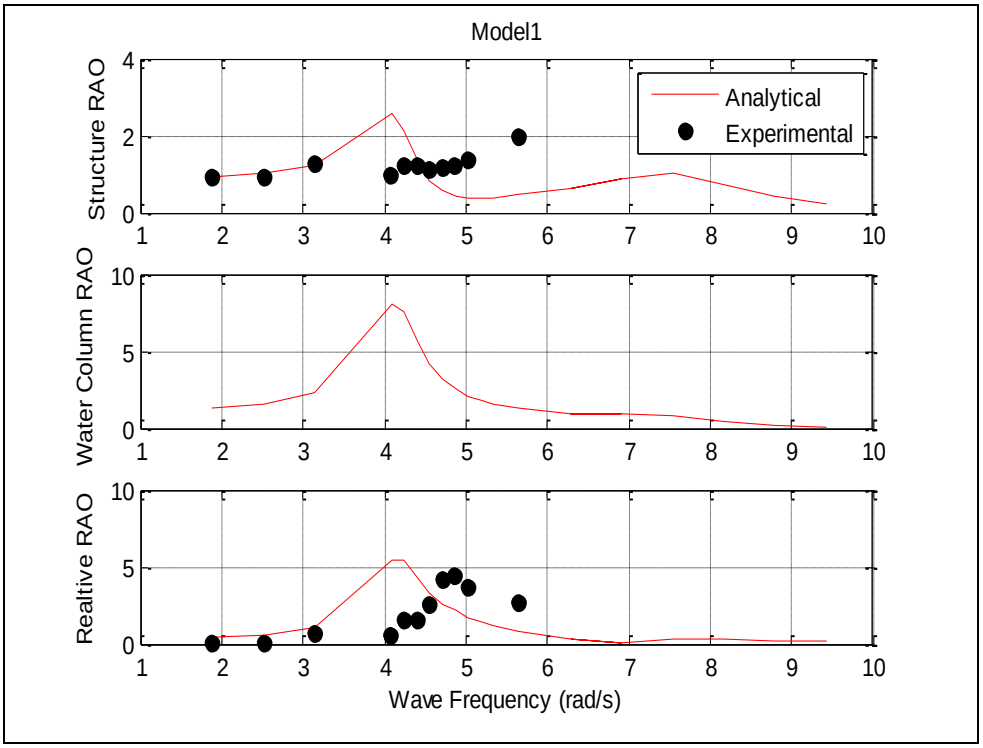

Fig.6.7. Comparison between analytical and experimental structure heave, water oscillations and relative motion RAOs vs. wave frequency for experimental model1, open tube; simplified 2DOF model, viscous damping using half power bandwidth method.

Fig.6.7 showed that the measured relative RAO showed a clear peak at 4.8rad/s which is the water column natural frequency in case the structure is captive.

The predicted relative RAO peaks at 4.1rad/s and 8rad/s corresponding to the water column and structure natural frequencies presented in Table 6.4.

It is noticed that the structure heave response is better described in chapter 4 when the water column was not considered.

The predicted frequency responses of the spar and the relative motion become very close to each other and failed to match the measured peaks corresponding to the structure and water column natural frequencies. In order to validate the analytical procedure, Matlab scripts are developed to solve the same equations numerically using the procedure discussed earlier. Comparison between analytical, numerical and experimental results of structure heave and relative motion RAOs for experimental model 1 is presented in Fig.6.8 within the range of frequencies tested experimentally.

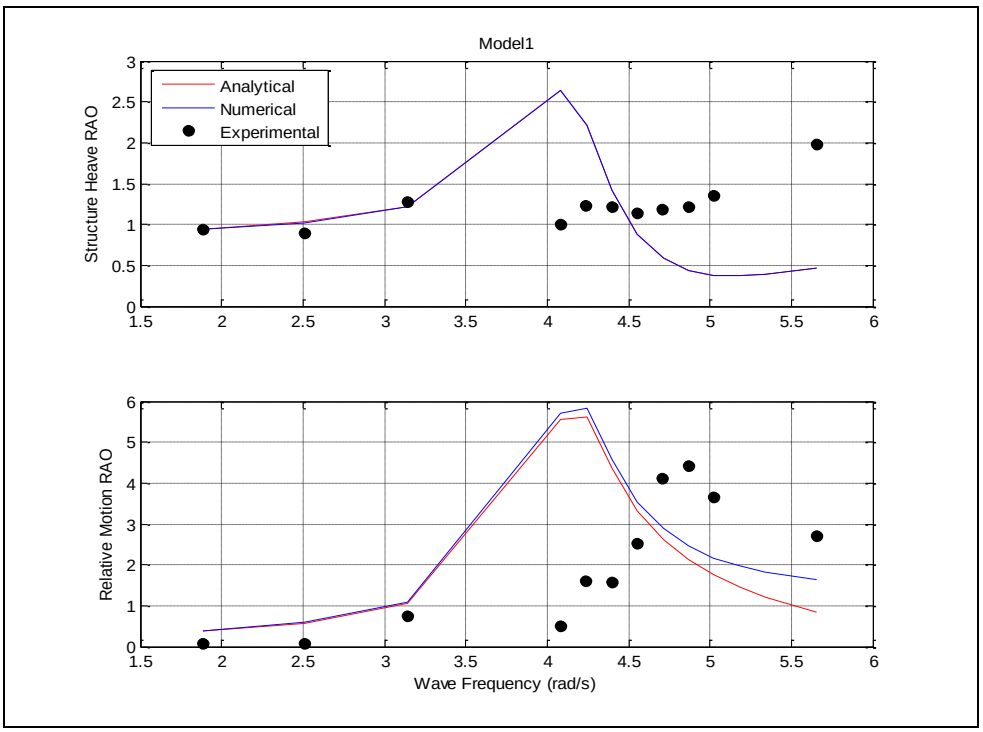

Fig.6.8. Comparison between analytical, numerical and experimental structure heave and relative motion RAOs vs. wave frequency for experimental model1, open tube; simplified 2DOF model, viscous damping using half power bandwidth method.

Fig.6.8 showed that both analytical and numerical procedures failed in predicting the spar heave and the relative motions responses which raised doubts about the suitability of the dynamic model. However, Fig.6.9 and Fig.6.10 present comparison between the numerical and experimental spar heave and the relative motions RAOs for experimental models 1&2 in case of open tube and different number of orifices.

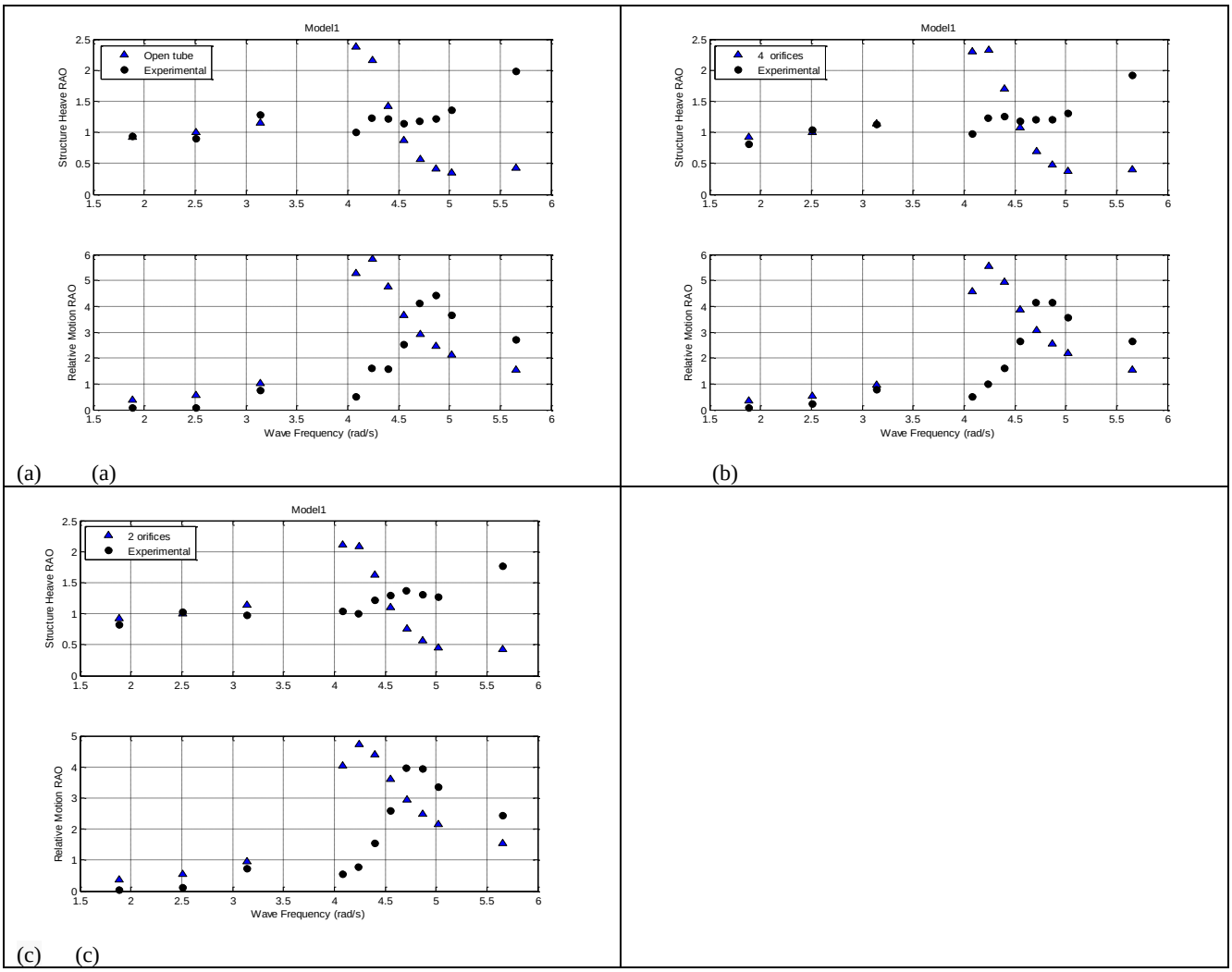

Fig.6.9. Comparison between numerical and experimental structure heave and relative motion RAOs vs. wave frequency for experimental model1; simplified 2DOF model, viscous damping using half power bandwidth method; (a) Open tube, (b) 4 orifices, (c) 2 orifices

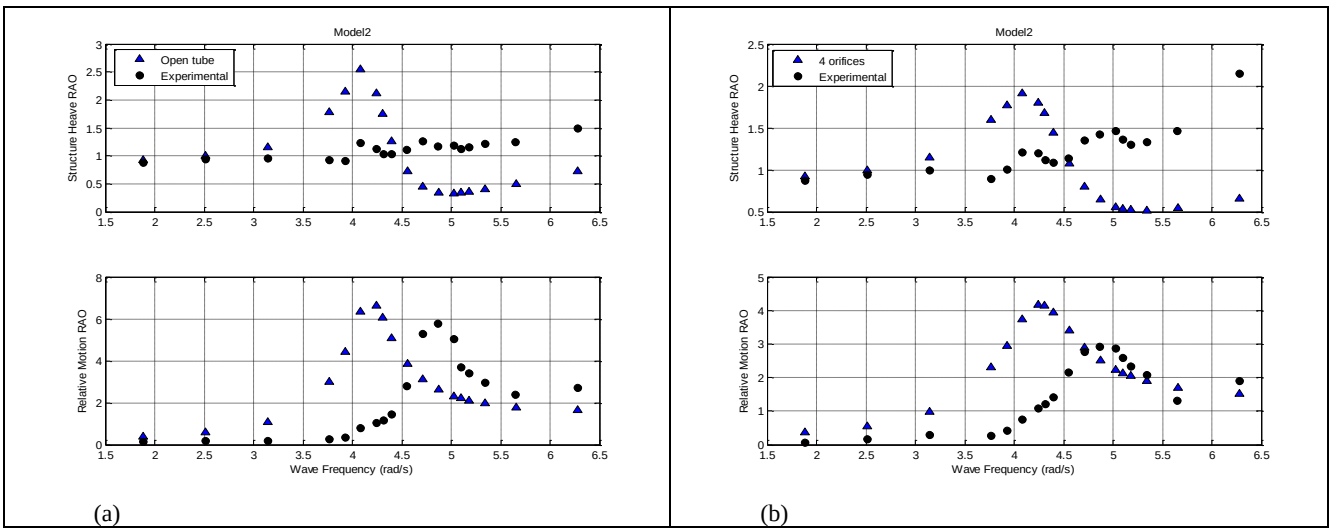

Fig.6.10. Comparison between numerical and experimental structure heave and relative motion RAOs vs. wave frequency for experimental model2; simplified 2DOF model, viscous damping using half power bandwidth method; (a) Open tube, (b) 4 orifices.

Fig.6.9 and Fig.6.10 proved that the simplified 2DOF model results did not agree with the experimental results. It is noticed that the peak frequencies are shifted.

The phase angles between waves and structure heave; and between waves and water column oscillations as calculated from Eq.6.19 and Eq.6.21 are presented in Fig.6.11 and Fig.6.12 for experimental models 1 and 2 respectively.

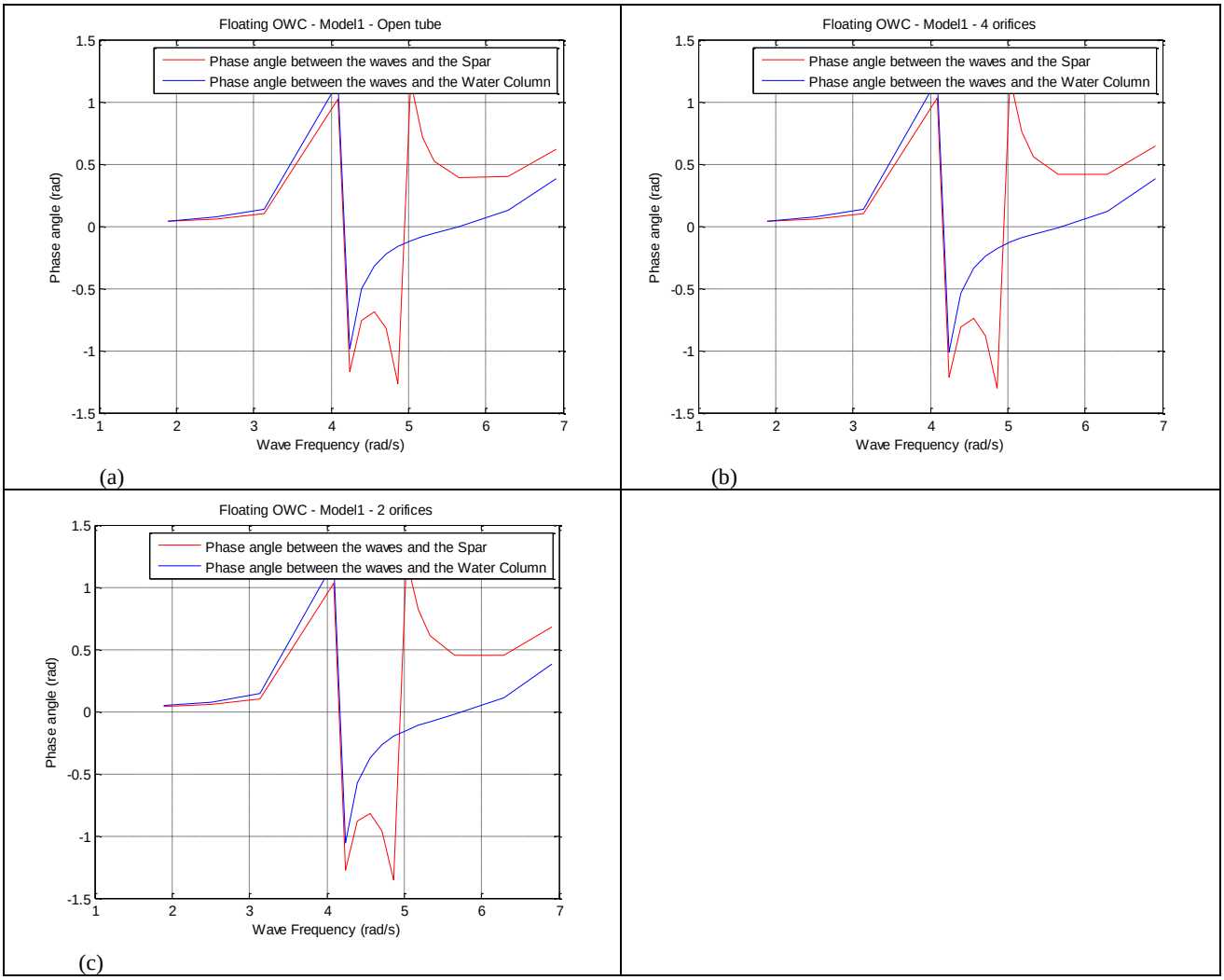

Fig.6.11. Predicted phase angles between waves and structures; and wave and water column oscillations for experimental model1; simplified 2DOF model; (a) Open tube (b) 4 Orifices (c) 2 Orifices

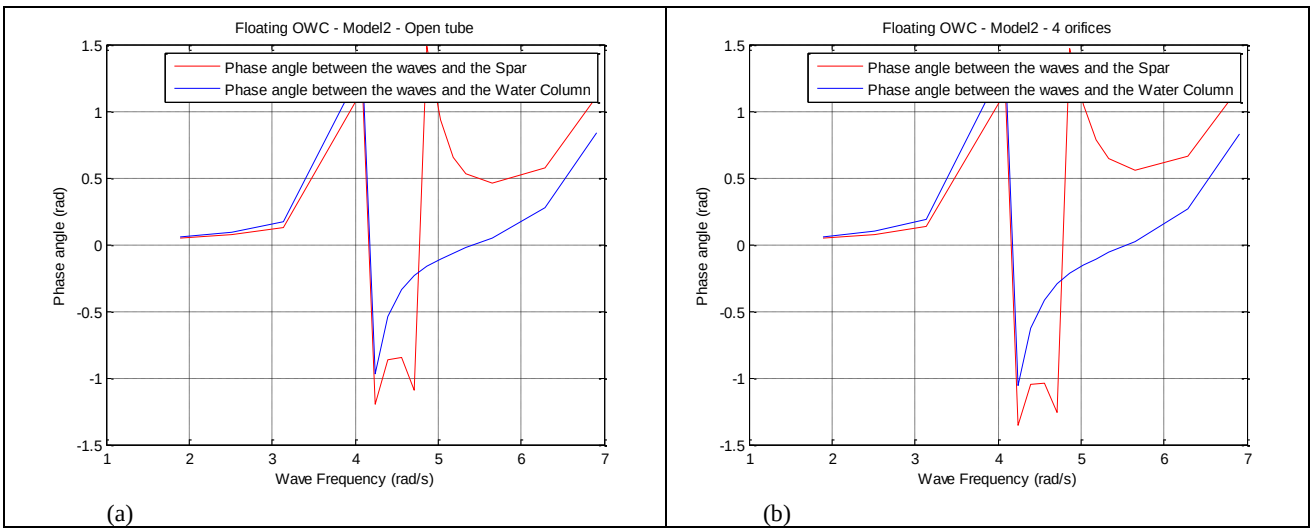

Fig.6.12. Predicted phase angles between waves and structures; and wave and water column oscillations for experimental model2; simplified 2DOF model; (a) Open tube (b) 4 Orifices

From the above figures it is seen that the resonance conditions are satisfied at the same frequencies.

The results obtained from the simplified 2DOF model question the dynamic model originally and not the numerical procedures. In other words, the arrangement of the mass, springs and dampers does not describe the coupling occurring in reality. That is why the model proposed by Szumko was used later. However, three different approaches were adopted to investigate the similarity between the responses of the two masses and improve the results obtained by the simplified 2DOF model.

First, the idea that the damping applied is not high enough to numerically model the coupling was considered. Therefore simulations have been performed assuming higher damping values. Fig.6.13 presents a comparison between numerical results using constant structure damping ratio of 0.5 and higher water column damping ratio. On the other hand, Fig.6.14 presents a comparison between numerical results using constant water column damping ratio of 0.5 and higher structure damping ratio.

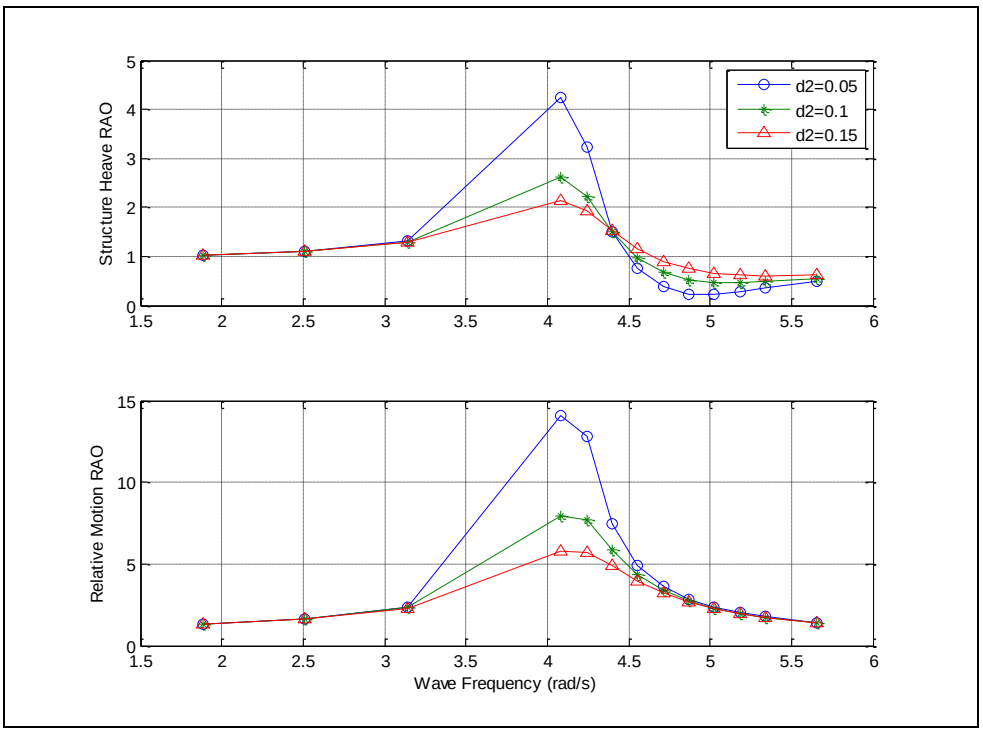

Fig.6.13. Comparison between numerical structure heave and relative motion RAOs vs. wave frequency for simplified 2DOF model, constant structure damping ratio (d1=0.05) and different water column damping ratios (d2)

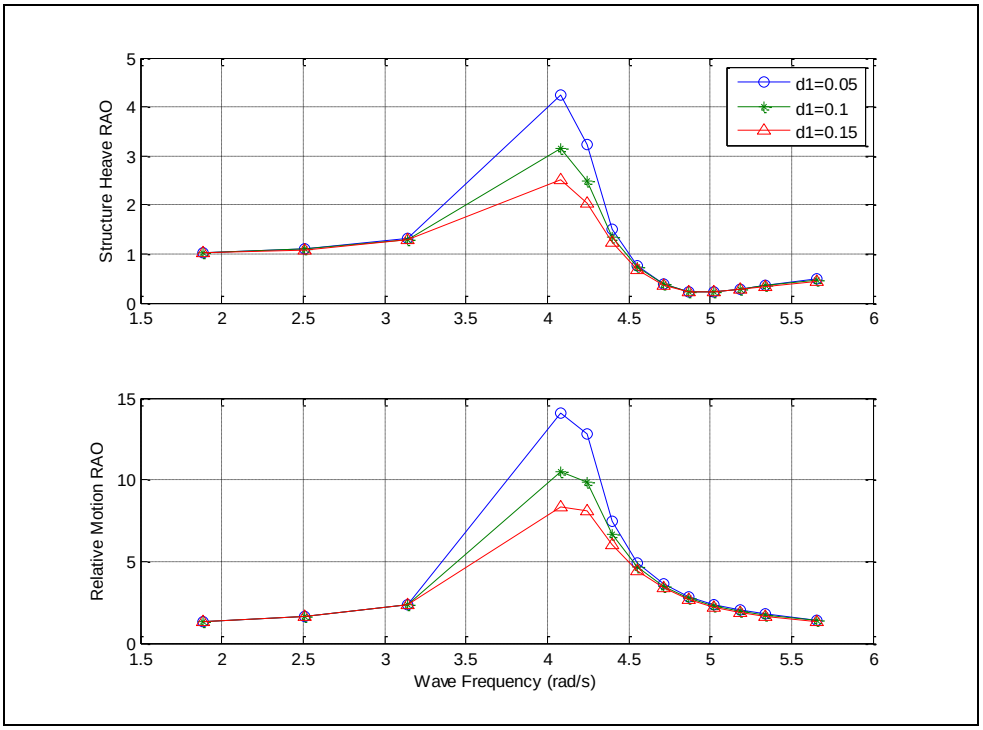

Fig.6.14. Comparison between numerical structure heave and relative motion RAOs vs. wave frequency for simplified 2 DOF model, constant water column damping ratio (d2=0.05) and different structure damping ratio (d1)

Modelling of floating OWC by the simplified 2DOF model using higher damping values did not solve the problem since the structure heave and relative motion peak frequencies occur at the same frequency as presented in Fig.6.13 and Fig.6.14. which does not agree with the experimental results.

The second approach was to investigate the effect of the mass ratio on the modelling. Therefore numerical modelling was performed using lower mass ratios by increasing the mass of the structure. Numerical results obtained are presented in Fig.6.15.

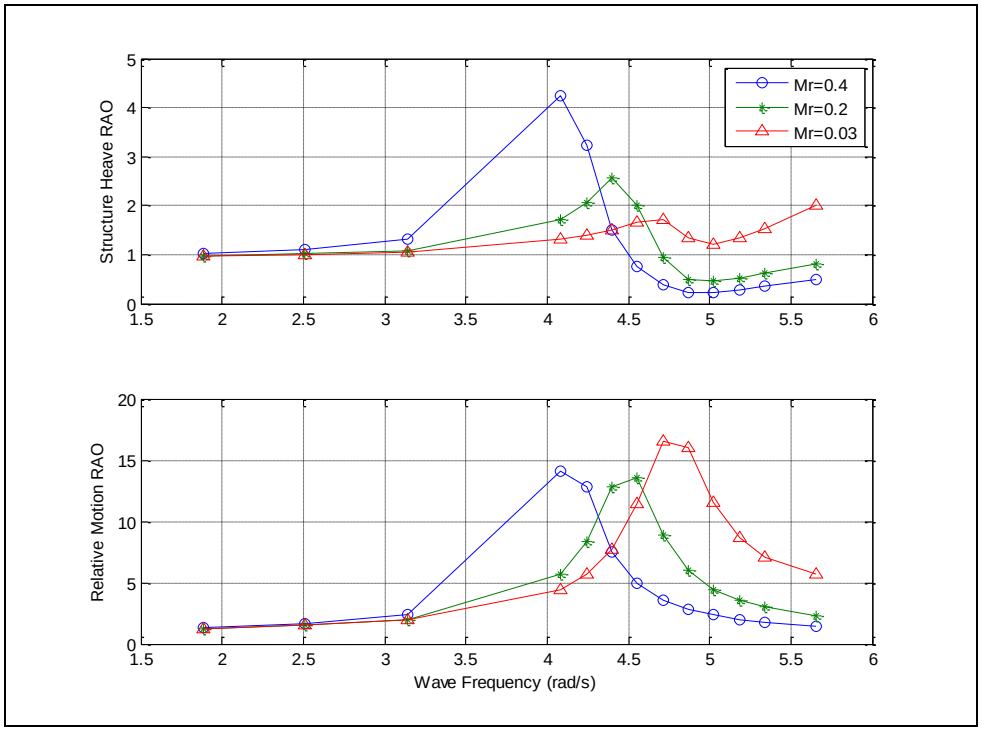

Fig.6.15. Comparison between numerical structure heave and relative motion RAOs vs. wave frequency for simplified 2 DOF model, constant structure and water column damping ratios (d1=d2=0.05) and different mass ratio.

From Fig.6.15 it is noticed that as the mass ratio decreases, the relative motion peak frequency moves towards the expected correct value. In order to validate this approach experimental model3 was used to validate the results obtained.

Experimental model1 was fitted inside a larger diameter floater (0.35m diameter instead of 0.14m) having the same draught and freeboard of the initial one. The new model will be referred to as experimental model3. The model was tested undamped (open tube) and with cover plate containing one orifice only. Fig.6.16 presents comparison between the numerical and experimental spar heave and the relative

motions RAOs. The damping in case of one orifice is assumed to be 15% of the critical damping and the spar damping is assumed to be 5%.

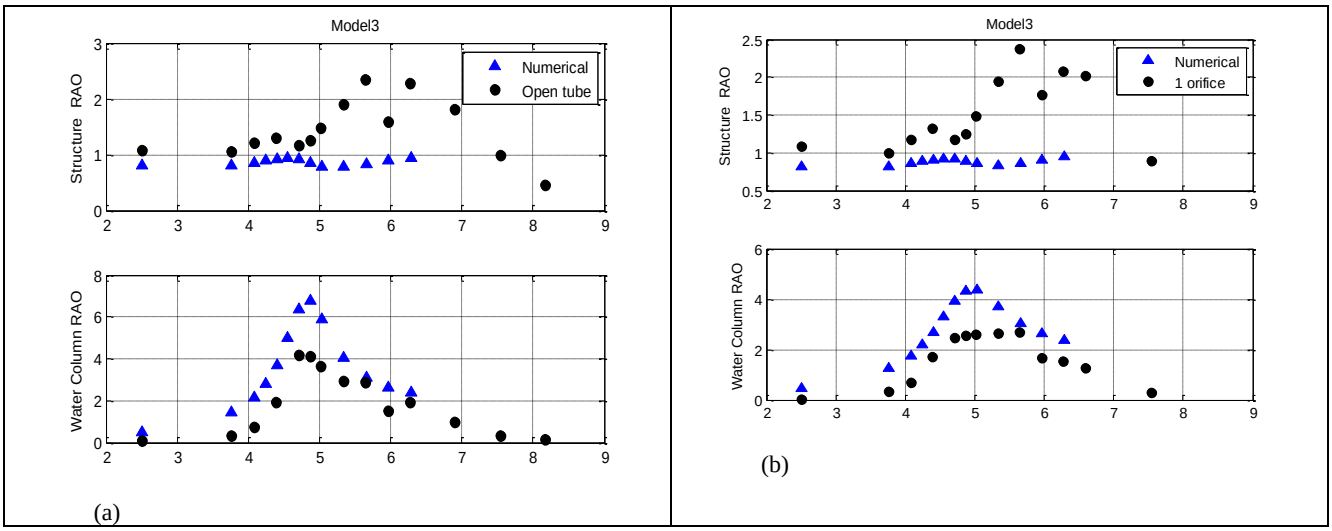

Fig.6.16. Comparison between numerical and experimental structure heave and relative motion RAOs vs. wave frequency for experimental model3; simplified 2 DOF model, viscous damping using half power bandwidth method; (a) Open tube, (b) 1 orifices.

From the above figures, predicted relative motion response showed better agreement with experimental results for both cases: open tube and 1 orifice. In contrast, predicted spar heave motion response did not agree with the experimental results for frequencies over 5rad/s, and this is expected due to the limitations of linear wave theory. The first peak appeared correctly at 4.7rad/s corresponding to the buoy coupled natural frequency.

Experimental model 3 was test for a wider range of frequencies as we can see in Fig. 6.16. The second peak in the relative RAO appeared at 5.6rad/s which is the structure uncoupled natural frequency.

Therefore, the third approach adopted to obtain better modelling results from the simplified 2DOF model is discussed in section6.6 and will be referred to in the text as one way coupling model. One-way coupling between the two masses is achieved by treating the structure heave motion as single DOF system while keeping the equation of motion of the water column as it is in case of the simplified 2DOF model (see Eq.29 & Eq.30). Comparison between numerical and experimental results of

structure heave, water column oscillations and relative RAOs for experimental model1 is presented in Fig.6.17.

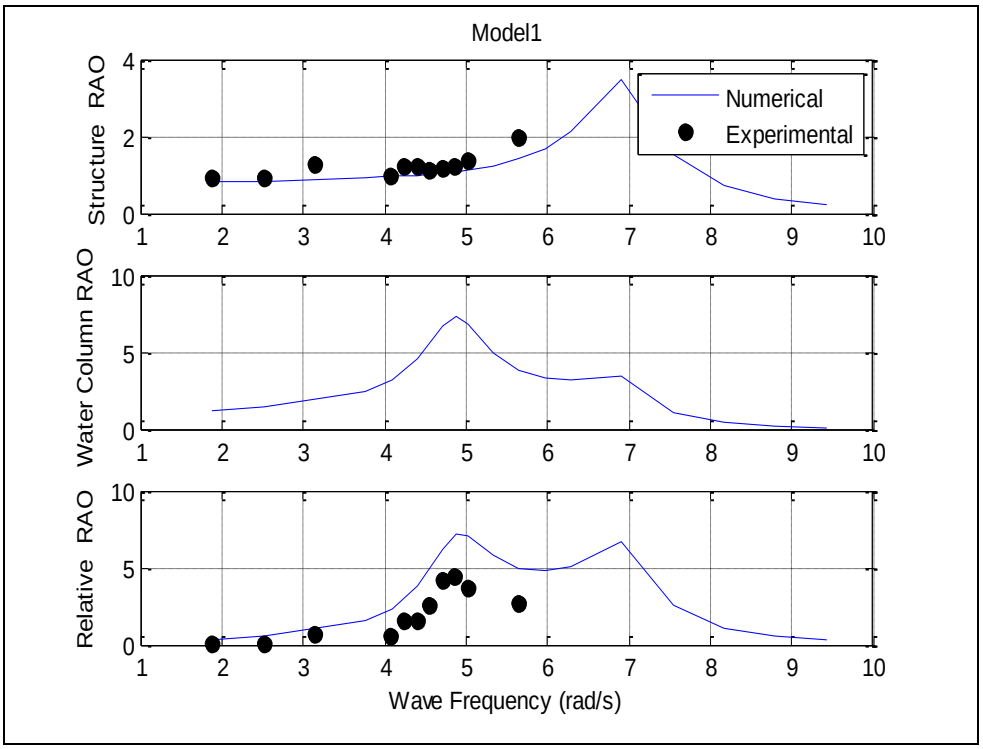

Fig.6.17. Comparison between numerical and experimental structure heave, water oscillations and relative motion RAOs vs. wave frequency for experimental model1, open tube; one-way coupling, 2DOF model, viscous damping using half power bandwidth method.

The above figure showed that only one peak appeared in the structure heave RAO at 7rad/s which corresponds to the uncoupled structure heave natural frequency (as if the spar heave is modelled as a 1DOF system).

The water column and relative RAOs showed close behaviour with two peaks. The first peak at 4.8rad/s, corresponds to the uncoupled water column natural frequency (as if the structure is captive), the second peak appeared at 7rad/s corresponding to the uncoupled structure heave natural frequency.

Fig.6.18, Fig.6.19, and Fig.6.20 present comparison between numerical and experimental spar heave and relative RAOs for experimental models 1, 2&3 respectively within the experimentally validated range of frequencies.

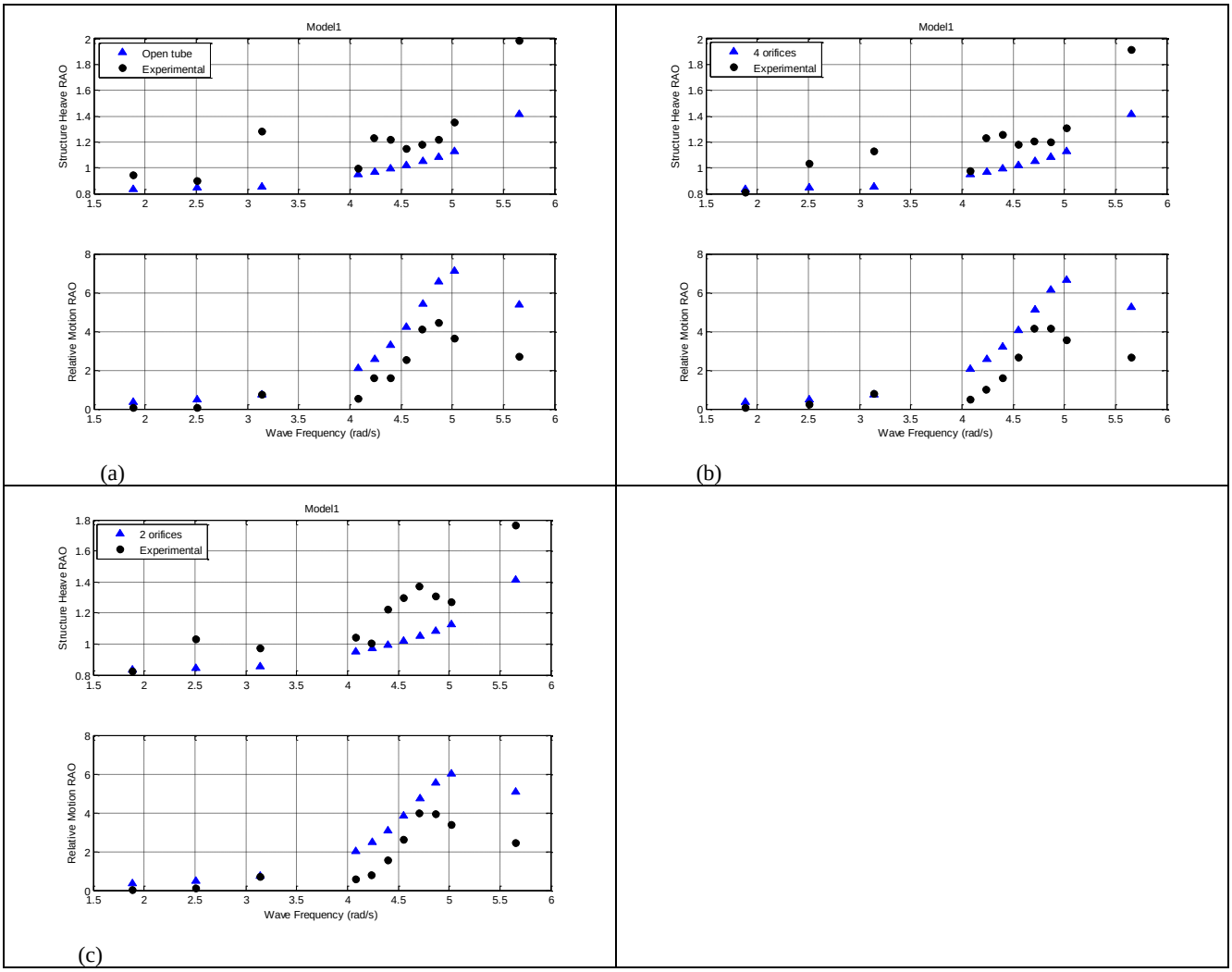

Fig.6.18. Comparison between numerical and experimental structure heave and relative motion RAOs vs. wave frequency for experimental model1; one-way coupling, 2DOF model, viscous damping using half power bandwidth method; (a) Open tube, (b) 4 orifices, (c) 2 orifices

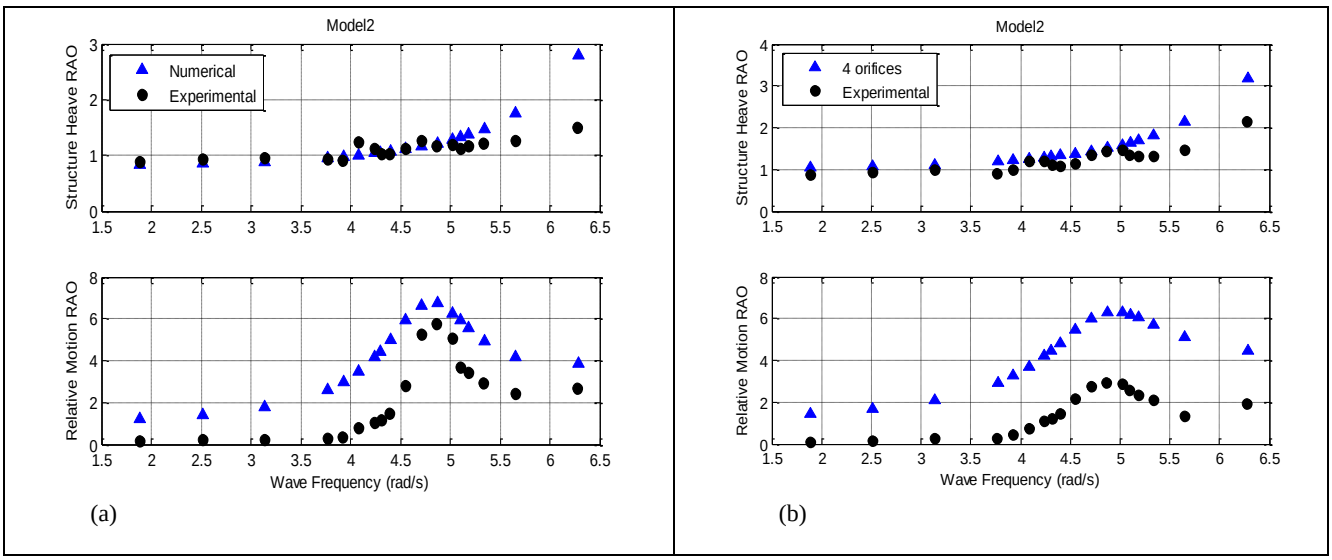

Fig.6.19. Comparison between numerical and experimental structure heave and relative motion RAOs vs. wave frequency for experimental model2; one-way coupling, 2DOF model, viscous damping using half power bandwidth method; (a) Open tube, (b) 4 orifices.

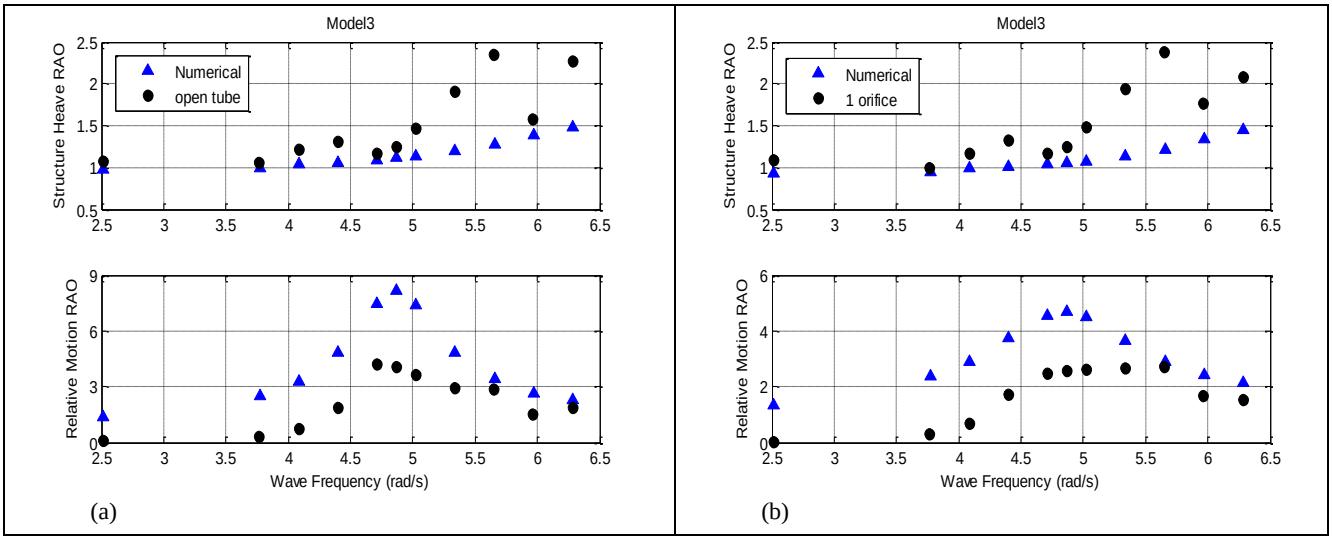

Fig.6.20. Comparison between numerical and experimental structure heave and relative motion RAOs vs. wave frequency for experimental model3; one-way coupling, 2DOF model, viscous damping using half power bandwidth method; (a) Open tube, (b) 1 orifice.

Predicted spar heave response obtained from the one-way coupling model showed better agreement with the experimental response than the response obtained from the simplified 2DOF model for the three experimental models. The predicted relative motion response expressed higher values than the simplified 2DOF results since damping terms were set to zero in the equation of motion, while peak frequency agrees with the experimental peak unlike the relative motion peak frequency obtained from the simplified 2DOF model.

The second dynamic model used to describe the floating OWC motions is the model proposed by Szumko and presented in Fig.6.2. Fig.6.21 presents comparison between numerical and experimental results of structure heave, water column oscillations and relative RAOs for experimental model1 over a wide range of frequencies.

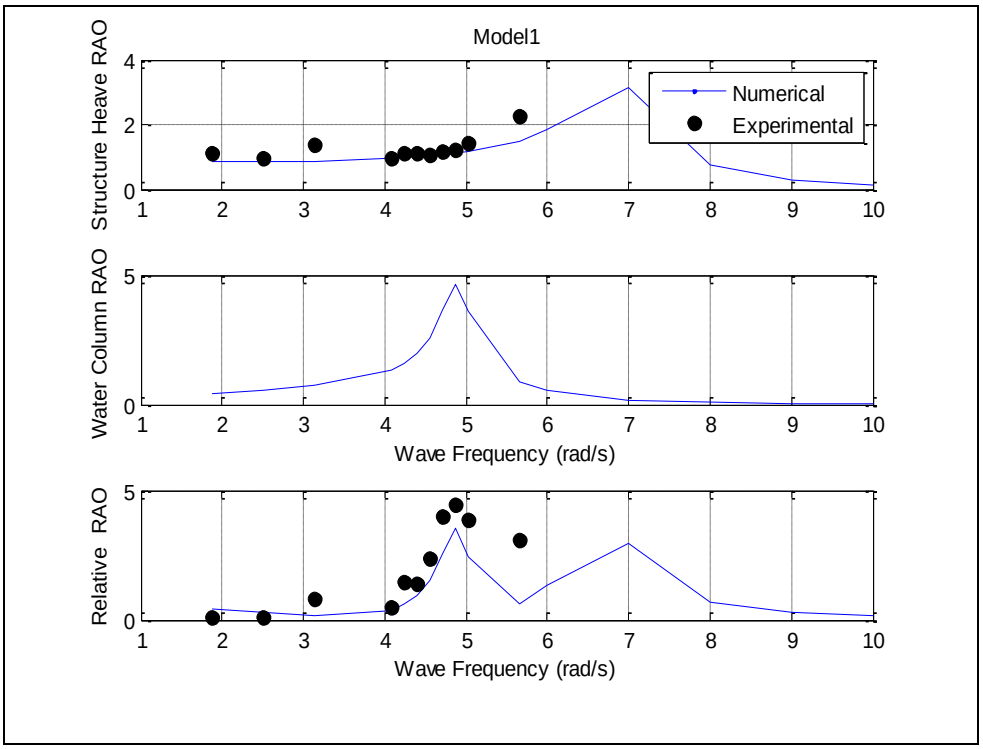

Fig.6.21. Comparison between numerical and experimental structure heave, water oscillations and relative RAOs vs. wave frequency for experimental model1, open tube; Szumko model, viscous damping using half power bandwidth method.

Fig.6.22, Fig.6.23 and Fig.6.24 present comparison between the numerical and experimental spar heave and relative motions RAOs for experimental models 1,2&3 within the experimentally validated range of frequencies using Szumko model.

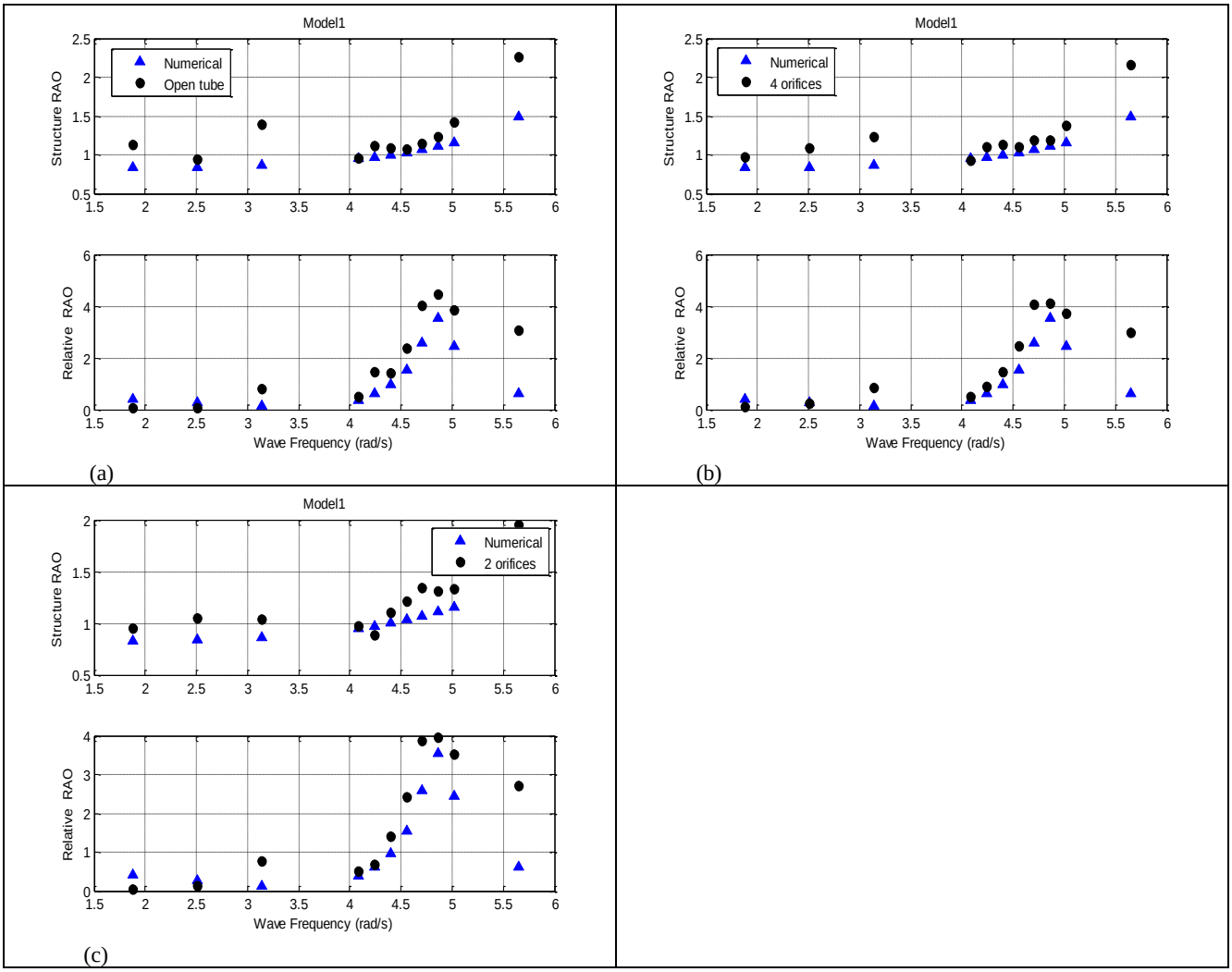

Fig.6.22. Comparison between numerical and experimental structure heave and relative motion RAOs vs. wave frequency for experimental model1; Szumko model, viscous damping using logarithmic decrement method; (a) Open tube, (b) 4 orifices, (c) 2 orifices.

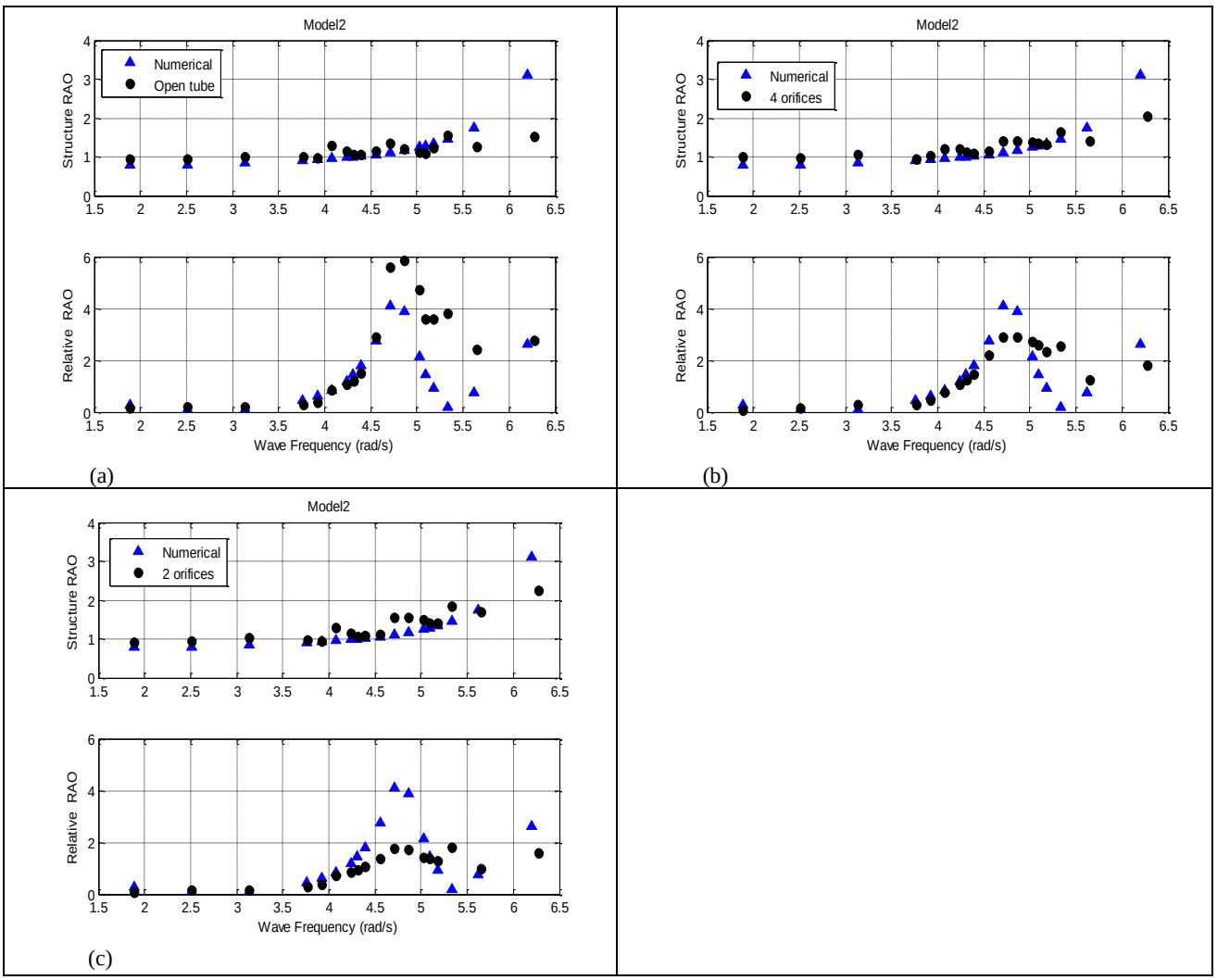

Fig.6.23. Comparison between numerical and experimental structure heave and relative motion RAOs vs. wave frequency for experimental model2; Szumko model, viscous damping using logarithmic decrement method; (a) Open tube, (b) 4 orifices, (c) 2 orifices

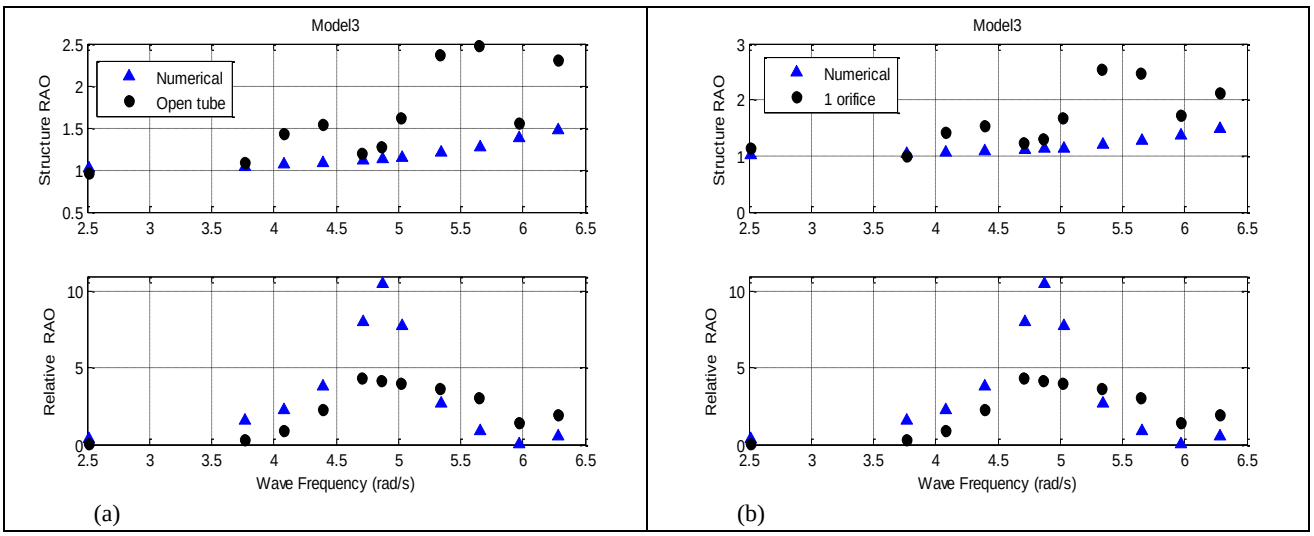

Fig.6.24. Comparison between numerical and experimental structure heave and relative motion RAOs vs. wave frequency for experimental model3; Szumko model, viscous damping using logarithmic decrement method; (a) Open tube, (b) 1 orifice

Modelling results of szumko model showed the best agreement with the experimental results. The disagreement between the predicted and measured relative RAO around the peak frequency is due to the adoption of viscous damping approach. For experimental model3 the measured response has wider bandwidth than the predicted one.

Moreover the relative RAO falls to zero between the two peaks, which does not agree with the experimental results. This is in addition to the sensitivity of the modelling results to the pneumatic stiffness and damping values. Szumko model arranged the spring and damper in series as shown in Fig.6.2.

A modelling problem appeared during the solution of the equations of motion, which is the pneumatic stiffness and damping should have a value not equal to zero. It should be mentioned that during the modelling of the open tube case those values were set to be very small ($0.1*10^{-3}$). Therefore Szumko model has been modified so that the pneumatic spring and damper is parallel. The phase caused by the spring in the first case has been ignored. However the phase between the forces on the two masses is still introduced by the area ratio.

Fig.6.25 presents comparison between numerical and experimental results of structure heave, water column oscillations and relative RAOs for experimental model1 over a wide range of frequencies using the modified Szumko model.

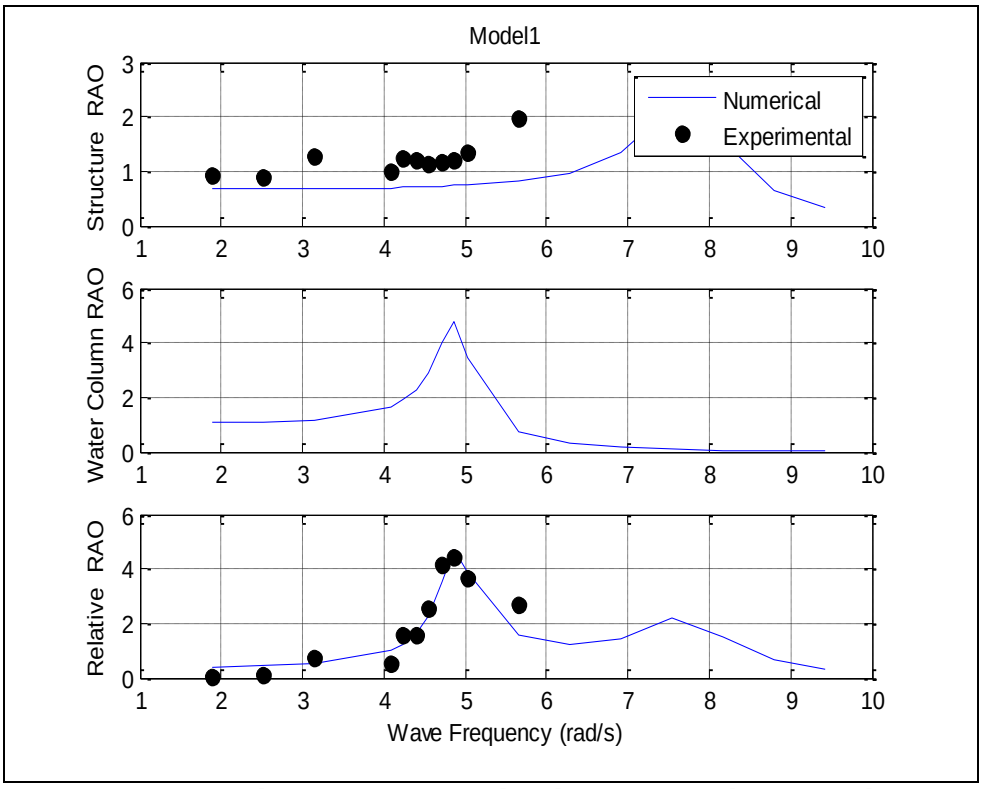

Fig.6.25. Comparison between Numerical and experimental structure heave, water oscillations and relative RAOs vs. wave frequency for experimental model1, open tube; Modified Szumko model, viscous damping using half power bandwidth method.

From the above Fig. it can be seen that results obtained are similar to those obtained from the Szumko model, only two differences appeared. The relative RAO did not fall to zero between the two peaks and agreed with the measured RAO. On the other hand the structure natural frequency is shifted from 7 to 7.5rad/s which caused the deviation between the predicted and measured RAOs.

Concerning the investigation of the performance of the WEC in case the structure is captive, the measured oscillations amplitudes and the predicted ones using the 1DOF model were used to calculate the captured pneumatic power and performance measures. Since results obtained adopting the logarithmic decrement techniques in damping calculation were very high, oscillations amplitudes obtained using the half power bandwidth method were used. It is important to mention that the predicted power captured and performance measures are not realistic. This is due to the use of

the same orifice plates for testing both models without any scaling. But it is important to figure the power absorption behaviour along frequencies. It is expected that full scale results will be significantly different due to the PTO damping used in real conditions. The pneumatic power captured by captive experimental models 1 and 2 calculated using Eq.6.31 are presented in Fig.6.26 and Fig.6.27 respectively.

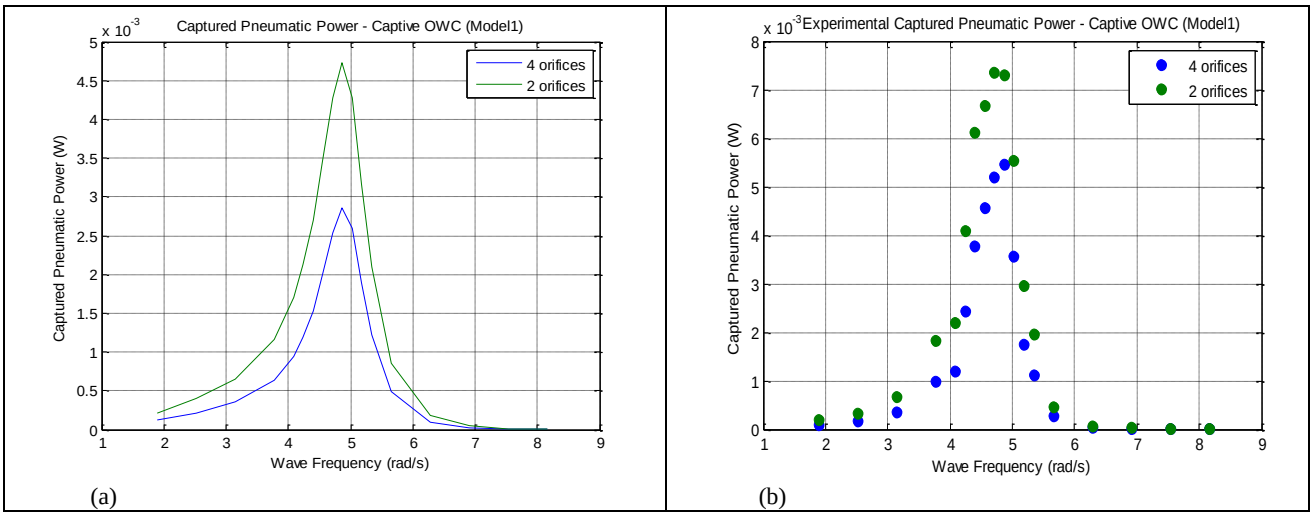

Fig.6.26. Captured pneumatic power by captive experimental model1; (a) Numerical; (b) Experimental

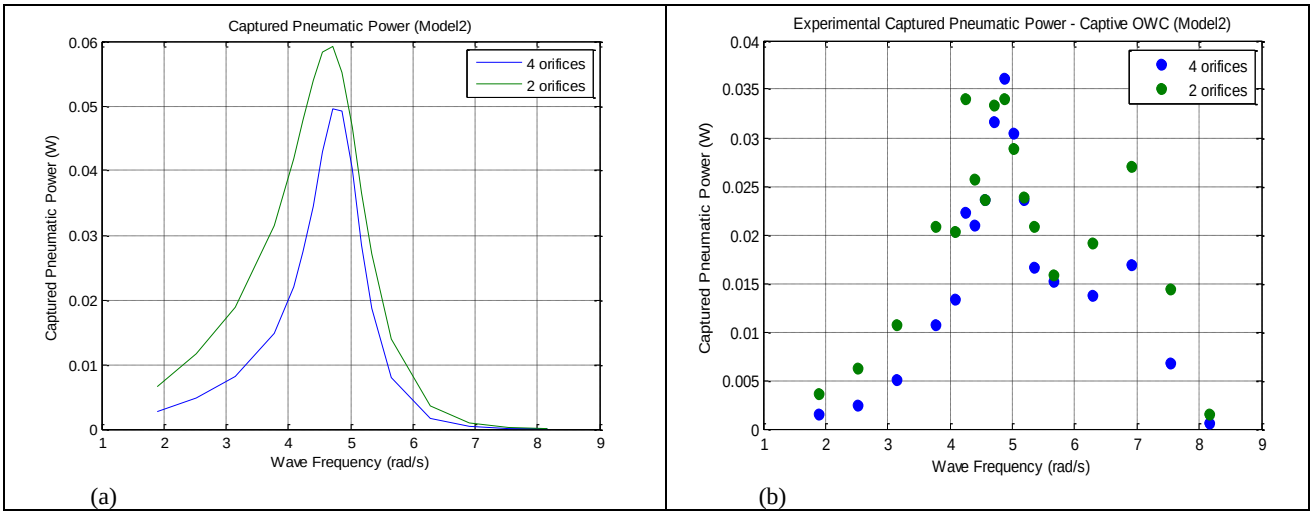

Fig.6.27. Captured pneumatic power by captive experimental model2; (a) Numerical; (b) Experimental

From Fig.6.26 and Fig.6.27 one may notice that as the damping increases, it broadens the region over which significant power capture is achieved especially at excitation frequencies not coincident with the natural frequency. Gomes et al., 2012 reported that the pneumatic stiffness effect on the device increases as the OWC

chamber height increases. In addition, as the height increases, the power absorption single peak (at the peak frequency) becomes smaller and forms two new peaks, one at a higher and other at a lower frequency. As these peaks increase, they move away from the central frequency, reducing the power absorption at that frequency. This effect reduces the annual average power. From Fig.6.27(b) it is noticed that the increase of stiffness due the decrease of orifice area ratio has the same effect.

The dimensionless mean power capture defined as the ratio of the maximum achievable captured power to the power captured by the device. Results obtained from Eq.6.33 are plotted in Fig.6.28 and Fig.6.29 for both experimental models.

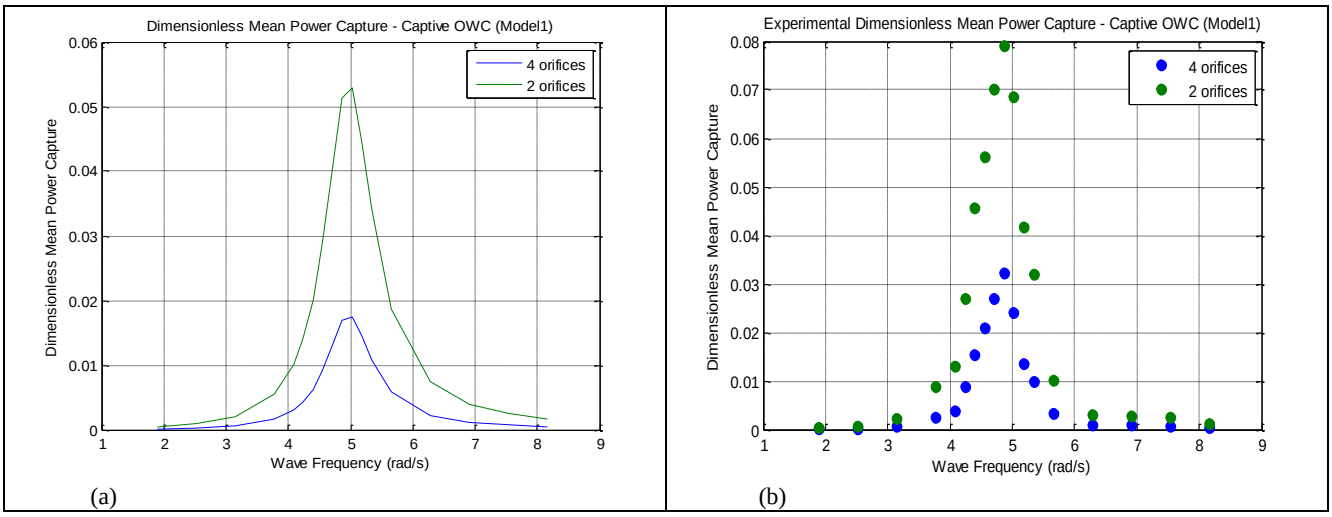

Fig.6.28. Dimensionless mean power capture of captive experimental model 1; (a) Numerical; (b) Experimental

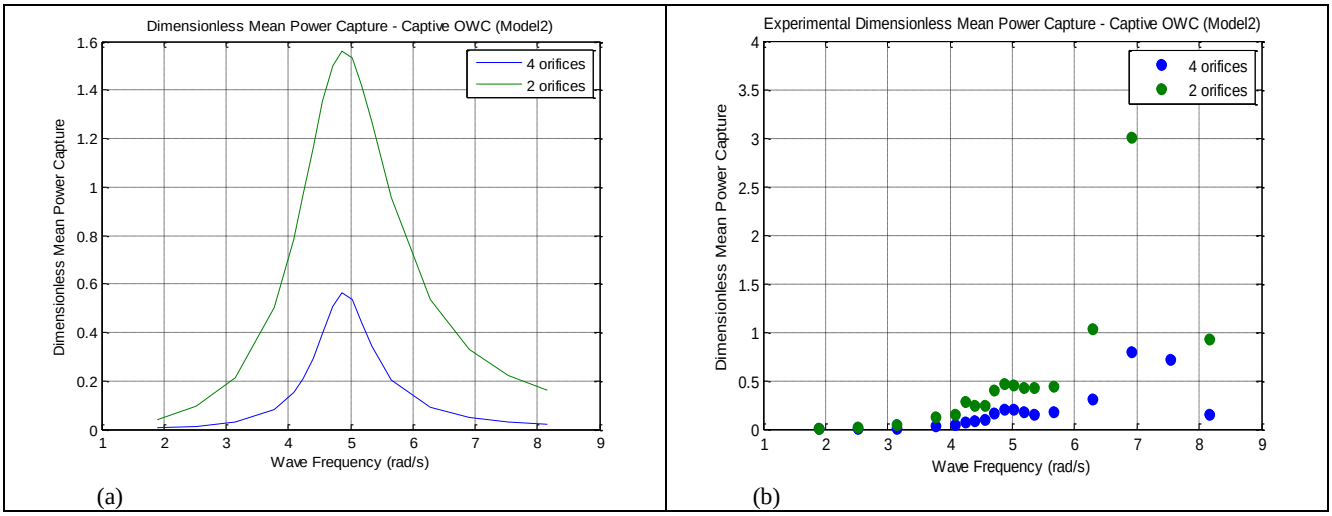

Fig.6.29. Dimensionless mean power capture of captive experimental model 2; (a) Numerical; (b) Experimental

It is clear that results obtained from experimental model2 are extremely higher than those obtained from experimental model 1. This is due to the use of the same orifice plates for testing both models.

It is also noticed that for experimental model2 the numerical and experimental dimensionless mean power capture have the same behaviour for frequencies less than 5.5rad/s, then the pneumatic stiffness affects the system.

The same equation used to calculate the capture width and capture factor of a full scale OWC (Eq.6.34 and Eq.6.35) were used with the reduced scale models, it is important to mention here that wave height of 0.06m was used to calculate the wave power per meter width of a wave used to plot both capture width and factor graphs.

Capture factor of captive device were calculated by dividing the capture width by the water column diameter. Capture width results of the two models are presented in Fig.6.30 and Fig.6.31 capture factor results are presented in Fig.6.32 and Fig.6.33

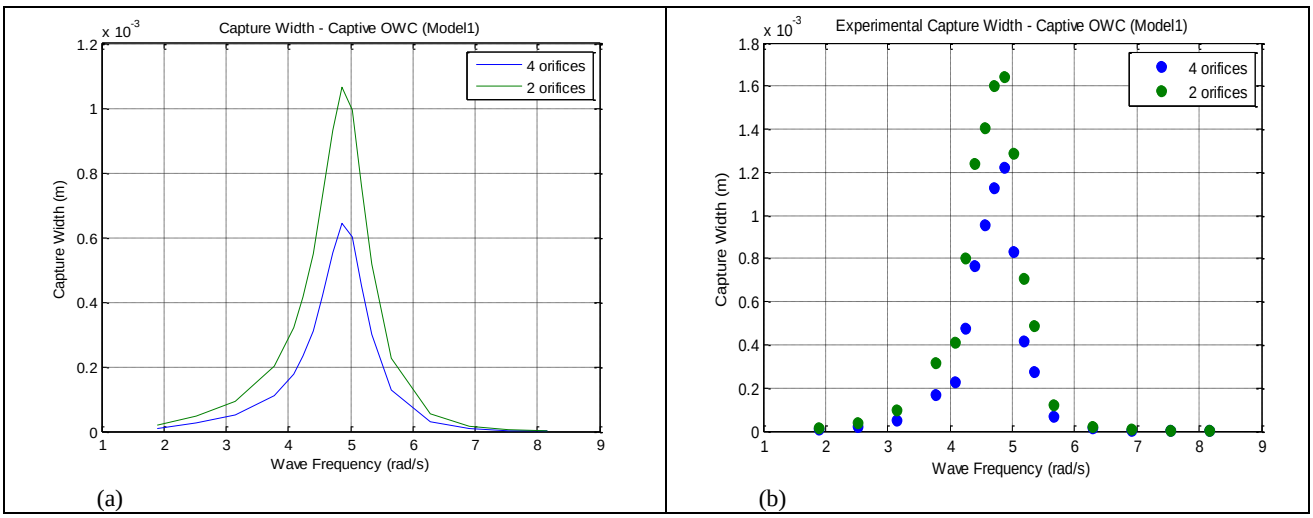

Fig.6.30. Capture width of captive experimental 1; (a) Numerical; (b) Experimental

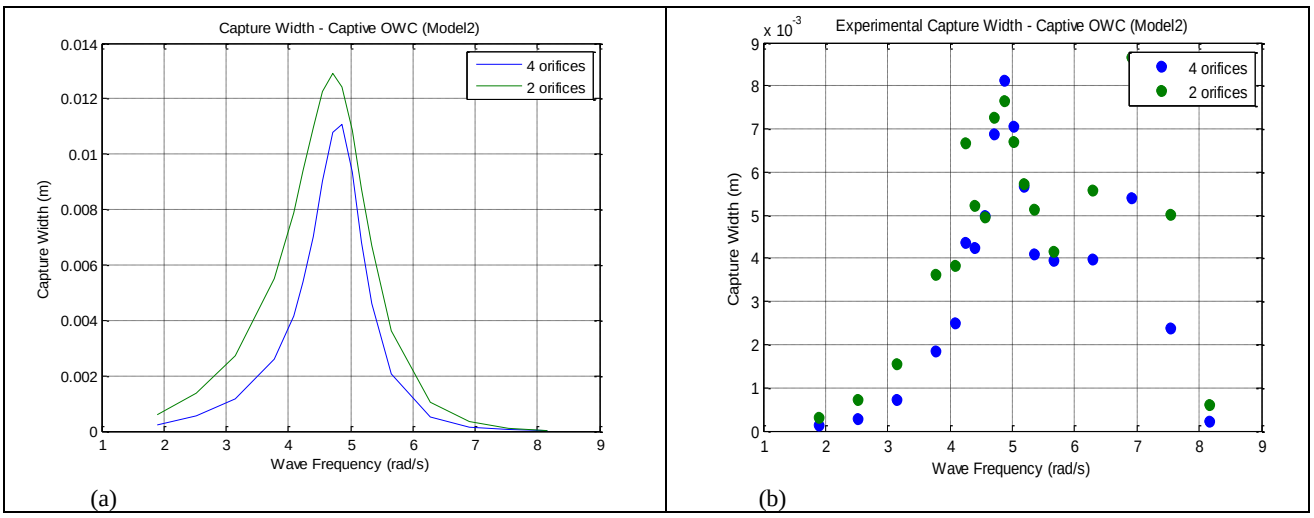

(a) (b)

Fig.6.31. Capture width of captive experimental 2; (a) Numerical; (b) Experimental

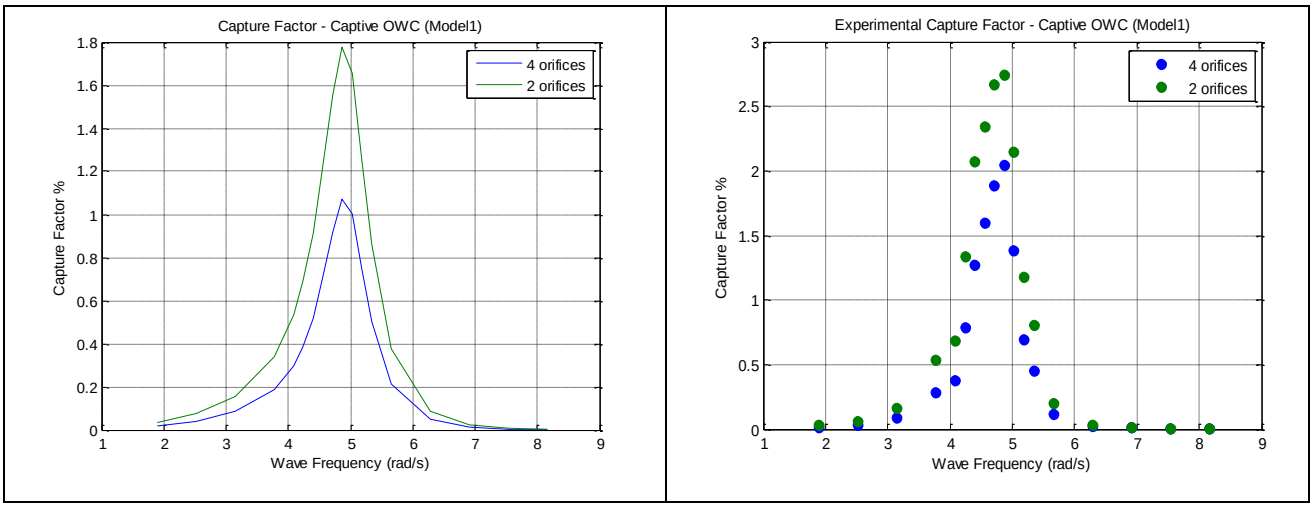

Fig.6.32. Capture factor of captive experimental 1; (a) Numerical; (b) Experimental

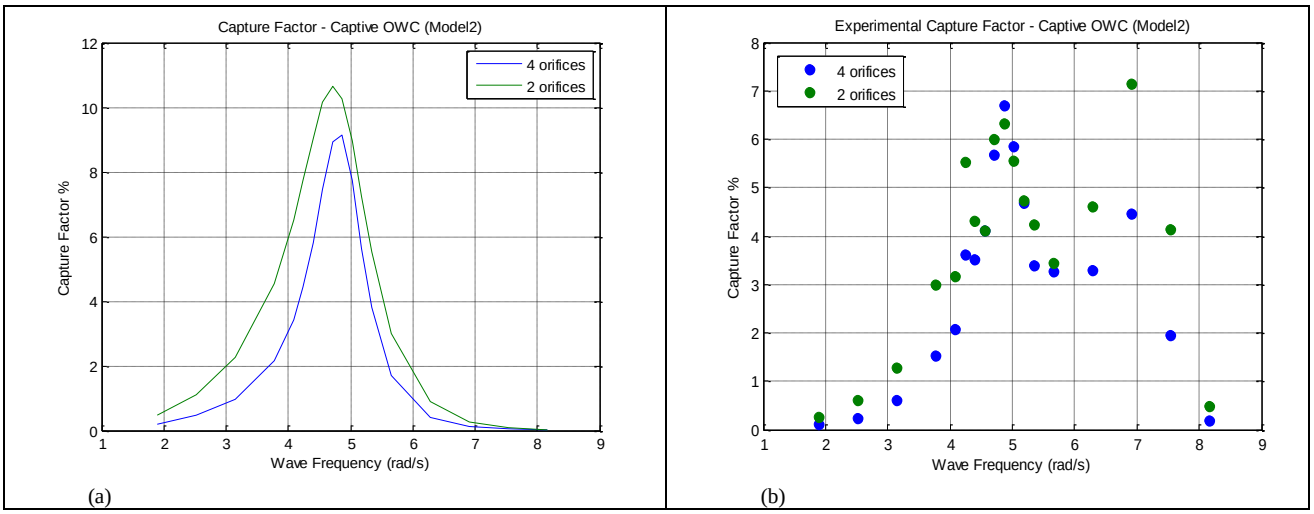

(a) (b)

Fig.6.33. Capture factor of captive experimental 1; (a) Numerical; (b) Experimental

The same procedure adopted to plot the performance measures of captive OWC will be used in case of floating OWC. Instead of using the water column oscillations amplitudes, the relative motion amplitudes between the structure and the water column will be used in calculations. Unfortunately, the water column response around the structure natural frequency was not validated experimentally due to time limitations.

The pneumatic power captured by floating experimental models 1 and 2 are calculated using Eq.6.31 and presented in Fig.6.34 and Fig.6.35 respectively.

Wave height of 0.02m were used to calculate the wave power per meter width of a wave front used to plot both capture width and factor graphs. The diameter of the structure was used to calculate the capture factor from the capture width.

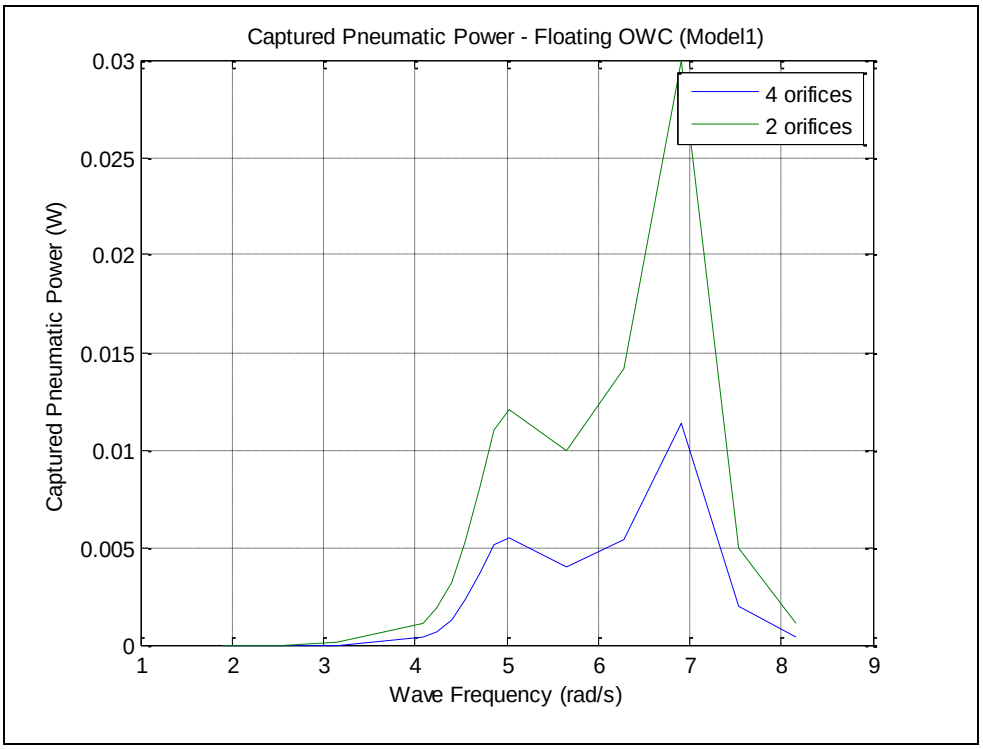

Fig.6.34. Captured pneumatic power by floating experimental 1

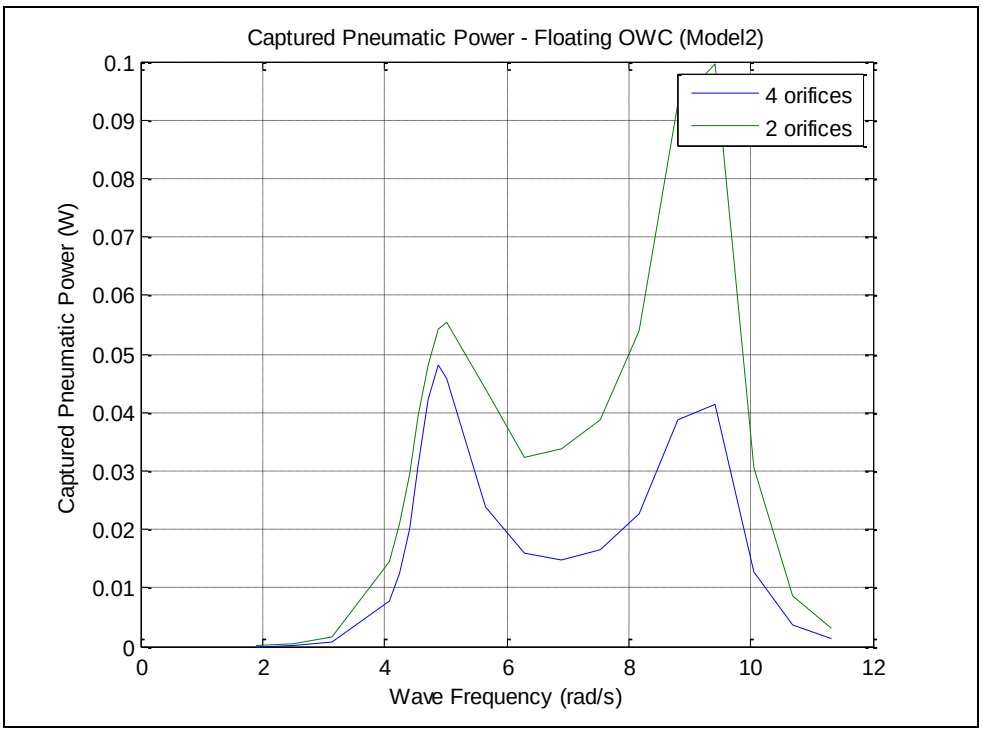

Fig.6.35. Captured pneumatic power by floating experimental 2

The peaks corresponding to the OWC and floating structure natural frequencies are visible in the power capture plots. This is consistent with the floating OWC experimental results from the study by Sykes et al., (2009).

It is noticed that at high damping, the power captured at the structure natural frequency is higher the power captured at the water column natural frequency. This implies that a structural natural frequency lower than the water column natural frequency is favourable in optimising power capture.

Moreover, it is evident from these figures that a significant increase in power capture is achieved when the natural frequencies of the OWC and floating structure are separated compared to the power captured results in case of captive OWC when the structure peak didn't exist and this agrees with Stappenbelt & Cooper (2009).

Capture width results of the two models are presented in Fig.6.36 and Fig.6.37 capture factor results are presented in Fig6.38 and Fig.6.39

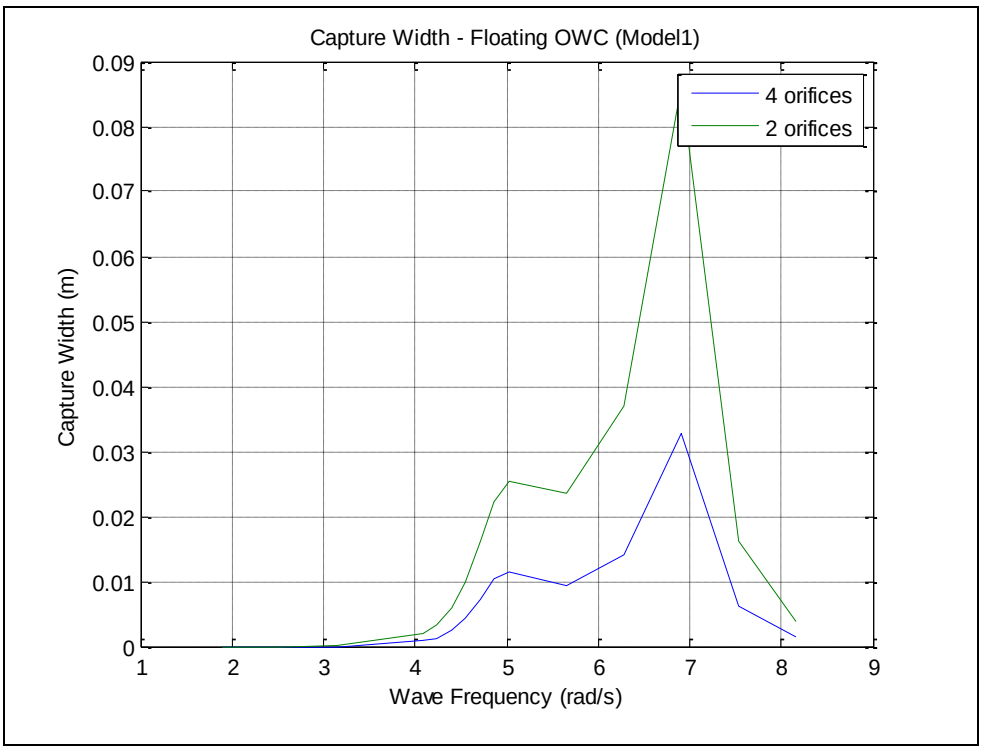

Fig.6.36. Capture width of floating experimental 1

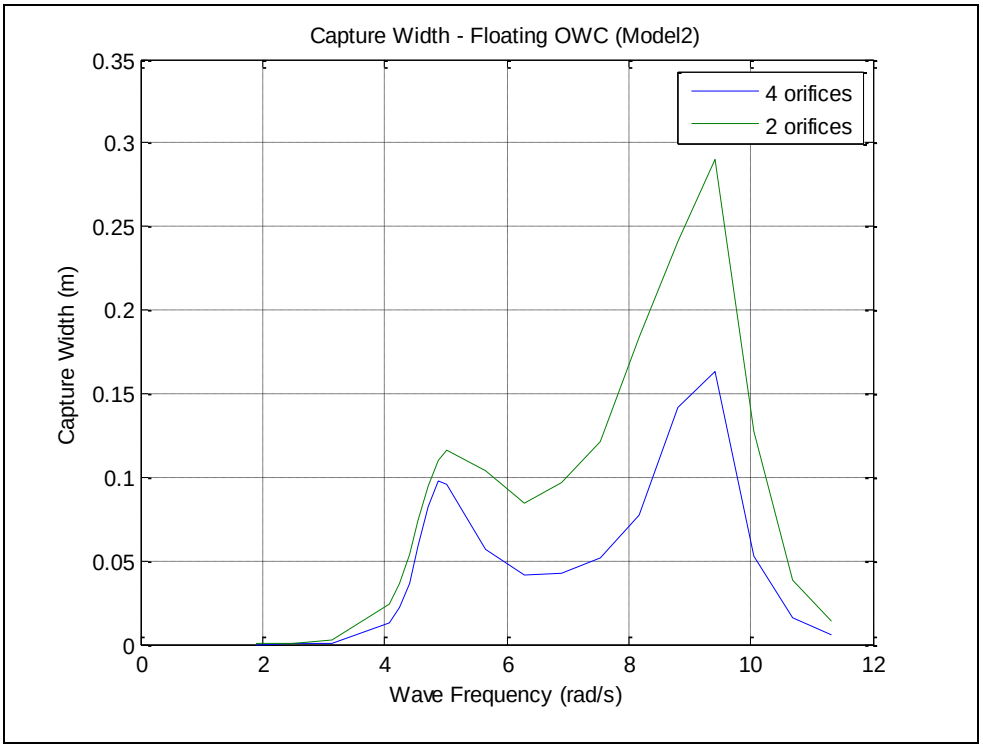

Fig.6.37. Capture width of floating experimental 2;

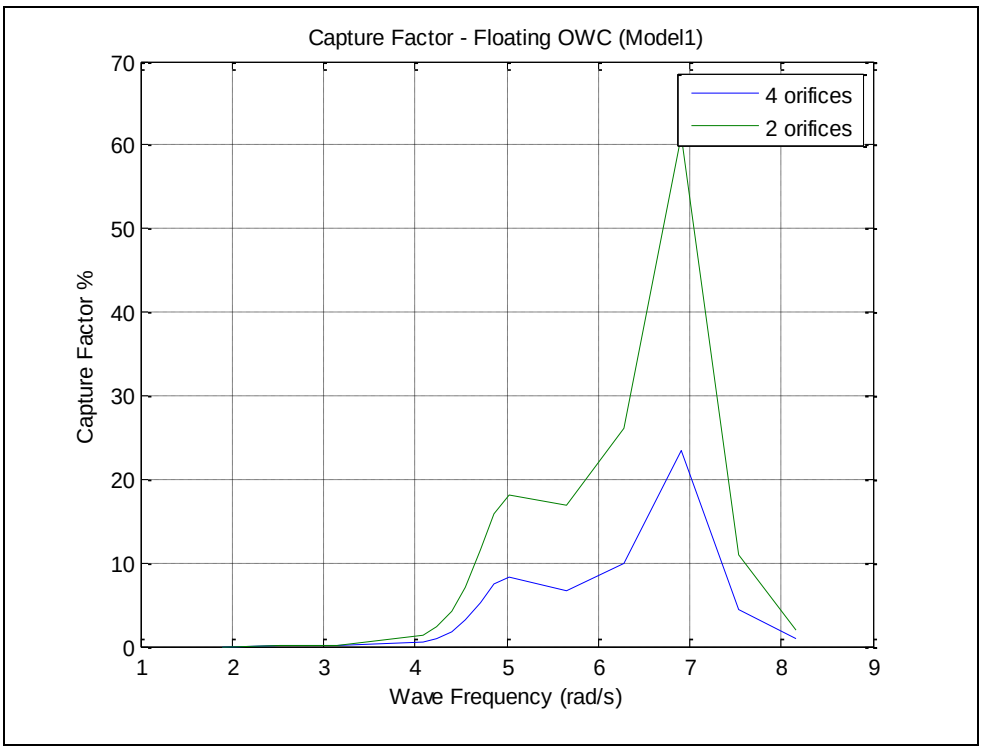

Fig.6.38. Capture factor of floating experimental 1

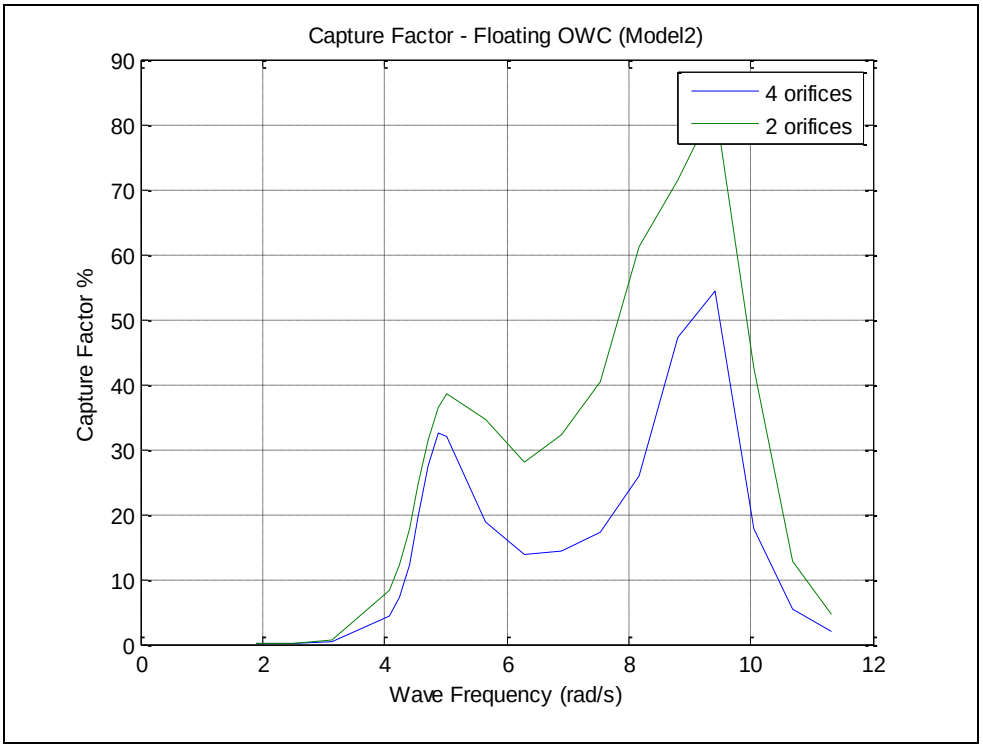

Fig.6.39. Capture factor of floating experimental 2

References of Chapter 6

Aalbers A.B. 1984, 'The water motions in a moonpool', Ocean Engineering Vol. 11 No. 6, pp 557-579

Ayres Frank, 1952, **Theory and problems of differential equations**. Schaums Outline series, McGraw-Hill Book company.

Brendmo A., Falnes J., Lillebekken P.M., 1996, 'Linear modelling of OWCs including viscous loss'. Applied Ocean Research, Vol. 18, pp 65–75.

Falnes J., 2002, **Ocean waves and oscillating systems.** Cambridge: Cambridge University Press

Falcão António F.O., Henriques João C.C., Cândido José J., 2012, 'Dynamics and optimization of the OWC spar buoy wave energy converter'. Renewable Energy Vol. 48 pp 369 - 381

Folley, M. & Whittaker, T., 2005, 'The effect of plenum chamber volume and air turbine hysteresis on the optimal performance of oscillating water columns', In *Proceeding of 24th International Conference on Offshore Mechanics and Arctic Engineering* (OMAE2005), Halkidiki, Greece.

Gervelas R., Trarieux F. amd Patel M., 2011,' A time domain simulator for an oscillating water column in irregular waves at model scale' Ocean Engineering, Vol. 38, pp 1007–1013.

Gomes R.P.F., Henriques J.C.C., Gato, A.F.O. Falcão L.M.C., 2012, 'Hydrodynamic optimization of an axisymmetric floating oscillating water column for wave energy conversion' Renewable Energy Vol. 44 328-339

Hals Jørgen, 2010, 'Modelling and phase control of wave-energy converters', PhD. Thesis Norwegian University of Science and Technology, Norway

Ikoma T, Masuda K, Watanabe Y, and Maeda H, 2012, 'Hydro-elastic responses and performance of owc type wecs of a large scale floating structure'. *In Proceeding of the 6th International Conference on HYDROELASTICITY in Marine Technology* (Hydroelasticity 2012), Tokyo, JAPAN

Incecik, A., 1982, 'Design aspects of hydrodynamic and structural loading on floating offshore platforms under wave excitation', Ph.D. thesis, University of Glasgow, U.K

Jefferys E.R., 1984, 'Simulation of wave power devices'. Applied Ocean Research, Vol. 6, No. 1, pp 31-39.

Matlab 2008, version 7.4, The Mathworks Inc. http://www.mathworks.com

Nunes Guilherme, Duarte Valério, Pedro Beirão, and José Sá da Costa, 2011, Modelling and control of a wave energy converter, Renewable Energy, Vol 36, pp 1913-1921.

Oosthuizen, P.H., and Carscallen W.E., 1997, 'Compressible Fluid Flow, Some Fundamental Aspects of Compressible Flow', The McGraw-Hills, Companies, Inc.,

Singiresu S. Rao, 1991, **Mechanical Vibration**, Third edition, Addison-Wesley Publishing Company, ISBN 0-201-52686-7

Sphaier S. H., Torres F.G.S, Masetti I.Q., Costa A.P. &Levi C, 2007, 'Monocolumn behaviour in waves: Experimental analysis', Ocean Engineering Vol. 34, pp 1724-1733

Stappenbelt Brad and Cooper Paul, 2009, 'Mechanical Model of a Floating Oscillating Water Column Wave Energy Conversion Device', Annual Bulletin of the Australian Institute of High Energetic Materials pp. 34-45. USBN: 978-0-9806811-3-0

Suleman zahid, and Bin khaleeq hammad, 2010, 'Design analysis of power extracting unit of an onshore OWC based wave energy power plant using numerical

simulation'. Mehran university research journal of engineering & technology, volume 30, no. 3, [ISSN 0254-7821]

Szumko, S., 1989, 'Mechanical Model for Oscillating Water Column with Compressibility', *Journal of Engineering Mechanics*, Vol. 115, No.9, pp 1851-1865

Thiruvenkatasamy, K., Neelamani, S. and Sato, M., 1998, 'On the hydrodynamic parametric comparisons of MOWC wave energy caissons in array', Eighth International Offshore and Polar Engineering Conference, Montreal, Canada, pp 119-126

Chapter 7

Nonlinear Modelling of Oscillating Water Column

7.1. Introduction

If nonlinearities can be assumed to be small, frequency domain solutions are sufficient. There are, however, nonlinearities which cannot be reproduced at present in frequency domain solutions. If these other nonlinearities are considered significant or must be investigated a time domain solution is necessary. Such nonlinearities are associated with the drag forces or the nonlinearity associated with the forces in the displaced position of the structure. Second-order diffraction formulations allow higher nonlinear effects to be included (Anam and Roesset, 1994).

7.2. Non-linearity due to large wave forces

The small amplitude wave theory is adopted to predict the forces and resulting responses of the WEC, which is valid for most of the WEC operational life (Cruz, 2008). However, from the survivability perspective the small amplitude wave theory may not be valid. In this section linearized and nonlinear approaches are proposed to predict nonlinear effect associated with incident large waves. For simplification Froude-Krylov approximation is adopted to calculate the wave forces. Linearized approach was adopted to predict nonlinearity in water column oscillations in frequency domain. Later on, time domain nonlinear approach is presented.

7.2.1. Linearized frequency domain model

There are several methods to find approximate solutions for nonlinear problems in the frequency domain, such as perturbation technique or harmonic balance based methods (Nayfeh, 1981). For the model reported herein nonlinear oscillations are analysed asymptotically by means of perturbation method. This approach doesn't require the wave force to be calculated in the time domain. In this case the problem may be formulated by adding a small (perturbed) term to the mathematical description of the linear (auxiliary) problem to represent the nonlinearity and solve the coupled equations in the frequency domain (Nayfeh and Mook, 1979). The equation of motion of the water column oscillations in captive OWC assuming Froude-Krylov approximation is:

$$\boldsymbol{M\ddot{y} + b\dot{y} + ky = 0.5\, H_w A_{wc}\, \rho g \frac{cosh(-dK + w_d K)}{cosh(w_d K)} cos(\omega t)} \qquad \textbf{Eq. 7.1}$$

In order to include the nonlinear effect due to large waves the draft *d* should vary simultaneously with the water column oscillation amplitude *y*.

Assume that:

$$\boldsymbol{d(t) = d_0 - y(t)} \qquad \textbf{Eq. 7.2}$$

where;

d(t) is the instantaneous draft

d_0 is the initial draft

y(t) is the instantaneous oscillation amplitude

Therefore the pressure force *F* becomes:

$$\boldsymbol{F = 0.5\, H_w\, A\, \rho g \frac{cosh(-(d_0 - y)K + w_d K)}{cosh(w_d K)} cos(\omega t)} \qquad \textbf{Eq. 7.3}$$

Let:

$$\boldsymbol{F = B\, \mathbf{cosh}[-(d_0 - w_d)k + yk]\, \mathbf{cos}(\omega t)} \qquad \textbf{Eq. 7.4}$$

where:

$$\boldsymbol{B = \frac{0.5\, H_w\, A\, \rho g}{cosh(w_d K)}} \qquad \textbf{Eq. 7.5}$$

If, $|w_d - d| \gg y$, The equation can be linearized and its solution is to be composed of 2 solutions in the form of $y = y_0 + y_1$using classical perturbation technique, so that the equation of motion may be written as:

$$\boldsymbol{M(\ddot{y}_0 + \ddot{y}_1) + b(\dot{y}_0 + \dot{y}_1) + k(y_0 + y_1) = B\cosh[-(d_0 - w_d) + yk]\cos(\omega t)} \qquad \textbf{Eq .7.6}$$

Reduced to:

$$\boldsymbol{M(\ddot{y}_0 + \ddot{y}_1) + b(\dot{y}_0 + \dot{y}_1) + k(y_0 + y_1) = B[cosh(-(d_0 - w_d)K)\, cosh(yK) + sinh(-(d_0 - w_d)K)\, sinh(yK)]\, cos(\omega t)} \qquad \textbf{Eq. 7.7}$$

Reduced to

$$\boldsymbol{M(\ddot{y}_0 + \ddot{y}_1)\dot{y} + b(\dot{y}_0 + \dot{y}_1) + k(y_0 + y_1) = B[cosh(-(d_0 - w_d)K)(1) + sinh(-(d_0 - w_d)K)\,(yK)]\, cos(\omega t)} \qquad \textbf{Eq. 7.8}$$

Reduced to

$$\boldsymbol{M(\ddot{y}_0 + \ddot{y}_1) + b(\dot{y}_0 + \dot{y}_1) + k(y_0 + y_1) = B\, cosh(-(d_0 - w_d)K)\, cos(\omega t) + BK\, sinh(-(d_0 - w_d)K) y\, cos(\omega t)} \qquad \textbf{Eq. 7.9}$$

Reduced to:

$$\boldsymbol{M(\ddot{y}_0 + \ddot{y}_1) + b(\dot{y}_0 + \dot{y}_1) + k(y_0 + y_1) = [F_0 + F_1 y]\cos(\omega t)} \qquad \textbf{Eq. 7.10}$$

Reduced to:

$$\boldsymbol{M(\ddot{y}_0 + \ddot{y}_1) + b(\dot{y}_0 + \dot{y}_1) + k(y_0 + y_1) = [F_0 + F_1(y_0 + y_1)]\, cos(\omega t)} \qquad \textbf{Eq. 7.11}$$

where;

$$F_0 = Bcosh(-(d_0 - w_d)K) \quad \textbf{Eq. 7.8}$$

$$F_1 = BK\,sinh(-(d_0 - w_d)K) \quad \textbf{Eq. 7.9}$$

From Eq.7.11 – Eq.7.13, we thus have:

$$M\ddot{y}_0 + b\dot{y}_0 + ky_0 = F_0\,cos(\omega t) \quad \textbf{Eq. 7.10}$$

$$M\ddot{y}_1 + b\dot{y}_1 + ky_1 = F_1(y_0 + y_1)\,cos(\omega t) \quad \textbf{Eq. 7.11}$$

Now the Eq.7.14 & Eq.7.15 are to be solved simultaneously for y_0 and y_1 using Matlab.

7.2.2. Non-linear time domain model

For more accurate prediction numerical nonlinear approach is adopted. This requires the calculation of wave force in time domain, which is obtained by taking into account the instantaneous draft. Matlab ode23 allows the solution of the equation in this form.

Therefore the force may be written directly as:

$$F(t) = 0.5\,H_w\,A\,\rho g\frac{cosh(-(d+y(t))K+w_dK)}{cosh(w_dK)} \quad \textbf{Eq. 7.12}$$

7.3. Non-linearity due to damping forces

Damping coefficients relate the floating structures rigid body velocities to the hydrodynamic damping forces. Two types of damping forces may be experienced on the floating structures which oscillate near or on the free surface.

First, wave damping forces due to the dissipation of energy in the form of surface waves which are generated as a result of rigid body motion of floating structures (radiated waves).

Second, viscous damping forces which are due to the turbulent flow in the lee of a body.in other words it is due to a deviation of the pressure distribution from its ideal fluid value (Incecik, 1982). In case of OWC, PTO mechanism adds more damping which extracts energy from the system. Equivalent Viscous Damping (EVD) methodology based on linear and quadratic damping coefficients will be adopted for both frequency and time domain analysis. The linear and quadratic damping coefficients b_L and b_Q can be derived from the decrease in the water elevation for two successive cycles from the decay test, and then the equivalent viscous damping corresponding to particular water elevation amplitude may be calculated as:

$$\boldsymbol{b_{eq} = b_L + b_Q \frac{16y}{3T}} \qquad \textbf{Eq. 7.13}$$

where, T is the natural period. b_L and b_Q are obtained by plotting (the decrease in oscillation amplitude /mean amplitude) against (oscillation amplitude). Then the data is fitted using the least squared technique to yield a linear equation of the form $Y = nX + c$. The slope, n, is related to the quadratic damping coefficient and its y-axis intercept, c, is related to the linear damping coefficient as follow:

$$\boldsymbol{b_Q = \frac{3}{8} M\, n} \qquad \textbf{Eq. 7.18}$$

$$\boldsymbol{b_L = 2c \frac{M}{T}} \qquad \textbf{Eq. 7.19}$$

where, M and T are the mass and natural period of the oscillating body.

7.3.1. Iterative (optimised) frequency domain model

The analytical solution of the equation of motion of a single DOF system in frequency domain gives:

$$y = \frac{F/k}{\sqrt{\left[1-\left(\omega/\omega_n\right)^2\right]^2+\left[2\xi_{eq}\left(\omega/\omega_n\right)\right]^2}} \qquad \textbf{Eq. 7.20}$$

Similarly to the method suggested by Blagoveschchensky, 1962 to optimize the linear and quadratic coefficients, Matlab script is used to solve Eq. (7.19) with EVD Eq. (7.16) as an iterative solver. This is achieved by assuming amplitude of motion, the damping coefficients are calculated and then the equation of motion is solved. Motion amplitudes obtained from these equations can now be used to determine new damping coefficients and the equation of motion is again solved. This iteration procedure continues until two successive linear damping coefficients are close enough to each other (1% relative error) (Incecik, 1982).

7.3.2. Time domain non-linear model

In this model numerical nonlinear approach is adopted. This requires the calculation of damping force in time domain, which is achieved by taking into account the instantaneous oscillation amplitude as in Eq. (6.16). Therefore the EVD is used to substitute the viscous damping coefficient in the equation of motion Eq. (6.1). So that it can be written as:

$$M\ddot{y} + \left(b_L + b_Q\frac{16y}{3T}\right)\dot{y} + ky = F\cos(\omega t) \qquad \textbf{Eq. 7.21}$$

The equivalent system of first-order differential equation used for Matlab in this case becomes:

$$\dot{u}_1 = u_2 \qquad \textbf{Eq. 7.22}$$

$$\dot{u}_2 = -\frac{\left(b_L+b_Q\frac{16u_1}{3T}\right)}{m}u_2 - \frac{k}{m}u_1 + \frac{f}{m}\cos(\omega t) \qquad \textbf{Eq. 7.23}$$

The linear and quadratic damping coefficients are not optimized in this case but taken as constants which are obtained experimentally.

7.4. Nonlinearity due to air compressibility

Perturbation techniques previously discussed in section 7.2.1 may be used to linearize the air compressibility effects in case analysis is required to be performed in frequency domain. In this section nonlinear effect due to air compressibility is modelled in time domain by considering the instantaneous pneumatic chamber volume in calculations.

In this case the stiffness due to air compressibility (pneumatic stiffness) is in the form:

$$\boldsymbol{k_{air}(t) = \frac{\gamma\, p\, {A_{wc}}^2}{V(t)}} \qquad \textbf{Eq. 7.24}$$

where;

V(t) is the instantaneous volume calculated as:

$$\boldsymbol{V(t) = A_{wc}\left(h - y(t)\right)} \qquad \textbf{Eq. 7.25}$$

Where, h is the pneumatic chamber height. Once again, Matlab ode23 allows the solution of the equation of motion in the new form:

$$\boldsymbol{M\ddot{y} + b\dot{y} + (k_{wc} + \frac{\gamma\, p\, A_{wc}}{(h-y)})y = F\cos(\omega t)} \qquad \textbf{Eq. 7.26}$$

7.5. Results and discussions

This chapter aimed to investigate nonlinear response of water column inside captive OWC-WEC due to large wave and nonlinear damping in both time and frequency domains. Time domain representations of linear, perturbed and linearized water column oscillation amplitudes obtained originally from frequency domain analysis using perturbation theory (section 7.2.1) are presented in Fig.7.1 and Fig.7.2 for experimental model1 at different wave frequencies.

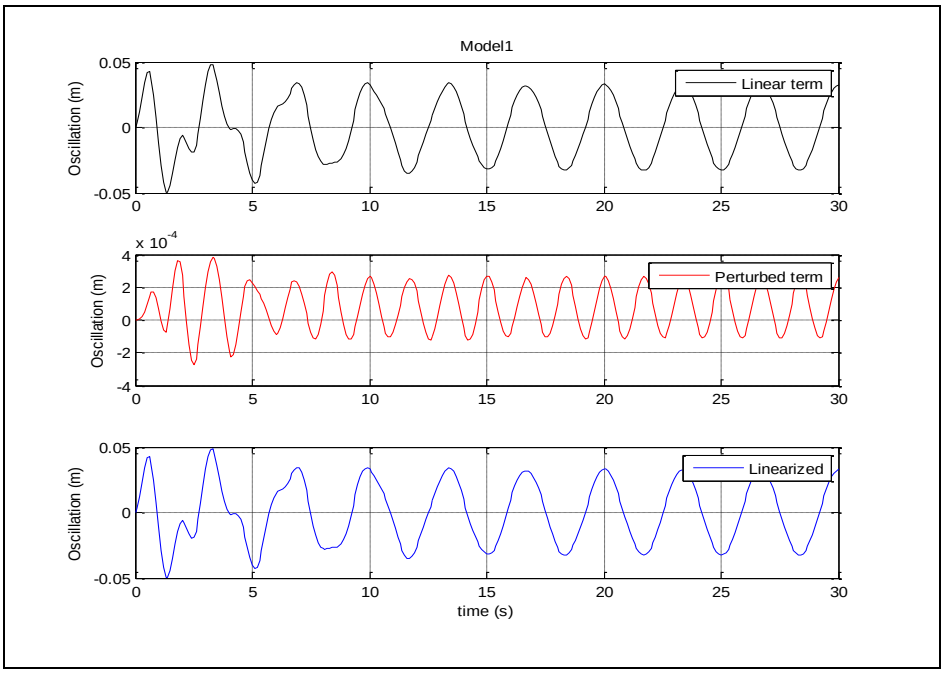

Fig.7.1. Time domain representation of linear, perturbed and linearized water column oscillation amplitude for experimental model1; 1DOF, large wave model; $H_W = 0.06m$, $\omega = 1.8rad/s$

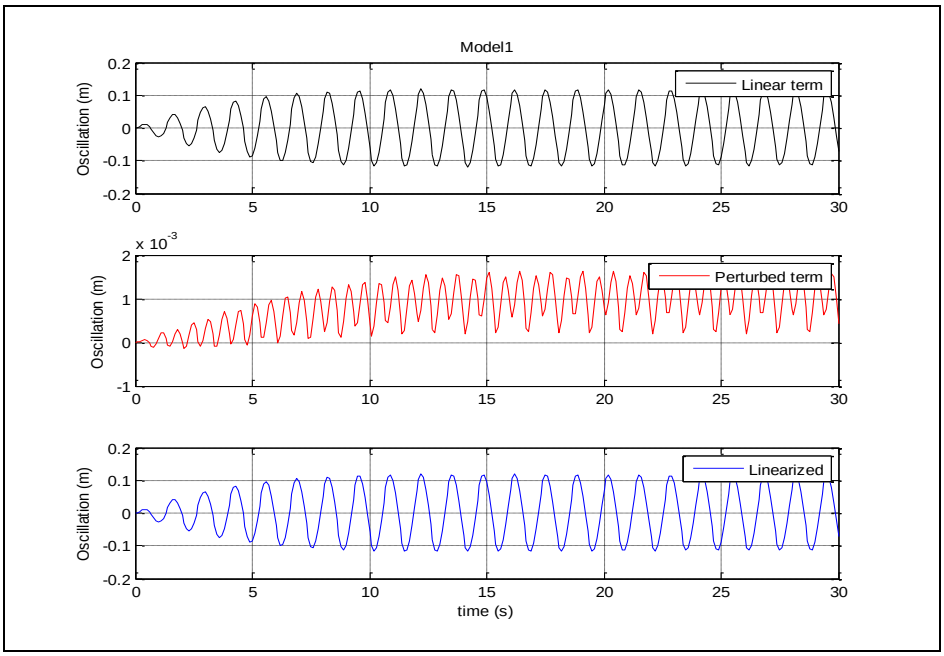

Fig.7.2. Time domain representation of linear, perturbed and linearized water column oscillation amplitude for experimental model1; 1DOF, large wave model; $H_W = 0.06m$, $\omega = 4.8rad/s$

Fig.7.1 and Fig.7.2 showed that the perturbed term is very small compared to the linear one which clarify the similarity between the linear and linearized results.

Fig.7.3 shows comparison between linear, linearized and nonlinear water column oscillations (nonlinear approach discussed in section 7.2.2).

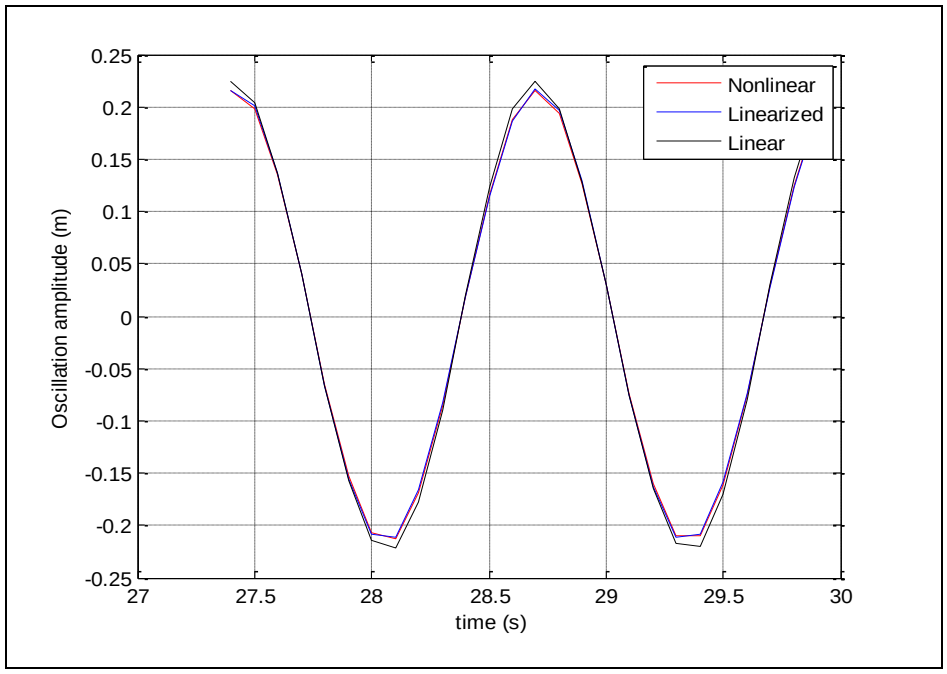

Fig.7.3. Comparison between linear, linearized and nonlinear water column oscillations (due to large waves) vs. time for experimental model1, open tube; 1DOF model, $H_W = 0.09$m, $\omega = 4.8$rad/s

Frequency domain representation comparing the experimental water column oscillations RAO and the results obtained from linear, linearized and nonlinear approaches is presented in Fig.7.4 (using the damping values calculated by the logarithmic decrement method). It is clear that results of the three approaches are very close. However linear results are the highest followed by the linearized then the nonlinear approach results.

Differences between the results obtained from the three approaches increase as the response amplitude increases. Therefore comparison is performed at the water column natural frequency and higher wave amplitudes. This comparison is shown in Fig.7.5. Note that the y-axis scale is very small.

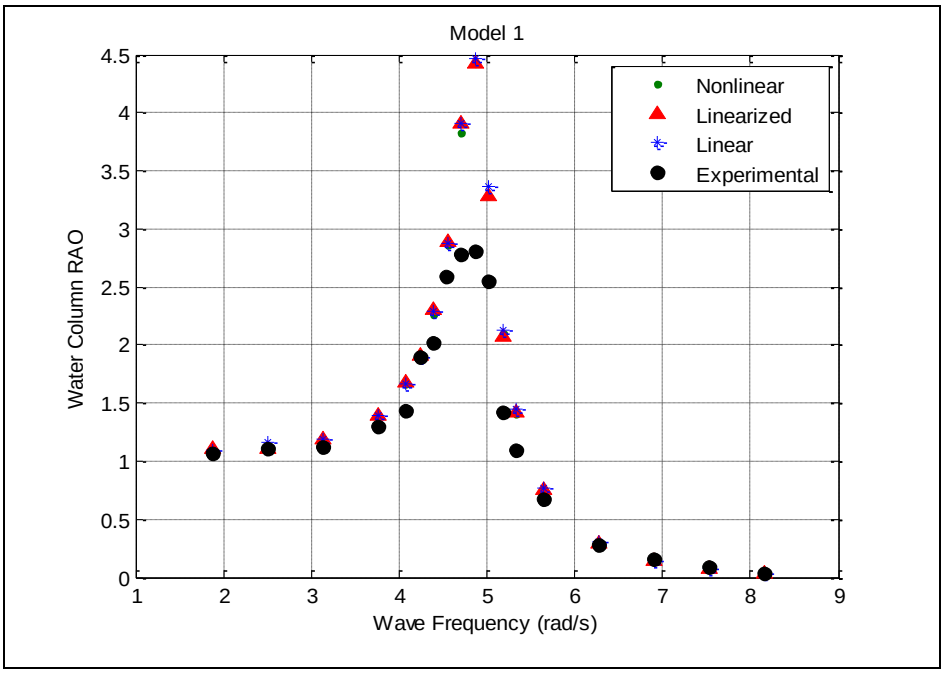

Fig.7.4. Comparison between numerical (linear, linearized and nonlinear due to large waves) and experimental water column oscillations RAOs vs. wave frequency for experimental model1; 1DOF model

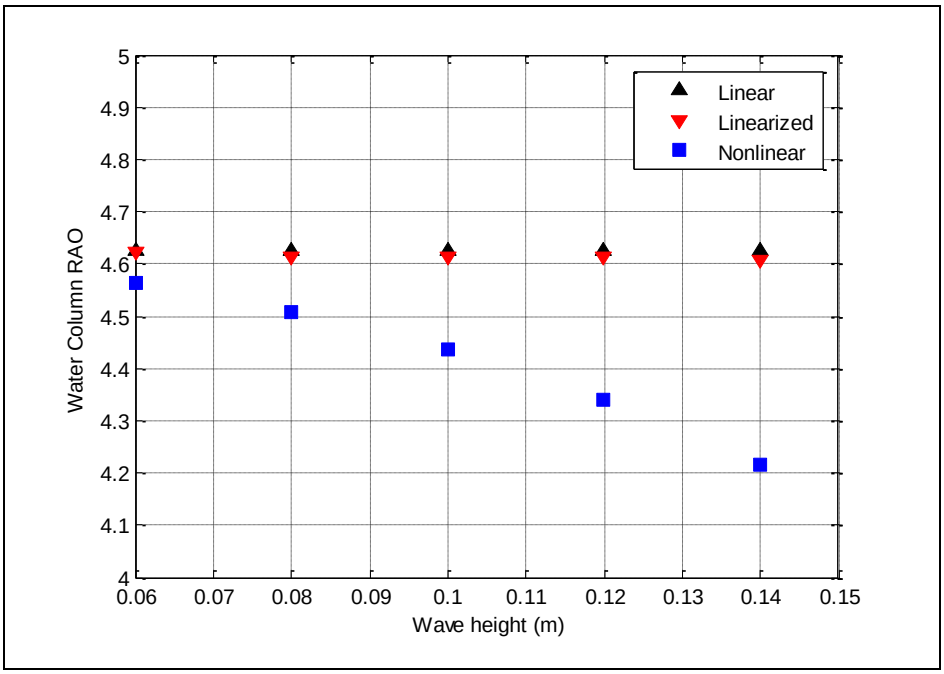

Fig.7.5. Comparison between linear, linearized and nonlinear water column RAO (due to large waves) vs. incident wave height for experimental model1, open tube; 1DOF model, $\omega = 4.8$rad/s

For normal ships, nonlinear response is slightly lower than the linear one, since the water-plane area of the ship corresponding to the hydrostatic stiffness increases with

higher heave amplitudes due to the hull shape. Unlike ships, spars have a constant diameter, consequently constant stiffness, but the pneumatic stiffness due to air compressibility increases in addition to friction losses. Fig.7.5 shows that linearized solution is much closer to the linear solution than the nonlinear one, which questions the suitability of this approach to this type of nonlinearity.

The second type of nonlinearity investigated herein is due to nonlinear damping.

Fig.7.6, presents sample of the water elevation decay test where the oscillations peaks and troughs are detected, in order to plot the decrease in water elevation /mean water elevation against the water elevation.

It shows that the linear least squared fitting technique is suitable in this case to yield a linear equation of the form $Y=nX+c$, leading to The linear and quadratic damping coefficient. The linear least squared is a technique used to arrive at the regression equation by minimizing the sum of the squares of the vertical distances between the actual Y values and the predicted values of Y.

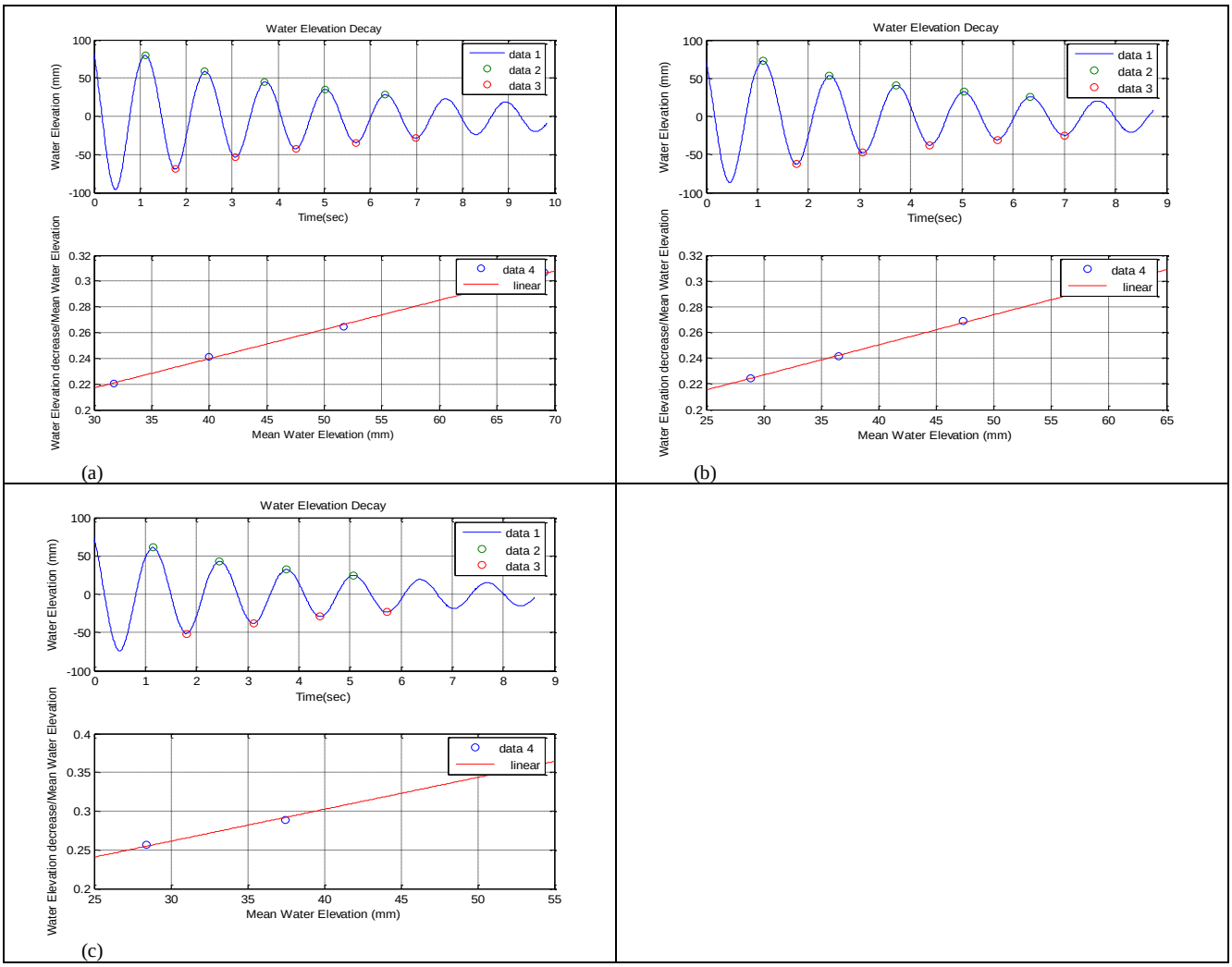

Fig.7.6. Linear least squared fit results, Experimental model1 (a) open tube, (b) 4 orifices, (c) 2 orifices

The equivalent damping ratio increases slightly with the increase of the water elevation amplitude since the equivalent viscous damping is related to the water elevation amplitude. The logarithmic decrement calculated from selected cycles of the decay test is presented in (Fig.7.7)

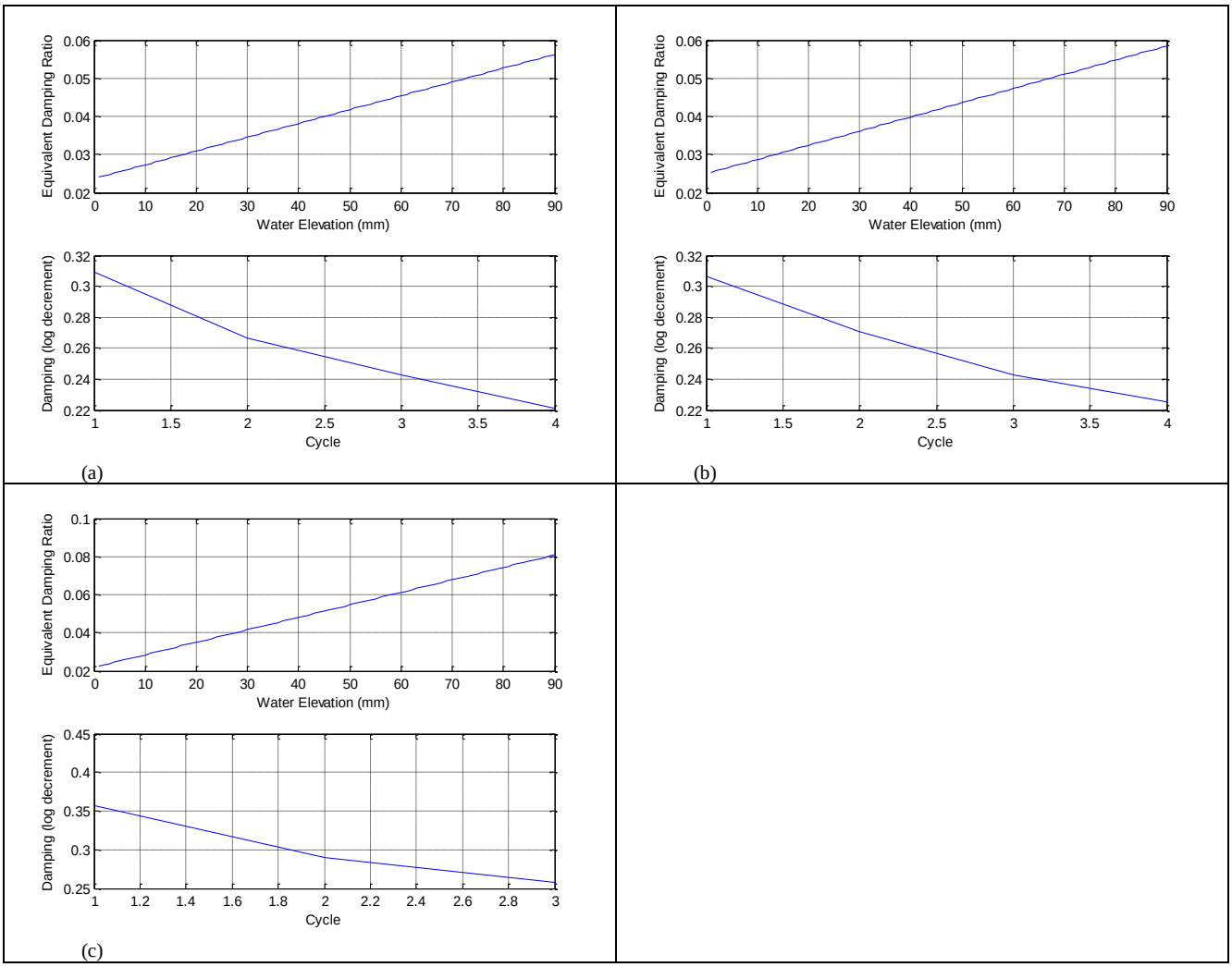

Fig.7.7. Equivalent viscous damping ratio vs water elevation and Logarithmic decrement vs cycles, (a) open tube, (b) 4 orifices, (c) 2 orifices

Linear and quadratic damping results obtained from the Matlab program analysing the decay are presented in Table 7.1

Table 7.1: Linear and quadratic damping coefficients

	Experimental model 1			**Experimental model 2**		
	Open tube	4 orifices	2 orifices	Open tube	4 Orifices	2 Orifices
Linear coefficient	0.279	0.280	0.285	0.340	0.39	0.42
Quadratic coefficient	0.0009	0.002	0.003	0.005	0.017	0.067

In order to achieve better agreement with the experimental results the iterative procedure discussed in section is applied to optimise the damping coefficients.

Optimized damping values for experimental model 1 and 2 in case of open tube, 4 orifices and 2 orifices are presented in Fig.7.8 and Fig.7.9.

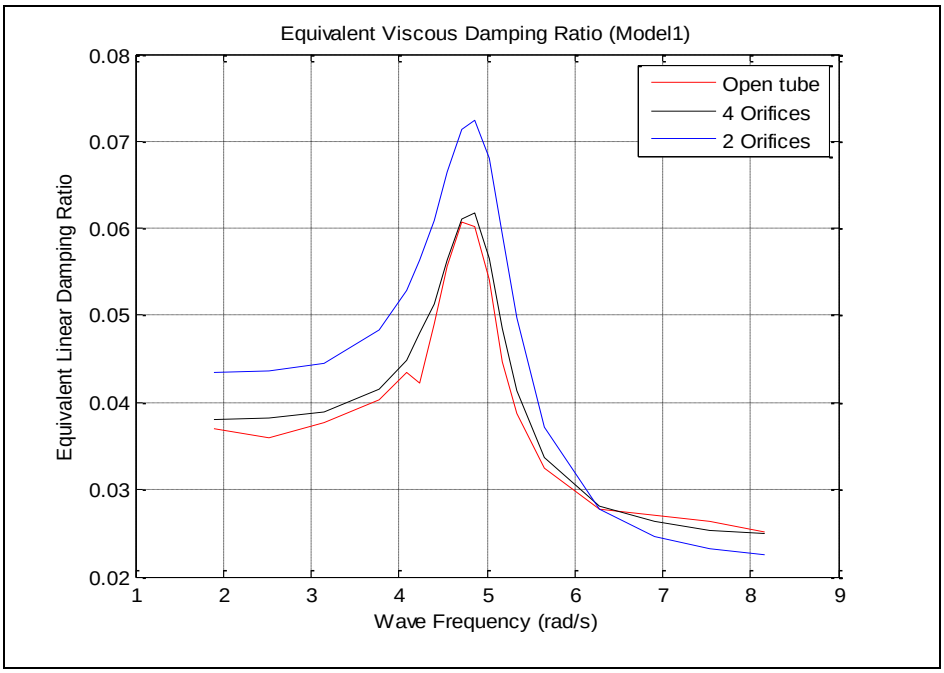

Fig.7.8. Optimized equivalent viscous damping ratios of experimental model 1

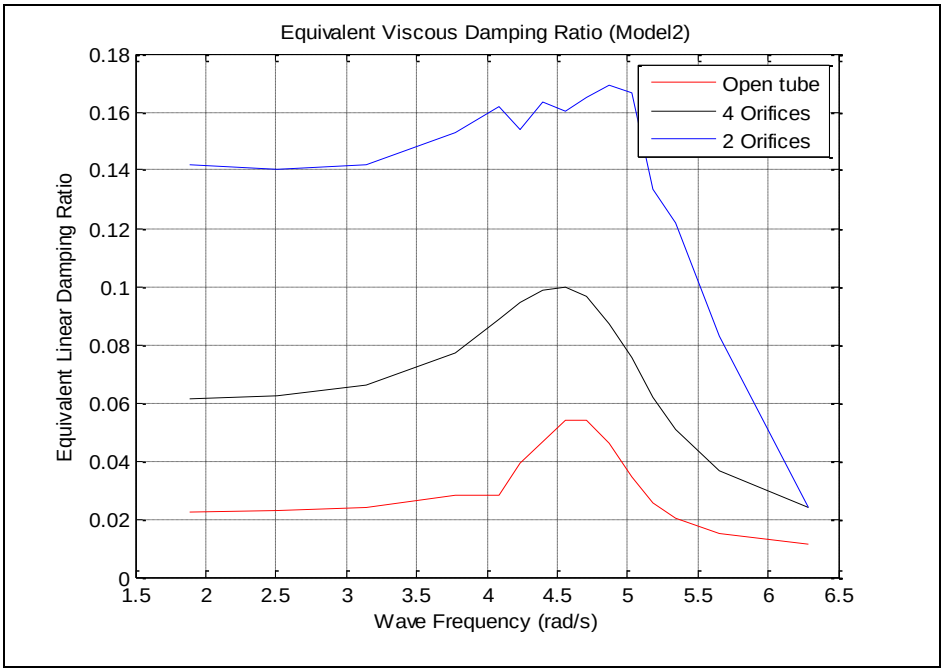

Fig.7.9. Optimized equivalent viscous damping ratios of experimental model 2

Results obtained adopting the two methodologies discussed in sections 7.3.1 and 7.3.2 are presented in Fig.7.10 in comparison with the experimental results and those

obtained from linear modelling discussed in chapter 6 using the damping values calculated by the logarithmic decrement method.

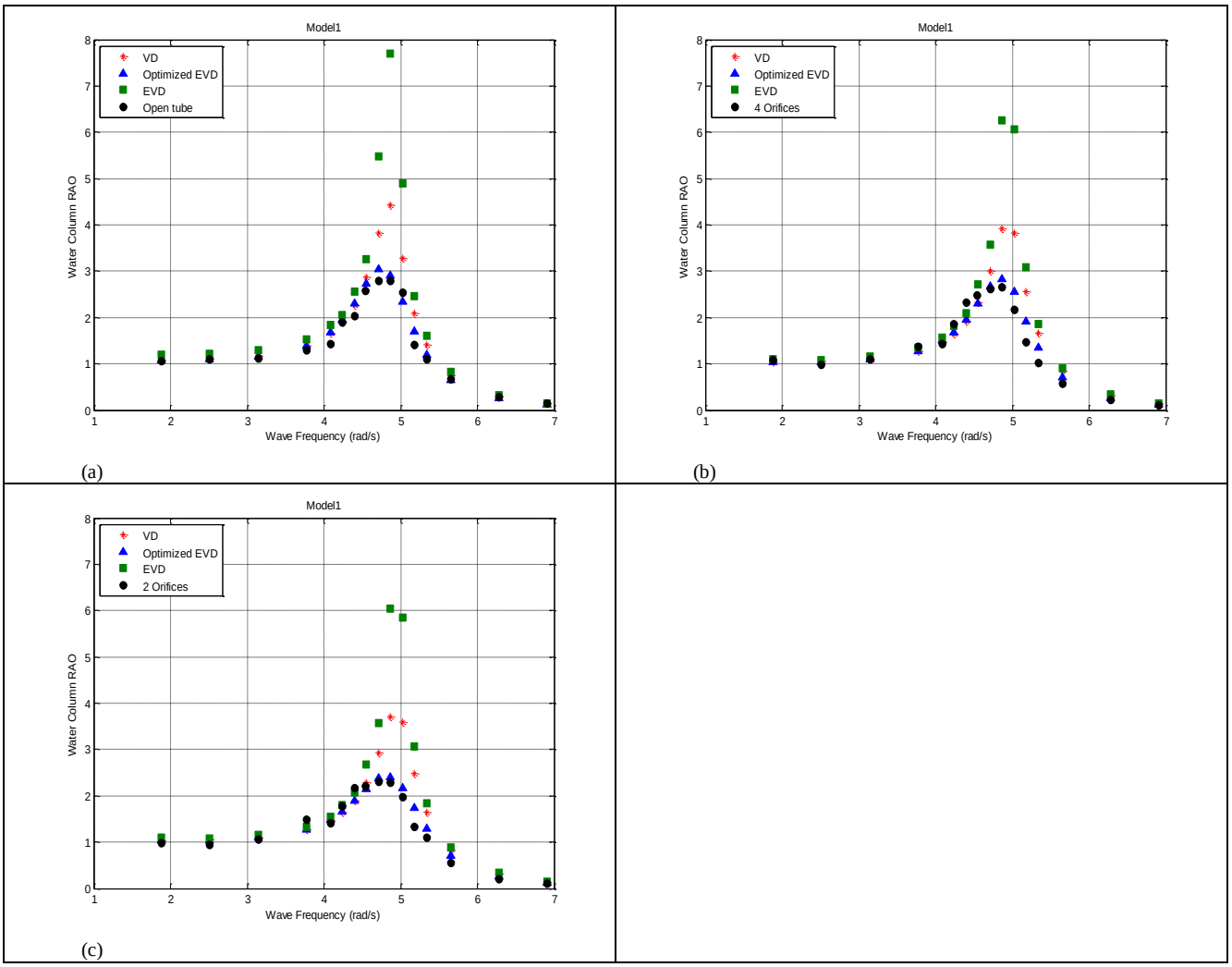

Fig.7.10. Comparison between numerical (viscous, equivalent viscous and optimised equivalent viscous damping) and experimental water column oscillations RAOs vs. wave frequency for experimental model 1; 1DOF model; (a) Open tube, (b) 4 orifices, (c) 2 orifices.

The clear disagreement between the experimental results and the EVD approach results near resonance in Fig.7.10 is caused by the inaccurate prediction of the linear and quadratic damping coefficients from the free oscillation tests of the water column.

In contrast, the adopted iterative procedure used to optimize the damping coefficients was very successful leading to a very good agreement with the experimental results

and allows the analysis to be performed in frequency domain. Comparison of the experimental results of model 2 and the predicted result are presented in Fig 7.11.

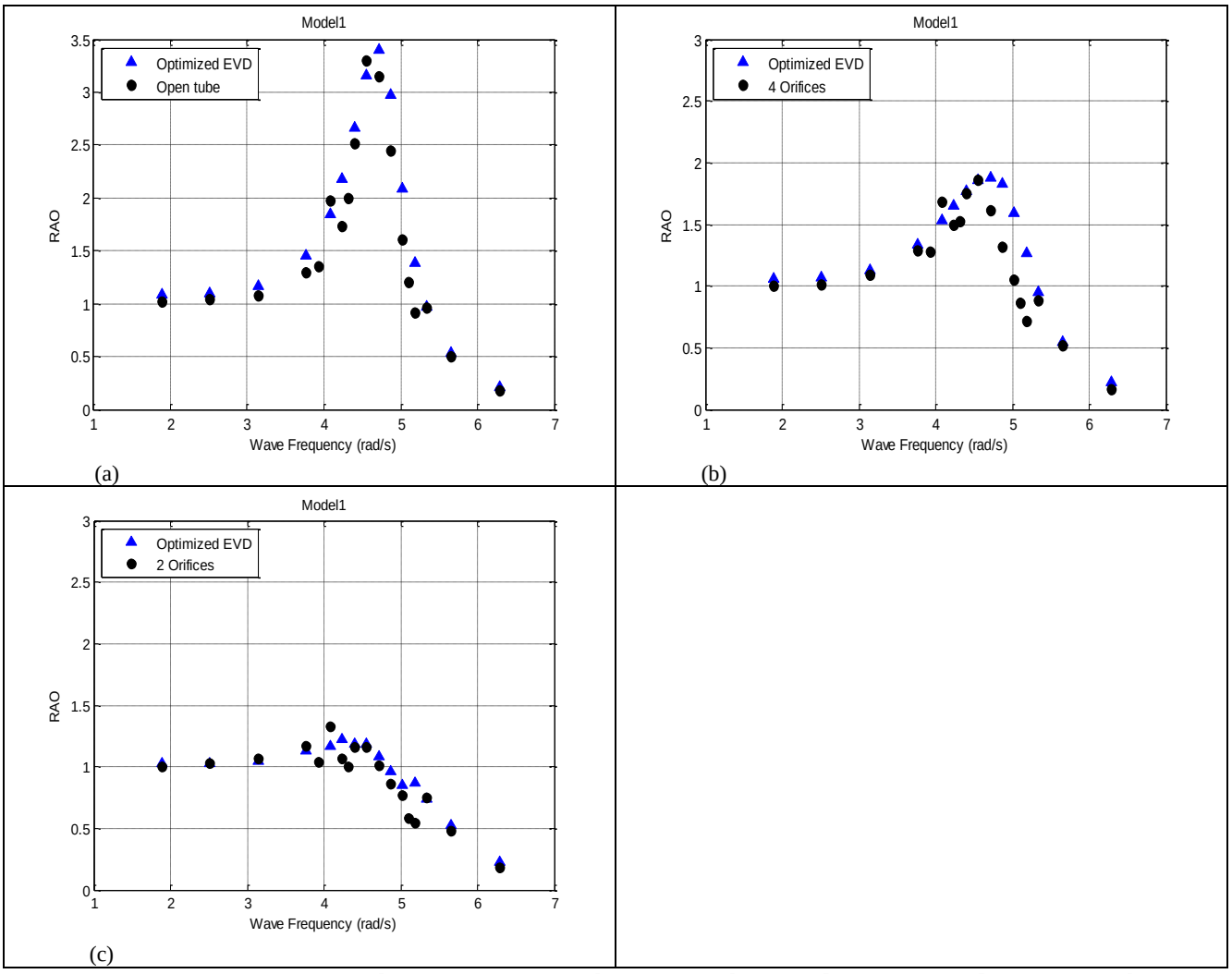

Fig.7.11. Comparison between numerical (optimised equivalent viscous damping) and experimental water column oscillations RAOs vs. wave frequency for experimental model 2; 1DOF model; (a) Open tube, (b) 4 orifices, (c) 2 orifices

Once again, the iterative procedure leaded to a very good agreement with the experimental results. However, in order to investigate the disagreement between the experimental results and the EVD approach results near resonance in Fig.7.10, water column decay tests have been modelled numerically using VD and EVD approaches. Results are presented in Fig.7.12 and 7.13 respectively.

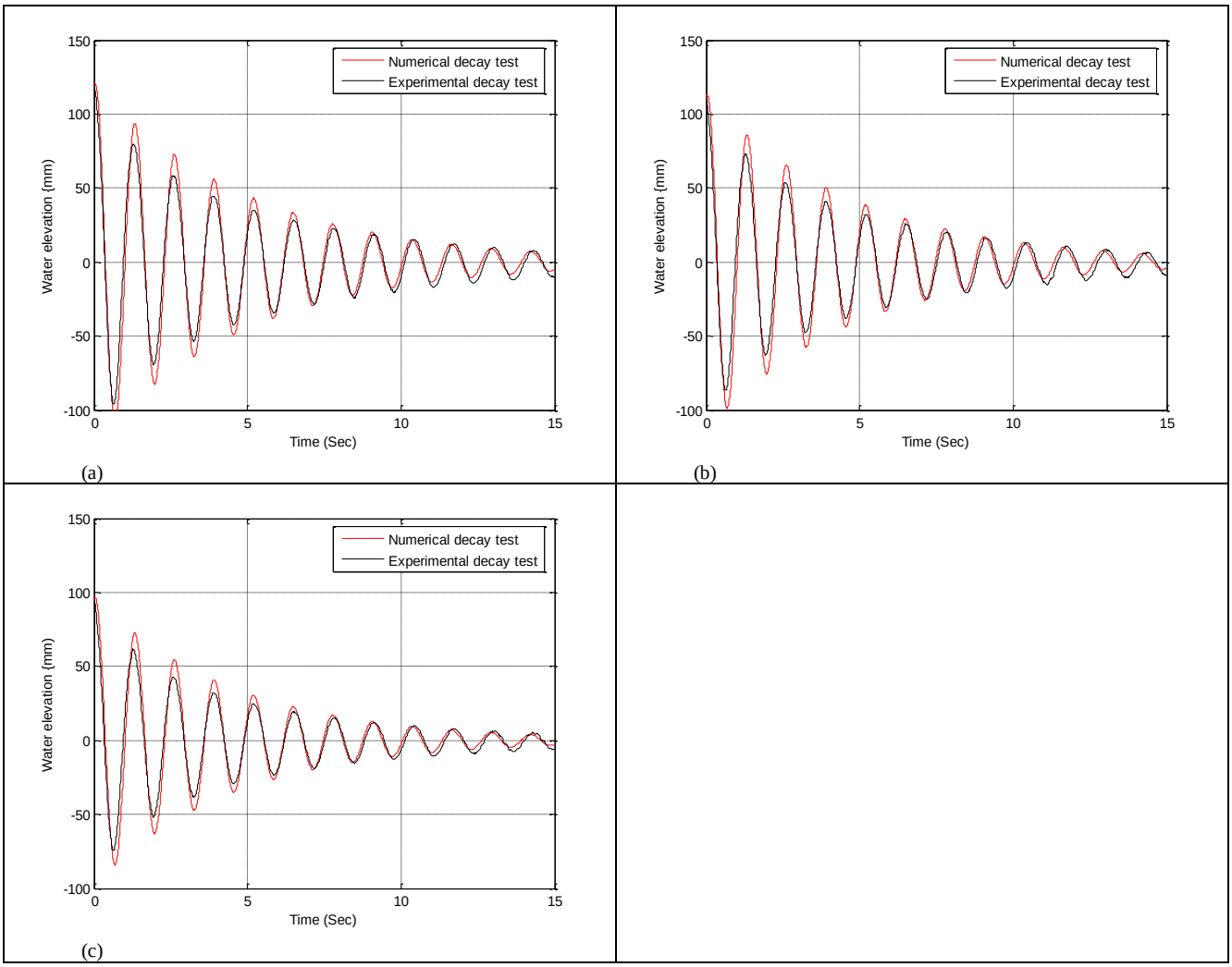

Fig.7.12. Comparison between numerical and experimental water column decay motion: VD using logarithmic decrement (a) open tube, (b) 4 orifices, (c) 2 orifices

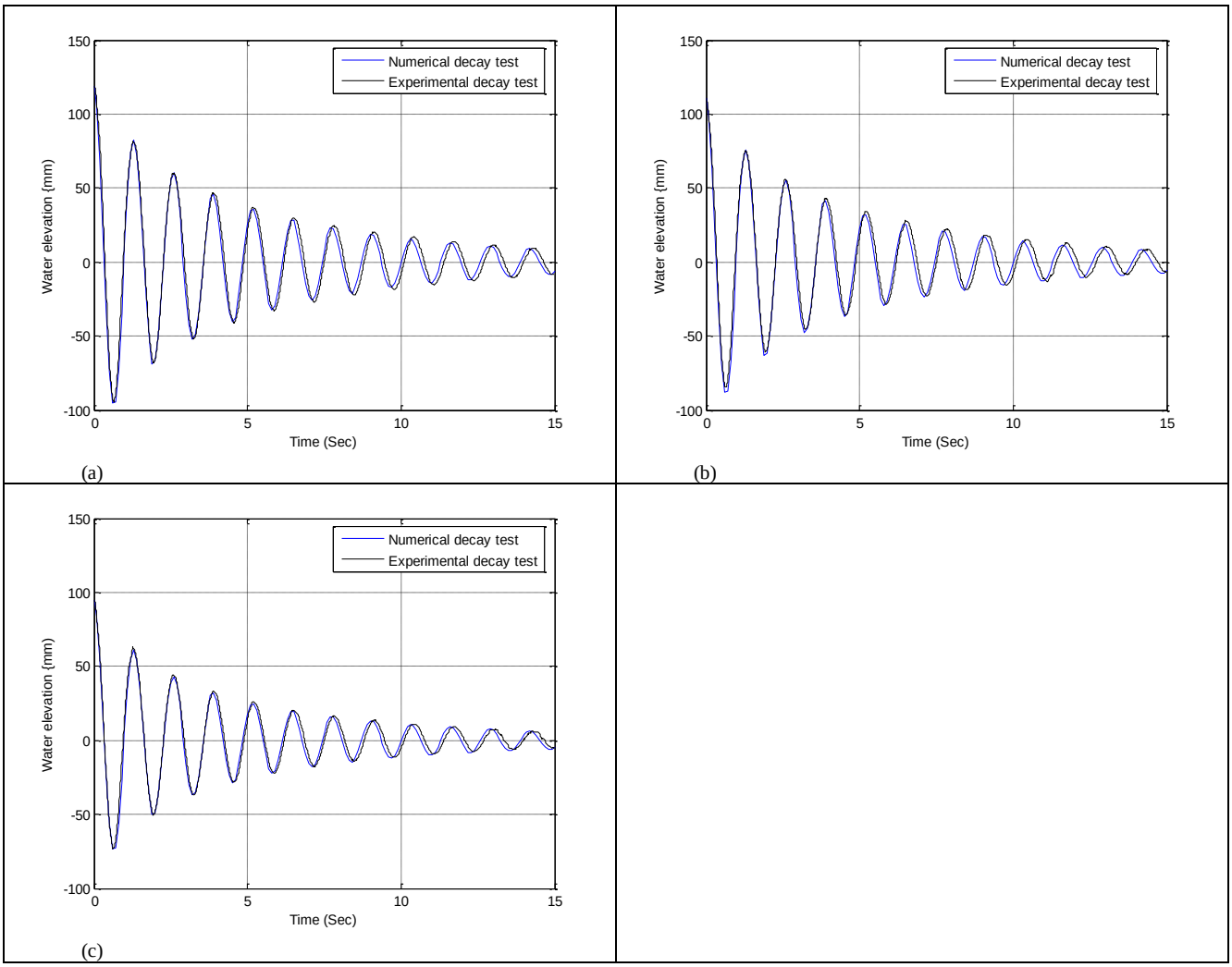

Fig.7.13. Comparison between numerical and experimental water column decay motion: EVD using linear and quadratic coefficients (a) open tube, (b) 4 orifices, (c) 2 orifices

The good quality of fit in Fig.7.13 compared to Fig.7.12 proves that the EVD approach describes the physical process accurately. It should be noted that the quality of fit in the first part of the decay motion depends mainly on the quadratic damping coefficient. The tail of the curve depends mostly on the linear damping coefficient. According to the theory, the quadratic damping has a slight influence on the zero-crossing period, but this effect was very small compared to its influence on the first part of the motion decay curve. It is also noted that the water column amplitude in the beginning of the decay tests was around 100mm, while oscillations amplitudes in case forced oscillations tests did not reach this value. This explains how the VD model results showed better agreement with the experimental results the EVD model results in Fig.7.10.

Results obtained from the time domain model developed to model nonlinear effects due to air compressibility in section 7.4 are presented through Fig.7.14 and Fig.7.15 In this model the stiffness varies instantly according to the water column oscillations amplitude inside the OWC. Fig presents comparison between linear water column hydrostatic stiffness and max pneumatic stiffness at different oscillations amplitude.

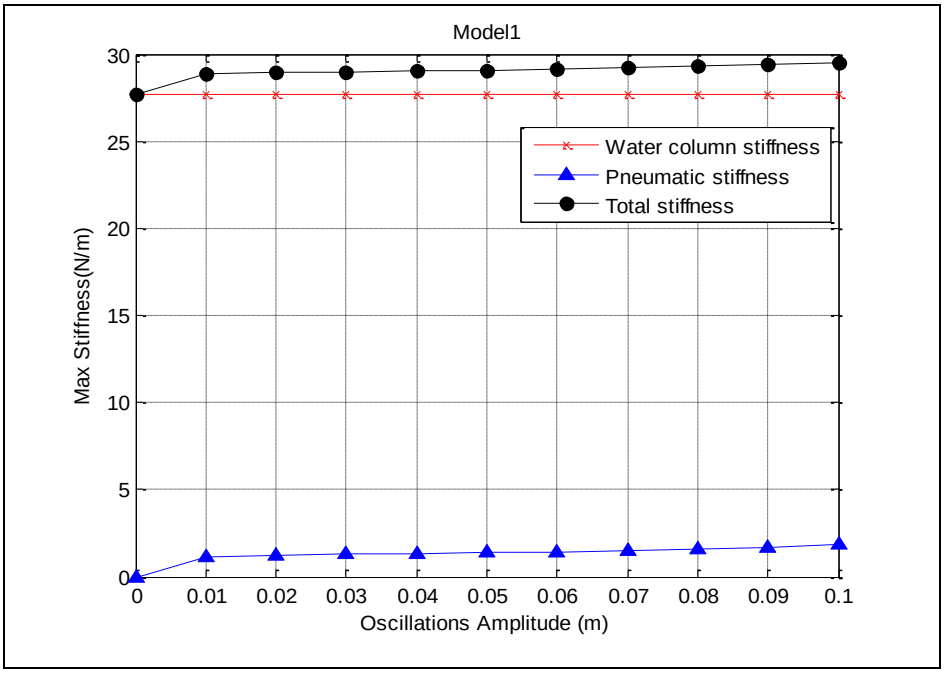

Fig.7.14. Comparison between water column hydrostatic stiffness, and max pneumatic stiffness vs. oscillations amplitudes for experimental model1, 4 orifices; 1DOF model, $\omega = 4.8$rad/s

Fig.7.14 showed that the max pneumatic stiffness is not just small compared to the water column hydrostatic stiffness but the increase in the pneumatic stiffness due to the increase in oscillation amplitude is very small.

Fig.7.15 presents results obtained using nonlinear pneumatic stiffness in comparison with the experimental results and those obtained from linear modelling discussed in chapter 6.

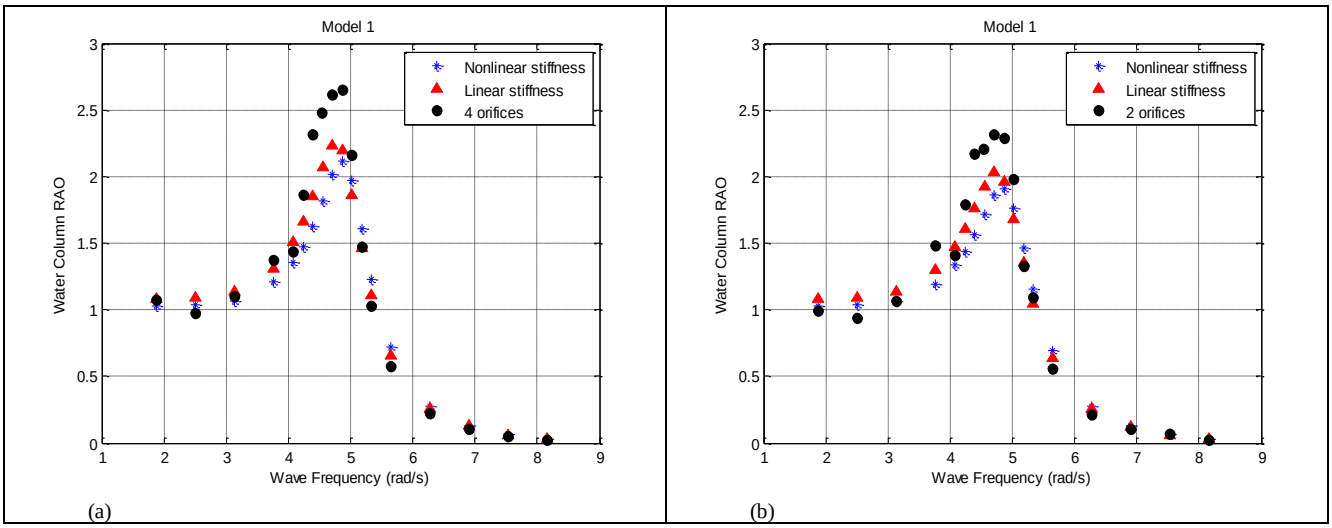

Fig.7.15. Comparison between numerical (linear and nonlinear due to air compressibility) and experimental water column oscillations RAOs vs. wave frequency for experimental model1; 1DOF model (a) 4 orifices (b) 2 orifices

From the above figure it is noticed that the increase in stiffness due to the introduction of the nonlinear pneumatic effects over estimated the total stiffness. Consequently, a small shift of peak frequency is noticed in addition to the reduction in water column RAO. For this reason reasons we may conclude that linear modelling of air compressibility is more suitable in this case. Note that the damping values used are calculated by the half-power bandwidth method.

References of Chapter 7

Anam Iftekhar & Roësset José M. (2004),' Slender-body approximations of hydrodynamic forces for spar platforms', international journal of offshore and polar engineering Vol. 14, No.2

Blagoveshchensky, S.N., (1962). '**Theory of Ship Motions**', Dover.

Cruz J., (2008), **Ocean wave energy**. ISBN 978-3-540-7489-6. Springer.

Incecik, A. (1982), 'Design aspects of hydrodynamic and structural loading on floating offshore platforms under wave excitation', Ph.D. thesis, University of Glasgow, U.K

Nayfeh, A. H., Mook, D. T.: **Nonlinear oscillations**. New York: Wiley 1979.

Nayfeh, A. H.: **Introduction to perturbation techniques**. New York: Wiley 1981

Chapter 8

Renewable Energy Converting Platform

8.1. Introduction

Offshore renewable energy devices have attracted interest because of the higher levels of annual average incident wave and wind power that occur in deeper water and the minimal topographical constraints for their deployment (Folley et al., 2007).

The main challenge for offshore floating renewable energy devices remains to build a structure capable of withstanding the challenging ocean environment while financially viable in a competitive global energy market. That's why the pioneer wave energy researchers Falnes and Budal, 1978 promoted an idea of wave energy power plant consisting of many relatively small units, in contrast to large-scale converters reaching several megawatts.

Muliawan et al., 2013 reported that by the end of 2009, 1.3% of the global installed wind power capacity was installed offshore. Since then the number of offshore wind farms grew up in water depths of less than 20 m to minimize the initial and running costs of the plant. Several floating platform types have been proposed to support offshore wind turbines. They include Spar, tension-leg platform, barge and semi-submersible types, which are similar to the proven offshore floating platforms used by the oil and gas industry.

The concentration of several devices on one platform has both economic and operational advantages. Considering a platform equipped with wind and wave energy converters, they can share the electrical cable and power transfer equipment to

transport the electricity to shore. Capital costs are also reduced overall provided that the design of the foundation can be adapted to multiple devices with minimum modifications. Access to multiple devices would be simplified, resulting in cost-saving at the operational level (Aubault et al., 2011). Fig.8.1 provided by (Davies, 2005) presents the average costs distribution for wave power plant.

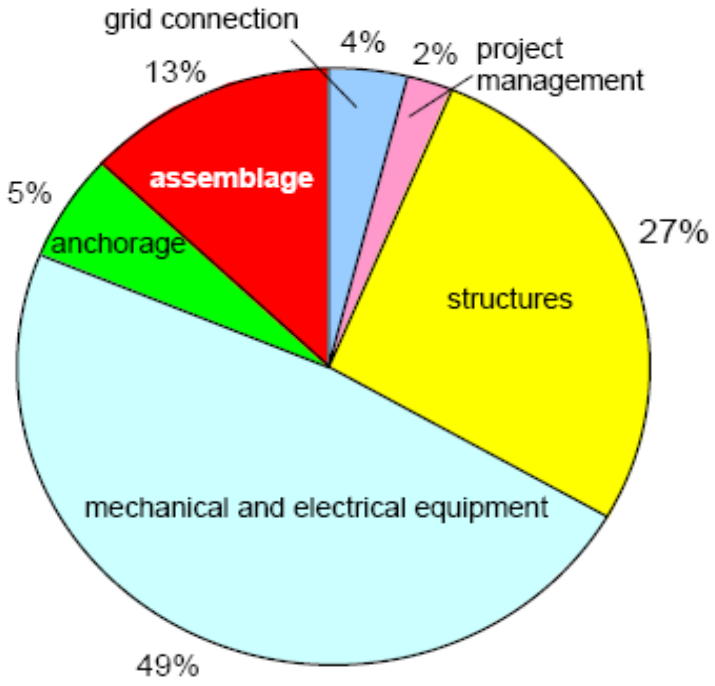

Fig.8.1. Costs distribution for wave power plant

Moreover, the proposed platform may have other purposes such as navigation and communication towers, weather monitoring stations and other purposes in order to reduce the economic value of the total project. In addition the platform offers a wide area exposed to sun light and it is equipped with the infra-structure required for power conditioning and transformation. Therefore mounting photovoltaic solar panels on this area would be an option to increase the output power of the platform.

The main objective of this chapter is to study the feasibility of producing a floating platform equipped with multi-OWC-WEC supporting a wind turbine to reduce the total costs as mentioned earlier and consequently reduce the cost of electricity.

In the present study the wind turbine is completely ignored and experiments have been performed to test the behaviour of the platform, assess the wave energy converters and validate the numerical work.

8.2. Description of the platform

The platform proposed herein consists of four similar SparBuoy WECs rigidly attached together by trusses forming a square platform where spars are located at the corners. Heavy ballast is put at the bottom of each spar, bringing the centre of gravity below the centre of buoyancy. This gives the platform sufficient stability to carry a wind turbine on top. Fig.8.2 presents a only a conceptual drawing for the platform.

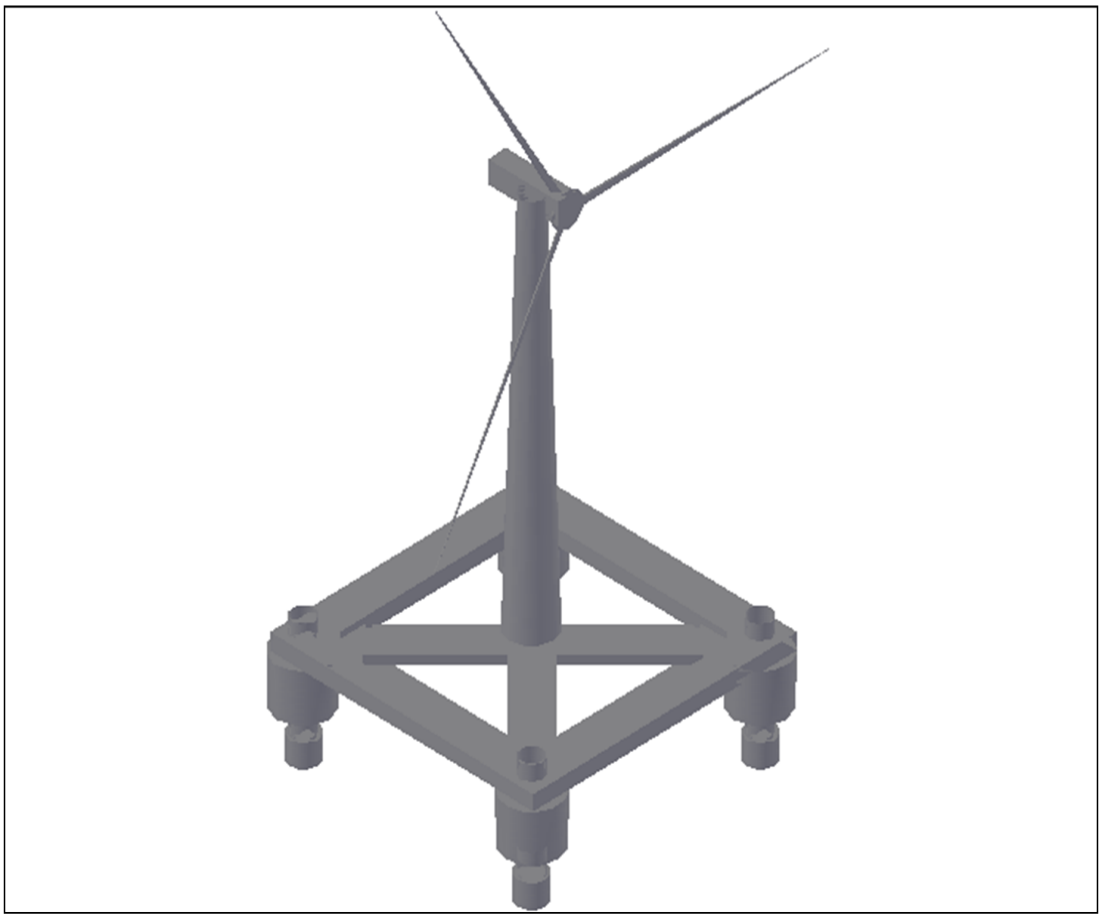

Fig.8.2. 3D view of renewable energy converter platform

The platform was originally designed to investigate if the power captured by the device would increase by making use of the pitch motion of the whole structure.

In order to maximise the pitch motion, Therefore the front and rear pairs of spars are separated by a distance B that matches the structure pitch and water column oscillations natural frequencies. Obviously this distance would be the half of the dominant wave length. The following calculations were performed to validate this assumption.

The sum of pressure forces should be equal to zero since the pressure on the front and rear parts are equal and have different signs, in this case:

$$\boldsymbol{P = \sigma\, cos\left(\frac{KB}{2} - \omega t\right) + \sigma\, cos\left(-\frac{KB}{2} - \omega t\right) = 0} \qquad \textbf{Eq. 8.1}$$

where;

$$\boldsymbol{\sigma = 0.5\, H_w\, 0.5\, \rho\, g\, e^{kd}} \qquad \textbf{Eq.8.2}$$

Therefore;

$$\boldsymbol{\sigma\left(cos\left(\frac{KB}{2}\right) cos(\omega t) + sin(\omega t)\, \mathbf{sin}\left(\frac{KB}{2}\right)\right) + \sigma\left(cos\left(-\frac{KB}{2}\right) cos(\omega t) + sin(\omega t)\, \mathbf{sin}\left(\frac{KB}{2}\right)\right) = 0} \qquad \textbf{Eq. 8.3}$$

At (t=0); Eq.8.3 is reduced to:

$$\boldsymbol{\sigma\left[cos\left(\frac{KB}{2}\right) + cos\left(-\frac{KB}{2}\right)\right] = 0} \qquad \textbf{Eq. 8.4}$$

Since

$$\boldsymbol{cos\left(\frac{KB}{2}\right) = cos\left(-\frac{KB}{2}\right)} \qquad \textbf{Eq. 8.5}$$

Therefore;

$$2cos\left(\frac{KB}{2}\right) = 0 \qquad \textbf{Eq. 8.6}$$

From the above equation the distance between the front or the rear rows and the origin at which the pressure is calculated (centre of the platform) is one quarter of the wave length.

8.3. Modelling of the proposed platform

The global reference system (X, Y, Z) is chosen in such a way that the origin of the system is at the centre of gravity of the floating structure. Therefore wave forces on front and rear buoys will be calculated differently. And similarly to the wave force calculations presented in Chapter 3, Heave forces will be assumed to consist of pressure and acceleration components while surge forces will be assumed to consist of inertia and drag components. It is important to mention that during the experiments buoys were connected to each other by supports above the water level. Therefore wave forces on truss connecting the buoys in real case are neglected.

In order to predict the rigid body motions of the platform, methodology presented in chapter 4 will be adopted. Although, some modifications should be applied to the calculation procedures since the platform consists of several cylinders.

Free hanging catenary or multi-catenary moorings (spread mooring) appear to be the suitable options at present. Several procedures have been proposed to spread mooring system. (Fatlinsen, 1990) stated that the procedures adopted in case of single catenary mooring line analysis may be generalized to a spread mooring system. In this case the relationship between mean external loads on the structure and its position can be found by considering the contributions from each mooring line separately. However, the methodology proposed by (Johanning et al., 2006) and presented in section 5.7 is more simplified and just require the load excursion and reaction curves of four orthogonal lines.

8.4. Calculations

8.4.1. Added mass and inertia

Considering the structure to be consisted of four spars, the total added mass in heave and surge directions will be the sum of added masses of the four spars. Therefore added mass in surge and heave will be calculated for each cylinder using Eq.4.6 and Eq4.7 respectively. However, added inertia in pitch direction will be calculated differently using parallel lines theory since cylinders doesn't rotate about their centre but they rotate about the centre of the whole platform. In this case, the total inertia in pitch will be calculated as:

$$\boldsymbol{I_{pt} = 4\left(\left(I' + m_{act}\left(\frac{B}{2}\right)^2\right) + \left(I'_{ap} + m_{avm}\left(\frac{B}{2}\right)^2\right)\right)} \qquad \textbf{Eq. 8.7}$$

Where,

I' and I_{ap} are the actual and added inertia in pitch direction of one cylinder. m_{act} and m_{avm} are the actual and added mass in heave direction of one cylinder.

8.4.2. Wave forces

Assuming the front and rear parts are at distance B from each other, the pressure force on the front two cylinders is:

$$\boldsymbol{F_{FY} = 2 \times 0.5\, H_w\, \rho g A \frac{cosh(-dK + w_d K)}{cosh(w_d K)} \cos\left(\frac{KB}{2} - \omega t\right)} \qquad \textbf{Eq. 8.8}$$

The pressure force acting on the rear buoys are then obtained as:

$$\boldsymbol{F_{RY} = 2 \times 0.5\, H_w\, \rho g A \frac{cosh(-dK + w_d K)}{cosh(w_d K)} \cos\left(\frac{-KB}{2} - \omega t\right)} \qquad \textbf{Eq. 8.11}$$

The total heave force acting on the structure is simply the sum of forces acting on each part while preserving the (+/-) signs.

$$F_{TY} = F_{FY} + F_{RY}$$ **Eq. 8.14**

For surge forces acting on the front buoys, inertia forces are calculated as:

$$F_{FX} = 2 \times 0.5\, H_w\, \rho\, g\, C_M \omega^2\, A \left(\frac{1}{K} - Exp(-Kd)\right) \sin\left(\frac{KB}{2} - \omega t\right)$$ **Eq. 8.15**

And for rear buoys inertia and drag forces are calculated as:

$$F_{RX} = 2 \times 0.5\, H_w\, \rho\, g\, C_M\, \omega^2 A \left(\frac{1}{K} - Exp(-Kd)\right) \sin\left(\frac{-KB}{2} - \omega t\right)$$ **Eq. 8.18**

The total surge force on the whole structure:

$$F_{TX} = F_{FX} + F_{RX}$$ **Eq. 8.21**

8.4.3. Stability index and reference heights

Centre of buoyancy KB

$$KB = \frac{4}{4} \frac{\left[\left(\nabla_b\left(d_t - \frac{d_b}{2}\right)\right) + \left(\nabla_t\left(\frac{d_t}{2}\right)\right) + \left(\nabla_c\left(\frac{d_c}{2}\right)\right)\right]}{\nabla_T}$$ **Eq. 8.22**

Metacentric radius BM

$$BM = \frac{j_{yy}}{\nabla_T}$$ **Eq. 8.23**

$$j_{yy} = 4\left[j_{yyb}\, A_b \left(B/2\right)^2\right]$$ **Eq. 8.24**

$$j_{yy} = 4\left[\frac{\pi}{64}\left(D_{bo}^4 - D_{bi}^4\right) + \frac{\pi}{4}\left(D_{bo}^2 - D_{bi}^2\right)\left(B/2\right)^2\right]$$ **Eq. 8.25**

Centre of gravity KG

$$KG = \frac{M_b\, CG_b + M_t\, CG_t + M_c\, CG_c}{M_b + M_t + M_c}$$ **Eq. 8.26**

8.5. Results

It is important to evaluate the effect on the OWC on the platform motions, for this reason, platform motions were measured in experiments with un-damped and damped OWC. Comparison between the platform motion responsse in these cases is presented in Fig.8.3.

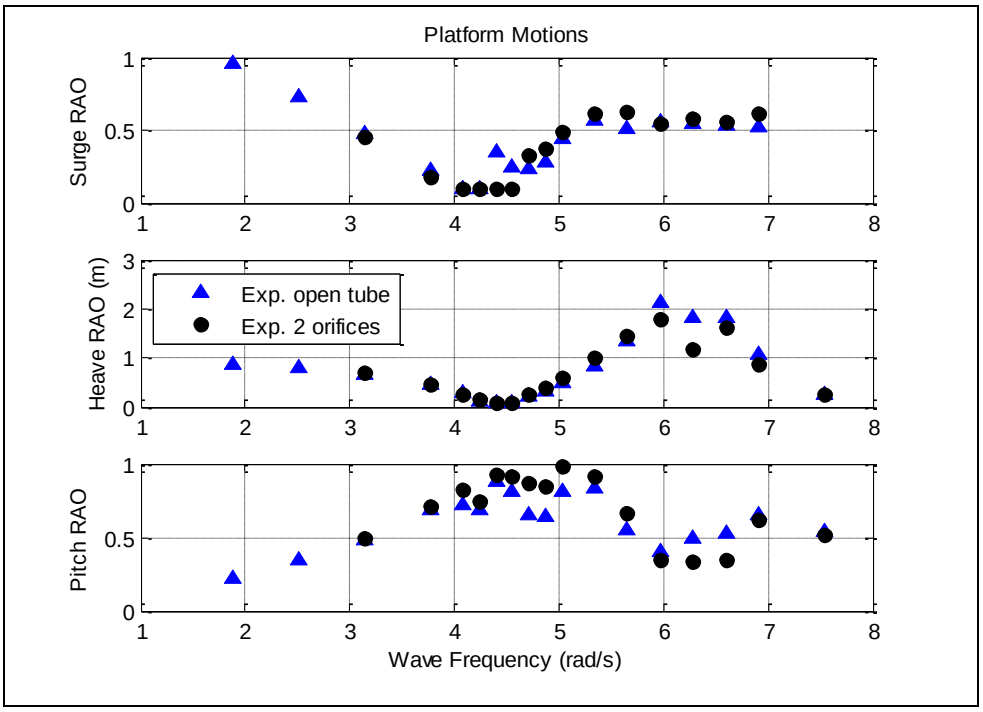

Fig.8.3. Comparison between the platform motions in case un-damped OWC (open tube) and damped OWC (2 orifices)

The above figure showed that the OWC has negligable effect on the platform response which agrees with Aubault et al., 2011.

The modelling procedure discussed herein predicts the surge, heave and pitch motions of the platform ignoring the existance of the OWCs. Fig.8.4 presents comparison between measured and predicted RAOs adopting linear wave theory and viscous damping approach.

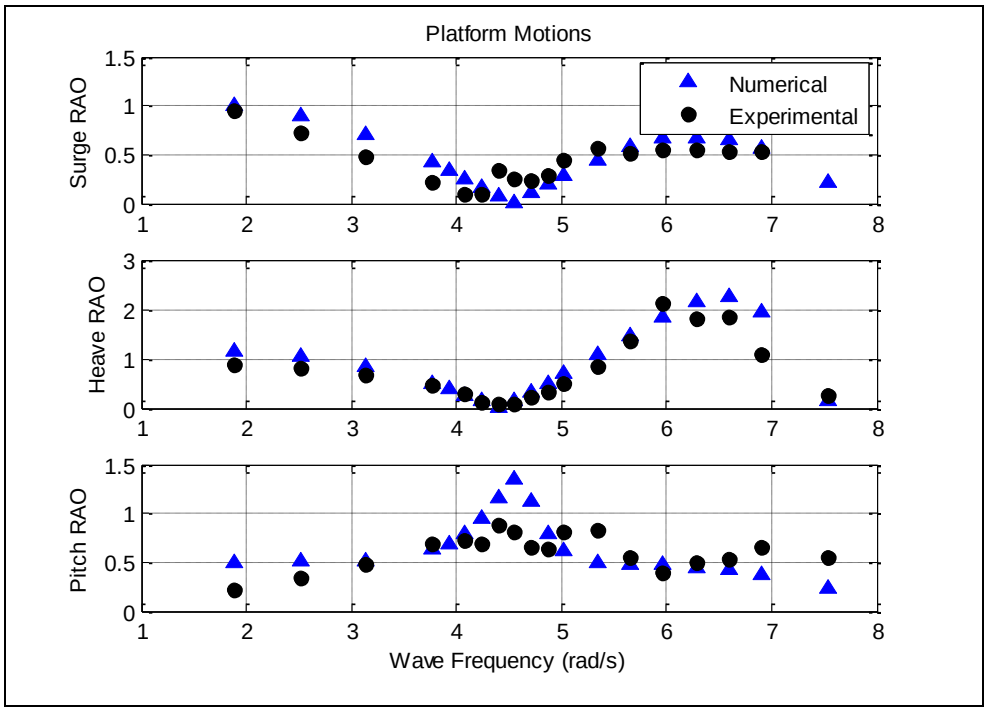

Fig.8.4. Comparison between numerical and experimental surge, heave and pitch RAOs vs. wave frequency for experimental model 4

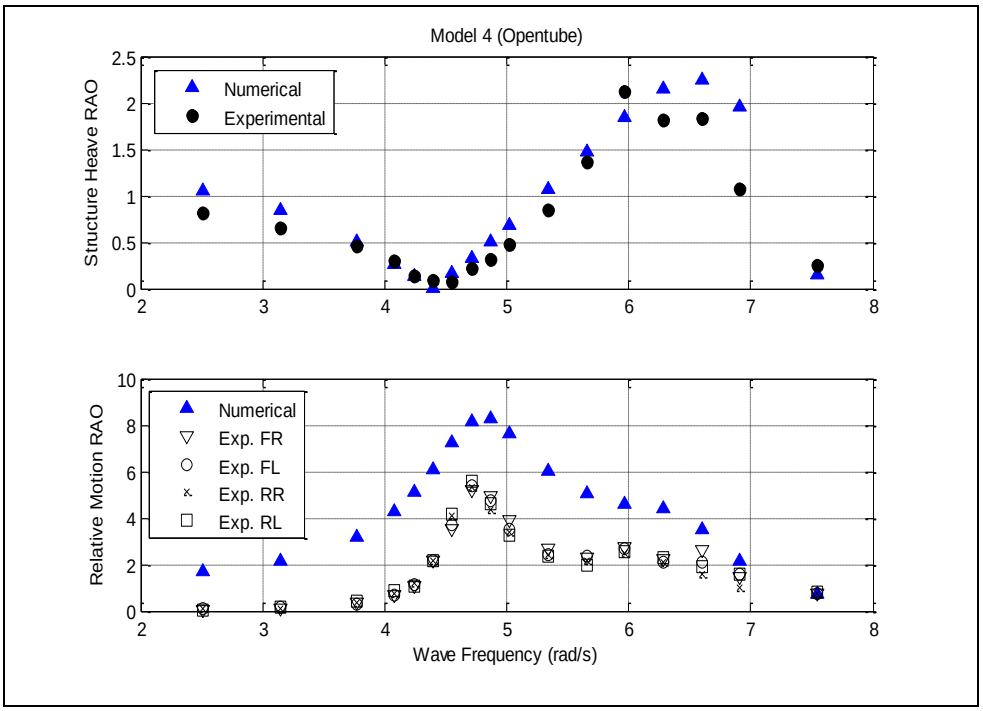

Fig.8.5. Comparison between numerical and experimental structure heave and relative motion RAOs vs. wave frequency for experimental model4; one-way coupling, 2DOF model, viscous damping using half power bandwidth method; Open tube

Fig.8.4 showed that the numerical tool modelled the motions accurately, In order to model the OWC motions, the 'one way coupling approach' discussed previously was

applied. Experimental platform heave and relative motion RAO in case of open tubes are compared to those obtained from the numerical model (see Fig.8.5).

In Fig.8.5, FR, FL, RR, RL, stand for Front Right, Front Left, Rear Right and Rear Left water columns.

From Fig.8.5 it is shown that relative motion RAO has two peaks the first corresponding to the water column natural frequency at 4.8rad/s. the second minor peak at 6rad/s corresponding to the platform heave natural frequency.

It is noted that the measured relative motion RAO inside the four OWCs are similar to each other and similar to the relative motion RAO of a single SparBuoy. The difference between the two devices is the peak frequency of the structure.

References of Chapter 8

Aubault A, Alves M, Sarmento A, Roddier D, Peiffer A., 2011, 'Modelling of an oscillating water column on the floating foundation windfloat'. In Proc. of the 30th international conference on ocean, offshore and arctic engineering, paper No. OMAE2011-49014, Rotterdam; The Netherlands.

Davies P.A., 2005, 'Wave-powered desalination: resource assessment and review of technology', Desalination Vol. 186 pp 97–109.

Falnes J, Budal K., 1978, 'Wave-power conversion by point absorbers', Norwegian Maritime Res Vol. 6 No. 4, pp 2–11

Folley M., Whittaker T.J.T., & Henry A., 2007, 'The effect of water depth on the performance of a small surging wave energy converter', Ocean Engineering Vol.34 pp 1265–1274

Made Jaya Muliawan, Madjid Karimirad, Torgeir Moan, 2013, 'Dynamic response and power performance of a combined Spar-type floating wind turbine and coaxial floating wave energy converter', Renewable Energy Vol. 50, pp 47-57

Chapter 9

Experimental Modelling

9.1. Introduction

Model testing has been an integral part of the development of offshore structures starting with the shallow water structures in the early fifties to the present day. Experimental testing of physical models became the traditional way of investigating the behaviour of offshore structure/vessels. Model testing involves design and construction of scale model, generation of environment in an appropriate facility, measuring responses of the model subjected to the scaled environment and scaling up of the measured responses to the design values. It is recognized as the most reliable tool for reproducing realistic and extreme situations an offshore structure is expected to experience in its life time (Chakrabarti, b.2003).

Most laboratory programs have followed the same course as the parallel theoretical studies, in which the initial work has been in two dimensions (2-D) and then extended to three dimensions (3-D). The terminology Narrow Tank is usually reserved for experiments which investigate genuinely 2-D phenomena and Wide Tank refers to the 3-D case, which usually allows for the possibility of directional seas. Testing, in both narrow and wide tanks, has played an important role in the progress of wave energy studies and is widely agreed to be essential due to the common benefits of tank testing involving:

- Calibration and validation of mathematical and numerical models
- Validation of design values
- Determination of empirical coefficients

- Verification of offshore operation, and;
- Evaluation of higher order effects normally ignored in the analysis (Chakrabarti, b.2003).

9.2. Similarity laws and scale factor

One of the most commonly acknowledged difficulties of conducting experiments with offshore structures is the presence of scale effects. Modelling and similarity laws relate the behaviour of a prototype to that of a scaled model in a prescribed manner. The three areas where attention must be given so that the model truly represents the prototype behaviour are structure geometry, fluid flow and interaction of the two. Therefore the following criteria are required:

- Geometric similarity – All linear dimensions must have the same scale ratio.
- Kinematic similarity – The flow and model(s) will have geometrically similar motions in model and full scale (fluid streamlines are similar)
- Dynamic similarity – Ratios between different forces in full scale must be the same in model scale.

In the present study Froude law of similitude has been used to achieve similitude between the prototype and reduced scale model, Froude number should be kept the same. The Froude number is defined as the fraction between the inertial forces divided by gravitational forces. This means that gravity is considered to be preponderant over the other forces acting on the structure. The different aspects of similitude according to Froude model are defined in Table 9.1.

(Cruz, 2008) categorised the various fluid-structure interactions which occur and suggested suitable scales for experimental investigation of the mechanisms (Table 9.2). The suggested scales are the minimum values which should be used and larger scales are often more desirable, but there is a balance to be drawn between financial cost, available facilities and meaningful results.

Table 9.1: Froude scaling table (Sarpkaya & Isaacson (1981)

Parameter	Unit	Scale factor
Length	[m]	S
Area	[m^2]	S^2
Volume	[m^3]	S^3
Time	[s]	$S^{½}$
Frequency	[s^{-1}]	$S^{-½}$
Force	[N]	S^3
Mass	[kg]	S^3
Velocity	[m s^{-1}]	$S^{½}$
Acceleration	[m s^{-2}]	1

Table 9.2: suitable scales for experimental investigation (Cruz, 2008)

Investigation	Suggested scale	
	1st choice	**2nd choice**
Offshore device behavior	1:50	1:100
Validation of numerical models / optimization	1:20	1:33
Nonlinear and hydrodynamics	1:7	1:5
Component testing	1:5	1:1

9.3. Experimental Aims & Objectives

The first aim of the experimental work is to validate the models proposed to predict the behaviour and performance of a single Spar Buoy OWC and set of Spar Buoys OWCs rigidly connected together forming a platform.

The second aim is to determine the conditions for maximum wave-pneumatic energy conversion. To achieve the experimental aims, the following objectives were proposed:

- Design and fabrication of the experimental models
- Select and calibrate the suitable instruments
- Investigate the six DOF motions of the structure and the water column oscillations
- Investigate the natural frequencies of each model.
- Measure the damping coefficients.
- Vary and measure the PTO damping applied on each model.
- Measure the performance of each model under different damping conditions over a suitable range of wave frequencies.
- Apply some experimental data to the numerical models to measure the overall performance over the designed bandwidth of wave frequencies.

9.4. Reduced-scale models

Four experimental models have been produced to achieve the aims of the research. Two models have been used to test single un-moored Spar Buoy OWCs with different dimensions. The third model was used to validate the one-way coupling model discussed in chapter 6.

Model 1 is 1:100 reduced scale of the devices presented in (Incecik, 2003). For the second model the horizontal dimensions of model 1 were double while the vertical dimensions remained the same. Each Spar Buoy OWC model consists of transparent acrylic tube for visualization purpose fitted in a cylindrical buoy made of solid foam (floater). A brass collar is attached to the bottom of the tube to stabilise the structure and to enhance the damping. In order to simulate turbine damping, different sets of flat covers with different number of circular orifices of 10mm diameter each are to be placed on the top end of each tube. Fig.9.1. presents schematic views of the experimental models.

It is important to mention here that the same orifice dimensions were used for different models regardless the chambers volume. In other words the orifices were not scaled.

The fourth model consists of four similar SparBuoy OWCs rigidly connected forming a square platform where spars are located at the corners.

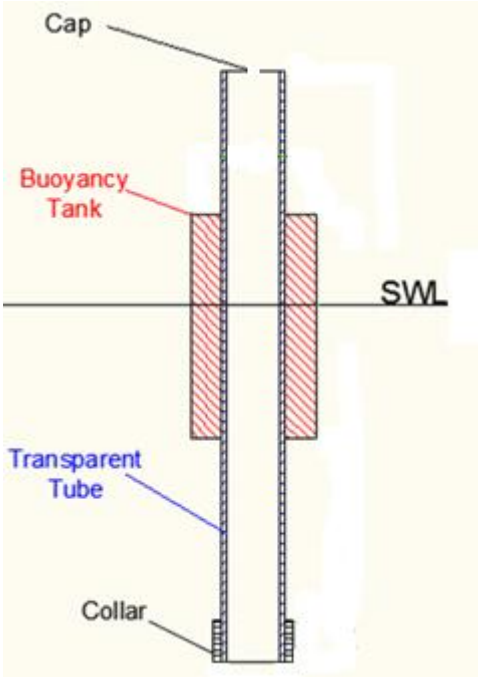

Fig.9.1 Vertical section of experimental model1

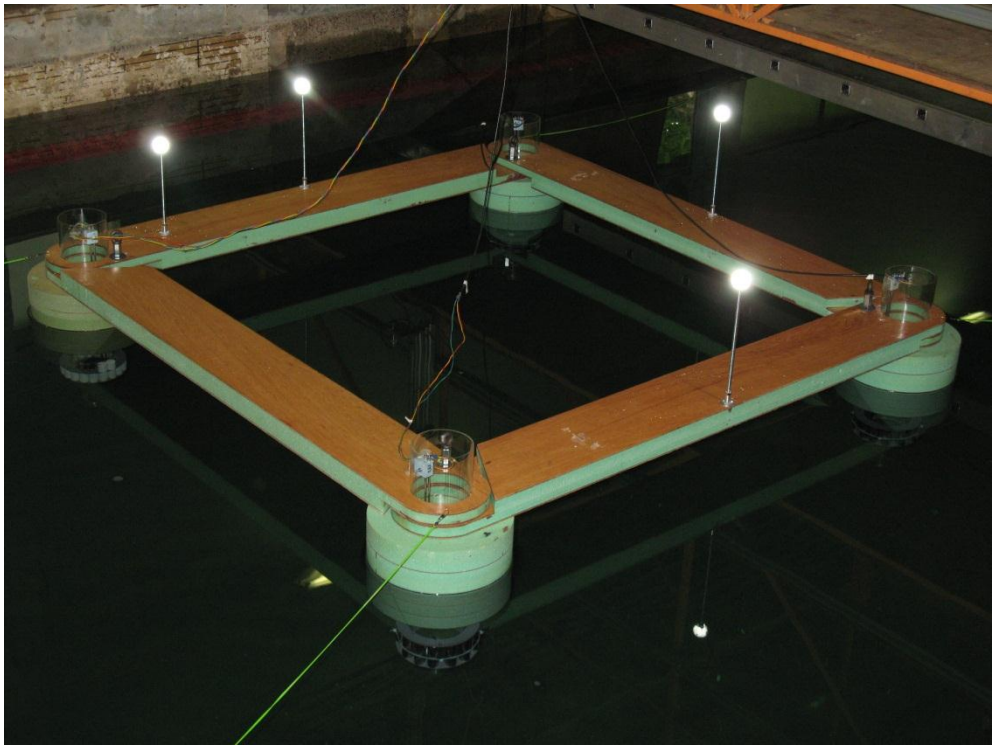

Fig.9.2 Photo of experimental model 4

Due to the limitation of the available tubes at the workshop, the closest tubes dimensions to those provided by (Incecik, 2003) have been selected. The reason for increasing the horizontal dimensions only in the second model is to avoid the effect of the tank floor on the bottom of the device. The dimensions in cm of the three experimental models are presented in Table 9.3.

Table 9.3: Experimental models dimensions (in cm)

	Model 1	**Model 2**	**Model 3**
Buoy outer diameter	14	30	40
Buoy inner diameter	7	12.7	7
Buoy draft	15	15	15
Buoy freeboard	10	10	10
Tube outer diameter	7	12.7	7
Tube inner diameter	6	12.1	6
Tube draft	40	40	40
Tube freeboard	26	26	26
Collar outer diameter	8.9	16.7	16.9
Collar inner diameter	7	12.7	7
Collar draft	4.75	9.5	9.5

9.5. Experimental facilities and measuring instrumentation

9.5.1. Wave tank

The tests have been accomplished in the tank located at the Kelvin Hydrodynamics Laboratory shown in Fig.9.3. The tank is commonly used for a wide range of marine hydrodynamics tests.

Fig.9.3. The tank located at Kelvin Hydrodynamics Laboratory

The tank has the dimensions of 76m x 4.6m x 2.5m equipped with a Computer-controlled digital drive carriage its max speed reaches 5m/s. outfitted with digitally-controlled sub-carriage. Variable-water-depth computer-controlled four-flap absorbing wave maker generating regular or irregular waves over 0.5m height (subject to water depth) is installed in this tank. High quality variable-water-depth sloping beach, with reflection coefficient typically less than 5% over frequency range of interest is available. PC based modular data acquisition/control system. Up to 64 input and 20 output channels, is used to condition, monitor and record the output data with sample rate up to 60 kHz.

9.5.2. Wave probes

The wave probes used for the measurement of the amplitude of the passing waves and the water elevation of the water column inside the tube are a “resistance" type probe (see Fig. 9.4.). These probes produce a voltage proportional to the submerged length. This voltage can be logged by a computer at a prescribed sampling rate. As waves pass the probe, the computer will display the amplitude of the free surface as a function of time.

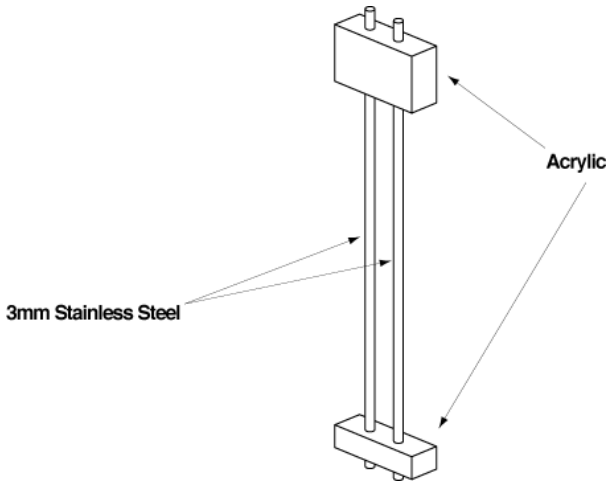

Fig.9.4. Schematic of resistance type wave probe

The wave probes were calibrated in terms of wave height by varying the depth of immersion of the probe in still water by measured height (50 mm) and noting the change in output signal. (Calibration data are presented in Appendix…)

9.5.3. Pressure transducer

The pressure transducers used are able to measure very low pressure changes. The transducers best suited are the Honeywell 163PC01D75 (±622.72Pa) low differential pressure transducers. The electrical output of the transducer is in the range 3.5V ±2.5V. The voltage is directly proportional to the change in pressure with atmospheric being 3.5V.

Fig.9.5. Pressure transducer

Fig.9.5 shows the pressure transducer in details. The protruding ports visible are the inputs. For gauge measurements, the port 2 should be used with port 1 open to atmosphere. If both ports are used the differential pressure is measured.

9.5.4. Motion detection cameras

The optical tracking systems core product is an advanced infrared camera (Fig.9.6). Using data from two or more cameras the system calculate the 3D positions of the markers attached to a model (ship or floating structure) the surge/sway/heave/roll/pitch/yaw, 6DOF motion is calculated and transferred over a TCP-IP connection in real-time. Further can the 6DOF data be output in analogue form in real time to be used for real-time control of the carriage.

Fig.9.6. Motion detection cameras

The QTM® software provides an easy-to-use Windows™ interface to record and calculate real-time 2D, 3D and 6DOF motion data. Optionally, captured data can be post-processed and re-tracked if desired. QTM offers a number specially designed features for ship hydrodynamic testing and the cameras can be used with a desktop or laptop. The cameras are daisy-chained and therefore easy to setup.

The two alternatives of output data are either regular 3D tracking or a 6DOF tracking which in each frame locates the position and orientation of one or more rigid bodies

in the measurement volume. The data output is available in real time and may be visualised as graphs on the computer monitor in real time.

9.5.5. Spike software

Spike software capture and analyse waveform, event and marker data and output precisely timed pulses and voltages using the familiar and easy to use Windows environment. The minimum supported hardware for Spike2 version 6 is a 486 computer running Windows 98SE with 256 MB of memory. The more powerful the processor and the more memory the system has, the better Spike2 runs. During tests Spike software was used to fit the experimental data sinusoidal within the steady state selected by the cursors on the screen. For better analysis the decay tests output was filtered by low pass filter to remove the noise in the signal.

9.6. Experiments

In order to achieve the objectives highlighted in section 9.2., different types of experiments have been performed. Forced oscillation tests in both captive and floating modes have been performed with different PTO damping controlled by the number of orifices in the top flat cover of the tube (these conditions varied from model to another and presented in Table 9.4). All forced oscillation tests readings were taken at the steady state.

Table 9.4: Test matrix

	Inclining test	Decay test							Forced test	
		Structure			Water column				Captive	Floating
		Heave	Pitch	Surge	Opentube	4 orifices	2 orifices	1 orifice		
Model1		X	X		X	X	X		X	X
Model2	X	X	X		X	X	X		X	X
Model3					Same as M1	Same as M1	Same as M1	X		X
Model4		X	X	X	Same as M2	Same as M2	Same as M2			X

9.6.1. Inclining tests

The metacentric height (GM position) may be experimentally determined by moving weights transversely and/or longitudinally to produce a known overturning moment. Knowing the restoring properties (buoyancy) of the structure from its dimensions and floating position. By measuring the equilibrium angle of the structure, the GM is calculated. The inclining test has been performed for the second experimental model only to validate the methodology of calculations.

9.6.2. Decay tests

Decay tests were performed to determine natural frequencies and damping coefficients. It could be performed in all 6 DOF in case of moored models. During the tests the models were located in the middle of the tank to avoid the reflected waves from the side walls of the tank. Tests were performed in calm water. Nearly single DOF motion was achieved during each test to avoid any coupling effect.

9.6.2.1. Water column heave decay

Free oscillations tests of the water column have been accomplished by exciting the water column inside the tube once while the Spar Buoy structure is captive and the water oscillations die out freely, in order to identify the water column natural frequency and damping coefficients for each orifice plate and in case of open tube. Water column decay tests have been performed as presented in Table 9.4.

9.6.2.2. Structure motion decay tests

Structure decay tests have been performed by exciting the whole structure in a particular direction and the motion dies out freely, in order to identify the structure heave and pitch natural frequencies and damping coefficients in addition to mooring lines stiffness and damping in surge direction). Mooring line tests have been performed for models only since models 1, 2 and 3 have been tested un-moored.

9.6.3. Forced oscillation tests

Forced oscillation tests are generally used to establish a transfer functions for all measured responses in regular monochromatic wave conditions; and to observe any nonlinearity in the response by varying the wave height at few selected frequencies. During the experiment the data sampling rate and test duration were chosen so that the steady state of the response is obtained accurately. About 10 cycles of steady state data are recorded.

9.6.3.1. Captive mode tests

Captive mode tests were carried by fixing the device in the wave tank at 20m from the wave maker. The model was subjected to regular waves of 30mm amplitude and the wave frequency varied from 0.3 to 1.3Hz with different steps. Several wave probes were used for data collection. One wave probe was fixed at 10 m from the wave maker. The second one was fixed in-line with the model at a reasonable distance and the third one was located inside the tube. The pressure of the pneumatic chamber was measured and recorded as well. Captive test have been done for model 1and 2 only since the same tubes have been used to contain the OWC.

9.6.3.2. Floating mode tests

Floating mode tests have been conducted by letting the device floats in the tank while it is subjected to regular waves of 10mm amplitude and the frequency varies from 0.3 to 1Hz with different steps. In this case the structure 6DOF motions are measured in addition to the measured parameters of the captive mode tests. The experimental set-up of the forced oscillation tests is illustrated in Fig.9.7. It was important to use compliant (elastic) slack mooring during the forced oscillation tests of models 4 and 5 due to the significant drift. In this case mooring forces are considered negligible once steady state conditions have been established in the tank and the transient regime has been completed.

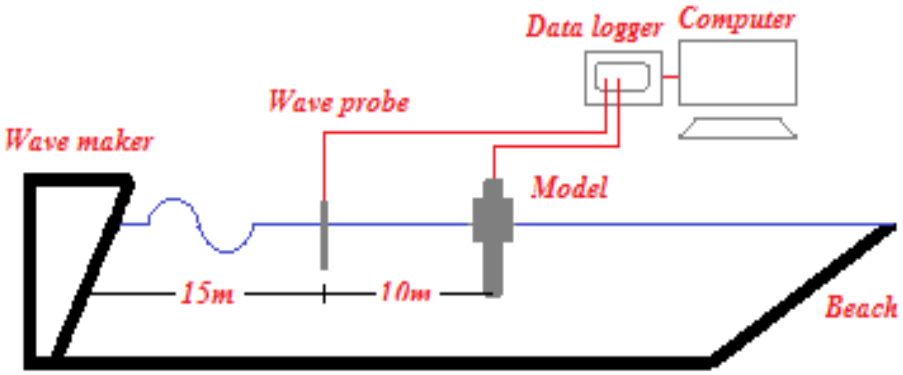

Fig.9.7. Experimental set-up

9.7. Sources of experimental error

Several sources of error appear with the experimental equipment and procedures and include:

- The calibration of the wave probes used could not be carried out to accuracy greater than 5%, given the very small amplitudes of waves or oscillations and the size of the tube.
- The diffraction of waves around the model would be affected by the close proximity of the tank walls, and the cross-waves caused by this effect have influence on the results obtained.
- The suspended wires connecting the wave probes to the computer on the carriage may apply an additional load on the floating device.

References of chapter 9

Chakrabarti, S., 2005b, **Handbook of Ocean Engineering vol. 2**. Plainfield: Elsevier

Cruz J., 2008, **Ocean wave energy**. ISBN 978-3-540-7489-6. Springer, 2008.

Incecik A. 2003, 'Dynamic motion response analysis of a spar buoy', Report prepared for WAVEGEN Limited, Inverness

Sarpkaya T., Isaacson. M.,1981, **Mechanics of Wave Forces on Offshore Structures**, Van Nostran Reinhold Company, New York, 1981

Chapter 10

Conclusions

10.1. Conclusions of chapter 3

Surge/pitch wave force/moment have been assumed to be consisted of inertia and drag components while heave wave forces have been assumed to be consisted of pressure and acceleration components.

In this context, the drag contribution in the total horizontal force and pitch moment is very small compared to the inertia contribution. Heave force consists mainly of the pressure components and that acceleration component may be neglected. This case corresponds to Froude-Krylov approximation.

Concerning wind force calculations, results obtained following API and ABS recommendations are very close.

In order to validate the wave forces calculations presented above, Keulegan-Carpenter and the diffraction parameters have been calculated. Results showed that $KC<1$ and $D/\lambda<0.2$, therefore viscous forces may be ignored, forces are to be calculated in diffraction regime, and Froude-Krylov approximation is valid which verify the results obtained. In addition results are compared to (Incecik, 2003) results and showed very good agreement.

10.2. Conclusions of chapter 4

The dynamic model adopted to predict the floating structure's motions produced three uncoupled linear second order differential equations describing surge, heave and pitch motions. The model did not include interactions between different modes of motions or the interaction between the structure and water column. The structure heave and pitch numerical results have been validated experimentally by the use of two experimental models (models 1 & 1).

Predicted structure heave RAOs agrees with the measured ones. The disagreement between the predicted and measured pitch RAOs around the resonant frequencies is due to the inaccuracy of determining the pitch damping coefficient. Better agreement has been achieved by adopting the EVD approach based on linear and quadratic damping coefficient.

10.3. Conclusions of chapter 5

Mooring system has been introduced to model the structure surge motion using static and quasi-static modelling approaches.

Load excursion curve and reaction curves have been plotted analytically by applying a range of horizontal forces that are to be expected on the WEC at the installation location, for specific mooring line length, submerged weight per unit length and water depth.

Finite element multi-static model have been developed to validate the analytical results. Comparison between analytical and computational reaction curve showed good agreement and agree with (Johanning et al, 2006) results.

Constant line stiffness has been used for static modelling while reaction curve obtained has been used to estimate the instant resultant mooring line tension at different offsets. It is fount that surge RAO obtained from quasi-static modelling did not show big discrepancies than RAO obtained from static approach.

10.4. Conclusions of chapter 6

One DOF mechanical oscillation model has been presented to simulate the water column oscillations inside captive cylindrical OWC where PTO damping and stiffness due to air compressibility inside the pneumatic chamber have been taken into account linearly. Experiments have been carried out to calculate the damping coefficients and to validate the proposed model.

Predicted water column RAOs agrees with the measured RAOs except around resonance. This has been expected due to the adoption of viscous damping approach.

Damping in this case have been experimentally determined using two different techniques. It is noted that modelling using damping obtained from the logarithmic decrement method over estimated the water column response at resonance while the use of the half power bandwidth method in damping determination resulted in under estimation of the water column response at resonance.

Results also showed that the pneumatic stiffness has a minor influence on the water column response and may be ignored.

Two different dynamic models have been implemented to describe floating OWC. Both models considered two translational modes of motions in heave direction. Experiments have been carried out again to calculate the new damping coefficients and to validate the proposed models

The simplified two DOF model adopted in the beginning of the research failed to predict the structure heave and relative motions RAOs correctly. The predicted frequency responses of the spar and the relative motion became very close to each other and failed to match the measured peaks corresponding to the structure and water column natural frequencies.

In order to validate the analytical procedure, Matlab scripts have been developed to solve the same equations of motions numerically using Matlab ODE toolbox.

Comparison between analytical, numerical results showed that this failure is not due to calculations error.

Three different approaches have been adopted to modify the simplified two DOF model in order to obtain a satisfactory agreement between the predicted and measured results.

Modelling using higher damping values did not solve the problem since the structure heave and relative motion peak frequencies occurred at the same frequency again.

Modelling using lower mass ratio improved the agreement between the predicted and measured results of the experimental model especially developed for the validation.

Neither modelling using higher damping nor modelling using lower mass ratio helped to achieve a satisfactory agreement between the predicted and measured results.

Therefore, One-way coupling approach between the two masses have been proposed by treating the structure heave motion as single DOF system while keeping the equation of motion of the water column as it is in case of the simplified two DOF model.

The adoption of the one-way coupling approach resulted in good agreement with the measured results. The model succeeded to predict the structure heave RAO and slightly over estimated the relative motion RAO.

The results obtained from the former approach questioned the dynamic model originally and not the numerical procedures. In other words, the arrangement of the mass, springs and dampers does not describe the coupling occurring in reality. That is why the model proposed by Szumko has been used.

Unlike the simplified two DOF model coupling between the two masses in case of Szumko model did not include the water column stiffness and damping. The masses are assumed to be coupled by the pneumatic chamber only. Coupling between the

structure and water column considered the air compressibility stiffness and PTO damping.

Modelling results of szumko model showed better agreement with the experimental results. The disagreement between the predicted and measured relative RAO around the peak frequency is due to the adoption of viscous damping approach.

Although, the relative RAO falls between the two peaks, which does not agree with the experimental results. This is in addition to the sensitivity of the modelling results to the pneumatic stiffness and damping values.

Therefore Szumko model has been modified so that the pneumatic spring and damper be in parallel. The phase caused by the spring in the first case has been ignored. However the phase between the forces on the two masses is still introduced by the area ratio.

Results obtained from the modified Szumko model showed that the relative RAO did not fall to zero between the two peaks and agreed with the measured RAO. On the other hand the structure natural frequency is a little shifted which caused the slight deviation between the predicted and measured structure heave RAOs.

By calculating the power captured by the device it is noticed that as the damping increases, it broadens the region over which significant power capture is achieved especially at excitation frequencies not coincident with the natural frequency.

In addition the power absorption response of captive OWC expected to have single peak but using the experimental data (in case of high pneumatic damping and stiffness) to calculate the power absorption resulted in two smaller new peaks, one at a higher and other at a lower frequency.

Gomes et al., 2012 reported this incident and correlated it to the pneumatic stiffness effect on the device which increases as the OWC chamber height increases. In the research reported herein, using small orifices in case of the bigger experimental model had the same effect. As these peaks increase, they move away from the central

frequency, reducing the power absorption at that frequency. This effect reduces the annual average power.

Moreover, it is evident that a significant increase in power capture is achieved when the natural frequencies of the OWC and floating structure are separated compared to the power captured results in case of captive OWC when the structure peak didn't exist. However the separation between the natural frequencies of the two masses should be optimised for maximum power absorption.

It is also noticed that at high damping, the power captured at the structure natural frequency is higher the power captured at the water column natural frequency. This implies that a structural natural frequency lower than the water column natural frequency is favourable in optimising power capture and this agrees with Stappenbelt & Cooper (2009).

10.5. Conclusions of chapter 7

Nonlinearities in water column oscillations due large waves and due to nonlinear damping have been investigated in both frequency and time domains in case of captive OWC.

Linearized model based on classical perturbation theory have been used to predict non-linear water column response due to large wave amplitude in frequency domain. Results showed that the perturbed term is very small compared to the linear term which clarify the similarity between the linear and linearized results. Comparison with time domain non-linear model proved that the proposed linearization technique is not suitable in this case where higher non-linearity should be considered and therefore calculation of wave force in time domain is necessary.

A mathematical model has been presented to consider equivalent viscous damping coefficient calculated in time domain by taking into consideration the instant oscillation amplitude. The disagreement between experimental and EVD approach

results near resonance is caused due to the inaccurate detection of the linear and quadratic damping coefficients from the free oscillation tests of the water column.

In contrast, the adopted iterative procedure used to optimize the damping coefficients was very successful leading to a very good agreement with the experimental results.

10.6. Conclusions of chapter 8

The idea of concentration of several devices on one platform has been successfully accomplished.

A floating platform consists of four similar SparBuoy OWC WECs rigidly attached together by trusses where spars are located at the corners have been tested experimentally.

It is noted that the measured relative RAO inside the four OWCs are similar to each other and similar to the relative RAO in case of single SparBuoy. Consequently, the power captured by the platform is almost four times the power captured by single SparBuoy OWC WEC. In addition to the wind power expected to be captured by wind turbine mounted on top of the platform.

In addition the platform offers a wide area exposed to sun light and it is equipped with the infra-structure required for power conditioning and transformation. Therefore mounting photo voltaic solar panels on this area would be recommended to increase the output power of the platform.

10.7. Recommendations for future work

In the present study the first power conversion process (wave to pneumatic) has been successfully modelled. In the future it is possible to involve the aerodynamic problem based on the experimental results collected.

The numerical program developed can extend to estimate the responses in irregular waves for more accurate annual power prediction.

A CFD model may be developed to simulate the air flow inside the OWC chamber and through the turbine in order to estimate the pneumatic power transferred to the electrical generator or for proper selection of the turbine.

This may be achieved by using the time series water oscillations measured experimentally as input data for CFD model.

The CFD modelling allows the investigation of chamber shape and volume and there effects on the system. Moreover the effect of adding water-droplet separator to protect the turbine and pressure relief valve may be studied.

The differences between the exhalation and inhalation processes and there effects on the air flow may be examined accurately by combining the CFD and measurements.

Advanced investigations may be carried out to compare between the performance of Well's turbine and impulse turbine based on experimental measurements and performance curves provided by their suppliers.

It is also important to develop geometrical optimisation procedure to maximise the power output of the device.

Furthermore, study may be developed to couple the renewable energy platform 6DOF motions and the water column oscillations inside each OWC in addition to the investigation considering the wind turbine and the synchronisation between different machineries.

References of Chapter 10

Gomes R.P.F., Henriques J.C.C., Gato, A.F.O. Falcão L.M.C., 2012, 'Hydrodynamic optimization of an axisymmetric floating oscillating water column for wave energy conversion' Renewable Energy Vol. 44 pp 328-339

Incecik A., 2003, 'Dynamic motion response analysis of a spar buoy', Report prepared for WAVEGEN Limited, Inverness

Johanning L., Smith G H, and Wolfram J., 2006, 'Mooring design approach for wave energy converters', Proc. IMechE Vol. 220 Part M: J. Engineering for the Maritime Environment

Stappenbelt Brad and Cooper Paul, 2009, 'Mechanical Model of a Floating Oscillating Water Column Wave Energy Conversion Device', Annual Bulletin of the Australian Institute of High Energetic Materials pp. 34-45. USBN: 978-0-9806811-3-0

APPENDIX A: SURGE FORCES CALCULATIONS

Surge forces are assumed to consist of inertia and drag components. In the following Appendices subscripts 1, 2 and 3 denote buoy, water column and collar respectively, while subscripts o and i denote outer and inner diameters.

Surge force on buoy

Inertia force, F_{1XI}

$$\boldsymbol{F_{1XI} = 0.5\, H_w\, \rho\, g\, CM_1\, \frac{\pi}{4} D_{1o}^2 \omega^2 \left(\frac{1}{K} - Exp(-k\, d_1)\right)} \qquad \textbf{Eq. A.1}$$

Drag force, F_{1XD}

$$\boldsymbol{F_{1XD} = 0.5\, H_w\, 0.5\, \rho\, g\, CD_1\, \frac{4}{3\pi} D_{1o}^2 \omega^2 \left(\frac{1}{2K} - Exp(-2\, k\, d_1)\right)} \qquad \textbf{Eq. A.2}$$

Total surge wave forces on buoy, F_{1X}

$$\boldsymbol{F_{1X} = \sqrt{F_{1XI}^2 + F_{1XD}^2}} \qquad \textbf{Eq. A.3}$$

Surge force on water column

Inertia force, F_{2XI}

$$\boldsymbol{F_{2XI} = 0.5\, H_w\, \rho\, g\, CM_2\, \frac{\pi}{4} D_{2o}^2 \omega^2 \left(\frac{1}{K} - Exp(-k\, d_2)\right)} \qquad \textbf{Eq. A.4}$$

Drag force, F_{2XD}

$$\boldsymbol{F_{1XD} = 0.5\, H_w\, 0.5\, \rho\, g\, CD_2\, \frac{4}{3\pi} D_{2o}^2 \omega^2 \left(\frac{1}{2K} - Exp(-2\, k\, d_2)\right)} \qquad \textbf{Eq. A.5}$$

Total surge wave forces on water column, F_{2X}

$$\boldsymbol{F_{2X} = \sqrt{F_{2XI}^2 + F_{2XD}^2}} \qquad \textbf{Eq. A.6}$$

Surge force on collar

Inertia force, F_{3XI}

$$\boldsymbol{F_{3XI} = 0.5\, H_w\, \rho\, g\, CM_3\, \frac{\pi}{4} D_{3o}^2 \omega^2 \left(\frac{1}{K} - Exp(-k\, d_3)\right)} \qquad \textbf{Eq. A.7}$$

Drag force, F_{3XD}

$$\boldsymbol{F_{3XD} = 0.5\, H_w\, 0.5\, \rho\, g\, CD_3\, \frac{4}{3\pi} D_{3o}^2 \omega^2 \left(\frac{1}{2K} - Exp(-2\, k\, d_3)\right)} \qquad \textbf{Eq. A.8}$$

Total surge wave forces on collar, F_{3X}

$$\boldsymbol{F_{3X} = \sqrt{F_{3XI}^2 + F_{3XD}^2}} \qquad \textbf{Eq. A.9}$$

Total surge force on the structure, F_{TX}

$$\boldsymbol{F_{TX} = F_{1X} + F_{2X} + F_{3X}} \qquad \textbf{Eq. A.10}$$

APPENDIX B: HEAVE FORCES CALCULATIONS

Heave forces are assumed to consist of pressure and acceleration components.

Heave force on buoy

Pressure forces, F_{1YP}:

$$\boldsymbol{F_{1YP} = \frac{\pi}{4}\left(D_{1o}^2 - D_{1i}^2\right)P_{dw}} \quad \textbf{Eq. B.1}$$

$$\boldsymbol{P_{dw} = 0.5\, H_w\, \rho g \frac{cosh(-d_1 K + w_d K)}{cosh(w_d K)}} \quad \textbf{Eq. B.2}$$

Acceleration forces, F_{1YA}:

$$\boldsymbol{F_{1YA} = M_{avm,w} a_{y,w}} \quad \textbf{Eq. B.3}$$

$$\boldsymbol{M_{avm,w} = \frac{4}{3}\rho\left[\left(\frac{D_{1o}}{2}\right)^3 - \left(\frac{D_{1i}}{2}\right)^3\right]} \quad \textbf{Eq. B.4}$$

$$\boldsymbol{a_{y,w} = -0.5\, H_w\, g\, K \frac{sinh(-d_1 K + w_d K)}{sinh(w_d K)}} \quad \textbf{Eq. B.5}$$

Total heave forces on buoy, F_{1Y}

$$\boldsymbol{F_{1Y} = \sqrt{F_{1YP}^2 + F_{1YA}^2}} \quad \textbf{Eq. B.6}$$

Heave force on water column

Pressure forces, F_{2YP}:

$$\boldsymbol{F_{2YP} = \frac{\pi}{4}\left(D_{2o}^2\right)P_{dw}} \quad \textbf{Eq. B.7}$$

$$\boldsymbol{P_{dw} = 0.5\, H_w\, \rho\, g \frac{cosh(-d_2 K + w_d K)}{cosh(w_d K)}} \quad \textbf{Eq. B.8}$$

Acceleration forces, F_{2YA}:

$$F_{2YA} = M_{avm,w} a_{y,w} \quad \textbf{Eq. B.9}$$

$$M_{avm,w} = \frac{4}{3}\,\rho \left(\frac{D_{2o}}{2}\right)^3 \quad \textbf{Eq. B.10}$$

$$a_{y,w} = -0.5\, H_w\, g\, K \frac{sinh(-d_2 K + w_d K)}{sinh(w_d K)} \quad \textbf{Eq. B.11}$$

Total heave forces on water column, F_{2Y}

$$F_{2Y} = \sqrt{F_{2YP}^2 + F_{2YA}^2} \quad \textbf{Eq. B.12}$$

Heave force on collar

Pressure forces, F_{3YP}:

$$F_{3YP} = \frac{\pi}{4}\left(D_{3o}^2 - D_{3i}^2\right) P_{dw} \quad \textbf{Eq. B.13}$$

$$P_{dw} = 0.5\, H_w\, \rho\, g \frac{cosh(-d_1 K + w_d K)}{cosh(w_d K)} \quad \textbf{Eq. B.14}$$

Acceleration forces, F_{3YA}:

$$F_{3YA} = M_{avm,w} a_{y,w} \quad \textbf{Eq. B.15}$$

$$M_{avm,w} = \frac{4}{3}\rho \left[\left(\frac{D_{3o}}{2}\right)^3 - \left(\frac{D_{3i}}{2}\right)^3\right] \quad \textbf{Eq. B.16}$$

$$a_{y,w} = -0.5\, H_w\, g\, K \frac{sinh(-d_1 K + w_d K)}{sinh(w_d K)} \quad \textbf{Eq. B.17}$$

Total heave forces on collar, F_{3Y}

$$F_{3Y} = \sqrt{F_{3YP}^2 + F_{3YA}^2} \quad \textbf{Eq. B.18}$$

Total heave force on the structure, F_{1TY}

$$F_{1TY} = F_{1Y} + F_{3Y} \quad \textbf{Eq. B.19}$$

Total heave force on the water column, F_{2TY}

$$F_{2TY} = F_{2Y} \qquad \textbf{Eq. B.20}$$

APPENDIX C: PITCH MOMENT CALCULATIONS

Pitch moment is assumed to consist of inertia and drag components.

Pitch moment on buoy

Inertia moment, P_{1M1}

$$\boldsymbol{P_{1MI} = 0.5\, H_w\, \rho\, g\, CM_1\, K\, \frac{\pi}{4}\left(D_{1o}^2 - D_{1i}^2\right)\left(\frac{d_1}{K}\, Exp(-K\, d_1) - \frac{1}{K^2}\left(1 - Exp(-K\, d_1)\right)\right)} \quad \textbf{Eq. C.1}$$

Drag moment, P_{1MD}

$$\boldsymbol{P_{1MD} = 0.5\, H_w\, 0.5\, \rho\, g\, CD_1\, K\, \frac{8}{3\pi}\left(D_{1o} - D_{1i}\right)\left(\frac{d_1}{2K}\, Exp(-2K\, d_1) - \frac{1}{4K^2}\left(1 - Exp(-2K\, d_1)\right)\right)} \quad \textbf{Eq. C.2}$$

Total pitch moment on buoy, P_{1M}

$$\boldsymbol{P_{1M} = \sqrt{P_{1MI}^2 + P_{1MD}^2}} \quad \textbf{Eq. C.3}$$

Pitch moment on water column

Inertia moment, P_{2M1}

$$\boldsymbol{P_{2MI} = 0.5\, H_w\, \rho\, g\, CM_2\, K\, \frac{\pi}{4} D_{2o}^2\left(\frac{d_2}{K}\, Exp(-K\, d_2) - \frac{1}{K^2}\left(1 - Exp(-k\, d_2)\right)\right)} \quad \textbf{Eq. C.4}$$

Drag moment, P_{2MD}

$$\boldsymbol{P_{2MD} = 0.5\, H_w\, 0.5\, \rho\, g\, CD_2\, K\, \frac{8}{3\pi} D_{2o}^2\left(\frac{d_2}{2K}\, Exp(-2K\, d_2) - \frac{1}{4K^2}\left(1 - Exp(-2K\, d_2)\right)\right)} \quad \textbf{Eq. C.5}$$

Total pitch moment on water column, P_{2M}

$$\boldsymbol{P_{2M} = \sqrt{P_{2MI}^2 + P_{2MD}^2}} \qquad \textbf{Eq. C.6}$$

Pitch moment on collar

Inertia moment, P_{3M1}

$$\boldsymbol{P_{3MI} = 0.5\, H_w\, \rho\, g\, CM_3\, K\, \frac{\pi}{4}\left(D_{3o}^2 - D_{3i}^2\right)\left(\frac{d_3}{K}\, Exp(-K\, d_3) - \frac{1}{K^2}\left(1 - Exp(-k\, d_3)\right)\right)} \qquad \textbf{Eq. C.7}$$

Drag moment, P_{3MD}

$$\boldsymbol{P_{3MD} = 0.5\, H_w\, 0.5\, \rho\, g\, CD_1\, K\, \frac{8}{3\pi}(D_{3o} - D_{3i})\left(\frac{d_3}{2K}\, Exp(-2K\, d_3) - \frac{1}{4K^2}\left(1 - Exp(-2K\, d_3)\right)\right)} \qquad \textbf{Eq. C.8}$$

Total pitch moment on collar, P_{3M}

$$\boldsymbol{P_{3M} = \sqrt{P_{3MI}^2 + P_{3MD}^2}} \qquad \textbf{Eq. C.9}$$

Total Pitch moment on the structure, P_{TM}

$$\boldsymbol{P_{TM} = F_{1X}(d_2 + Lever_1 - KG) + F_{2X}(d_2 + Lever_2 - KG) + F_{3X}(d_2 + Lever_3 - KG)} \qquad \textbf{Eq. C.10}$$

The sign for levers is negative

Levers

$$\boldsymbol{Lever_1 = \frac{P_{1M}}{F_{1X}} \quad Lever_2 = \frac{P_{2M}}{F_{2X}} \quad Lever_3 = \frac{P_{3M}}{F_{3X}}} \qquad \textbf{Eq. C.11}$$

APPENDIX D: ANALYTICAL SOLUTION OF SINGLE DEGREE OF FREEDOM MODEL

The standard equation of motion of a single DOF model is in the form:

$$\boldsymbol{m\ddot{x} + b\dot{x} + kx = F\, e^{i\omega t}} \qquad \textbf{Eq. D.1}$$

Assuming harmonic excitation force, the forcing function is given by:

$$\boldsymbol{F(t) = F_0 \cos \omega t} \qquad \textbf{Eq. D.2}$$

The particular solution of the equation of motion is also assumed to be harmonic in the form of:

$$\boldsymbol{x(t) = X \cos\,(\omega t - \phi)} \qquad \textbf{Eq. D.3}$$

where X and ϕ denote the amplitude and the phase angle of the response respectively. By substituting Eq.A.3 in Eq.A.1, we get:

$$\boldsymbol{X[(k - m\omega^2)\cos(\omega t - \phi) - b\omega \sin(\omega t - \phi)] = F_0 \cos \omega t} \qquad \textbf{Eq. D.4}$$

Using the trigonometric relations

$$\boldsymbol{\cos\,(\omega t - \phi) = \cos \omega t \cos \phi + \sin \omega t \sin \phi} \qquad \textbf{Eq. D.5}$$

$$\boldsymbol{\sin\,(\omega t - \phi) = \sin \omega t \cos \phi - \cos \omega t \sin \phi} \qquad \textbf{Eq. D.6}$$

By equating the coefficient of cos ωt and sin ωt on both sides of the resulting equation, we get:

$$\boldsymbol{X[(k - m\omega^2)\cos \phi + b\omega \sin \phi] = F_0} \qquad \textbf{Eq. D.7}$$

$$\boldsymbol{X[(k - m\omega^2)\sin \phi - b\omega \cos \phi] = 0} \qquad \textbf{Eq. D.8}$$

Solution of the above equations gives:

$$X = \frac{F_0}{\left[\left(k - m\omega^2\right)^2 + b^2\omega^2\right]^{1/2}} \qquad \textbf{Eq. D.9}$$

and,

$$\phi = \tan^{-1}\left(\frac{b\omega}{k - m\omega^2}\right) \qquad \textbf{Eq. D.10}$$

Dividing both the numerator and the denominator of the above equations by *k* and making the following substitutions:

$$\omega_n = \sqrt{\frac{k}{m}} \qquad \textbf{Eq. D.11}$$

where ω_n is the undamped natural frequency

$$\xi = \frac{b}{b_c} = \frac{b}{2m\omega_n} = \frac{b}{2\sqrt{mk}} \qquad \textbf{Eq. D.12}$$

where ξ is the damping ratio, the deflection under static force is:

$$\Delta_{st} = \frac{F_0}{k} \qquad \textbf{Eq. D.13}$$

we obtain:

$$X = \frac{\Delta_{st}}{\left\{\left[1 - \left(\frac{\omega}{\omega_n}\right)^2\right]^2 + \left[2\xi\frac{\omega}{\omega_n}\right]^2\right\}^{1/2}} \qquad \textbf{Eq. D.14}$$

and;

$$\phi = \tan^{-1}\left\{\frac{2\xi\frac{\omega}{\omega_n}}{1 - \left(\frac{\omega}{\omega_n}\right)^2}\right\} \qquad \textbf{Eq. D.15}$$

APPENDIX E: ANALYTICAL SOLUTION OF TWO DEGREE OF FREEDOM MODEL

The standard equation of motion of a two DOF model is in the form:

$$\boldsymbol{M_1\ddot{y}_1 + (b_1 + b_2)\dot{y}_1 + (k_1 + k_2)y_1 - b_2\dot{y}_2 - k_2y_2 = F_{1TY}\,cos(\,\omega t)} \qquad \textbf{Eq. E.1}$$

$$\boldsymbol{M_2\ddot{y}_2 + b_2\dot{y}_2 + k_2y_2 - b_2\dot{y}_1 - k_2y_1 = F_{2TY}\,cos(\,\omega t)} \qquad \textbf{Eq. E.2}$$

The general form of the characteristic equation:

$$\begin{aligned}&(m_{11}m_{22} - m_{12}m_{21})S^4 + (m_{11}c_{22} + m_{22}c_{11} - m_{21}c_{12} - m_{12}c_{21})S^3 + \\ &\quad (m_{11}k_{22} + m_{22}k_{11} + c_{11}c_{22} - m_{12}k_{21} - m_{21}k_{12} - c_{12}c_{21})S^2 + \\ &\qquad (c_{11}k_{22} + c_{22}k_{11} - c_{12}k_{21} - c_{21}k_{12})S + (k_{11}k_{22} - k_{12}k_{21}) = 0\end{aligned} \qquad \textbf{Eq. E.3}$$

It is a fourth order linear equation in *S* and has four roots; each pair is conjugate and represents a mode. They are in the form:

$$\boldsymbol{S_1 = \alpha_1 + i\beta_1} \qquad \textbf{Eq. E.4}$$

$$\boldsymbol{S_2 = \alpha_1 + i\beta_1} \qquad \textbf{Eq. E.5}$$

$$\boldsymbol{S_3 = \alpha_2 + i\beta_2} \qquad \textbf{Eq. E.6}$$

$$\boldsymbol{S_4 = \alpha_2 + i\beta_2} \qquad \textbf{Eq. E.7}$$

where:

$$\boldsymbol{\alpha_1 = -\xi_1\omega_1} \qquad \textbf{Eq. E.8}$$

$$\boldsymbol{\alpha_2 = -\xi_2\omega_2} \qquad \textbf{Eq. E.9}$$

The natural frequencies of the two masses are calculated as:

$$\boldsymbol{\omega_1^2 = \alpha_1^2 + \beta_1^2} \qquad \textbf{Eq. E.10}$$

$$\boldsymbol{\omega_2^2 = \alpha_2^2 + \beta_2^2} \qquad \textbf{Eq. E.11}$$

Therefore the characteristics equation may be written as follow:

$$(m_{11}m_{22} - m_{12}m_{21})(S^2 + 2\xi_1\omega_1 + \omega_1^2)(S^2 + 2\xi_2\omega_2 + \omega_2^2) = 0 \qquad \textbf{Eq. E.12}$$

The mass, damping, and stiffness matrices from the spar and water column equations (Eq.6.2 & Eq.6.3) are:

$$[m] = \begin{bmatrix} m_{11} & m_{12} \\ m_{21} & m_{22} \end{bmatrix} = \begin{bmatrix} m_1 & 0 \\ 0 & m_2 \end{bmatrix} \qquad \textbf{Eq. E.13}$$

$$[b] = \begin{bmatrix} b_{11} & b_{12} \\ b_{21} & b_{22} \end{bmatrix} = \begin{bmatrix} (b_1 + b_2) & -b_2 \\ -b_2 & b_2 \end{bmatrix} \qquad \textbf{Eq. E.14}$$

$$[k] = \begin{bmatrix} k_{11} & k_{12} \\ k_{21} & k_{22} \end{bmatrix} = \begin{bmatrix} (k_1 + k_2) & -k_2 \\ -k_2 & k_2 \end{bmatrix} \qquad \textbf{Eq. E.15}$$

Therefore

$$\begin{vmatrix} m_{11} & m_{12} \\ m_{21} & m_{22} \end{vmatrix} = m_1 m_2 \qquad \textbf{Eq. E.16}$$

$$\begin{vmatrix} f_1 & k_{12} \\ f_2 & k_{22} \end{vmatrix} = f_1 k_2 + k_2 f_2 \qquad \textbf{Eq. E.17}$$

$$\begin{vmatrix} f_1 & c_{12} \\ f_2 & c_{22} \end{vmatrix} = f_1 c_2 + c_2 f_2 \qquad \textbf{Eq. E.18}$$

$$\begin{vmatrix} f_1 & m_{12} \\ f_2 & m_{22} \end{vmatrix} = f_1 m_2 \qquad \textbf{Eq. E.19}$$

$$\begin{vmatrix} k_{11} & f_1 \\ k_{21} & f_2 \end{vmatrix} = f_2(k_1 + k_2) + k_2 f_1 \qquad \textbf{Eq. E.20}$$

$$\begin{vmatrix} c_{11} & f_1 \\ c_{21} & f_2 \end{vmatrix} = f_2(c_1 + c_2) + c_2 f_1 \qquad \textbf{Eq. E.21}$$

$$\begin{vmatrix} m_{11} & f_1 \\ m_{21} & f_2 \end{vmatrix} = f_2 m_1 \qquad \textbf{Eq. E.22}$$

The amplitudes and the phase angles of the two bodies may be written as:

$$Y_1 = \frac{1}{\omega_{n1}^2\omega_{n2}^2 m_1 m_2}\sqrt{\frac{\left((f_1k_2+k_2f_2)-\omega^2(f_1m_2)\right)^2+\left(\omega(f_1c_2+c_2f_2)\right)^2}{\left[(1-r_1^2)^2+(2\xi_1r_1)^2\right]\left[(1-r_2^2)^2+(2\xi_2r_2)^2\right]}} \quad \textbf{Eq. E.23}$$

$$\Phi_1 = tan^{-1}\left(\frac{2\xi_1r_1}{1-r_1^2}\right)+tan^{-1}\left(\frac{2\xi_2r_2}{1-r_2^2}\right)-tan^{-1}\left(\frac{\omega(f_1c_2+c_2f_2)}{(f_1k_2+k_2f_2)-\omega^2(f_1m_2)}\right) \quad \textbf{Eq. E.24}$$

$$Y_2 = \frac{1}{\omega_{n1}^2\omega_{n2}^2 m_1 m_2}\sqrt{\frac{\left((f_2(k_1+k_2)+k_2f_1)-\omega^2(f_2m_1)\right)^2+\left(\omega(f_2(c_1+c_2)+c_2f_1)\right)^2}{\left[(1-r_1^2)^2+(2\xi_1r_1)^2\right]\left[(1-r_2^2)^2+(2\xi_2r_2)^2\right]}} \quad \textbf{Eq. E.25}$$

$$\Phi_2 = tan^{-1}\left(\frac{2\xi_1r_1}{1-r_1^2}\right)+tan^{-1}\left(\frac{2\xi_2r_2}{1-r_2^2}\right)-tan^{-1}\left(\frac{\omega(f_2(c_1+c_2)+c_2f_1)}{(f_2(k_1+k_2)+k_2f_1)-\omega^2(f_2m_1)}\right) \quad \textbf{Eq. E.26}$$

Since the system is damped, the masses vibrate with the same frequency with a time lag; assuming that:

$$y_1 = Y_1e^{i(\omega t-\Phi_1)} \quad \textbf{Eq. E.27}$$

$$y_2 = Y_2e^{i(\omega t-\Phi_2)} \quad \textbf{Eq. E.28}$$

$$\dot{y}_1 = Y_1i\omega e^{i(\omega t-\Phi_1)} \quad \textbf{Eq. E.29}$$

$$\dot{y}_2 = Y_2i\omega e^{i(\omega t-\Phi_2)} \quad \textbf{Eq. E.30}$$

$$\ddot{y}_1 = -Y_1\omega^2 e^{i(\omega t-\Phi_1)} \quad \textbf{Eq. E.31}$$

$$\ddot{y}_2 = -Y_2\omega^2 e^{i(\omega t-\Phi_2)} \quad \textbf{Eq. E.32}$$

Therefore the relative motion between the water column and the structure may be expressed as:

$$RM = y_1\cos(\omega t+\phi_1)-y_2\cos(\omega t+\phi_2) \quad \textbf{Eq. E.33}$$

APPENDIX F: FIRST ORDER EQUATIONS OF CAPTIVE OWC

In case of captive structure, the water column equation of motion following the linear approach (Eq.6.1) can be integrated in a close form using Matlab by decomposing the second order equation into 2 coupled first order equations as follow:

Let;

$$\boldsymbol{y_2 = u_1} \qquad \textbf{Eq. F.1}$$

$$\boldsymbol{\dot{y}_2 = u_2} \qquad \textbf{Eq. F.2}$$

Therefore Eq.6.1 may be re-written as:

$$\boldsymbol{M_2\dot{u}_2 + b_2u_2 + k_2u_1 = F_{2TY}\,cos(\omega t)} \qquad \textbf{Eq. F.3}$$

The 2 coupled first order equations are in term of velocity and acceleration derivatives. From Eq.F.1 & Eq.F.2 the first equation is:

$$\boldsymbol{\dot{u}_1 = u_2} \qquad \textbf{Eq. F.4}$$

The second equation is formulated from Eq.F.3 in term of acceleration as:

$$\boldsymbol{\dot{u}_2 = -\frac{b_2}{M_2}u_2 - \frac{k_2}{M_2}u_1 - \frac{F_{2TY}}{M_2}cos(\omega t)} \qquad \textbf{Eq. F.5}$$

APPENDIX G: FIRST ORDER EQUATIONS OF FLOATING OWC

For the simplified 2DOF model used to describe floating OWC (Fig. 6.1(a)), the coupled equations of motion describing the structure and water column motions (Eq.6.2 & Eq.6.3) are integrated by decomposing the 2 coupled second order equations into 4 coupled first order equations.

Let;

$$\boldsymbol{y_2 = u_1} \qquad \textbf{Eq. G.1}$$

$$\boldsymbol{\dot{y}_2 = u_2} \qquad \textbf{Eq. G.2}$$

$$\boldsymbol{y_1 = u_3} \qquad \textbf{Eq. G.3}$$

$$\boldsymbol{\dot{y}_1 = u_4} \qquad \textbf{Eq. G.4}$$

Therefore Eq.6.2 & Eq.6.3 may be re-written as:

$$\boldsymbol{M_1\dot{u}_4 + (b_1 + b_2)u_4 + (k_1 + k_2)u_3 - b_2u_2 - k_2u_1 = F_{1TY}\,cos(\omega t)} \qquad \textbf{Eq. G.5}$$

$$\boldsymbol{M_2\dot{u}_2 + b_2u_2 + k_2u_1 - b_2u_4 - k_2u_3 = F_{2TY}\,cos(\omega t)} \qquad \textbf{Eq. G.6}$$

Similarly to the analysis performed in case of single DOF model, the 2 second order equations have to be reduced into 4 coupled first order equations. From Eq.G.1 – Eq.G.4, the first 2 equations are obtained:

$$\boldsymbol{\dot{u}_1 = u_2} \qquad \textbf{Eq. G.7}$$

$$\boldsymbol{\dot{u}_3 = u_4} \qquad \textbf{Eq. G.8}$$

The third and fourth equations are derived from the modified equations of motion (Eq.G.5 & Eq.G.6) as:

$$\boldsymbol{\dot{u}_2 = -\frac{b_2}{M_2}u_2 - \frac{k_2}{M_2}u_1 + \frac{b_2}{M_2}u_4 + \frac{k_2}{M_2}u_3 + \frac{F_{2TY}}{M_2}\cos(\omega t)} \qquad \textbf{Eq. G.9}$$

$$\dot{u}_4 = -\frac{(b_1+b_2)}{M_1}u_4 - \frac{(k_1+k_2)}{M_1}u_3 + \frac{b_2}{M_1}u_2 + \frac{k_2}{M_1}u_1 + \frac{F_{1TY}}{M_1}\cos(\omega t) \quad \textbf{Eq. G.10}$$

Considering the model proposed by Szumko, illustrated in Fig.6.2 the coupled equations of motions have to be treated similarly to the former model, so that the coupled equations are reduced to first order equations.

Let

$$y_1 = u_1 \quad \textbf{Eq. G.11}$$

$$\dot{y}_1 = u_2 \quad \textbf{Eq. G.12}$$

$$y_2 = u_3 \quad \textbf{Eq. G.13}$$

$$\dot{y}_2 = u_4 \quad \textbf{Eq. G.14}$$

$$y = u_5 \quad \textbf{Eq. G.15}$$

$$\dot{y} = u_6 \quad \textbf{Eq. G.16}$$

Therefore the coupled equations (Eq.6.4 – Eq.6.6) are to be written as:

$$M_1\dot{u}_2 + b_s u_2 + b_{PTO}(u_2 - u_6) + k_s u_1 = F_{1TY}\cos(\omega t) \quad \textbf{Eq. G.17}$$

$$b_{PTO}(u_6 - u_2) + k_{air}(u_5 - u_3) = 0 \quad \textbf{Eq. G.18}$$

$$M_2\dot{u}_4 + b_{wc}u_4 + k_{wc}u_3 + k_{air}(u_3 - u_5) = F_{2TY}\cos(\omega t) \quad \textbf{Eq. G.19}$$

In this case 5 first order differential equations have to be formulated. From Eq.G.11 – Eq.G.16 the first 3 equations are obtained:

$$\dot{u}_1 = u_2 \quad \textbf{Eq. G.20}$$

$$\dot{u}_3 = u_4 \quad \textbf{Eq. G.21}$$

$$\dot{u}_5 = u_6 \quad \textbf{Eq. G.22}$$

The fourth equation is obtained from Eq.G.17:

$$\dot{u}_2 = -\frac{b_s}{M_1}u_2 - \frac{b_{PTO}}{M_1}(u_2 - u_6) - \frac{k_s}{M_1}u_1 + \frac{F_{1TY}\cos(\omega t)}{M_1} \quad \textbf{Eq. G.23}$$

Similarly the fifth equation is obtained from Eq.G.19 as:

$$\dot{u}_4 = -\frac{b_{wc}}{M_2}u_4 - \frac{k_{wc}}{M_2}u_3 - \frac{k_{air}}{M_2}(u_3 - u_5) + \frac{F_{2TY}}{M_2}\cos(\omega t) \quad \textbf{Eq. G.24}$$

Now, u_6 should be defined. By multiplying Eq.G.18 by M_2 and Eq.G.19 by k_{air} we get:

$$M_2 b_{PTO}(u_6 - u_2) + M_2 k_{air}(u_5 - u_3) = 0 \quad \textbf{Eq. G.25}$$

$$M_2 k_{air}\dot{u}_4 + b_{wc}k_{air}u_4 + k_{wc}k_{air}u_3 + {k_{air}}^2(u_3 - u_5) = k_{air}F_{2TY}\cos(\omega t) \quad \textbf{Eq. G.26}$$

The sum of Eq.G.25 & Eq.G.26 gives:

$$b_{wc}k_{air}u_4 + k_{wc}k_{air}u_3 + {k_{air}}^2(u_3 - u_5) + M_2 b_{PTO}(u_6 - u_2) + M_2 k_{air}(u_5) = k_{air}F_{2TY}\cos(\omega t) \quad \textbf{Eq. G.27}$$

Finally Eq.G.22 may be written as:

$$\dot{u}_5 = u_2 + \frac{b_{wc}k_{air}}{M_2 b_{PTO}}u_4 - \frac{k_{wc}k_{air}}{M_2 b_{PTO}}u_3 - \frac{{k_{air}}^2}{M_2 b_{PTO}}(u_3 - u_5) + \frac{M_2 k_{air}}{M_2 b_{PTO}}(u_5) + \frac{k_{air}F_{2TY}}{M_2 b_{PTO}}\cos(\omega t) \quad \textbf{Eq. G.28}$$